Petrogenesis of low-Ti and high-Ti magmatic rocks of the Jurassic Ferrar Large Igneous Province, Antarctica

Dissertation

zur Erlangung des akademischen Grades doctor rerum naturalium
(Dr. rer. nat.)

vorgelegt dem Rat der Chemisch-Geowissenschaftlichen Fakultät

der

Friedrich-Schiller-Universität Jena

von Dipl.-Geol. Ricarda Hanemann

geboren am 25.08.1975 in Jena

Gutachter:

1. Prof. Dr. L. Viereck-Götte

2. Prof. Dr. F. Holtz

Tag der öffentlichen Verteidigung: 28.11.2007

ABSTRACT

The Mid-Jurassic Ferrar Large Igneous Province is one of the Mesozoic continental plateau basalt provinces associated with the break-up of the Gondwana supercontinent. The Ferrar magmatic rocks, exposed in a linear belt along the Palaeo-Pacific margin of Gondwana, comprise numerous sills, dikes and lava flow sequences as well as the Dufek layered mafic intrusion. Uniform crust-like trace element and isotope signatures indicate a single magma source for the > 3000-km long Ferrar magmatic province. A subcontinental lithospheric mantle source has been proposed characterised by crustal enrichment due to Palaeozoic subduction along the cratonic margin of Gondwana. However, the thermal source for the voluminous melt generation is still under debate as the crust-like isotope data obscure the detection of a possible mantle plume involvement. Furthermore, the genesis of the two magma series present within the Ferrar province, a low-Ti and a high-Ti series, is an unsolved issue up to now.

Against this background, the present thesis investigates Ferrar magmatic rocks from northern Victorialand and from George V Land aiming a better understanding of the petrogenesis of the Ferrar magmatic rocks. The main subject is directed towards the understanding of the evolution of the two compositionally distinct Ferrar magma series including the differentiation history, the melt generation and some magma source constraints. Beside major and trace elements (incl. rare earth elements – REE), platinum-group elements (PGE) were analysed in selected Ferrar rocks to further describe the evolutionary processes and additionally, to decipher mantle source characteristics, since the thermal source for the generation of the large volumes of Ferrar magmas is still a matter of debate.

The analysed basaltic andesites and andesites exhibit the common phase assemblage of tholeiitic differentiation sequences composed of varying amounts of pyroxenes, plagioclase, oxides and mesostasis. All samples have been categorised as low-Ti (LTS: TiO_2 ~ 0.4 – 1.2 wt%) and high-Ti series (HTS: TiO_2 ~ 1.7 – 2.1 wt%). In contrast to the LTS, rocks of the HTS generally lack orthopyroxene and contain clinopyroxene and plagioclase that are richer in FeO and Na_2O, respectively. They exhibit higher concentrations of incompatible elements (e.g. FeO, TiO_2, Y, Zr, REE) at only slightly enriched SiO_2 contents relative to the LTS.

The low-Ti rocks are characterised by wide petrographical as well as mineral- and whole-rock chemical variations. The mineral chemistry and specific element concentrations of low-Ti rocks exhibit good correlations with the degree of differentiation of the distinctly evolved samples. These variations are interpreted to result from fractional crystallisation during low-pressure *in situ* differentiation. From the chilled margins of low-Ti sills (Mg# ~ 62), which are suggested to represent the pre-intrusive composition of the low-Ti magmas, cumulates and differentiates (Mg# ~ 74 – 33) developed after magma intrusion in the upper crust. The mineral and bulk-rock chemical data further indicate that the magmas of the chemically more evolved but uniform HTS (Mg# ~ 31 – 24) are not generated by continued low-pressure fractionation of the LTS magmas. The uniform trace element signatures (and published isotope data) of the two Ferrar magma series indicate that commonly proposed models for the generation of distinct magma series in other LIPs, such as derivation from different magma sources or differences during melt generation, can be excluded. Assuming an identical primary magma for both Ferrar magma series, different conditions during their pre-emplacement differentiation are suggested to explain the two distinct compositions.

In consideration of previously published experimental results, the compositional differences observed for the two Ferrar magma series are used to develop a differentiation model suggesting distinctly different water activities, oxygen fugacities and pressure conditions for both magma series. The influence of these intensive parameters on the Ferrar magma evolution

has been examined by equilibrium crystallisation experiments performed at 1100 °C and 2 kbar in internally heated pressure vessels using a chilled margin sample from a low-Ti sill as starting material. The obtained phase relations and compositions exhibit systematic variations with changing run conditions. The comparison of the experimental results with the natural phase assemblage of the analysed low-Ti and high-Ti rocks indicates that the high-Ti magma series experienced pre-emplacement differentiation under lower pressure, lower water activity and lower oxygen fugacity than the low-Ti magma series.

From these results, it is suggested that the low-Ti magmas experienced the pre-emplacement differentiation mainly at the base of the continental crust, while the high-Ti magmas stagnated and differentiated at shallower crustal level. The complex interaction of the different intensive variables during magma differentiation in the proposed independent temporary magma reservoirs largely influenced the fractionating mineral phases and hence can well explain the distinct evolution of the two Ferrar magma series.

This simplified polybaric differentiation model including the transfer of the increasingly evolving low-Ti and high-Ti magmas to the upper crust is assumed to be essentially controlled by sudden major tectonic changes related to rifting processes associated with the initial break-up of the Gondwana supercontinent. Magma emplacement along pre-existing lithospheric discontinuities would explain the unusual distribution of the Ferrar magmatic rocks.

However, the present geochemical data do not give any evidence of a mantle plume contribution during generation of the Ferrar magmas. The PGE abundances, thought to shed some light on this problem, exhibit distinct correlations with the differentiation index of the samples indicating that the primary signatures are also largely influenced by the pronounced *in situ* differentiation. The mainly sulphur-undersaturated conditions during differentiation of the Ferrar magmas inferred from the PGE systematics confirm the refractory nature of their mantle source that has also been deduced from specific major and trace element features of the studied rocks. These signatures indicate a derivation of the primary Ferrar magmas by partial melting of a secondarily hydrated source within the subcontinental lithospheric mantle, depleted by previous events of melt extraction. Nevertheless, the controlling mechanism of melt generation producing the voluminous Ferrar magmas can not be evaluated conclusively by means of the present geochemical data and remains an outstanding issue for an interdisciplinary discussion.

KURZFASSUNG

Die Jurassische Ferrar Large Igneous Province (FLIP) repräsentiert eine der mit dem Gondwana-Zerfall assoziierten Mesozoischen Plateaubasaltprovinzen. Die magmatischen Gesteine der Ferrar Provinz treten in einem schmalen Gürtel entlang des Paläopazifischen Randes Gondwanas auf und umfassen zahlreiche Lagergänge, Gänge und Lavastromabfolgen sowie die geschichtete mafische Dufek Intrusion. Einheitliche krustenähnliche Spurenelement- und Isotopencharakteristika veranlassen zur Annahme einer identischen Magmenquelle für die sich über mehr als 3000 km erstreckende Ferrar Provinz. Eine subkontinentale lithosphärische Mantelquelle wird vorgeschlagen, welche im Zuge Paläozoischer Subduktionsprozesse entlang des Gondwana-Kratons an Krustenkomponenten angereichert wurde. Jedoch wird die Wärme-quelle für die großvoluminöse Schmelzbildung noch immer kontrovers diskutiert, da die krustalen Isotopensignaturen die Identifizierung der Beteiligung eines Mantelplumes verhindern. Des Weiteren ungeklärt ist die Genese der auftretenden low-Ti und high-Ti Ferrar Magmaserien.

Vor diesem Hintergrund wurden in der vorliegenden Arbeit magmatische Ferrar Gesteine aus dem nördlichen Victorialand und dem George V Land mit dem Ziel untersucht, einen wesentlichen Beitrag zum besseren Verständnis der Petrogenese der Ferrar Gesteine zu liefern. Zentrale Fragestellung ist die Entwicklung der beiden geochemisch verschiedenen Magmaserien, welche die Beschreibung ihrer Differentiationsgeschichte, ihrer Schmelzbildung sowie die Charakterisierung ihres Magmenursprungs beinhaltet. Zusätzlich zu Haupt- und Spurenelementen (einschließlich der Seltenen Erdelemente – REE) wurden an ausgewählten Proben die Konzentrationen der Platingruppenelemente (PGE) analysiert, um sowohl die magmengenetischen Prozesse als auch Mantelquellensignaturen detaillierter beschreiben zu können, da die thermische Quelle, erforderlich für die Bildung der enormen Magmenvolumina, noch immer umstritten ist.

Die analysierten basaltischen Andesite und Andesite weisen eine Mineralvergesellschaftung bestehend aus stark variierenden Anteilen an Pyroxenen, Plagioklas und Oxiden auf, die typisch ist für tholeiitische Differentiationsserien. Alle Proben lassen sich den bekannten low-Ti (LTS: TiO_2 ~ 0,4 – 1,2 Gew%) und high-Ti (HTS: TiO_2 ~ 1,7 – 2,1 Gew%) Magmaserien zuordnen. Im Gegensatz zur LTS enthalten die Gesteine der HTS keinen Orthopyroxen, jedoch Fe-reichere Klinopyroxene sowie Na-reicheren Plagioklas. Des Weiteren zeichnen sie sich durch erhöhte Konzentrationen an inkompatiblen Elementen (z. B. FeO, TiO_2, Y, Zr, REE) aus bei nur unwesentlich erhöhten SiO_2-Gehalten verglichen mit den Gesteinen der LTS.

Die low-Ti Gesteine sind gekennzeichnet durch ausgeprägte petrographische sowie mineral- und geochemische Variationen. Die mineralchemischen Daten sowie spezifische Elementkon-zentrationen der low-Ti Gesteine belegen gute Korrelationen mit dem Differentiationsgrad der verschieden stark entwickelten Proben. Diese Variationen werden auf fraktionierte Kristallisation während einer *in situ* Differentiation unter Niedrig-Druck-Bedingungen zurückgeführt. Ausge-hend von den rasch abgekühlten Rändern („chilled margins") der low-Ti Lagergänge (Mg# ~ 62), welche die prä-intrusive Zusammensetzung der low-Ti Magmen widerspiegeln, entwickelten sich Kumulate und Differentiate (Mg# ~ 74 – 33) nach der Magmenplatznahme in der oberen Erdkruste. Zudem belegen die mineral- und gesteinschemischen Daten, dass die Magmen der chemisch höher entwickelten aber homogenen HTS (Mg# ~ 31 – 24) nicht durch fortgesetzte Niedrig-Druck-Fraktionierung der low-Ti Magmen gebildet wurden. Die einheitlichen Spuren-elementsignaturen (sowie publizierte Isotopendaten) beider Magmaserien deuten ferner darauf hin, dass allgemein angenommene Modelle zur Bildung unterschiedlicher Magmaserien inner-halb anderer LIPs, wie z. B. die Abstammung aus unterschiedlichen Magmenquellen oder Unterschiede während des Schmelzbildungsprozesses, ausgeschlossen werden können. Unter

der Annahme eines identischen Ursprungsmagmas für die beiden Ferrar Magmaserien werden unterschiedliche Bedingungen während der Differentiation vor der oberkrustalen Magmenplatznahme vorgeschlagen, um die bestehenden geochemischen Unterschiede zu erklären.

Basierend auf den ermittelten Unterschieden beider Magmaserien wurde unter Berücksichtigung publizierter experimenteller Studien ein Differentiationsmodell entwickelt, welches die Annahme unterschiedlicher Wasseraktivitäten, Sauerstofffugazitäten sowie Druckbedingungen für beide Magmaserien postuliert. Der Einfluss dieser Parameter auf die Entwicklung der Ferrar Magmen wurde anschließend anhand von Gleichgewichtskristallisationsexperimenten untersucht. Die Experimente wurden bei 1100 °C und 2 kbar in intern beheizten Gasdruckanlagen durchgeführt; als Ausgangsmaterial wurde ein „chilled margin" eines low-Ti Lagerganges ausgewählt. Die ermittelten Phasenbeziehungen sowie deren Zusammensetzung belegen systematische Variationen mit variierenden experimentellen Bedingungen. Aus dem Vergleich der experimentell synthetisierten Proben und der natürlichen low-Ti und high-Ti Gesteine wird geschlussfolgert, dass die high-Ti Magmaserie eine Differentiation unter niedrigerem Druck, niedrigerer Wasseraktivität und niedrigerer Sauerstofffugazität als die low-Ti Magmen erfahren hat.

Anhand dieser Ergebnisse wird eine Differentiation der low-Ti Magmen an der Basis der kontinentalen Kruste vorgeschlagen, während die high-Ti Magmen in einem flacheren Krustenniveau stagnierten und differenzierten. Die komplexen Wechselwirkungen der unterschiedlichen Bedingungen während der Differentiation in den vorgeschlagenen voneinander unabhängigen, temporären Magmareservoiren beeinflussten maßgeblich die fraktionierenden Mineralphasen, womit die unterschiedliche Entwicklung der beiden Ferrar Magmaserien erklärt werden kann.

Es wird ferner angenommen, dass dieses vereinfachte polybare Differentiationsmodell sowie der Transport der sich zunehmend entwickelnden low-Ti und high-Ti Magmen in die Oberkruste entscheidend durch abrupte tektonische Veränderungen kontrolliert wird, welche im engen Zusammenhang mit dem initialen Zerfall des Gondwana-Superkontinents stehen. Die Magmenplatznahme entlang vorhandener lithsophärischer Diskontinuitäten ermöglicht es, die ungewöhnliche Verbreitung der Ferrar Gesteine zu erklären.

Die vorliegenden geochemischen Daten geben jedoch keinen Aufschluss über die Beteiligung eines Mantelplumes zur Bildung der Ferrar Magmen. Die PGE-Konzentrationen, welche ursprünglich eine Lösung dieser Fragestellung in Aussicht stellten, weisen eindeutige Korrelationen mit dem Differentiationsgrad der Proben auf. Dies belegt, dass die primären PGE-Signaturen ebenfalls stark von der ausgeprägten *in situ* Differentiation beeinflusst wurden. Die aus den PGE-Systematiken abgeleitete Interpretation von überwiegend Schwefel-untersättigten Differentiationsbedingungen steht im Einklang mit dem refraktären Charakter der Ferrar Mantelquelle, welcher anhand spezifischer Haupt- und Spurenelementsignaturen der untersuchten Gesteine ermittelt wurde. Diese Signaturen implizieren die Herkunft der primären Ferrar Magmen als Folge partieller Schmelzbildung einer sekundär überprägten subkontinentalen lithosphärischen Mantelquelle, die im Zuge vorangegangener Schmelzextraktionen abgereichert wurde. Jedoch können die Mechanismen, die die Schmelzbildung der Ferrar Magmen kontrollierten, nicht auf der Basis des vorhandenen geochemischen Datensatzes abschließend verifiziert werden und bleiben somit weiterhin ein interessanter Diskussionspunkt.

Contents

List of Figures

List of Tables

1   INTRODUCTION

1.1   LARGE IGNEOUS PROVINCES

Large igneous provinces (LIPs) have been studied intensely over the last decades. They represent some of the most significant periods of magmatic activity in Earth's history and are defined as regions of voluminous emplacement of predominantly mafic extrusive and intrusive rocks that originated from processes other than 'normal' sea-floor spreading (COFFIN & ELDHOLM 1992). Besides continental flood basalts and their associated intrusives, LIPs include large igneous bodies at volcanic passive margins, submarine ridges, some seamount chains as well as oceanic plateaus and ocean basin flood basalts (COFFIN & ELDHOLM 1994) which have been recognised as being the submarine counterparts to the continental provinces. These vast outpourings of mostly basaltic magma often produced volumes of several 10^6 km^3, which have been distributed over an area of 10^5 to 10^6 km^2. The largest is 'greater' Ontong Java with a volume of $> 5 * 10^7$ km^3 (COFFIN & ELDHOLM 1993, NEAL et al. 1997). Since considerable parts of LIPs (especially those of pre-Mesozoic age) may have been destructed due to processes like subduction, continent-continent collision or erosion, many of them presumably covered a much larger area than reported in literature. Hence, LIP magmatism reflects important geological events with a major contribution to the growth of both oceanic and continental crust.

Characteristic is the very short time span required to generate these immense volumes of predominantly tholeiitic magmas (e.g. COFFIN & ELDHOLM 1994). There are a number of examples of LIPs where the bulk of magmas were emplaced over a short period of time of about one million years or even less, e.g. the Siberian Traps at ~ 250 Ma (SHARMA 1997), the Deccan Traps at 65 Ma (COURTILLOT et al. 1986) or the Ferrar-Karoo provinces at ~ 184 Ma (ENCARNACIÓN et al. 1996, DUNCAN et al. 1997). This apparent short duration of magmatic activity of most LIPs, suggested by increasingly precise geochronological data for magma emplacement, is furthermore supported by palaeomagnetic data, the marked geochemical similarity of lava flows and supra-crustal intrusions as well as the general lack of significant amounts of palaeosols, subaerial weathering horizons and/or persistent sedimentary intercalations in the sequences of most provinces (MARSH et al. 1997).

The very high emplacement rates (e.g. COFFIN & ELDHOLM 1993), deduced from the exceptionally large melt volumes of these short-lived magmatic pulses, have widely been accepted as being linked to rifting processes of continents and to the involvement of upwelling mantle plumes (e.g. MCKENZIE & BICKLE 1988, WHITE & MCKENZIE 1989, 1995, CAMPBELL & GRIFFITH 1990, DUNCAN & RICHARDS 1991). However, although the majority of authors now agree with the starting-plume hypothesis for the origin of many LIPs (e.g. the Columbia River and Deccan provinces, HOOPER 1990), which has been encouraged by e.g. RICHARDS et al. (1989) and HILL (1991), in recent years a comprehensive discussion persists concerning the precise nature of the source region. Thereby, the role inferred for a plume is discussed in quite different ways. The outstanding problem is to establish whether LIPs result from the impingement of a deep-

seated mantle plume on the base at the lithosphere with the plume serving (at least partially) as a source of magma, or if LIPs are generated by adiabatic decompressional melting of anomalous hot mantle lithosphere involving conductive heat transfer from a mantle plume.

In more recent studies, a great number of modifications of these 'active' and 'passive' models have been proposed for the formation of individual LIPs by attributing variable importance to both a mantle plume and lithospheric extension, the two fundamental requirements to provide the enormous melt volumes (WHITE & MCKENZIE 1989, 1995). In this context, 'lithospheric-asthenospheric interaction' became a widely used term (e.g. ELLAM & COX 1991, ARNDT & CHRISTENSEN 1992, GIBSON et al. 1995, 1999). Since some of the geochemical signatures exhibited by many continental flood basalts differ markedly from those of their oceanic counterparts, they have been interpreted as emphasising the importance of continental lithospheric mantle as melting source for the generation of LIPs (e.g. HERGT et al. 1991, TURNER & HAWKESWORTH 1995, HARRY & LEEMAN 1995) with only subordinate plume impact. The most extraordinary model questioning the importance of any plume involvement is suggested by ANDERSON (1994a, 1994b) who refers to the presence of many LIPs at continental margins adjacent to Archaean cratons. His alternative model proposes lithospheric pull-apart at cratonic boundaries, rather than extension of uniform lithosphere, to cause small-scale convection due to lateral temperature gradients, which triggers the extensive continental magmatism by melting the hydrous subcontinental lithospheric mantle.

Much recent interest in LIP magmatism has been focussed on its implication for the thermal structure of the mantle, its importance for the global crustal production and hence, the understanding of continental growth and separation. A general consensus exists on the obvious temporal and causal association of LIPs with continental break-up processes (e.g. HILL 1991, STOREY et al. 1992b, ANDERSON 1994a, 1994b, STOREY 1995, DALZIEL et al. 2000). The time-space relationship between mantle plumes, LIP magmatism and continental separation has been thoroughly reviewed by e.g. WHITE & MCKENZIE (1989), COFFIN & ELDHOLM (1992) and COURTILLOT et al. (1999) who described in detail several cases of continental flood basalt volcanism followed by continental rifting and opening of ocean basins. Here too, the actual causes and the geodynamic mechanism driving the fragmentation of continents remain elusive.

One example for the causal link of flood basalt volcanism and continental break-up is the disintegration of the Gondwana supercontinent. This break-up was accompanied by large-scale mafic magmatism in Mesozoic times. The generated voluminous tholeiitic continental flood basalts are widespread across the southern hemisphere, forming three large igneous provinces: the Cretaceous Paraná-Etendeka Province (S-America, W-Africa), the Jurassic Karoo Province (S-Africa, Antarctica) and the Jurassic Ferrar Province (mainly Antarctica) (Fig. **1.1**). Compared to the former, the Ferrar Large Igneous Province (FLIP) forms the most extraordinary continental flood basalt province associated with the Gondwana break-up concerning the distribution as well as the geochemical features of its igneous rocks. Since the Karoo and the Paraná provinces mark positions of opening ocean basins, these provinces have been accepted to be closely related to continental separation. In contrast, the Ferrar igneous rocks were

emplaced along the palaeo-Pacific continental margin of Gondwana related to rifting processes. These igneous rocks possibly indicate a long failed rift arm of a triple junction (FORD & KISTLER 1980, ELLIOT 1992, COURTILLOT et al. 1999, WHITE & MCCLINTOCK 2001) and are therefore believed not to be direct precursors to continental separation and seafloor spreading. The unusual geometry of the FLIP has widely been discussed (e.g. DUNCAN et al. 1997) as well as the origin of the geochemical characteristics of the Ferrar tholeiites. While the Paraná and the Karoo magmatism may be attributed to plume-related heating and mantle upwelling (WHITE & MCKENZIE 1989), the tectono-thermal regime for the Ferrar province is poorly constrained and remains an unsolved issue up to now.
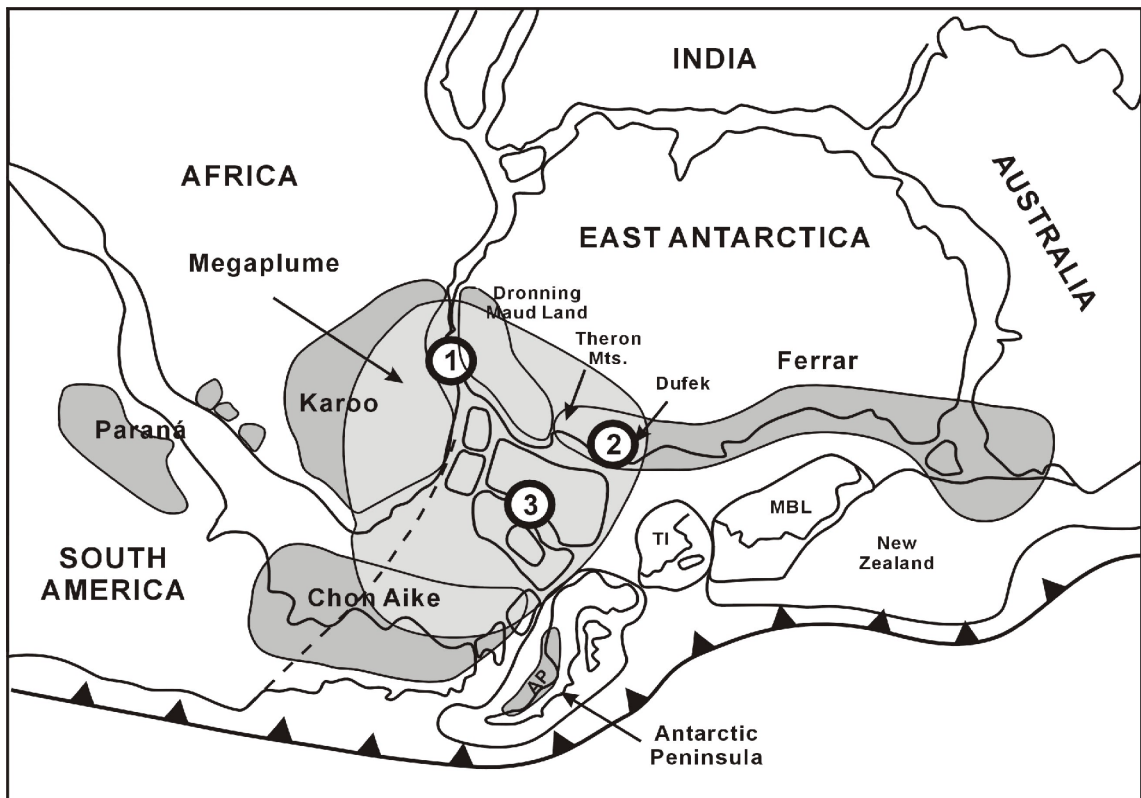
Fig. 1.1 – Sketch map showing a pre-break-up Gondwana reconstruction (~ 180 Ma) and the distribution of the continental plateau basalt provinces Paraná, Karoo, Ferrar and Chon Aike (modified after RILEY et al. 2003) as well as the megaplume of STOREY & KYLE (1997) and the location of the three individual hotspots (1) Discovery, (2) Bouvet and (3) Shona from STOREY et al. (2001).

Besides studies regarding magma source constraints and general geodynamic questions, LIP magmatism provides an enormous diversity of topics to investigate petrogenetic processes such as magma evolution during partial melting and differentiation. Aside from variable melting sources, the conditions (e.g. pressure, temperature, volatile content and volatile composition) under which a magma experiences the modification processes can be quite diverse. This is best reflected by the wide compositional variability of rock series generated in different LIPs or even within individual LIPs. Based on a comprehensive mineral- and geochemical characterisation of

these different magma types, detailed modelling describing the petrogenetically relevant processes has been performed for a large number of oceanic and continental LIPs in the last decades. The fundamentals applied in these petrogenetic models are widely supported by results of systematic experimental studies conducted to simulate melting and crystallisation processes in nature and to better understand igneous phase relations and their dependence on intensive parameters. Such experiments became more important in recent years since they provide valuable tools to test the predictions obtained from geochemical modelling.

In addition to the increasingly recognised petrological importance of LIP magmatism, recently, much focus of interest is directed towards the radical impact of plateau basalt magmatism on global environmental changes. These changes can be attributed to enormous emissions of climate-relevant volatiles into the atmosphere during eruption events (e.g. THORDARSON & SELF 1996, OLSEN 1999) causing among other things increased chemical weathering and modifications of ocean chemistry. In this context, WIGNALL (2001, and references therein) reviews the close temporal relationship of mass extinctions and ecosystem disruptions with formation ages of LIPs, as implicated by the coincidence of e.g. the Siberian or the Deccan Traps with biotic crises at the Permian-Triassic boundary (RENNE et al. 1995) and the Cretaceous-Tertiary boundary (DUNCAN & PYLE 1988, BAKSI 1987), respectively. Another example is given by PÁLFY & SMITH (2000), considering the synchrony of the Ferrar-Karoo plateau basalt volcanism with the mass extinction and oceanic anoxic event in early Jurassic times.

1.2   OBJECTIVES AND OUTLINE OF THIS THESIS

Within the scope of German geoscientific research in Antarctica, the break-up process of the Gondwana supercontinent has been considered one of the major subjects and hence, the knowledge of the closely related Mid-Jurassic Ferrar Large Igneous Province (FLIP) is of fundamental importance. In order to contribute to the understanding of the petrogenesis of Ferrar magmatic rocks, particularly the generation of two distinct magma series present within this province, intrusives and extrusives in northern Victorialand (NVL) and George V Land were sampled during the German Antarctic North Victoria Land Expedition VIIII (GANOVEX VIII), the joint German-Italian Antarctic Expedition in 1999/2000.

The motivation for the investigations presented here arose from the results gained during a preliminary study within the scope of my diploma thesis. This previous work comprised the petrographical and whole-rock chemical characterisation of selected Ferrar occurrences from NVL in order to extend the knowledge of the regional distribution of the two compositionally distinct magma series. The results have shown some marked differences to observations made e.g. by HORNIG (1993), which aroused further interest to examine.

The main issue of this thesis about the petrogenesis of the Ferrar tholeiitic rocks is directed towards the differences of the evolution of the two compositionally distinct magma series including considerations of the magma source, the melt generation and the magma differentiation paths. Since different magma series have been reported

from a large number of LIPs, e.g. from the Gondwana related Mesozoic Paraná and Karoo provinces, a number of models suggested to explain the petrogenesis of the respective rocks have been discussed controversially, each model corresponding to the tectonic framework and the geochemical features given by the particular LIP. The basically different assumptions proposed in these models are reviewed and discussed in more detail in the respective chapters of discussion and are thus only shortly listed here:

- magma derivation from distinct mantle sources (interaction of asthenospheric and lithospheric sources)
- different depths and/or degrees of partial melting
- different melt generation rates caused by variable amounts of extension
- different extent of crustal contamination of mantle-derived magmas
- subsequent differentiation from one magma series to the other
- distinct physico-chemical conditions during magma differentiation

Besides the evaluation of the evolution path of the two magma series considering the above listed models, this thesis further aims at deciphering mantle source characteristics since the thermal source for the generation of the large volumes of Ferrar magma is still a matter of debate (see Chapter 1.3.2). In this respect, platinum-group element (PGE) characteristics of basaltic rock suites were suggested to be useful tools to distinguish lower and upper mantle reservoirs (Chapter 2.4). Thus, in addition to whole-rock major and trace elements, PGE characteristics of selected Ferrar samples will be used to assess their significance to magma source constraints, however, not without consideration of the behaviour of this element group during differentiation processes and partial melting.

The presented thesis is structured as follows:

After the introduction into LIP magmatism in general, the Ferrar LIP is introduced in Chapter 1.3 including the basics of distribution, stratigraphy and age of Ferrar rocks as well as their general geochemical features and the present state models of magma origin. This is followed by a short review of the geological setting and history of the investigation area at the middle Rennick Glacier in NVL.

A description of the techniques and procedures applied for chemical analyses is given in Chapter 2 supplemented by short remarks on the motivation and expected benefit of the respective analysis. For this purpose, Chapter 2 also includes a brief survey of the general petrogenetic behaviour of platinum-group elements.

Chapter 3.1 documents the field relations and sampling of extrusive and intrusive Ferrar occurrences from within NVL and George V Land and describes the hand specimen as well as their appearance and modal composition determined under the microscope. The further characterisation of the sample material is based on mineral chemical data (Chapter 3.2) including a short summary of the obtained results. The inferred preliminary conclusions are tested by estimating some differentiation

conditions such as crystallisation temperature and oxygen fugacity by applying the mineral chemistry to conventional geothermobarometers and oxybarometers, respectively. Chapter 3.3 further characterises the sample material by means of their whole-rock chemistry comprising (besides the ordinary major and trace elements) rare earth element and platinum-group element concentrations of selected samples.

Based on this comprehensive sample characterisation, different aspects of the petrogenesis of the Ferrar rocks are discussed in Chapter 4, namely the differentiation history, the partial melting process and magma source composition, each aspect considering especially the petrogenetic differences between both magma series.

The implication that the differentiation process is the crucial factor causing the different evolution paths is discussed in more detail in Chapter 4.6. Therein, the consideration of distinct factors influencing the Ferrar magma differentiation is combined with a review of published results from experimental studies aiming at comparable issues. The obtained conclusions are summarised in a preliminary differentiation model suggesting distinct conditions during differentiation for both magma series.

This proposed model is tested by some crystallisation experiments (Chapter 5) performed under systematically modified conditions according to the assumptions outlined in the model before. The experimentally synthesised phase relations and their compositions will be used to evaluate the effect of oxygen fugacity and water activity on the Ferrar magma evolution during differentiation processes. A summary of the gained conclusions will be presented in a petrogenetic model (Chapter 6) that leads to a better understanding of the genesis of the two distinct magma series present within the Ferrar LIP.

The final implications drawn for the Ferrar province are not only of regional importance, but the results obtained from this study also contribute to generally enhance the understanding of magmatism generating continental large igneous provinces and of processes involved in their genesis. In particular, the results will help to understand the formation of distinct magma series as well as the geochemical behaviour of platinum-group elements.

1.3   THE FERRAR LARGE IGNEOUS PROVINCE

1.3.1   Regional Distribution, Stratigraphy and Age

Regional Distribution

Rocks of the Jurassic Ferrar LIP are exposed in a linear > 3,000 km long but only < 200 km wide belt along the western margin of the East Antarctic craton, parallel to the palaeo-Pacific margin of Gondwana. On the Antarctic continent, the FLIP comprises the Dufek-Forrestal layered mafic intrusion as well as widespread intrusives and extrusives with subordinate sedimentary and volcanogenic interbeds, the total volumes of which are in excess of 5×10^5 km^3 (KYLE et al. 1981). The igneous rocks crop out as erosional remnants in numerous occurrences from Horn Bluff / George V Land and Victorialand throughout the length of the Transantarctic Mountains (TAM) to the Theron Mountains in the Weddell Sea sector (Fig. **1.2**). Including plateau-forming

sills in Tasmania (HERGT et al. 1989) and single occurrences in South Australia (MILNES et al. 1982, HERGT et al. 1991) and New Zealand (MORTIMER et al. 1995), which are all characterised by Jurassic age and comparable geochemical features, the FLIP extends over more than 4000 km (Fig. **1.1**).
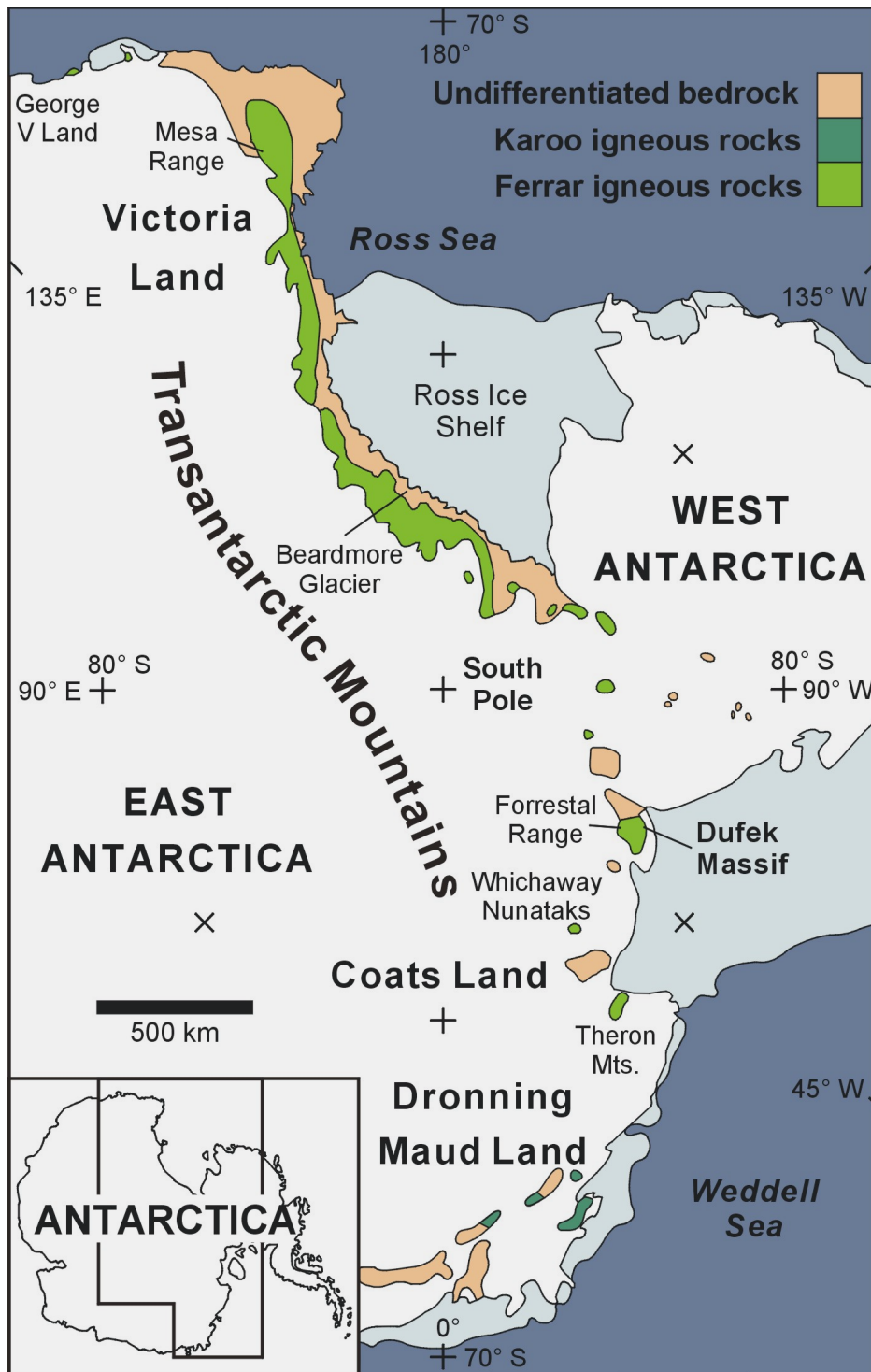
Fig. 1.2 – Distribution of Jurassic tholeiitic rocks in Antarctica including those of the Ferrar igneous province stretching along the Transantarctic Mountains, those of the Karoo igneous province exposed within Dronning Maud Land as well as the Coats Land dolerites which represent a transition zone between the two provinces.

Intensely discussed are the occurrences of Jurassic tholeiitic rocks from Coats Land exposed as sills and minor dikes in the Theron Mountains and the Whichaway Nunataks, which are situated transitionally between the Karoo province in Dronning Maud Land and the Ferrar Province along the TAM. Most of these Coats Land dolerites are geochemically transitional between the Karoo and the Ferrar tholeiites, but some are comparable to the latter and therefore, have been attributed to the FLIP as well (BREWER 1989, BREWER et al. 1992).

Stratigraphy

After BRADSHAW (1987b), the Ferrar magmatic activity can generally be subdivided into three stages: an initial explosive phase recorded by volcanic breccias, volcanogenic sediments and lahars, which was followed by a quieter flood basalt phase and an intrusive phase with sill and dike emplacement along with the subdued flood basalt extrusions. A simplified stratigraphic profile from the basement to the Ferrar rocks is given exemplarily for northern Victorialand in ROLAND & WÖRNER (1996).

Aside from the Dufek-Forrestal intrusion (see below), comprising the bulk volume of the known Ferrar rocks (FORD & HIMMELBERG 1991), the majority of Ferrar occurrences is represented by intrusives exposed as innumerable high-level sills and dikes, referred to as "Ferrar Dolerites" after HARRINGTON (1958). They predominantly intruded the sediments of the Devonian to Triassic Beacon Supergroup (BARRETT et al. 1986) and less frequently the Palaeozoic metamorphic or igneous basement units. Major sills commonly have a thickness of 150 – 200 m, but single sills can reach up to 400 m thickness (ELLIOT et al. 1985). In a given section, their total thickness may exceed 1,000 m. Also widely distributed, but volumetrically insignificant are dikes with thicknesses often below 10 m.

Generally, intrusives are geographically much more widespread than extrusives, which are confined to only few regions at the edge of the Polar Plateau, namely the Beardmore Glacier region in the central TAM and parts of Victorialand. They are referred to as "Kirkpatrick Basalts" after GRINDLEY (1963) and form lava flow sequences which document existent thicknesses of 450 – 780 m with single lava flows varying from 1 m up to 135 m (ELLIOT et al. 1986c). At selected localities, they include intermittent lacustrine sediment horizons as well as thin pahoehoe lava tongues and pillow lavas.

Based on mainly locally restricted field observations, the underlying and only slightly predating volcanogenic rock assemblages including pyroclastic deposits and associated tuffs have been attributed to distinct formations, e.g. the Prebble, the Mawson, the Exposure Hill or the Hanson formations (e.g. ELLIOT et al. 1986b, ELLIOT 1992, 1996, 1999, 2000, ELLIOT & FLEMING 2004). They reach a maximum thickness of a few hundred metres in the central TAM (ELLIOT et al. 1986a, ELLIOT 2000). The importance of these mainly phreatomagmatic rock units as precursors of the flood basalt volcanism is the main focus of several recent investigations (e.g. HANSON & ELLIOT 1996, ELLIOT & HANSON 2001, MCCLINTOCK & WHITE 2006 and references therein). Their appearance and distribution indicate a deposition of the volcanogenic sediments and subsequent magma emplacement into a volcano-tectonically active intra-continental rift environment related to the break-up of Gondwana (KYLE et al.

1981, ELLIOT 1992, ELLIOT & LARSEN 1993). Consistent with an evolving early Jurassic rift zone, the local presence of thin pillow lavas, lacustrine sedimentary interbeds and palaeosols within the extrusive profiles give evidence of a topographically differentiated surface with low-lying, water-rich depressions and furthermore, of a persistent regional subsidence which balanced the accumulation of the flood basalts (BRADSHAW 1987b).

Owing to erosion, which exposed the underlying system of sills and dikes, the lava flow sequences and the associated volcanoclastics are mainly restricted to post-magmatically developed depressions and thus, probably represent the remnants of an originally much larger flood basalt field.

An additional extraordinary feature of the Ferrar LIP is the presence of a layered mafic intrusion, the Dufek-Forrestal intrusion. Located in the Pensacola Mountains just south of the Weddell Sea (Fig. **1.2**), it forms one of the world's largest layered igneous complexes. According to early aeromagnetic and gravity surveys, the areal extension of this intrusion including its sub-glacial continuation was estimated to a minimum of $5 \times 10^4 \ km^2$ (BEHRENDT et al. 1981), which is comparable to the area covered by the Bushveld Complex of South Africa. Based on more recent modelling, the distribution area of the Dufek-Forrestal intrusion was reduced by nearly 80 % to $6.6 \times 10^3 \ km^2$ (FERRIS et al. 1998) and thus, it is rather similar in size to the Stillwater Complex in North America. After FORD & HIMMELBERG (1991), the Dufek-Forrestal intrusion is inter-preted to be generated by a single intrusive event forming an at least 3.5 km thick stratified body mainly composed of olivine-free gabbroic cumulates with minor inter-layers of pyroxenite, anorthosite and magnetite. This mafic cumulate sequence is overlain by several hundred meters of noncumulus granophyre. The unexposed section of the Dufek-Forrestal intrusion was estimated to comprise another 5 km based on geophysical results and petrological considerations including a comparison with other layered intrusions (BEHRENDT et al. 1974, FORD & HIMMELBERG 1991).

Largely unsettled is the question of the role and importance of this gabbro intrusion within the FLIP as a potential magma conduit for the widely distributed Ferrar igneous rocks (MINOR & MUKASA 1997, STOREY & KYLE 1997, ELLIOT et al. 1999).

Age

$^{40}Ar/^{39}Ar$ isotope ages on whole-rock samples or mineral separates from extrusive and intrusive Ferrar rocks are closely similar and demonstrate a brief period of < 1 Ma for the entire magma emplacement at about 177 Ma (FOLAND et al. 1993, HEIMANN et al. 1994, FLEMING et al. 1995, 1997). On the basis of newer baddeleyite and zircon U-Pb ages from sills in the central TAM and southern Victorialand (ENCARNACIÓN et al. 1996) and zircon U-Pb ages from the Dufek intrusion (MINOR & MUKASA 1997) the emplacement age of the Ferrar magmas was revised to ~ 184 Ma, but it was confirmed that igneous activity was confined to a short interval of possibly less than 1 million years. A recalculation of previous Ar isotope dates using the revised age of the neutron flux monitor (RENNE et al. 1994) shows that these ages are within the uncertainty of the mean U-Pb ages (ENCARNACIÓN et al. 1996).

1.3.2   Geochemistry and Models of Magma Origin

All Ferrar tholeiitic rocks belong to the Gondwana low-Ti province (COX 1988) and are characterised by a relatively homogeneous composition. They are geochemically distinct from the tholeiites of other Gondwana-related LIPs like those contemporaneous basaltic rocks exposed in Dronning Maud Land, which are geochemically related to the Karoo province of southern Africa (BREWER et al. 1992). The Ferrar tholeiitic rocks feature unusually elevated initial $^{87}Sr/^{86}Sr$ ratios, low ε_{Nd} values, low TiO_2 concentrations and Ti/Y ratios, generally higher SiO_2 contents and crust-like trace element characteristics, indicated by relatively high abundances of large ion lithophile (LILE) and light rare earth elements (LREE) associated with very low contents of high field strength elements (HFSE) (e.g. KYLE 1980, MENSING et al. 1984, SIDERS & ELLIOT 1985, BREWER et al. 1992, FLEMING et al. 1992, 1995, MOLZAHN et al. 1996). Previous studies on Ferrar rocks have established two different interpretations to explain these anomalous features: (1) magma derivation from a depleted mantle source, followed by extensive contamination of the magmas by assimilation of continental crust (e.g. COMPSTON et al. 1968, FAURE et al. 1974, HOEFS et al. 1980, ANTONINI et al. 1999) or (2) magma derivation from a subcontinental lithospheric mantle that has been enriched by a crustal component during Palaeozoic subduction processes (e.g. KYLE 1980, HERGT et al. 1989, 1991, FLEMING et al. 1992, 1995, MOLZAHN et al. 1996). In short, the discussion has been focussed mainly on the question whether the magma originated from a contaminated mantle source or, alternatively, crustal contamination occurred subsequently during the course of magma transport within the crust. However, the amount of assimilated crustal rocks, as previously stated by e.g. ANTONINI et al. (1999, 2000) to be crucial to explain the crustal signatures, has been confined to 2 – 3 % at most on the basis of Re-Os isotope modelling (MOLZAHN et al. 1996, BRAUNS et al. 2000, HERGT & BRAUNS 2001). This negligible impact of crustal assimilation on Ferrar magma composition is furthermore supported by the general lack of crustal xenoliths within the Ferrar rocks (e.g. MINOR & MUKASA 1997).

Concerning the large volumes and the high magma emplacement rates during the short-lived Ferrar magmatic activity, an elevated mantle temperature has to be assumed for the magma production according to WHITE & MCKENZIE (1989). The other Gondwana associated LIPs are mainly thought to be related to mantle plumes, at least to plume-derived conductive heat transfer to the lithosphere. In contrast, a thermal anomaly required for the large-scale melting event to generate the Ferrar magmas is still a matter of debate, especially due to the assumption of a subduction zone in the west of the Ferrar province at the same time (HERGT et al. 1991, TINGEY 1991, ELLIOT 1992, STOREY et al. 1992a). However, based on geochemical data, an involvement of asthenospheric plume material has not yet been identified clearly (HERGT et al. 1991), which can particularly be attributed to the contamination of the magma source by a crustal component altering the isotope and trace element signatures.

Furthermore, the Ferrar tholeiitic rocks can be subdivided into the compositionally distinct low-Ti and high-Ti magma series, referred to as the Mount Fazio Chemical Type (MFCT) and Scarab Peak Chemical Type (SPCT), respectively (SIDERS & ELLIOT

1985, FLEMING et al. 1992). Of both series, the latter is confined to very few regions scattered along the TAM comprising only a small volume of the known Ferrar occurrences. The majority of high-Ti rocks occur as homogeneous lava flows capping low-Ti lava flow sequences. Aside from some outcrops where the mode of emplacement of high-Ti magma as either a sill or a lava flow is not clearly definable from field relations, very few intrusive occurrences of high-Ti chemistry are known so far within the Theron Mountains and the Whichaway Nunataks in the Weddell Sea region (Fig. **1.2**; BREWER 1989, LEAT et al. 2006). The striking petrographic and geochemical homogeneity and the lack of intrusives within most of the high-Ti occurrences led ELLIOT et al. (1999) to postulate a single region of magma generation and long-distance magma transport within middle to upper crustal levels over thousands of kilometres from the Weddell Sea region to northern Victorialand and Tasmania.

In this context, the Dufek-Forrestal intrusion has an extraordinary position since it is the only layered mafic intrusion (*sensu stricto*) known within the Ferrar LIP. Therefore, it has been considered repeatedly as possible magma conduit for the widespread Ferrar igneous rocks. This assumption is supported by the proximity of this gabbroic intrusion to the Weddell triple junction (MINOR & MUKASA 1997, STOREY & KYLE 1997, FERRIS et al. 2000, ELLIOT & FLEMING 2000, LEAT et al. 2000) and its possible association with the Bouvet mantle plume (e.g. STOREY et al. 2001). A comparable example for the temporal and co-genetic relation between basalt flows and a large mafic intrusion is given by the Proterozoic Muskox Intrusion and the Mackenzie Dike Swarm of Northwest Canada (BARAGAR et al. 1996).

The magnitude of the Ferrar magmatic event is comparable with other magmatic events attributable to mantle plume activity, like e.g. the Karoo province. Since age determinations of Ferrar and Karoo tholeiitic rocks demonstrate an at least partly synchronous magma emplacement for both provinces, the Ferrar and southern Karoo magmatism are suggested to have been related to the same mantle thermal anomaly and rifting event (e.g. ENCARNACIÓN et al. 1996, RILEY & KNIGHT 2001).

However, the presence of compositionally different magma suites is characteristic for a large number of LIPs such as the Gondwana related Paraná-Etendeka and Karoo provinces. Interpretations explaining the generation of distinct magma series within one single plateau basalt province are based on highly variable assumptions. Aside from the suggestion of different magma sources (e.g. GIBSON et al. 1995, PEATE 1997, STOREY et al. 1999) or different degrees and/or conditions during melt generation from a single magma source (e.g. FODOR 1988, ARNDT et al. 1993, HORNIG 1993, HOOPER 1997), a derivation of one magma series from the other by subsequent differentiation (BROTZU et al. 1988) or variable degrees of crustal contamination for the distinct series (SHARMA 1997) have been proposed. Nevertheless, for the Ferrar LIP, neither the generation of the two distinct magma series present nor that of the Ferrar province in general has been satisfactorily explained by now.

1.3.3 Geological History of Northern Victorialand

Northern Victorialand (NVL) is located transitionally between the East Antarctic craton and the Ross Sea at the Pacific end of the Transantarctic Mountains (TAM). It is now widely accepted that the Late Precambrian to Early Palaeozoic basement of NVL can be subdivided into three major tectono-stratigraphic terranes, which were accreted onto the East Antarctic craton during westward-directed subduction within the framework of the Early Palaeozoic Ross Orogeny at about 500 Ma. From the Ross Sea to the craton, these crustal blocks are the Robertson Bay Terrane, the Bowers Terrane and the Wilson Terrane (WEAVER et al. 1984), which are bound by NNW-trending faults (Fig. **1.3**).
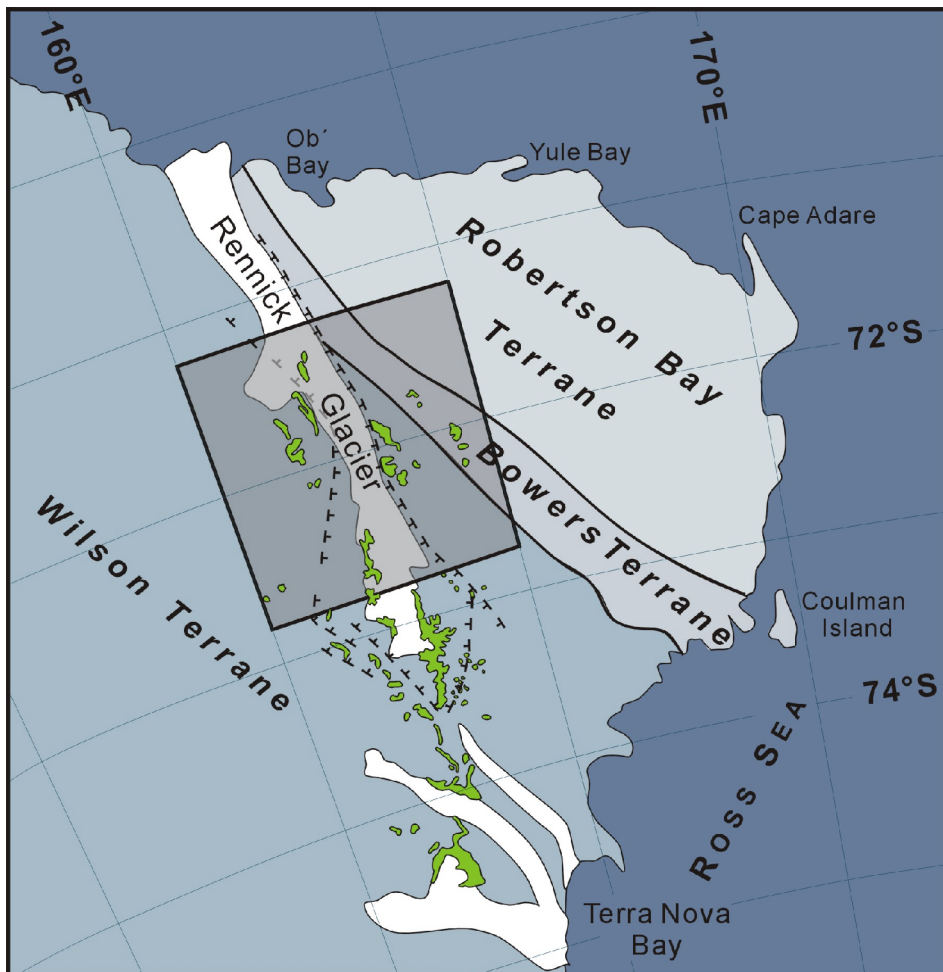
Fig. 1.3 – Schematic map of northern Victorialand illustrating the subdivision into three tectono-stratigraphic terranes at the western margin of the East Antarctic craton and the distribution of the Ferrar rocks (in green). The highlighted field marks the sampling area at the middle Rennick Glacier, which is displayed in detail in figure **3.1**.

The Robertson Bay Terrane comprises the Robertson Bay Group, a more than 2 km thick turbiditic succession of greywackes and mudstones of Late Cambrian to Early Ordovician age (WRIGHT 1981). In the Bowers Terrane, the Bowers Supergroup (BRADSHAW 1987a) is composed of at least 10 km thick Cambrian to Ordovician

volcanic and sedimentary rocks, of which the former show geochemical evidence of a primitive island-arc setting for the early Bowers rocks (WEAVER et al. 1984). While the sedimentary and volcanic rocks within these two terranes experienced a very low-grade to low-grade metamorphism, the Wilson Terrane contains various low- to very high-grade metamorphic rock suites (GREW et al. 1984) including mainly schists, gneisses and migmatites and local high-pressure mafic-ultramafic rocks showing more or less evidence of polyphase deformation.

However, the timing and modes of accretion of the three terranes onto the East Antarctic craton have been discussed controversially. KLEINSCHMIDT & TESSENSOHN (1987) suggested westward dipping subduction zones between all three terranes, which were accreted by a uniformly directed, long-lasting but episodic subduction process during the main phase of the Ross Orogeny (Fig. **1.4**). Contrary, BORG & STUMP (1987) suggested an Early Palaeozoic accretion of the Wilson Terrane against the craton and a post-Devonian accretion of an allochthonous crustal continental block consisting of the Bowers and the Robertson Bay terranes against the Wilson Terrane. Based on fission track data, LISKER (2002) provided further evidence in support of the latter model.

Based on several compilations of petrological, geochronological and structural results, the Wilson Terrane is interpreted to represent the active palaeo-Pacific continental margin of the Precambrian craton affected by the Ross Orogeny (e.g. TALARICO et al. 1995). In this context, ROLAND et al. (2004) proposed to abandon the term Wilson Terrane in favour of the newly suggested Wilson Mobile Belt.
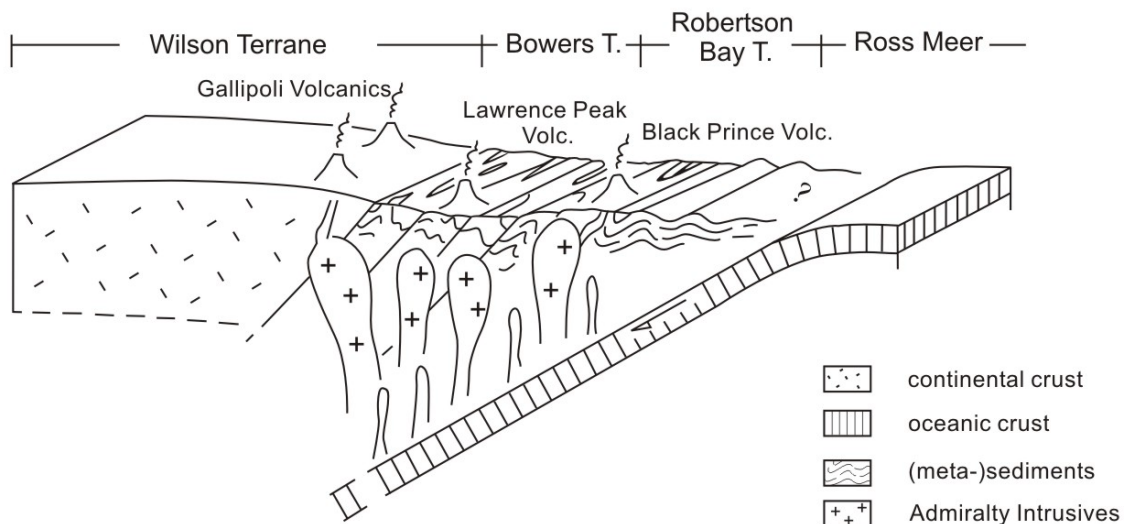
Fig. 1.4 – Schematic cross section through northern Victorialand illustrating the final of three stages of a westward directed subduction-accretion at the Pacific margin of Gondwana at about 360 Ma (post-Ross Orogeny) as proposed by KLEINSCHMIDT & TESSENSOHN (1987).

Besides the regionally distinct metamorphism and the formation of major tectonic structures, the Ross-orogenic subduction/accretion processes were accompanied by

different stages of granitoid plutonism. The Granite Harbour Intrusives, emplaced between 530 and 450 Ma (KREUZER et al. 1981, BORG et al. 1987), are confined to the Wilson Terrane, and both the Robertson Bay and the Bowers terranes were intruded by the Admiralty Intrusives in Devonian time between 390 and 360 Ma (KREUZER et al. 1981, BORG et al. 1987, BORG & DEPAOLO 1991). In addition to the Mid Palaeozoic plutonism, eruptions of mainly silica-rich volcanic rocks took place onto all three terranes at about 320 Ma (BORG 1984) including the Gallipoli, the Lawrence Peak and the Black Prince Volcanics.

In the course of denudation of the Ross Orogen, the metamorphic basement was cut by a Late Palaeozoic erosional unconformity forming the Kukri Peneplain. From the Mid Palaeozoic to the Early Jurassic, the TAM were affected by subsidence forming extensive depositional basin structures along the palaeo-Pacific margin of Gondwana. In these intra-cratonic or foreland basins, the Carboniferous to Triassic generally flat-lying continental sedimentary sequence of the Beacon Supergroup (COLLINSON et al. 1986, 1994, BARRETT 1991) was deposited in the Wilson and the Bowers terranes.

Associated with rifting processes along the TAM in Early Jurassic times (ELLIOT & FLEMING 2000), during Mid Jurassic, Ferrar magmatic activity commenced with the formation of volcanogenic breccias and associated tuffs (e.g. ELLIOT et al. 1986b). The initial phreatomagmatic phases were followed by voluminous extrusion of tholeiitic lava flows with local production of pillow lavas, lacustrine sediments and palaeosols. Contemporaneously with extrusion, numerous sills and dikes were emplaced predominantly within the sedimentary Beacon strata and at few places within the Granite Harbour or Admiralty intrusives. Extensive erosion has since reduced the subaerial lava flow sequences to isolated remnants, which are preserved mainly within post-magmatically developed depressions. Thus, in NVL extrusive profiles are restricted to few regions of limited extension within the interior of the Rennick Graben, namely the Mesa Range and its northernmost outlier Litell Rocks. Much more widespread are sills and dikes exposed at both shoulders of the Rennick depression.

Between 135 and 90 Ma, the Ferrar rocks experienced intense hydrothermal alteration, which has been dated by radiometric methods (FLEMING et al. 1992, 1999, FAURE & MENSING 1993, MOLZAHN et al. 1999) and supported by palaeomagnetic studies (DELISLE & FROMM 1984, 1989). These thermal events were considered to be related to rifting processes preceding the separation of Australia and Antarctica; alternatively, they were discussed by FLEMING et al. (1999) to be induced by hydrologic changes during initial stages of the uplift of the Transantarctic Mountains. Based on apatite fission track data, FITZGERALD & STUMP (1997) have shown that this episodic uplift and denudation history of the TAM was initiated in some sectors in early Cretaceous times at about 125 Ma and finally culminated in a principal phase of large-magnitude uplift of the entire mountain belt occurring in the early Cenozoic at 50 – 45 Ma.

Aside from Cenozoic glacial deposits, the only rocks younger than the Ferrar Group in NVL are Upper Cenozoic alkaline volcanic and plutonic rocks (KYLE 1990).

2   SAMPLE PREPARATION AND ANALYTICAL TECHNIQUES

2.1   SAMPLE PREPARATION

In a first preparation step, as much as possible of weathered crusts were removed from the samples during the sampling in the field in order to reduce secondary contamination of the samples during lab processing. Pieces from the samples were cut for the preparation of thin sections. The samples were sawed and crushed with a diamond saw and a steel jaw crusher, respectively, into pieces of approximately 1 cm in size. After removing sawed surfaces, the sample pieces were powdered in an agate ring-disc mill to a grain size suitable for analysis. Prior to analysis, the powdered samples were dried over night at 105 °C.

The selection of the samples for the mineral chemical and the distinct bulk-rock trace elemental analyses mainly followed from the petrographic results obtained under the microscope and the results of whole-rock major elemental determination by XRF.

2.2   MINERAL CHEMISTRY – ELECTRON MICROPROBE

2.2.1   Motivation

Analyses of the mineral chemistry of primary phases were performed in order to characterise the investigated samples. Thereby, major interest was directed towards compositional variations within single samples (including mineral zonations) as well as variations between the samples, especially between those of the two magma series. These variations will provide insights into the magma's differentiation history, possibly giving evidence of different crystallisation stages. This issue will finally be discussed in close relation to the whole-rock chemical variations. Moreover, the mineral chemical data can be applied to estimate intensive conditions during crystallisation such as temperature and oxygen fugacity by using conventional geothermo- / oxygen-barometers.

2.2.2   Technique

The chemical composition of primary mineral phases was determined by electron microprobe analysis on polished, carbon-coated thin sections using a JEOL JXA-8900 RL Superprobe equipped with five wavelength-dispersive spectrometers (WDS) at the Institut für Geowissenschaften, Universität Tübingen.

The operating conditions for silicate and oxide minerals were an accelerating voltage of 15 kV, a beam current of 15 nA and a focussed beam. In order to avoid fractionation of alkali elements under the electron beam, feldspar was analysed using a slightly defocussed beam width of about 5 µm. Counting times for major and minor elements were 16 s and 30 s, respectively, for peak positions and half the time for background measurement.

Standards for element calibration included both synthetic and natural materials. Instrument drift was monitored by measurement of standard materials prior to and between the mineral analyses. An internal correction of the raw data was applied by the $\varphi - \rho - Z$ routine from JEOL after ARMSTRONG (1991). Fe^{2+} and Fe^{3+} contents in pyroxenes were calculated according to the method of DROOP (1987).

2.3   WHOLE-ROCK CHEMISTRY – X-RAY FLUORESCENCE

2.3.1   Motivation

Since mobile major and trace elements are sensitive to the effects of alteration processes, the whole-rock data will firstly be applied to identify samples which experienced marked secondary modifications. These samples will not be considered in further petrogenetic interpretations.

The whole-rock chemistry will be used for the classification of the studied samples including their attribution to the known magma series and the determination of their magmatic affinities. Furthermore, the variation trends of major and trace elements will give information about the differentiation history. Due to the different partition coefficients of single elements with respect to distinct mineral phases, the phase assemblage, fractionated during differentiation of the Ferrar magma, can be deduced from the compatible or incompatible behaviour of these elements. Additionally, some considerations of the nature of the Ferrar magma source will be given, e.g. by primitive mantle normalised trace element pattern.

2.3.2   Technique

Whole-rock compositions were acquired by the standard wavelength dispersive X-ray fluorescence (WD-XRF) technique. The concentrations of major and trace elements were measured on glass fusion beads and pressed powder discs, respectively, using a Philips PW 2400 XRF spectrometer both at the Institut für Geowissenschaften, Universität Jena, and at the GeoForschungsZentrum (GFZ) Potsdam.

Processing of the raw data was performed by standard SuperQ software of Philips. Element (and instrument) calibration was done using international geochemical reference material. Additional rock standards were measured along with the samples for quality control.

For samples analysed in Jena, volatile contents were determined as loss on ignition (LOI) by placing crucibles filled with ~1.5 g dried sample powder into a muffle furnace and holding them for two hours at 900°C. Afterwards, the LOI is calculated as relative weight difference. The glass discs for major element analysis were made of a well-homogenised mixture of 0.4 g of the annealed sample powder and 4 g of lithium-tetraborate (Spectromelt A12, Fa. MERCK) fused in platinum crucibles using a high-frequency induction fusion furnace (Lifumat 1.2-Table Ox). The pressed powder pellets were prepared of 6 g of sample powder and 1 g of Hoechst wax C1 as binding agent pressed in an aluminium cap under ~130 kN.

At the GFZ Potsdam, the glass discs for determination of major elements and selected trace elements by XRF analysis were prepared of 1 g dried sample powder and 6 g Spectromelt. H_2O and CO_2 contents were measured by a LECO RC-412-Analyser. Additionally, the ferrous and ferric iron contents, not distinguishable by XRF analysis, were determined by $KMnO_4$ titration after sample digestion in $HF-H_2SO_4$.

Because of interlaboratory biases, all major element analyses are given recalculated on a volatile-free basis including total iron recalculated as $FeO_{(T)}$ [wt%].

2.4   RARE EARTH ELEMENTS – INDUCTIVELY COUPLED PLASMA – ATOMIC EMISSION SPECTROMETRY

2.4.1   Motivation

Since the group of the rare earth elements (REE) comprises widely incompatible elements with regard to most minerals, it is a useful tool to evaluate a number of petrological processes. However, for the individual REE, markedly different distribution coefficients with respect to distinct mineral phases, especially phases that are stable under mantle conditions, have been determined. Thus, rare earth element ratios and chondrite-normalised REE patterns can be applied to constrain differences in the degree of partial melting for magmatic rock series as well as the mineralogical and chemical composition of their melting sources and hence the depth of melt generation. Besides that, REE variations allow to asses the influence of fractional crystallisation on the magma composition.

2.4.2   Technique

To gain whole-rock rare earth element abundances of a subset of 10 samples, sample selection was designed to exclude altered samples and to span the range of observed compositional variations based on their appearance under the microscope as well as their major and trace element chemistry. REE and Y concentrations were analysed by a Varian Liberty 200 inductively coupled plasma – atomic emission spectrometer (ICP-AES) at the GeoForschungsZentrum Potsdam. The sample preparation and the determination of the REE followed the procedures outlined by ZULEGER & ERZINGER (1988).

The wet-chemical sample preparation was based on Na_2O_2-sinter dissolution of 1 g of dried sample powder. After the complete dissolution of the silicate material, the separation of the REE out of this solution was performed by ion-exchange chromatography using ion-exchange columns filled with an ion-exchange resin (Dowex 50 WX8). After subsequent filtering and evaporation procedures, the final REE-enriched residues were dissolved with 10 % HCl and stored in PE-bottles until measurement by ICP-AES. Further analytical details concerning the recovery of the REE and Y after the ion-exchange procedure or principal problems of spectral interferences during the element measurement by ICP-AES are discussed by ZULEGER & ERZINGER (1988). Based on replicate analyses of international reference samples, the reported precision of element

concentrations obtained by the described method is about 5 % for all elements, except for Pr (10 %).

2.5   PLATINUM-GROUP ELEMENTS – NIS FIRE-ASSAY AND INDUCTIVELY COUPLED PLASMA - MASS SPECTROSCOPY

2.5.1   Motivation

Even though in the last decades the application of platinum-group elements (PGE) experienced increasing importance for geochemical studies, their behaviour during most petrogenetic processes is not yet completely understood. Thus, a short introduction into their basic characteristics is given before the intentions to analyse the PGE in the studied suite of Ferrar samples will be addressed.

Platinum-group elements comprise a group of coherent siderophile elements, which have been enriched together with Fe and Ni in the earth's core due to its separation from the mantle during the early differentiation of the earth. Therefore, the earth's mantle should generally by depleted in PGE when compared to bulk earth showing so-called chondritic concentrations of these elements. Nevertheless, numerous mantle rocks have been analysed showing higher, non-chondritic concentrations of PGE than would be expected if the mantle were in chemical equilibrium with the core (e.g. PATTOU et al. 1996, REHKÄMPER et al. 1999a). In order to explain the increased PGE concentrations of the earth's mantle, KIMURA et al. (1974) established the model of an introduction of these elements by a meteorite impact referred to as "late veneer" hypothesis during the early earth's history after the core-mantle separation. This hypothesis is supported by some experimental investigations from HOLZHEID et al. (2000). Furthermore, a PGE transfer from the core to the mantle at the core-mantle boundary (SNOW & SCHMIDT 1998), a secondary influx of PGE-bearing sulphides via metasomatism in the upper mantle (ALARD et al. 2000) and partial melting processes within the earth's mantle (REHKÄMPER 2000) are discussed controversially as being responsible for the non-chondritic PGE abundances in mantle rocks.

However, in the crust and the mantle, PGE are generally present at very low trace element concentration levels (ppt to ppb). Rocks with elevated PGE abundances are often related to Cu and Ni bearing deposits generally associated with mafic and ultramafic rocks (e.g. the Sudbury, the Bushveld or the Stillwater complexes). The petrogenesis of such igneous ore deposits has often been reported to require differentiation processes of mantle-derived magmas at crustal levels, whereby conditions are met at which PGE-containing phases crystallise and accumulate in distinct horizons of such intrusive complexes. Additionally, secondary redistribution of some of the PGE within the igneous body due to post-magmatic processes (e.g. hydrothermal alteration) may play an important role.

Therefore, besides their economic importance, PGE are valuable geochemical tools to investigate petrogenetic processes within the earth's mantle and crust as well as processes during the formation of the earth. In order to understand the behaviour of the PGE during these processes, a comprehensive knowledge of the fundamental physico-chemical features of these highly siderophile elements is of great importance. In spite

of their similar chemical affinities, they can be subdivided into two subgroups: the Ir-group (IPGE: Os, Ir, Ru) with higher melting points than the Pt-group (PPGE: Rh, Pt, Pd) (BARNES et al. 1985). This classification reflects the geochemically distinct behaviour of both subgroups during melt generation and subsequent magma evolution resulting in a fractionation of the individual PGE from each other. This fractionation of the IPGE from the PPGE is often attributed to the segregation of early crystallising mineral phases like olivine and chromite, which enclose micro-inclusions of IPGE-bearing phases such as alloys (e.g. BARNES et al. 1985, KEAYS 1995). In contrast to the mostly compatible behaviour of the IPGE, the PPGE behave rather as incompatible elements during partial melting and differentiation processes.

In this context, significantly differing partition coefficients have been determined experimentally for the individual noble metal elements with respect to distinct mineral phases (e.g. PEACH et al. 1990, 1994, FLEET & STONE 1991, FLEET et al. 1991, 1993, 1996, BEZMEN et al. 1994, CAPOBIANCO et al. 1994, LI et al. 1996). The obtained diversity of partition coefficients for single PGE can partly be related to the strongly varying conditions of the numerous experiments (BARNES & MAIER 1999). However, major phases incorporating PGE are metal alloys, monosulphide solid solutions (mss), sulphides and oxides. Despite their primarily siderophile nature, sulphides are often described as containing the main portion of Pt and Pd besides metal alloys. The fractionation of sulphides strongly depends on the sulphur saturation of the magma, which is controlled by different factors such as the composition of the magma source, the degree of partial melting, the differentiation process and/or the pressure during melting and differentiation.

In the last decades, a considerable knowledge of the geochemical behaviour of PGE during the formation of layered mafic intrusions has been compiled within the scope of the exploration of mineral deposits. In contrast, there are only a few PGE studies on small-scale sheet-like intrusions, and thus detailed investigations of the fractionation behaviour of this element group at upper crustal conditions, as prevailing in these mostly surface-near intrusions, are of increasing importance.

Furthermore, until recently PGE characteristics of basaltic rock suites were suggested to be powerful petrogenetic indicators to distinguish lower and upper mantle reservoirs. For the Ferrar province, only very few PGE analyses have been previously reported from the Dufek layered mafic intrusion (FORD & HIMMELBERG 1991), but no systematic investigations of the PGE behaviour in Ferrar rocks have been carried out so far. Thus, the basic interest of analysing the PGE within Ferrar rocks was directed towards the identification of a contribution of asthenospheric mantle since the thermal source for the generation of the huge amounts of melt is still under debate as it is obscured by the crust-like trace element and isotope data. However, at first the PGE behaviour during differentiation processes will be considered in order to distinguish between the PGE signatures being discussed with respect to magma source aspects and those that reflect modifications during subsequent magma evolution.

2.5.2 Technique

In addition to the mineral and bulk-rock chemical characterisation of the Ferrar samples, a subset of 24 intrusive samples was selected for analyses of their PGE abundances based on the results from previous analyses with the purpose of excluding altered material and of completely comprising the compositional variations displayed by samples of both magma series.

The samples were analysed for the platinum-group elements Ir, Ru, Rh, Pt and Pd at the Institut für Mineralogie und Geochemie, Universität Karlsruhe. The preparation of the sample material for ICP-MS measurement of the PGE was performed by nickel sulphide fire-assay. This is a well-known PGE pre-concentration technique for analysis of materials with very low-level concentrations of PGE using nickel sulphides as PGE collectors (e.g. JACKSON et al. 1990, OGURI et al. 1999).

For the fire-assay, 30 g of dried sample powder were weighed into fireclay crucibles filled with ¾ of a thoroughly stirred mixture composed of 100 g sodium tetraborate, 30 g sodium carbonate, 7.5 g of sulphur (sublimated), 25 g pure silica and 10 g nickel (99.99 %). The use of a large sample portion (30 g) minimises a possible nugget effect. Before covering the sample material with the residual ¼ of the flux mixture, 500 µl of a specially prepared multi-element spike solution were added. This solution contains the isotopes ^{99}Ru, ^{191}Ir, ^{105}Pd and ^{198}Pt in order to determine the PGE concentrations within the samples using the isotope dilution method during ICP-MS measurement (e.g. YI & MASUDA 1996).

After complete fusion of the sample charges in a muffle furnace at 1140 °C for 1 hour, the melt was allowed to cool down to room temperature within an iron mould. During subsequent cooling, the PGE partition into sulphides and/or alloys forming a NiS bead, which is separated easily from the silicate matrix after cooling.

Afterwards, the mechanically crushed NiS bead was dissolved in 400 ml hydrochloric acid (36 %) in a water quench at 90 °C for 12 hours. After complete digestion special attention had to be paid to avoid PGE loss by further dissolution of the PGE compounds. The solution containing the PGE as finely dispersed particles was filtered through a PTFE-filter under vacuum. The filtrate was washed with 1M HCl, dissolved in 50 ml 12 M HCl and 10 ml H_2O_2 together with the PTFE filter. The obtained solution was then filtered through a paper filter and washed again with 1 M HCl. The residue was evaporated to a volume of ~ 2 – 3 ml and finally diluted with 1 % HNO_3. The solutions are transferred into 10 ml PE-bottles and stored in a fridge until analysis by ICP-MS.

The prepared sample solutions were measured by high-resolution ICP-MS using an AXIOM VG Elemental mass spectrometer. Measurement calibration was performed by analysing freshly prepared multi-element standard solutions with concentrations varying between 0 and 200 ppb PGE. They were made of a stock solution before running the batch of samples for analyses. To adjust instrumental drift, the isotopes ^{115}In and ^{169}Tm were added to these standard solutions as internal standards. Selected standard solutions with concentrations comparable to those expected in the samples were analysed repeatedly between the sample analyses. Possible interferences with

some oxides and Ar clusters were corrected if necessary. Element concentrations were finally calculated using the isotope ratios $^{99}Ru/^{101}Ru$, $^{99}Ru/^{102}Ru$, $^{105}Pd/^{106}Pd$, $^{105}Pd/^{108}Pd$, $^{105}Pd/^{110}Pd$, $^{191}Ir/^{193}Ir$, $^{195}Pt/^{198}Pt$ and $^{196}Pt/^{198}Pt$. ^{103}Rh was determined from the calibration curve of the standard solutions.

Lower limits of detection were calculated for each element from the average of blank reagents plus 3σ above background. Blanks were prepared and analysed in the same way as the sample materials. In the majority of the samples, the PGE concentrations are above the detection limits for all elements except for Ir, Ru and Rh in some of the more evolved samples with very low MgO contents. The detection limits for Ir, Ru, Rh, Pt and Pd are 0.1, 0.2, 0.1, 0.5 and 0.5 ppb, respectively.

For checking the accuracy and precision of the method, replicate analysis of arbitrary selected samples and an in-house reference standard material treated together with every charge of samples during the NiS fire-assay and during the PGE separation afterwards have been performed. Since standard matrices should be similar to the material being analysed, an ODP standard with PGE concentrations comparable to those expected for the Ferrar samples was chosen as reference material. However, due to the relative small number of samples analysed and thus a very small number of analyses of the in-house reference standard, the accuracy and precision of the analytical procedure is given as reported in previous PGE studies of comparable rock materials. These samples have been prepared and analysed using the same technique and equipment at the Institut für Mineralogie und Geochemie in Karlsruhe. Within the scope of two Ph.D. theses, PHILIPP (1999) and SCHEIBNER (2003) emphasised the reliability of the obtained PGE concentrations giving an accuracy of analysis within 3 to 12 % for Ir, Rh, Pt and Pd and 20 % for Rh, and a precision of the method of 15 % at most.

3   RESULTS AND INTERPRETATION

The following chapter introductorily describes the field relations and the petrographic characteristics of the sampled Ferrar igneous rock occurrences. Afterwards, the results from analyses of the modal mineral chemistry and the whole-rock chemistry are presented including major, trace and rare earth elements as well as platinum-group elements. Short summaries are given after the mineral and the whole-rock geochemical analyses including the estimation of temperatures and oxygen fugacities prevailing during magma crystallisation as well as preliminary conclusions.

3.1   FIELD RELATIONS AND PETROGRAPHY

3.1.1 Field Relations

The studied area encompasses the region around the middle Rennick Glacier in NVL and few sites in George V Land (Fig. **1.2**). In NVL, about 60 samples from intrusive and extrusive Ferrar occurrences within the Wilson and Bowers terranes were taken within a three-week field campaign during the first leg of the joint German-Italian Antarctic Expedition 1999/2000. The sample locations are illustrated in figure **3.1**. Access to the outcrops was supported by helicopter transport. The sampled sites comprise both, already known but unsampled and a few previously unmapped (unknown?) outcrops of Ferrar igneous rocks. For analytical comparison, reference samples were taken at some localities previously investigated during earlier expeditions. Supplementary sample material from George V Land was provided by N.W. Roland (BGR Hannover) taken during the second leg of the expedition. It extends the investigated area by some hundred kilometres to the west.

A more detailed list of all samples is given in the appendix **1** including GPS data for the exact positions and, if sufficiently indicated by the field relations, with some remarks on the mode of magma emplacement.

Low-Ti Series – Intrusives

Intrusive low-Ti rocks occur predominantly as flat-lying sills and rarely as dikes, which mainly intruded the Beacon sediments (Fig. **3.2**). Minor intrusions are found within the Palaeozoic granitoids close to unconformity between basement rock units and the Beacon sediments. In NVL, Ferrar intrusives are widespread on the western and eastern shoulder of the Rennick Graben structure. In the West, they were sampled in the Outback Nunataks, Helliwell Hills and Morozumi Range; in the East, samples were taken in the Lanterman Range, Alamein Range, Freyberg Mountains, Salamander Range, Neall Massif and Crown Hills.

The sills exhibit existent thicknesses varying between several tens and a few hundreds of metres. Lower contacts are often covered by debris; upper contacts are mostly removed by erosion. Near the contacts, sills frequently enclose various-sized rafts of Beacon sediments. Within the sills, cooling patterns vary with proximity to the chilled margins, with a rather compact appearance near the contacts grading into platy

fracturing, followed by regular columnar jointing towards the centre of the sills. Except for the slightly porphyritic rocks near the contacts, all samples appear aphyric in hand specimen. The crystal size of the dense, middle to dark grey rocks rapidly increases with distance from the aphanitic chilled contacts. For all rocks, aside from the chilled margins, signs of weathering are noticeable by rusty red surfaces, but internally most of the samples appear to be fresh.
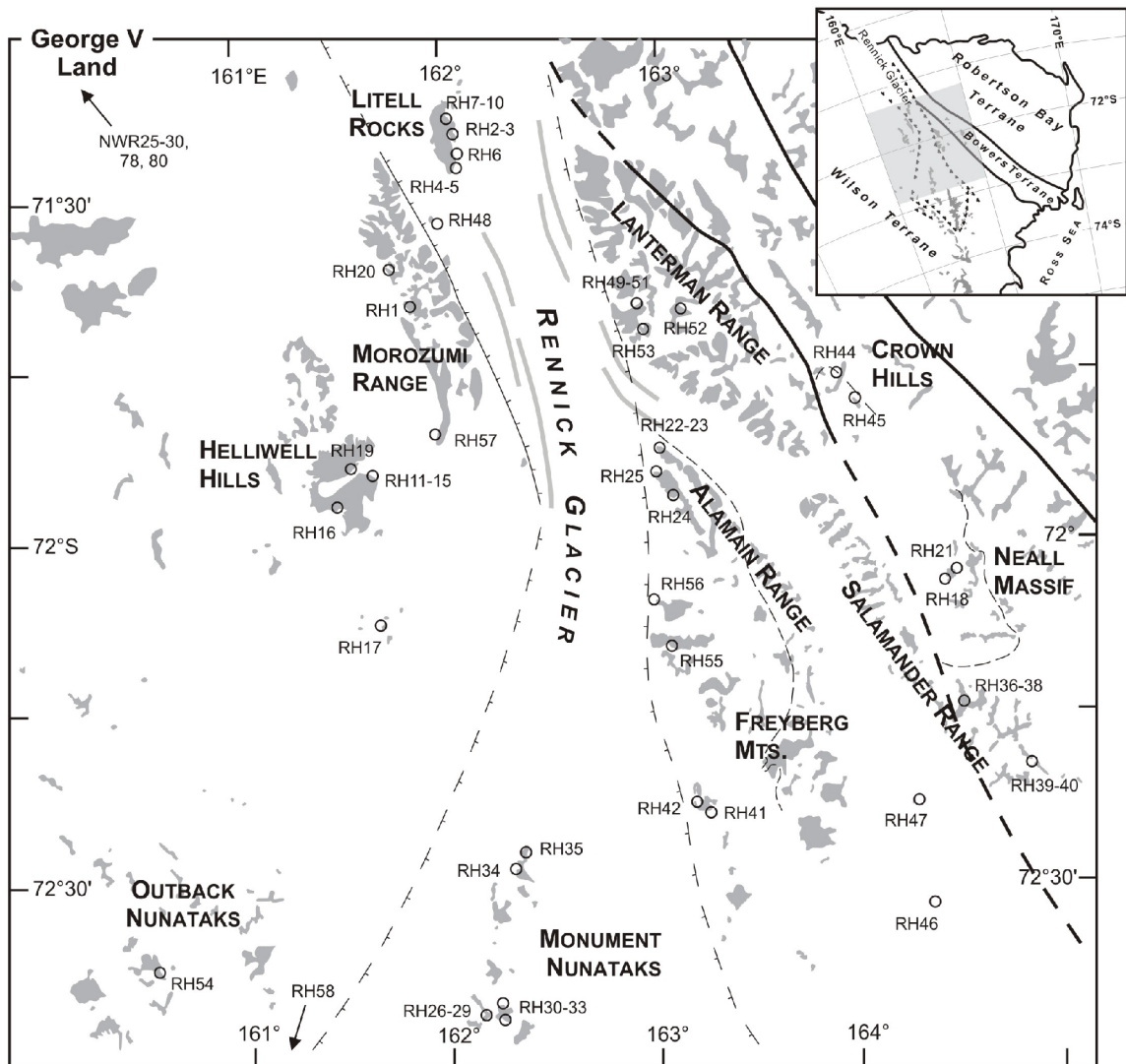
Fig. 3.1 - Sketch map showing the sampling sites of Ferrar magmatic rocks along the middle Rennick Glacier in northern Victorialand. The investigated area covers a SW-NE trending belt crossing the Rennick Graben structure and the boundary between the Wilson and the Bowers terranes, represented by the Lanterman Fault. Original map modified after GANOVEX-TEAM (1987).

Samples from sills were taken at different outcrop heights depending on accessibility, but no systematic sampling throughout single intrusions was performed. Samples, in the following referred to as 'chilled margins', do not represent the direct contacts with country rocks. They were sampled within the first few decimetres or metres from the

contact and still show typical chilled margin characteristics like being aphanitic or very fine-crystalline. The direct contacts were avoided, since they may be influenced by secondary alteration, possibly due to increased fluid migration. Furthermore, contamination due to fusion with country rocks cannot be excluded there.

Fig. 3.2 – View to the East on Mt. Engel in the Unconformity Valley, Morozumi Range (NVL). The exposure exhibits the typical profile observed in the sampling area: The metamorphic basement (lower part to the left) is overlain unconformably by light-coloured Beacon sediments followed by an approximately 100 m thick Ferrar sill showing marked columnar jointing.

At some localities, where no contacts with country rocks are exposed, no clear evidence exists for an intrusive or extrusive mode of magma emplacement. However, the appearance of the vesicle-free rocks and their cooling patterns compared to clearly identified intrusions led to an interpretation as sills (or dikes) for all sampled outcrops outside the Rennick Graben.

A few dikes, with maximum thicknesses of 5 m, were found within flat-lying Beacon sediments in the Neall Massif within the Bowers Terrane. The strike direction of these dikes is approximately NE-SW. This widely corresponds to dike directions mentioned by WILSON (1993), who investigated orientation patterns of fault arrays and Jurassic igneous dike swarms from southern Victoria Land in the Transantarctic Mountains.

Samples from George V Land were collected at Horn Bluff, Anxiety Nunataks and SCAR Bluff. Field relations indicate that these northernmost Antarctic Ferrar rocks have an intrusive origin. HORNIG (1993) described the columnar jointing of the medium- to coarse-crystalline, vesicle-free rocks of these nunataks. Some of the samples are

exceptionally coarse-crystalline with crystal sizes up to 1 cm in length. They probably represent the core of a massive sill intrusion.

Low-Ti Series – Extrusives

Extrusive occurrences were investigated at Litell Rocks and about 130 km to the south in the Monument Nunataks (Fig. **3.1**). The latter represent the northernmost part of a group of widespread mesas called the Mesa Range. Located within the Rennick Glacier, these sequences of numerous Ferrar lava flows are preserved as erosional remnants due to post-Jurassic subsidence of the Rennick Graben structure.

For the Monument Nunataks, the exposed total stratigraphic thicknesses of subaerial flow sequences can be estimated to be at least 600 m with strongly varying single lava flow thicknesses. In the Mesa Range, a few kilometres southward, they range from less than 1 m to as much as 135 m (ELLIOT et al. 1986c). Within the single lava flows, crystallinity increases with distance from the basis and the top of the flows, even though not as pronounced as in the sills due to the faster subaerial cooling. However, thicker flows are described by SIDERS & ELLIOT (1985) to reach internally a coarse crystallinity giving the dark grey rocks a diabasic appearance, which makes them nearly indistinguishable from their intrusive counterparts. Typical features of the lava flows are the amygdaloidal contacts with abundant zeolites, quartz and calcite as vesicle fillings. Very thin flows are vesicular throughout. Depending on flow thicknesses, an irregular to regular columnar jointing is developed. Samples were taken at few localities from several lava flows at different topographic heights between 1750 and 2300 m in order to check possible spatial and temporal variations of composition.

The Ferrar units from Litell Rocks were described in detail by SKINNER et al. (1981), HORNIG (1993) and others. In the south-eastern part of this low-lying outcrop, at the Mandel Cliffs, a sequence of five strongly altered low-Ti lava flows is exposed reaching a total thickness of a few decametres. It is overlain by a black high-Ti unit (see below). The massive interiors of the dark grey to greenish low-Ti lava flows exhibit a more or less regular columnar jointing. The vesicular contacts of the single flows are most intensely altered. Vesicle fillings predominantly include quartz, prehnite, chalcedony and calcite, but no zeolites. Reference samples were taken from less altered parts of these low-Ti lavas for analytical comparison with published data as well as for comparison to the lava flows from the Monument Nunataks.

High-Ti Series

From within NVL, the rare occurrences of high-Ti Ferrar rocks are mainly reported to be of extrusive origin. SIDERS & ELLIOT (1985) described black high-Ti lava flows from the Mesa Range (Fig. **1.2**) occurring as capping units of the low-Ti lava flow sequences. On top of some of the Monument Nunataks, a few kilometres north of the Mesa Range, these lava flows could be observed, but were not sampled due to difficult access.

At Litell Rocks, comparable lava flows of high-Ti chemistry cover the low-Ti lava flows in the SE at the Mandel Cliffs. SKINNER et al. (1981) described them as dense, finely crystalline basalt flows including pillow structures. Samples were taken a few

kilometres north of the Mandel Cliffs and additionally, from the topographically higher, northeastern parts of Litell Rocks. The exposed black, fine- to medium-crystalline, aphyric rocks exhibit a sharp-edged platy fracturing and do not include amygdales like the low-Ti extrusives from the SE of Litell Rocks. In contrast to the latter, the occurrences in the NE were interpreted as sill and dike intrusions by SKINNER et al. (1981). No contacts with country rocks were observed. Thus, due to the lack of any distinctive feature that allows the characterisation of the mode of magma emplacement, these high-Ti occurrences will be referred to as "high-Ti unit" following WILHELM & WÖRNER (1996), who described a similar unit from the Prince Albert Mountains in southern Victorialand.

One additional high-Ti occurrence was localised in the Alamein Range in the north-western Freyberg Mountains on the eastern rift shoulder of the Rennick Graben. The dark-coloured, medium to coarse-crystalline and vesicle-free sample taken near the top of the outcrop (~ 1850 m a.s.l.) is nearly indistinguishable from the intrusive low-Ti samples by its appearance in the field. The lower contact is covered by ice and the surface is eroded. However, due to its comparability to other clearly identified sills and due to the presence of light-coloured Beacon sediment strata below the Ferrar sills exposed at the north-eastern flank of this mountain range, it was identified as being of intrusive origin. However, this occurrence is different from the commonly flat-lying sills of low-Ti chemistry, because its rather platy cooling cleavage is inclined at ~ 40° to approximately west. The field relations indicate this occurrence to be a sill tilted towards the centre of the Rennick depression, which is likely to be related to the block-faulting tectonics described by LÄUFER & ROSSETTI (2001). The position of this occurrence outside the Rennick Graben furthermore supports its intrusive origin since extrusives are commonly restricted to the graben interior.

3.1.2 Petrography

All investigated Ferrar rocks feature the common tholeiitic mineral assemblage composed of varying amounts of pyroxenes, plagioclase, oxide phases and mesostasis. Estimations of the mineral modes are obtained from thin section analysis using traditional point counting techniques. They are listed in the appendix **2**. The entire suite of samples exhibits a broad variation in texture and composition according to thickness of the occurrence, cooling mode and sampling position within the vertical profile.

Low-Ti Series – Intrusives

Chilled margins of low-Ti sills and dikes are aphanitic to fine-crystalline and predominantly aphyric to weakly phyric. Phenocrysts of orthopyroxene and plagioclase, altogether making up almost 10 vol%, are set in a matrix consisting of plagioclase needles, granular clinopyroxene, and minor glass, arranged to form intersertal to intergranular rock fabrics. Some phenocrysts occur as glomerocryst clusters. Euhedral orthopyroxene is often replaced by greenish secondary minerals, and some slightly corroded crystals are rimmed by pigeonite or augite. Plagioclase exhibits twinning and

zonation of the tabular, euhedral to subhedral crystals. Opaques occur very finely dispersed in the groundmass in most of the samples. Glassy matrix often includes quenched crystals of opaques and pyroxene.

Towards the centre of the sills, the crystal size rapidly increases, involving a gradual textural transition from subophitic to ophitic intergrowths of euhedral plagioclase laths and granular pyroxene. Most samples from George V Land are unusually coarse-crystalline and contain anhedral, poikilitic pyroxene up to 1 cm in diameter enclosing plenty of plagioclase laths. In general, the modal abundance of the hypo- to micro-crystalline mesostasis varies between 6 and 39 vol% and comprises microphenocrysts of plagioclase, pyroxene, and opaques. In coarse-crystalline samples, granophyric intergrowths of low-birefringent cryptocrystalline material (alkali feldspar and silica) and patches of brown glass including skeletal opaques are common in the mesostasis.

The proportions of pyroxenes, plagioclase and the interstitial mesostasis suggest a correlation with the sample positions within the sills. Samples from lower parts include subhedral to anhedral orthopyroxene up to 13 vol%, subhedral crystals are again often surrounded by pigeonite or augite. Clinopyroxenes together vary between 22 and 51 vol%, whereby pigeonite dominates over augite if orthopyroxene is present. One sample contains 51 vol% pigeonite, minor orthopyroxene (inverted pigeonite) and no augite. In general, the abundance of low-Ca pyroxenes decreases with increasing amounts of high-Ca clinopyroxene and increasing granophyric quartzo-feldspathic intergrowths in the mesostasis, typical for samples from higher sections of sills. Plagioclase, varying from 31 to 44 vol%, mostly displays core-to-rim zoning.

Exsolution features are common within pyroxenes: low-Ca pyroxene often includes abundant 'granules' of augite; simply twinned inverted pigeonite with fine-scale augitic lamellae shows the typical herring-bone pattern. In contrast to observations by HORNIG (1993), phenocrysts of primary orthopyroxene are still preserved in some intrusive samples.

Apart from disseminated micro-crystalline opaques in the groundmass, Fe-Ti oxides are common in nearly all samples as euhedral or corroded crystals with modal contents up to 2 vol%. In more evolved samples, they increase in both crystal size and modal abundance (up to 4 vol%), often exhibiting magnetite-ilmenite exsolution lamellae.

Signs of alteration are patches of secondary phases (sheet silicates) replacing the mesostasis and to a certain degree the primary mineral phases, e.g. orthopyroxene crystals in chilled margin samples.

Low-Ti Series – Extrusives

In terms of mineral assemblage and texture, the examined finely to medium-crystalline extrusive low-Ti rocks are largely comparable to their intrusive equivalents. As for the intrusives, compositional variations according to the flow thicknesses are common.

All samples taken from these lava flows are characterised by a profound secondary alteration. The alteration products replace greater amounts of the mesostasis and primary minerals and occur furthermore as abundant vesicle fillings, together reaching up to about 35 vol%.

By comparison, the extrusives from the Monument Nunataks and from Litell Rocks show apparent differences in their assemblages of the secondary phases. The samples from the Monument Nunataks contain several zeolites, amorphous silica, calcite, chlorite, smectite, and chlorite-smectite-mixed-layered minerals filling amygdales and cavities and occurring as irregular patches replacing the groundmass. At Litell Rocks, the alteration assemblage in filled vesicles and cavities comprises mainly quartz, aggregates of prehnite, amorphous silica, chlorite, minor pumpellyite, and epidote. Neither zeolites were found nor have they been described in literature for Litell Rocks. These differences in the secondary mineral assemblage are interpreted to reflect distinct conditions during the secondary alteration. The reasons for this finding will be discussed later.

High-Ti Series

A characteristic feature of the investigated aphyric high-Ti samples from Litell Rocks is their overall-homogeneous appearance. These fine- to medium-crystalline rocks exhibit a hypo- to microcrystalline mesostasis. The major constituents, microphenocrysts of pyroxene, plagioclase and oxides, build up an intersertal to intergranular texture. Sample RH24 from the Alamein Range contains the same phenocryst phases, but is exceptional for its coarse crystallinity. At first glance, it is not distinguishable from the coarser low-Ti intrusive samples.

The amount of mesostasis (34 – 45 vol%) slightly exceeds that of most low-Ti samples. The mesostasis consists predominantly of brown glass with radiating intergrowths or cryptocrystalline patches of silica and alkali feldspar, which contain quench crystalline pyroxene and skeletal opaques. In sample RH24, thin needles of silica with an aspect ratio > 50 are common in the mesostasis. The high amounts of primary glassy mesostasis, the fine crystallinity and the quenched and skeletal growth of microphenocrysts in the high-Ti rocks from Litell Rocks indicate a rapid cooling of the magma. This could be indicative for a rather extrusive than intrusive emplacement of these magmas.

In general, all samples exhibit comparable contents in the major constituents plagioclase (25 – 32 vol%) and pyroxene (23 – 29 vol%). Pyroxene includes both augite and pigeonite, with generally higher modal contents of augite than pigeonite. In contrast to the description by Hornig (1993), (1) no orthopyroxene has been identified in any of the high-Ti samples, and (2) up to 6 – 8 vol% of oxides occur in euhedral to subhedral crystals often showing typical exsolution lamellae. Abundant opaques, finely dispersed in the mesostasis, could not be distinguished quantitatively. The high abundances of mesostasis and oxide minerals and the lack of orthopyroxene in high-Ti samples are the most distinctive attributes compared to low-Ti samples.

Secondary mineralisations partly replace the major phases as well as the mesostasis. They comprise sheet silicates present as aggregates of smectite and chlorite in the matrix, sericite in plagioclase and titanite around the oxide phases.

## 3.2	MINERAL CHEMISTRY

For electron microprobe analysis of the primary mineral phases (plagioclase, pyroxene, oxides), the samples were chosen based on the texture and bulk-rock composition in order to comprise the range of the observed petrographic and geochemical variations. Due to the considerable alteration of the extrusives, as determined under the microscope, only samples from intrusive occurrences were taken. Additionally, microprobe data published by other workers (e.g. HABAN & ELLIOT 1986, HORNIG 1993) indicated comparable mineral composition for intrusive and extrusive rocks. Representative chemical analyses of pyroxenes, plagioclase and oxide phases are listed in the appendix **3a**, **3b** and **3c**, respectively.

### 3.2.1	Pyroxenes

Pyroxenes in Ferrar igneous rocks have been analysed as Ca-Mg-Fe pyroxenes, which lack appreciable non-quadrilateral components in the diopside-enstatite-ferrosilite-hedenbergite system. Thus, the pyroxene end-member compositions have been recalculated into enstatite (En), ferrosilite (Fs) and wollastonite (Wo) components given in mole fractions [mol%].

Pyroxene in the analysed Ferrar samples is composed of low-Ca members (ortho-pyroxene – opx, pigeonite – pig), high-Ca members (augite – aug) and 'subcalcic' augitic pyroxenes. They exhibit a very wide compositional range documented by core-to-rim zonations of single crystals as well as large differences between different samples. In the pyroxene quadrilateral (Fig. **3.3**), these compositional variations of low-Ca and high-Ca pyroxenes indicate systematic trends of steadily decreasing MgO in favour of the FeO content in samples of both the low-Ti and the high-Ti series. Concomitant with this iron-enrichment trend, CaO generally decreases in augites and slightly increases in pigeonite, but late-stage Ca-enrichment in augite is observed as well.

These chemical variation trends of low-Ca and high-Ca pyroxenes within the suite of analysed Ferrar samples are similar to those, which are characteristic of differentiated tholeiitic magmas. Hence, they are compared with pyroxenes of the Skaergaard layered intrusion, Greenland (BROWN & VINCENT 1963), the Bushveld Complex, South Africa (ATKINS 1969) as well as those of the Dufek Intrusion (HIMMELBERG & FORD 1976), which all indicate significant enrichment in iron during magmatic evolution (Fig. **3.4**). Even the generally observed late-stage Ca-enrichment of augite is shown by very few highly evolved augites from the analysed Ferrar low- and high-Ti samples.

By comparison, pyroxenes in the high-Ti rocks show similar evolution trends like the low-Ti rocks, but at somewhat more evolved, iron-enriched composition. Below, the variations of low-Ca and high-Ca pyroxenes as well as some subcalcic augites in the analysed Ferrar rock samples are described in more detail.
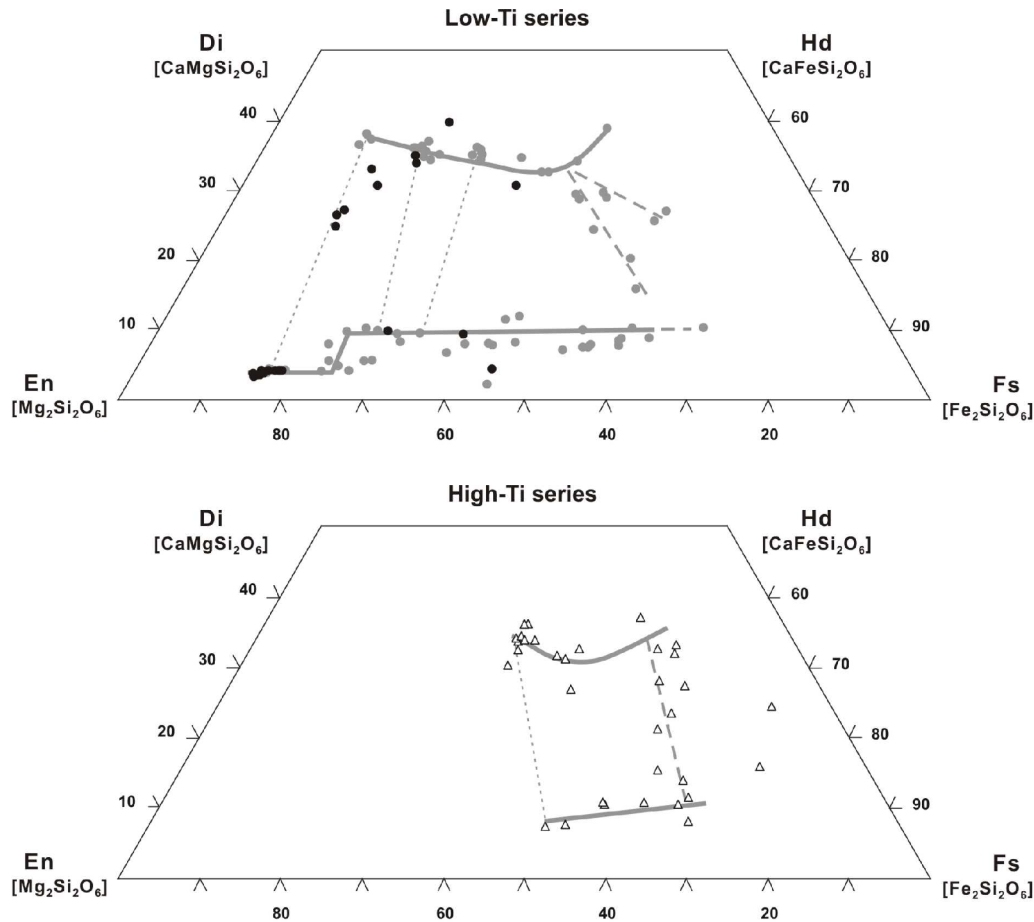
Fig. 3.3 – Compositional variations of pyroxenes analysed in selected Ferrar samples of the low-Ti and high-Ti magma series from NVL and George V Land in the diopside-enstatite-ferrosilite-hedenbergite (Di-En-Fs-Hd) quadrilateral. Symbols: black circles = chilled margins of low-Ti sills, grey circles = samples from interior parts of low-Ti sills, open triangles = high-Ti samples. Solid lines underline the Fe-enrichment trends of low-Ca and high-Ca pyroxenes. Dotted lines connect analyses of the most mafic coexisting pyroxenes in individual samples. Pyroxenes following the dashed lines or lying close to them are within the field of metastable phase relations after LINDSLEY (1983) at least under low-pressure conditions (see text and figures **3.10** and **3.11**).
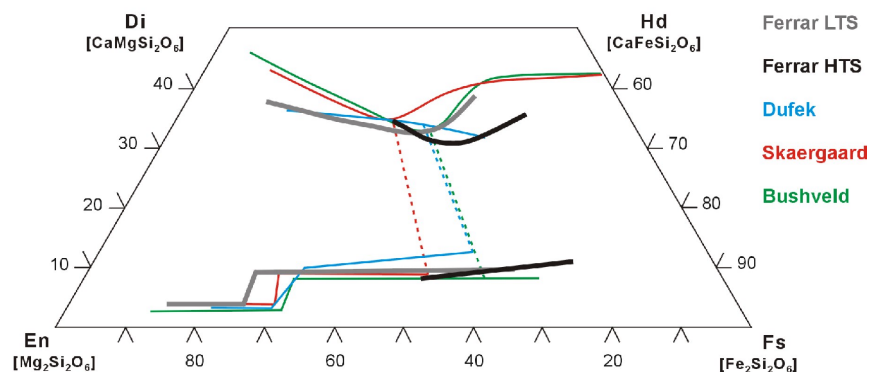
Fig. 3.4 – Comparison of the compositional variation trends of pyroxenes in the analysed Ferrar rocks and of characteristic pyroxenes from the Skaergaard layered intrusion (BROWN & VINCENT 1963), the Bushveld Complex (ATKINS 1969) and the Dufek Intrusion (HIMMELBERG & FORD 1976) in the Di-En-Fs-Hd quadrilateral. Dashed lines mark the two-pyroxene limit, the point at which pigeonite disappears from the crystallisation assemblage.

Low-Ca pyroxenes

Low-Ca pyroxenes are represented mainly by pigeonite and rarely by orthopyroxene. The latter, referred to as enstatite after the pyroxene nomenclature of MORIMOTO (1989), occurs as larger phenocrysts in chilled margin samples of low-Ti sills and dikes as well as in the few less evolved low-Ti rocks. In contrast to HORNIG (1993), no orthopyroxene could be identified in any of the high-Ti samples.

Orthopyroxene is essentially unzoned with the most magnesian composition in the chilled margin samples with $En_{81}Fs_{15}Wo_4$ varying only slightly to $En_{77}Fs_{18}Wo_5$. The latter with slightly lower pyroxene Mg-number (Mg# = 100*Mg / [Mg + Fe]) commonly occurs in samples with somewhat more mafic bulk-rock composition (Fig. **3.5**). Large orthopyroxene crystals have narrow rims of widely varying composition. Most frequently, they are surrounded by late-stage pigeonite or augite with pronounced enrichment in iron. Rarely, orthopyroxene has rims of higher evolved orthopyroxene chemistry ($En_{54-51}Fs_{44}Wo_{2-5}$), which can be compared with secondary 'hypersthene' reported by GUNN (1962) for a low-Ti sill from the central Transantarctic Mountains. They were formed by the inversion of pigeonite and can be distinguished from primary orthopyroxene by the occurrence of granular or lamellar augitic exsolutions as observed in thin section. In figure **3.3**, this is exemplarily shown by the two ortho-pyroxenes at En_{51} and En_{54} plotting markedly below the characteristic variation trend line for low-Ca pyroxene.
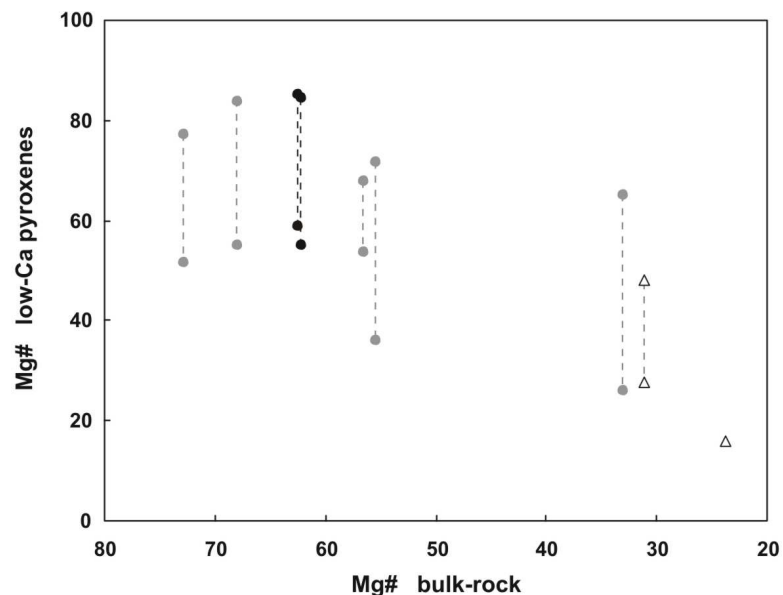
Fig. 3.5 – Variation of maximum and minimum Mg-numbers (Mg#) of low-Ca pyroxenes (opx + pig) analysed in selected samples with their bulk-rock Mg# as differentiation index (Mg# = 100*Mg / [Mg+Fe^{2+}] assuming Fe$_2$O$_3$/FeO = 0.15). Dashed lines reflect the Mg# range of pyroxene within individual samples, whereby maximum values mark the core chemistry of phenocrysts, and minimum values document both the rim chemistry of phenocrysts and groundmass pyroxene composition. Symbols as in figure **3.3**.

Pigeonite is present in all analysed low-Ti samples and exhibits a strongly varying chemistry between $En_{72}Fs_{22}Wo_6$ and $En_{23}Fs_{66}Wo_{11}$. Here, the composition of pigeonite

cores and corresponding rims depends on the degree of differentiation of the rocks samples as demonstrated in figure **3.5**, where the Mg-number of low-Ca pyroxene is plotted against the bulk-rock Mg-number as differentiation index. From the most mafic low-Ca pyroxene (orthopyroxene) in the chilled margin samples, the Mg# of low-Ca pyroxene decreases slightly with increasing bulk-rock Mg#, but decreases more significantly with decreasing bulk-rock Mg#. In high-Ti samples, pigeonite evolving from $En_{44}Fs_{48}Wo_8$ to $En_{13}Fs_{71}Wo_{16}$ shows the same trend of iron-enrichment as in the low-Ti rocks, but exhibits a comparatively smaller chemical range starting from more evolved core compositions than low-Ti samples at similar bulk-rock SiO_2 content.

High-Ca pyroxene

High-Ca pyroxene (augite) occurs as phenocrysts, as rims around low-Ca pyroxenes and as matrix minerals. As well as low-Ca pyroxenes, augitic clinopyroxene spans a wide compositional range of $En_{52-19}Fs_{11-53}Wo_{37-28}$ in low-Ti rocks and $En_{37-7}Fs_{32-68}Wo_{31-25}$ in high-Ti rocks. This strong iron-enrichment trend with decreasing MgO and CaO contents (Fig. **3.3**) documents both chemical zoning within individual pyroxenes and chemical differences between the distinctly evolved samples. In general, coexisting high- and low-Ca pyroxenes correspond in their chemistry and thus the composition of high-Ca pyroxene changes systematically with the bulk-rock composition (Fig. **3.6**) as already pointed out for the low-Ca pyroxenes. Samples with higher degree of differentiation contain more evolved augitic clinopyroxene. Comparing augite from low-Ti and high-Ti rocks with similar bulk-rock SiO_2 concentrations, those in the high-Ti rocks are characterised by more evolved, iron-enriched composition.
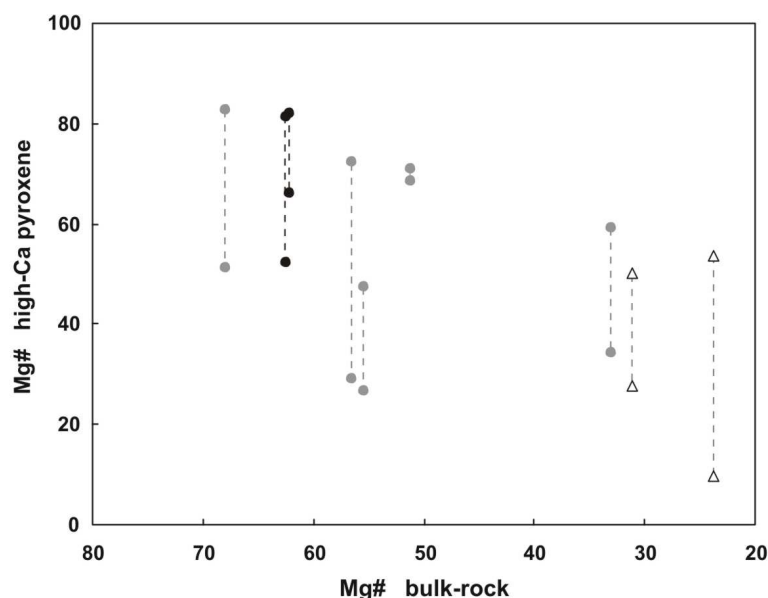
Fig. 3.6 – Variation of maximum and minimum Mg-numbers (Mg#) of high-Ca pyroxene analysed in selected samples with their bulk-rock Mg# as differentiation index. Dashed lines reflect the Mg# range of pyroxene in individual samples, whereby maximum Mg# values represent the core chemistry of augitic phenocrysts or innermost rims around low-Ca pyroxenes, and minimum Mg# values represent outer rims of pyroxene phenocrysts as well as matrix minerals. Symbols as in figure **3.3**.

Furthermore, very few augites within the most evolved low-Ti sample ($En_{20}Fs_{41}Wo_{39}$) and the high-Ti samples ($En_{17-15}Fs_{46-52}Wo_{37-32}$) exhibit a late-stage increase in their CaO contents, similar to some higher evolved augites (ferrohedenbergite) from the Skaergaard or the Bushveld intrusions (BROWN & VINCENT 1963, ATKINS 1969). This trend is extended by some hedenbergite reported by BROTZU et al. (1988) for Ferrar rocks from sills in southern Victorialand.

Subcalcic augite and others

Subcalcic augite covers the compositional range between low-Ca and high-Ca pyroxenes, where actually a miscibility gap exists between coexisting pyroxenes. Some of the pyroxenes analysed do not exactly match with the main trends of iron-enrichment described above; instead, they plot in the field of immiscibility. Most likely, they may reflect analyses of fine-scale lamellar intergrowths of exsolved pyroxene formed during secondary low-temperature exsolution reactions. Such subsolidus phase relations of pyroxenes from slowly cooled igneous rocks are very complex as discussed in detail by e.g. RIETMEIJER & CHAMPNESS (1982). However, some of these data are not included in the variation diagrams above and will not be considered in further interpretations.

Furthermore, some of the Mg-rich augites, present as microphenocrysts and rims around early phenocrysts (namely orthopyroxene) in the chilled margin samples, show a marked decrease of MgO and moderate increase in FeO accompanied by a significant enrichment in CaO (Fig. **3.3**). Their chemical range is $En_{61-39}Fs_{14-21}Wo_{25-40}$. According to MÜNTENER et al. (2001), the Ca-enrichment trend can be attributed to sub-solidus re-equilibration, whereas the above described iron-enrichment trend in augite with slightly decreasing CaO clearly indicates processes such as cooling and fractionation of magma. However, the strong increase in CaO may also result from rapid quenching of magma at the chilled margins of sills intruding into cooler country rocks.

In addition to these iron-poor augites, most of the very iron-rich calcic and subcalcic augites (Fig. **3.3**) in the higher evolved low-Ti and in the high-Ti samples, lie beyond the boundary of the "forbidden zone", where only metastable pyroxene relations exist at least at low-pressures (see below). The comparison with the Bushveld and the Skaergaard pyroxenes (Fig. **3.4**) shows that these pyroxenes are beyond the two-pyroxene limit, where pigeonite actually ceases to crystallise. These pyroxene data are not subject of further discussion.

3.2.2 Plagioclase

order to display and discuss the plagioclase composition of the analysed Ferrar rocks, plagioclase analyses have been recalculated into the end-member components anorthite (An), albite (Ab) and orthoclase (Or) given as mole proportions [mol%].

Within samples of the low-Ti series, plagioclase shows normal zoning and exhibits a wide interval of chemical composition with anorthite decreasing from An_{88} to An_{32} in favour of albite correlating with a small but clearly increasing orthoclase component

(Fig. **3.7**). Euhedral to subhedral phenocrysts within chilled margin samples document the most calcic chemistry and are chemically uniform. Only rarely, they are surrounded by narrow but strongly zoned rims of significantly Ab-richer composition. This pronounced chemical zoning causes variations of the anorthite content of up to 30 mol% within single plagioclase crystals. Similar to phenocryst rims of strongly zoned crystals, groundmass plagioclase generally shows a more evolved chemistry than phenocryst cores.
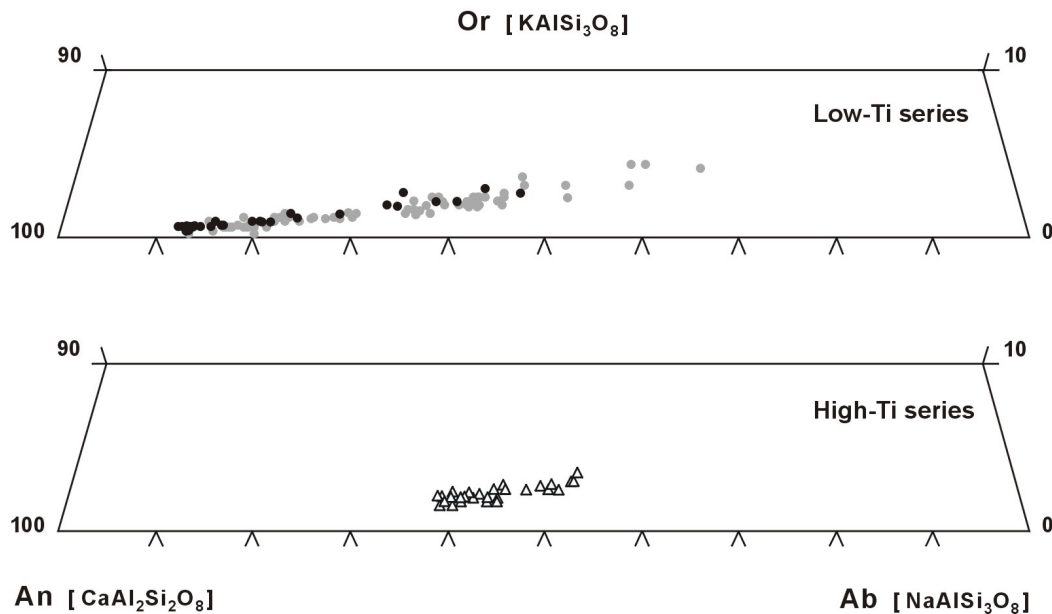
Fig. 3.7 – Chemical variation of plagioclase analysed in selected samples of the Ferrar low-Ti and the high-Ti magma series from NVL and George V Land in the anorthite-albite-orthoclase (An-Ab-Or) ternary plot. Symbols as in figure **3.3**.

Within the low-Ti samples, the composition of plagioclase cores systematically changes with the degree of differentiation of the samples (Fig. **3.8**), indicated by the bulk-rock Mg-number. From the most calcic plagioclase phenocryst cores (An_{88}) in chilled margin samples, the CaO content of plagioclase cores only slightly decreases towards An_{83} in least differentiated rocks. In contrast to that, samples of more evolved bulk-rock composition show significantly decreasing CaO contents in plagioclase in favour of Na_2O (and K_2O); the most evolved low-Ti sample contains plagioclase with a core chemistry varying from An_{61} to An_{54}.

In high-Ti samples, plagioclase is weakly zoned compared to low-Ti samples. The core chemistry varies between An_{60} and An_{53}, and the zoned crystals exhibit steadily decreasing An contents towards the outer rims up to An_{46}. Compared to plagioclase cores in low-Ti rocks, those in high-Ti rocks have lower An contents at similar bulk-rock SiO_2 contents but do not reach the low An and high Ab and Or contents detected for plagioclase rims in the most evolved low-Ti samples.
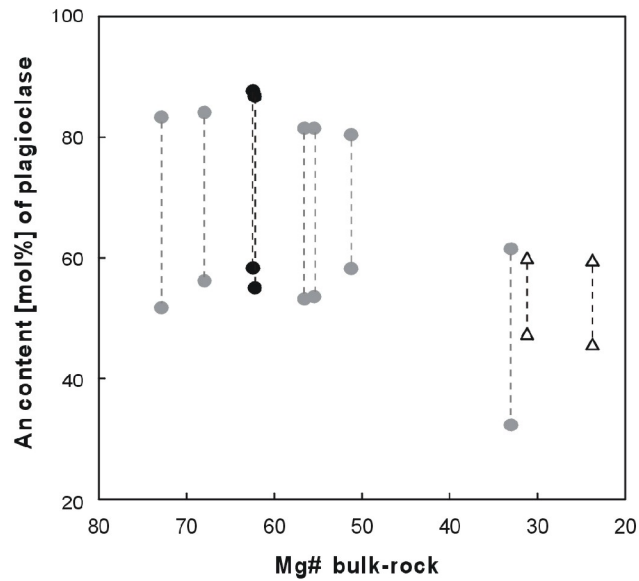
Fig. 3.8 – Chemical variation of plagioclase shown by maximum and minimum anorthite (An) contents in different investigated rock samples with respect to their degree of differentiation indicated by the bulk-rock Mg-number (Mg#). Symbols as in figure **3.3**. Dashed lines document the range of An content within the individual samples: maximum An contents represent the core chemistry of phenocrysts, and minimum An contents represent the rim chemistry of phenocrysts as well as groundmass plagioclase.

3.2.3   Oxide Phases

Oxides occur both as phenocrysts and microlites disseminated within the matrix in most of the analysed samples and often show marked exsolution features. In chilled margin samples, oxides are restricted to the groundmass with crystal sizes too small for chemical analysis. In higher evolved samples, they increase in size and total amount, which is highest in samples of the high-Ti series.

The oxides have been identified as iron-titanium oxides, predominantly titaniferous magnetite and ilmenite. At magmatic temperatures, both belong to continuous binary solid solution series between the end-members ulvöspinel (Fe_2TiO_4) and magnetite ($FeFe_2O_4$) and between ilmenite ($FeTiO_3$) and hematite (Fe_2O_3), respectively. The phase stability of both solid solution series is a sensitive function of the prevailing oxygen fugacity (fO_2).

Since only subordinate portions of further elements other than Fe and Ti are present in the analysed oxides, the chemical analyses have been recalculated to molecular fractions of ulvöspinel (Usp) and ilmenite (Ilm) using the program ILMAT from LEPAGE (2003), which provides different end-member calculation procedures after CARMICHAEL (1967), ANDERSON (1968), LINDSLEY & SPENCER (1982) and STORMER (1983). The oxide end-member compositions calculated by using the different schemes do not vary significantly. However, the results given in mol% Usp and mol% Ilm in the appendix **3c** are consequently calculated after STORMER (1983). The partitioning of total iron contents into FeO and Fe_2O_3 has been estimated by the method of CARMICHAEL (1967).

Both microlites and phenocrysts vary in composition, with the main variations in ulvöspinel content, ranging from 37 to 77 mol% in low-Ti rock samples and from 57 to 81 mol% in high-Ti rock samples. Within the samples of the low-Ti series, the oxides lack true systematic chemical variations with the degree of differentiation. Compared to oxides in the low-Ti rocks, those in the high-Ti rocks exhibit a narrow compositional range at generally higher ulvöspinel contents (higher TiO_2 concentrations). In all studied samples, ilmenite is exclusively present as exsolution lamellae in titano-magnetite and exhibits a very narrow compositional range compared to the spinel phase with 93 – 97 mol% Ilm in low-Ti rocks and 96 – 99 mol% Ilm in high-Ti rocks.

The occurrence of exsolution lamellae is characteristically observed in most of the larger oxide crystals. During and/or after cooling, ulvöspinel has been oxy-exsolved from primary titano-magnetite to form separate magnetite and ilmenite domains according to the following equation:

$$3Fe_2TiO_4 + \tfrac{1}{2}\,O_2 \; à \; 3FeTiO_3 + Fe_3O_4$$
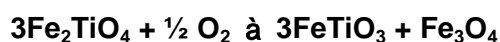
$$\textbf{ulvöspinel} \; à \; \textbf{ilmenite + magnetite}$$

This oxidation reaction under subsolidus temperatures proceeded to different extents within the analysed samples. It explains the wide variation of the spinel composition, which is observed even within individual samples. Considering the terminology of BUDDINGTON & LINDSLEY (1964), the most commonly occurring lamellae of ilmenite in titano-magnetite can be referred to as Trellis-type exsolutions (Fig. **3.9**).
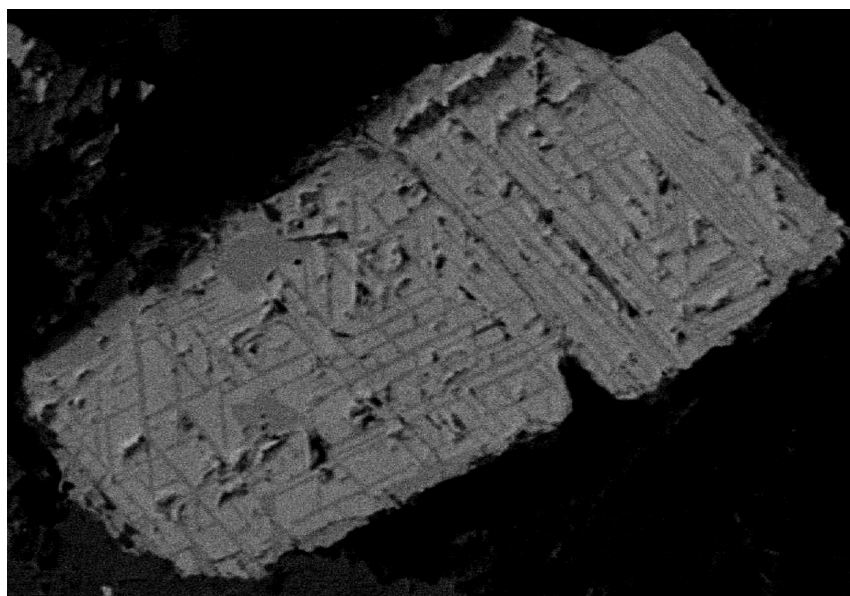
Fig. 3.9 – Back-scattered electron (BSE) image showing a typical example of oxides in low-Ti sample RH45. The primary titaniferous magnetite exhibits Trellis-type oxy-exsolution textures (after BUDDINGTON & LINDSLEY 1964) formed by ilmenite lamellae (96 mol% Ilm) within an ulvöspinel-rich host (67 mol% Usp). Width of image is ~ 150 µm.

No marked differences in these exsolutions were detected for the samples of both magma series, except from varying abundances and thicknesses of the lamellae.

These variations can serve to deduce conditions during the formation of the lamellae (e.g. the cooling rates, PRICE 1982) as it is driven by changes of physical and chemical conditions (e.g. temperature, redox conditions, HAGGERTY 1991, CRAIG 2001). However, since these features result from subsolidus oxidation reactions, no systematic analysis has been performed. In some of the mafic low-Ti samples investigated, lamellae of ilmenite are the only oxide phases quantitatively analysed, since analyses of the host titano-magnetite were not of reasonable quality due to complete secondary alteration.

3.2.4   Summary and Inferred Conclusions

In general, the new microprobe data of primary mineral phases in intrusive Ferrar rocks from NVL and George V Land largely resemble the range of compositional variations previously analysed in intrusive as well as extrusive Ferrar rocks from widely distributed occurrences within the FLIP and the Dufek Intrusion (e.g. HIMMELBERG & FORD 1976, ABEL et al. 1979, ELLIOT et al. 1986, HABAN & ELLIOT 1986, HAENSEL et al. 1986, BROTZU et al. 1988, HORNIG 1993, ELLIOT et al. 1995, ANTONINI et al. 1999, DEMARCHI et al. 2001). Only the phenocryst compositions published by HORNIG (1993) are contradictory to the present data in some striking points. The most primitive phenocryst compositions are described within a high-Ti rock sample from Litell Rocks including orthopyroxene (Mg# ~ 80), augite (Mg# ~ 85) and plagioclase (An$_{86}$). This mineral assemblage seems incompatible with the evolved iron-rich bulk-rock composition of this high-Ti rock. However, no orthopyroxene has been found in the present high-Ti samples at all and the most primitive mineral compositions are restricted to chilled margin samples of low-Ti sills. Furthermore, the high-Ti rocks are described by HORNIG to lack Fe-Ti oxides, but the present high-Ti rocks include the highest amount of Fe-Ti oxides (6 – 8 vol%) of all investigated samples.

As demonstrated above, the mineral chemical data exhibit systematic variations in the analysed Ferrar samples displayed by coexisting plagioclase and pyroxene becoming increasingly enriched in sodium and iron, respectively. This gives evidence that the present rocks belong to a suite of cogenetic magmas generated by differentiation. Thereby, the wide compositional range of the distinct mineral types indicates a strong influence of fractional crystallisation over a longer period. Following features are of importance:

- The compositional variations within individual samples reflect core-to-rim zonations of larger phenocrysts as well as variations between phenocrysts and micro-phenocrysts / groundmass phases.

- The compositional variations between the investigated samples exhibit a correlation between the mineral core compositions and the bulk-rock composition as higher evolved rocks contain mineral phases of more evolved composition.

- Conspicuously, the chilled margin samples of low-Ti sills contain the most primitive mineral phases although they do not exhibit the most primitive bulk-rock composition.

Commonly, the presence of crystals of two distinct average sizes – phenocrysts and groundmass crystals – can be interpreted as resulting from a two-stage crystallisation history of a magma caused by external factors (LATYPOV 2003a). In the present chilled margin samples of low-Ti sills, this is documented by the large phenocrysts of ortho-pyroxene and plagioclase on one hand and by the narrow rims around the phenocrysts and the microphenocrysts / ground mass minerals on the other hand. This reflects at least two distinct episodes of crystallisation during differentiation of the Ferrar magmas.

In this context, the large, essentially unzoned phenocryst cores represent an earlier stage of fractionation, which took place under approximately isothermal conditions. The assumption that these early phases crystallised at presumably higher temperature is inferred from their primitive composition, which furthermore indicates that they crystallised from a nearly primary melt. After this early fractionation event, the con-ditions (temperature, pressure, redox conditions) presumably changed during magma evolution, for example, related to magma ascent into higher levels, causing changes in the composition of the subsequently crystallising mineral phases. During this later fractionation stage under steadily changing conditions, the narrow but strongly zoned rims of phenocrysts and the groundmass minerals crystallised with more evolved compositions. These late mineral phases probably reflect crystallisation during and after magma emplacement. If these considerations are correct, this might explain the presence of the most primitive minerals within the chilled margin samples of sills, since the phenocryst-bearing magma has been rapidly cooled after its emplacement at crustal levels.

The implication of differences in crystallisation conditions for mineral phases crystallised during earlier and later fractionation stages will be tested by conventional geothermobarometers in the next chapter. The inferred two-phase differentiation history of the Ferrar magmas will be discussed in detail in chapters **4.2** and **4.3** combining the mineral and the bulk-rock chemical variations, the latter of which will be described in chapter **3.3**.

3.2.5   Estimation of Intensive Crystallisation Parameters

Since minerals provide an archive of pressure, temperature and redox conditions, at which a magma stagnated and partially crystallised, the above described assumption of an at least two stages comprising differentiation history of the Ferrar magmas will be tested by evaluating the conditions at which the magma experienced differentiation. These parameters can be described by applying compositions of primary mineral phases to geothermobarometers. A large number of these tools have been provided by many investigators over the last decades. These thermo/-barometers are primarily based on the exchange of different elements between distinct phases that are sensitive to varying conditions and have been calibrated using experimentally synthesised and / or natural mineral phases.

Based on the observed compositional variations of pyroxenes, plagioclase and Fe-Ti oxides, adequate conventional thermo- / barometers will be applied to estimate the crystallisation temperature and the oxygen fugacity of the Ferrar magmas considering

the influence of pressure on the respective estimates, too. The major intention is not to determine the exact values for distinct conditions but rather to identify relative differences in these conditions for mineral phases analysed in individual rocks and for the entire range of rock compositions, especially the differences between low-Ti and high-Ti rocks.

Crystallisation Parameters from Pyroxene Composition

Even if the large number of previous geothermometers (e.g. NIELSEN & DRAKE 1979), developed to estimate crystallisation temperatures from pyroxene composition, have been improved by several revised thermodynamic models (e.g. PUTIRKA et al. 1996), their application does not always give satisfactory results, as is seen for example by comparison to recent experimental data (FREISE 2004). Thus, the crystallisation temperature of pyroxenes in the Ferrar rocks was estimated by applying the graphic thermometer after LINDSLEY (1983) and the thermobarometer after BREY & KÖHLER (1990).

The principle of the two-pyroxene thermometer of LINDSLEY (1983) is based mainly on the partitioning of Ca between coexisting low-Ca and high-Ca pyroxenes since there is a strong temperature dependence of Ca-exchange between both. With decreasing temperature Ca increases in high-Ca pyroxenes and decreases in low-Ca pyroxenes at a given Mg/Fe ratio for the pyroxenes. In the analysed Ferrar samples, the opposite behaviour is observed when the entire sample set is considered: the major trends show that the Ca-content mainly decreases in augite and increases in orthopyroxene and pigeonite. This can primarily be attributed to the strong iron-enrichment during magma evolution (shifting the Mg/Fe ratio to markedly lower values), which outbalances the effect of Ca-distribution.

The applied two-pyroxene thermometer combines experimentally determined Mg-Fe-Ca pyroxene phase relations at different temperatures and pressures with calculated phase equilibria for the pure Mg-Ca- and the Fe-Ca-pyroxene joins. Since this graphic thermometer is based on the Di-En-Fs-Hd quadrilateral, it is applicable only to natural pyroxenes with negligible non-quadrilateral components (< 10 mol%) like those analysed in the Ferrar rocks. Figures **3.10** and **3.11** illustrate the polythermal pyroxene relations in the Di-En-Fs-Hd quadrilateral at different pressures (1 atm, 5 kbar and 10 kbar) applied to the studied Ferrar low-Ti and high-Ti samples, respectively. In general, the effect of variable pressures on temperature estimates is rather small but noticeable. Since no independent geobarometer could be used to estimate the exact pressure conditions, approximated values of temperatures for the crystallisation of the distinct pyroxenes are given in table **3.1** for the respective pressures. The accuracy of the thermometer is given with ± 50 °C (LINDSLEY 1983) including uncertainties of the exact placement of the isotherms as well as errors in pyroxene composition due to analytical inaccuracy and end-member calculations.
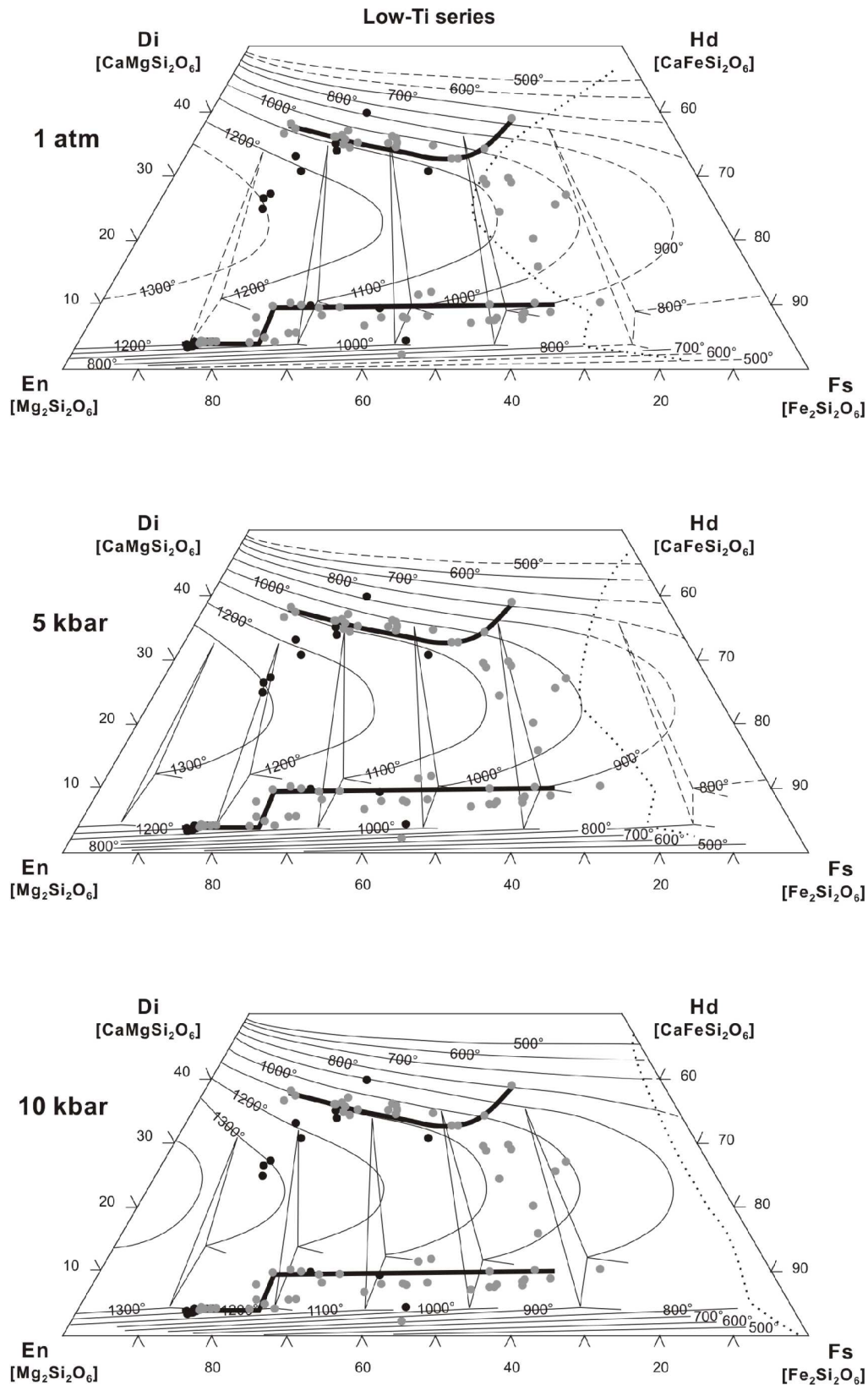
Fig. 3.10 – Polythermal relations of coexisting pyroxenes after L<small>INDSLEY</small> (1983) with isotherms contoured at 100 °C intervals at pressures of 1 atm, 5 kbar and 10 kbar to estimate crystallisation temperatures of pyroxene analysed in selected Ferrar low-Ti samples. Dashed lines mark fields of metastable phase relations, which decrease in dimension with increasing pressure. Symbols as in figure **3.3**, symbol size corresponds approximately to thermometer accuracy and analytical errors where isotherms are very close.
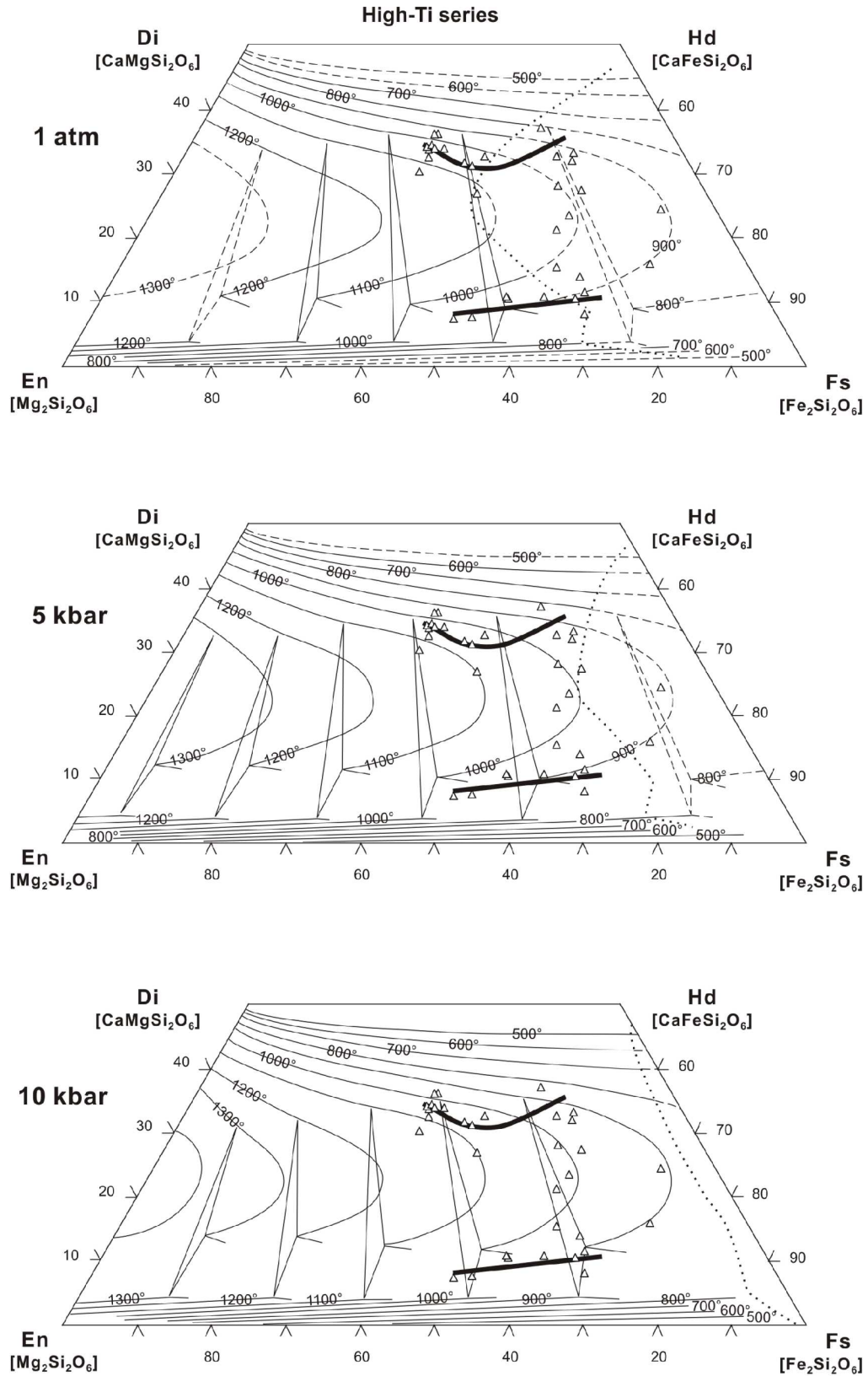
Fig. 3.11 – Polythermal relations of coexisting pyroxenes after LINDSLEY (1983) with isotherms contoured at 100 °C intervals at pressures of 1 atm, 5 kbar and 10 kbar to estimate crystallisation temperatures of pyroxene analysed in selected Ferrar high-Ti samples. Dashed lines mark fields of metastable phase relations, which decrease in dimension with increasing pressure. Symbols as in figure **3.3**, symbol size corresponds approximately to thermometer accuracy and analytical errors where isotherms are very close.

Tab. 3.1 – Crystallisation temperatures of pyroxenes estimated using the two-pyroxene thermo-
meter after LINDSLEY (1983) using mineral compositions of orthopyroxene, pigeonite
and augite from the studied Ferrar low-Ti and high-Ti rocks. The temperature range for
each of the pyroxenes includes the maximum values (Mg-rich px) and the minimum
values (Fe-rich px) at the respective pressures comprising pyroxenes from variably
evolved samples. Minimum values in parentheses are from pyroxenes that fall within
the field of metastable phase relations at low pressures.

Magma series	Pressure	Orthopyroxene Mg / Fe	Pigeonite Mg / Fe	Augite Mg / Fe
Low-Ti Series	1 atm	1200 – 770	1160 – 880 (860)	1120 – 760
	10 kbar	1250 – 820	1220 – 880	1140 – 790
High-Ti Series	1 atm	–	950 – 840	1120 – 950 (820)
	10 kbar	–	1020 – 890	1120 – 840

Although the temperatures obtained for the crystallisation of pyroxenes in the studied
Ferrar igneous rocks enclose the values given for low-Ti Ferrar rocks investigated by
HABAN & ELLIOT (1986), BROTZU et al. (1988) and ANTONINI et al. (1999), the present
temperatures, especially those obtained for the high-Ti rocks, provide new valuable
information and therefore, will be addressed in more detail.

The highest crystallisation temperature at all pressures (up to > 1300 °C) is obtained by
the few Mg-rich augitic microphenocrysts in chilled margins of low-Ti sills, which follow
a steep Ca-enrichment trend. Similar findings are interpreted by MÜNTENER et al.
(2001) to result from subsolidus re-equilibration. However, it is also possible that the
microphenocrysts crystallised during rapid quenching after magma emplacement. Their
steeply increasing CaO contents mark a trend line that crosses several isotherms and
indicate a wide temperature range of crystallisation. Since the origin of these micro-
phenocrysts is not clearly understood, the high temperatures inferred are not subject of
further discussions.

Aside from the values above, the highest temperatures obtained are those of ortho-
pyroxene, which is present as phenocrysts phase only in the chilled margins and some
mafic rocks from low-Ti sills. They range from 1200 °C at 1 atm to 1250 °C at 10 kbar.
The comparatively low temperatures of ~ 800 °C obtained from the few iron-rich
orthopyroxenes confirm their nature as inverted pigeonites as previously inferred from
the granular exsolutions observed under the optical microscope. The most Mg-rich
pigeonite in a mafic low-Ti sample yields temperatures of 1160 °C at 1 atm and
1220 °C at 10 kbar, whereas iron-rich pigeonite in higher evolved low-Ti samples yields
~ 880 °C at all pressures. Crystallisation temperatures of Mg-rich augite are about
1120 °C at 1 atm and 1140 °C at 10 kbar; those of Fe-rich augite are 760 and 790 °C
at 1 atm and 10 kbar, respectively.

Similar to the low-Ti rocks, the temperatures obtained for augites in high-Ti samples remain virtually unchanged at all pressures with 1120 °C for Mg-rich augites and ~ 840 °C for Fe-rich augites. Mg-rich pigeonite yields lower temperatures of about 950 °C to 1020 °C with pressure increasing from 1 atm to 10 kbar. Fe-rich pigeonite gives temperatures varying from 840 °C to 890 °C with increasing pressure.

It is noteworthy, that at low pressure only the more mafic augites and pigeonites yield reliable temperature estimates since most of the higher evolved clinopyroxenes fall within the field of metastable phase relations. As shown in the diagrams of LINDSLEY (1983), these pyroxenes are stable at higher pressures, but it is questionable if their presence really implies higher pressure conditions during differentiation or if they experienced subsolidus re-equilibration at low pressures. The latter interpretation is favoured since it agrees with the observation that most of the clinopyroxene in the higher evolved samples exhibit abundant exsolution features.

The crystallisation temperatures listed in table **3.1** comprise a wide range of > 300 K indicating a wide temperature interval of cooling and differentiation of the Ferrar magmas. During this process, decreasing temperatures result in the crystallisation of increasingly iron-rich low-Ca and high-Ca pyroxenes that is accompanied by a steadily evolving composition of the remaining magma. This observation corresponds to the iron-enrichment trends shown by many other tholeiitic rock suites such as those from the Dufek and the Bushveld intrusions. The correlation of pyroxene compositional variations with the evolution of the bulk-rock composition is displayed in figure **3.12** for the Ferrar rocks. It displays a graphical solution, also provided by LINDSLEY (1983), after which temperatures of minimum stability of pigeonite can be estimated as a function of $X = Fe / (Fe+Mg)$ at different pressures. The diagram illustrates that pyroxene becoming enriched in iron intersects each of the isobars at lower temperature. Applied to the determined compositions of pigeonite in the low-Ti and high-Ti Ferrar rocks, the obtained temperatures are in the range of those estimated before by the two-pyroxene thermometer.

The temperatures obtained from the "graphical" thermometer of LINDSLEY can partly be tested by the geothermobarometer of BREY & KÖHLER (1990). This calculation is based solely on the Ca-content in orthopyroxene that is in equilibrium with clinopyroxene; pressure dependence is considered as well. As already mentioned, orthopyroxene is only present in the chilled margin samples and some samples of more mafic bulk-rock composition taken from low-Ti sills. Temperatures exemplarily calculated for one of the most mafic orthopyroxene in one of the chilled margin samples range from 1249 °C over 1219 °C to 1189 °C for the applied pressures of 10 kbar, 5 kbar and 0 kbar, respectively. These values largely resemble those listed in table **3.1**, which have been estimated using the two-pyroxene thermometer of LINDSLEY (1983). The temperatures obtained for one of the iron-rich orthopyroxenes, which have been identified as inverted pigeonite, were significantly lower ranging from 557 at 10 kbar to 524 °C at 0 kbar. These temperatures confirm the secondary subsolidus reaction within this pyroxene. Compared to the values obtained from the graphical solution after LINDSLEY (1983, Fig. **3.10**), this temperature seems to be largely underestimated, however, it is considerably lower than that of the unexsolved primary orthopyroxenes.
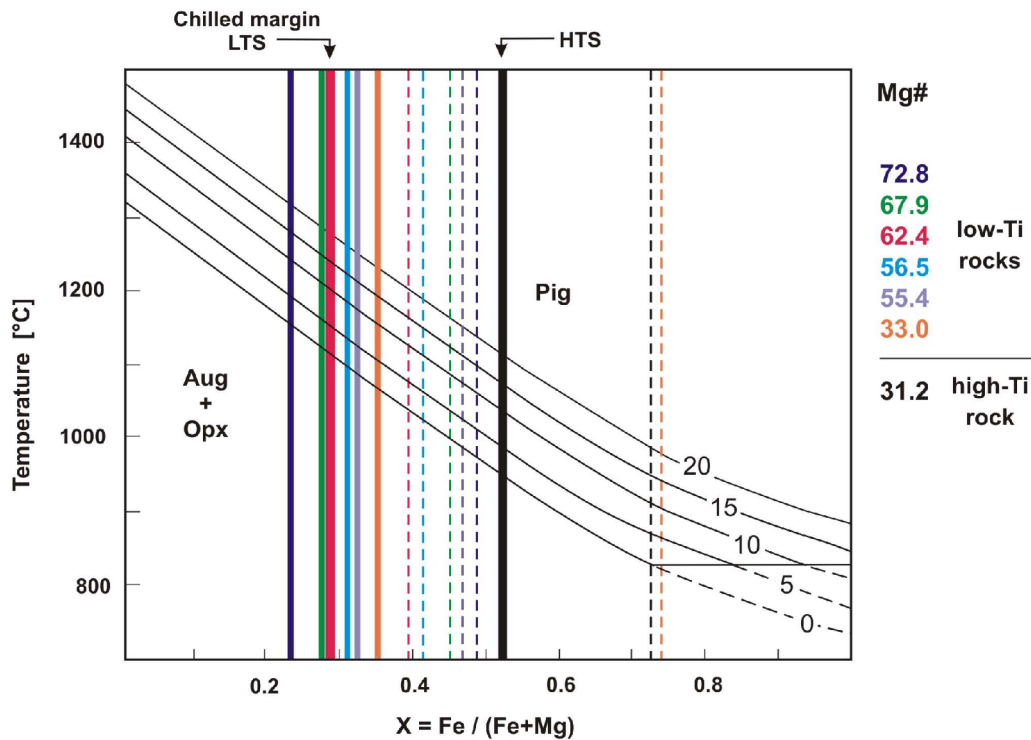
Fig. 3.12 – Minimum temperatures for the stability of pure Mg-Fe-Ca pigeonite as a function of X = Fe / (Fe+Mg) for five pressure values after LINDSLEY (1983). Pressure curves are labelled in kbar; dashed lines below 825 °C indicate that Mg-poor pigeonite is not stable. Vertical solid lines represent minimum values of X obtained for pyroxenes from variably evolved Ferrar samples; vertical dashed lines mark the respective maximum values of X for the same samples. The Mg# values on the right indicate the degree of differentiation of the respective samples.

In conclusion, the newly acquired thermometric data exhibit a wide range of crystallisation temperatures of pyroxenes emphasising that the iron-enrichment trends of low-Ca and high-Ca pyroxenes result from significant cooling and differentiation. The following observations are of main importance:

- Orthopyroxene phenocrysts in chilled margin samples have rims of pigeonite or augite that are significantly higher evolved and thus yield significantly lower crystallisation temperatures. This confirms the former conclusion that the Ferrar magmas experienced a multi-phase cooling history, in which orthopyroxene as liquidus phase may represent the earliest (preserved) crystallisation episode. It furthermore implies the possibility that this early differentiation event took place under higher pressure, and that during magma ascent and emplacement a later phase of crystallisation occurred at lower pressure.

- Comparing the temperature estimates from pyroxenes at 10 kbar within samples of both magma series, the highest temperature in low-Ti rocks is 1250 °C obtained from orthopyroxene, and in high-Ti rocks it is 1120 °C obtained from augite. Thus, the difference between crystallisation temperatures of low-Ti and high-Ti magmas is > 100 K. Assuming different pressures for the differentiation of the two magma series, this temperature difference between

both will change to a certain extent, however, the temperature for the given pyroxenes in high-Ti rocks will not exceed the temperature derived from orthopyroxene present in low-Ti rocks. This indicates that the low-Ti magma crystallised primarily at higher temperature than the high-Ti magma. This temperature difference is even more significant when higher pressures are assumed during the differentiation of the low-Ti magma and lower pressures for the high-Ti magma.

Crystallisation Parameters from Plagioclase Composition

Due to the significant temperature dependence of plagioclase compositions, numerous igneous geothermometers have been formulated to estimate their crystallisation temperatures. Most of the conventional plagioclase thermometers are based on exchange reactions between the plagioclase components anorthite and albite and the magmatic liquid. Similar to the thermodynamic approach from KUDO & WEILL (1970), the earlier thermometers have mainly been calibrated based on equilibrium melting experiments at low pressure. These models have later been improved by a large number of experiments on phase equilibria conducted for anhydrous and hydrous systems applied to a wide range of experimental conditions (temperature, pressure, oxygen fugacity) and liquid compositions (e.g. FUHRMAN & LINDSLEY 1988, ELKINS & GROVE 1990, HOUSH & LUHR 1991, GHIORSO & SACK 1995, SUGAWARA 2001, PUTIRKA 2005).

Similar to the pyroxenes, the present plagioclase data exhibit a very wide chemical range, both within single samples and between different samples of the Ferrar low-Ti and high-Ti rock series. The systematic changes from An_{88} to An_{32} with increasing SiO_2, K_2O and Na_2O and decreasing CaO and Al_2O_3 indicate significant differentiation over a certain period and hence, a large range of crystallisation temperatures for plagioclase has to be expected. It should be noted beforehand, that none of the mentioned geothermometers has been directly applied to estimate the crystallisation temperatures of plagioclase in the studied Ferrar igneous rocks. The reasons for this decision will be explained at first, before some approximations of relative differences of crystallisation temperature will be given for the present rocks.

Like in most models, the thermodynamic approach of KUDO & WEILL (1970) is based on the equilibrium of plagioclase and the coexisting liquid. Thus, this thermometer requires the possibility to measure or calculate the compositions of the two phases, provided that both are widely homogeneous. In the case of significantly zoned plagioclase crystals, only the outermost rims can be assumed to represent the equilibrium composition with the coexisting matrix. In contrast, the innermost plagioclase cores of more primitive composition are rather in equilibrium with the melt at the beginning of crystallisation (KUDO & WEILL 1970). Since this is the case for the wide compositional variations of plagioclase in the studied Ferrar samples, the application of compositions of plagioclase microphenocrysts and mesostasis to this thermometer would rather yield minimum crystallisation temperatures such as e.g. emplacement temperatures. However, temperature differences expected for distinct differentiation stages would be poorly recorded and possibly include large uncertainties due to the lack of equilibrium.

Compared to pyroxenes, plagioclase compositions and thus the deduced crystallisation temperatures are more sensitive to additional factors such as the presence of water and minor ternary components in plagioclase, but most of the geothermometer approaches do not adequately consider these effects. As outlined by SMITH & BROWN (1988) and references therein, most thermometers are based exclusively on phase relations in the binary An-Ab system, though most natural plagioclases contain at least small amounts of orthoclase. However, the relations in the ternary feldspar system are more complex and it is proven that the Or-component considerably influences temperature estimates: 1 mol% Or decreases the anorthite melting point for about ~ 100 K, whereas 1 mol% Ab causes only a temperature decrease of 5 K. Furthermore, it is well-known that increasing pressure raises the melting point of almost all solids. An increase of pressure of 1 kbar raises the temperature of anorthite and albite for about 2 K and 8 K, respectively (GOLDSMITH 1980, BOETTCHER et al. 1982), indicating that the effect of pressure on melting temperature of plagioclase is rather negligible unless very high pressures are assumed. A more significant influence is shown by an increase of water pressure, since water significantly lowers the melting temperature of anorthite (~ 65 K / 1 kbar P_{H2O}). The effect of variations in the water pressure during crystallisation of a silicate liquid can be deduced from the plagioclase phase diagram in figure **3.13**, given by JOHANNES (1978). It shows for example, that pure anorthite crystallises at very high temperatures of about 1550 °C at anhydrous conditions. This temperature is lowered significantly for more than 300 K when a water pressure of 5 kbar is assumed. This is in agreement with the given relation of temperature decrease of ~ 65 K / 1 kbar P_{H2O}.

These considerations emphasise the complexity of the plagioclase system and hence the difficulty to interpret chemical plagioclase data in a reasonable way. As the water pressure is only one of the unknown variables for the studied magmatic rock suite, temperatures obtained by the application of any of the above-mentioned thermometers would not give reliable absolute crystallisation temperatures but only approximations, which may bear considerable uncertainties.

Crystallisation temperatures of plagioclase in Ferrar igneous rocks have been estimated by BROTZU et al. (1988) for samples from low-Ti sills in southern NVL. Based on early (core) and late (rim or groundmass) plagioclase compositions, they calculated temperatures of about 1200 °C to 1100 °C for basaltic andesites using the thermo-dynamic approach of KUDO & WEILL (1970). HABAN & ELLIOT (1986) reported eruption temperatures of 1250 °C ± 50 °C for Ferrar low-Ti lava flows in the Mesa Range applying the plagioclase-liquid equilibria of MATHEZ (1973), a refined method of the Kudo-Weill thermometer. Temperatures calculated by ELLIOT et al. (1995) combining plagioclase core and whole-rock compositions of low-Ti and high-Ti lavas from the Mesa Range are given with 1227 – 1115 °C and 1105 – 1070 °C, respectively. ELLIOT et al. furthermore emphasised that the obtained temperatures widely agree with the degree of evolution of the rocks, an observation that has been reported by BROTZU et al. (1988) and ANTONINI et al. (1999) as well. Additionally, these studies show a correspondence of the plagioclase temperatures to the respective geothermometric data obtained from coexisting pyroxenes after LINDSLEY (1983). Even if no tempera-

tures are estimated directly from the plagioclase data of the newly analysed Ferrar rocks, the comparability to the mineral chemical data from HABAN & ELLIOT (1986), BROTZU et al. (1988) and ELLIOT et al. (1995) implies that similar temperatures like those estimated by these authors would be obtained by application of the same calculation methods. However, the reliability and quality of these data remain largely uncertain due to the facts outlined above. More important than the exact temperature values are the following considerations:
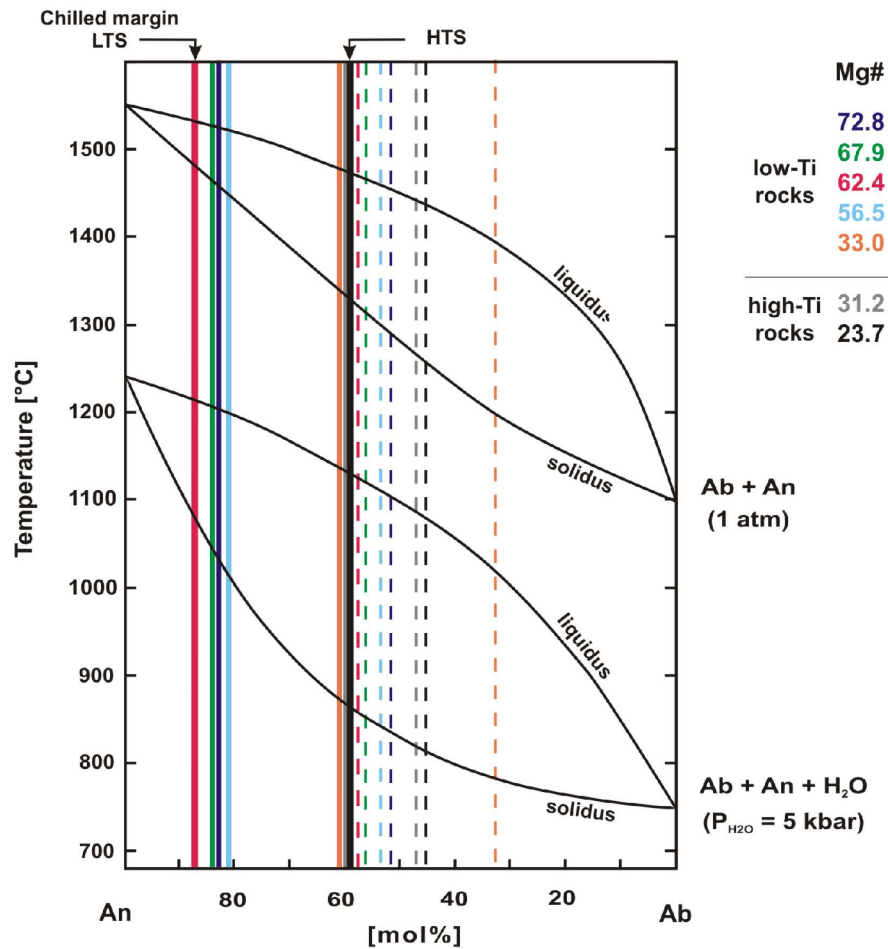
Fig. 3.13 – Phase diagram of the system albite-anorthite at different water pressures after JOHANNES (1978) indicating the pronounced influence of prevailing water pressures on plagioclase crystallisation temperatures and on its composition. Vertical solid lines represent maximum An contents of plagioclase obtained from variably evolved Ferrar samples; vertical dashed lines mark the respective minimum An contents for the same samples. The Mg# values on the right indicate the degree of differentiation of the respective samples.

The large compositional range of > 30 mol% An, shown between essentially unzoned phenocrysts (An_{88}) in chilled margins of low-Ti sills and the respective groundmass minerals (An_{55}), repeatedly emphasises the proposed two-stage differentiation history of the Ferrar magmas. Considering the difference of ~ 30 mol% Ab, the temperature decrease of 5 K per 1 mol% Ab mentioned above implies a difference in crystallisation temperature of at least 150 K within the chilled margin samples of sills. Applying the

most evolved composition of a plagioclase rim (An_{32}) in the most evolved low-Ti sample as a minimum estimate, the temperature range for cooling of the Ferrar low-Ti rocks is extended to ~ 280 K. This corresponds to the range of crystallisation temperature of 300 K obtained from the increase of the Or-content of about 3 mol% and furthermore, to the temperature estimations from coexisting pyroxenes. This wide temperature range obtained for plagioclase in the variably evolved low-Ti samples can be interpreted to reflect subsequent cooling and differentiation of the magma.

The comparatively narrow range of plagioclase compositions (An_{60-46}) determined within high-Ti rocks indicates a smaller range of crystallisation temperature. By comparison, the maximum anorthite content in plagioclase in the analysed low-Ti and high-Ti rocks shows an obvious difference of more than 25 mol%. This difference implies considerably lower crystallisation temperatures for more than 100 K for the high-Ti magma, confirming the estimations of ELLIOT et al. (1995). The reason for this difference remains elusive at this point, since the decisive influence of e.g. different pressures or water contents on plagioclase crystallisation temperature and composition can poorly be constrained. Thus, it is not easy to distinguish, whether this difference in An_{max} simply reflects a comparably higher differentiation degree of the high-Ti magma or if it is caused by a change in the physical conditions prevailing during the differentiation. This point can not be solved satisfactorily here and hence will be discussed later in combination with further data.

Crystallisation Parameters from Oxide Composition

Fe-Ti oxides are important accessory mineral phases in most igneous rocks. Since both temperature and oxygen fugacity (fO_2) control the TiO_2 contents of coexisting oxide phases, their compositions can be applied to estimate the temperature and redox conditions prevailing during their crystallisation or re-equilibration. Coexisting oxide pairs thus provide important constraints on the evolution of igneous rock suites.

The common methods developed for determination of T and fO_2 rely on the original version of BUDDINGTON & LINDSLEY (1964), which is based on the temperature and redox sensitive Fe and Ti exchange between coexisting cubic (e.g. magnetite-ulvöspinel$_{(SS)}$) and rhombohedral (e.g. ilmenite-hematite$_{(SS)}$) oxide pairs. From this Fe-Ti exchange, equilibrium temperatures can be calculated and the activities of magnetite and hematite in the cubic and rhombohedral oxides, respectively, are used to determine the oxygen fugacity at the estimated temperatures. Until recently, a large number of further developments of this basic model resulted in two widely applied thermo-oxybarometers: the thermodynamic model provided by GHIORSO & SACK (1991) and the thermodynamic calculations in the QUILF program of ANDERSEN et al. (1993). The latter considers the equilibria between Fe-Ti oxides, pyroxenes, olivine and quartz based on the theoretical background of studies from ANDERSEN & LINDSLEY (1988), FROST & LINDSLEY (1992) and LINDSLEY & FROST (1992).

However, similar to the thermometric pyroxene models, experimental results do not always agree with the calculated T and fO_2 values (even using more recently revised models), in particular at the high temperatures that are relevant for basaltic assemblages (LATTARD et al. 2005). This may partly be attributed to the limited number

of experimental data over wide T-fO_2 ranges applied for the calibration of the original models. Further problems can be ascribed to uncertainties in the estimates of ferric/ferrous iron ratios in the oxides and hence in the determination of the content of magnetite in the cubic oxide phase, which largely affects the fO_2 estimates (WOOD 1991).

In a recent study, DEVINE et al. (2003) pointed out that Fe-Ti oxide thermo-barometry applied on experimental products from natural andesites yields the closest fit between calculated temperatures and temperatures, which were thermocouple-measured during the experiments, when the solution model of STORMER (1983) in combination with the T-fO_2 formulations of ANDERSEN & LINDSLEY (1988, a later version of ANDERSEN & LINDSLEY 1985) are used. Therefore, the equilibration temperature and fO_2 from oxides in the present Ferrar rocks are determined by the thermodynamic approach after ANDERSON & LINDSLEY (1985) in conjunction with the magnetite and ilmenite end-member compositions calculated after the model of STORMER (1983), which both are integrated in the calculation scheme of LEPAGE (2003). The results are displayed in figure **3.14**.
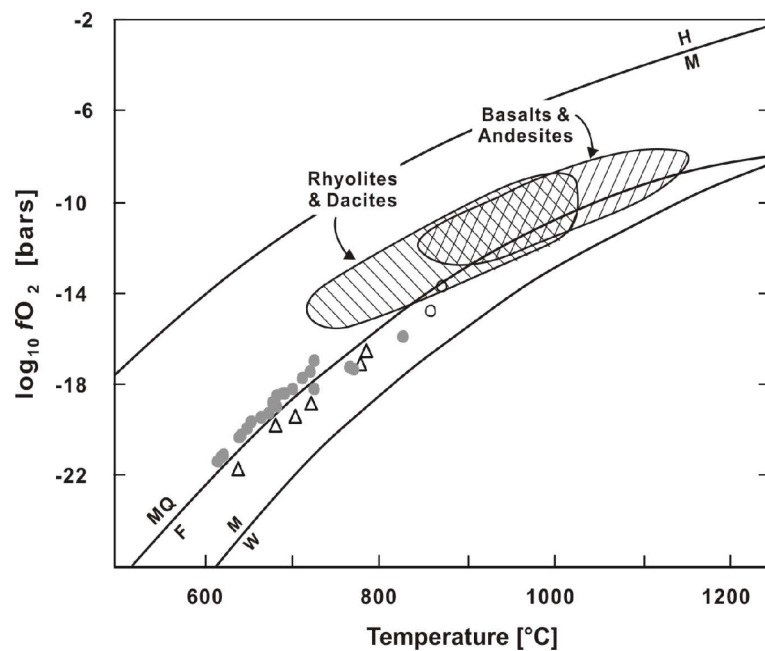
Fig. 3.14 – Oxygen fugacity against temperature calculated from compositions of coexisting Fe-Ti oxides in the studied Ferrar low-Ti (solid circles) and high-Ti (open triangles) rocks. The two open circles represent estimates for low-Ti Ferrar rocks from BROTZU et al. (1988) and ANTONINI et al. (1999). The fO_2 – T curves of the magnetite-hematite (MH) and the wüstite-magnetite (WM) oxygen buffers after MYERS & EUGSTER (1983) and the fayalite-magnetite-quartz (FMQ) oxygen buffer after SCHWAB & KÜSTNER (1981) have been included for reference. The hatched fields indicate equilibrium T and fO_2 for acid and basic lavas determined from Fe-Ti oxide compositions, which have been compiled by CARMICHAEL et al. (1974) and GILL (1981).

The temperatures estimated from the oxides in Ferrar low-Ti and high-Ti rocks vary from 600 to 800 °C, the corresponding oxygen fugacities range from 10^{-16} to 10^{-22} bars. No significant difference in the estimated temperatures is observable for the low-Ti and

high-Ti rocks, however, the more mafic rocks and the chilled margins of low-Ti sills (giving higher temperature estimates from pyroxenes) could not be considered since no primary Ti-magnetite is present or preserved. In general, the calculated temperatures are obviously too low to represent conditions on the liquidus as indicated by the discrepancy to the temperatures determined for a wide range of basalts and andesites (Fig. **3.14**). Since the naturally occurring oxides are prone to oxidation-induced exsolution until the final solidification of the residual melt fractions, the thermometric data from exsolved Ti-magnetite and ilmenite can be interpreted to represent rather minimum temperatures of re-equilibration of the oxides during the slow cooling than crystallisation temperatures of the magma.

This conclusion explains the large difference to temperatures obtained from pyroxene thermometry, an observation that is characteristic for a large number of slowly cooled igneous rock suites. The occurrence of granule or lamellar exsolutions is problematic in pyroxenes as well, indicating that they have reset their composition through subsolidus exchange (FROST & LINDSLEY 1992). Therefore, the primary bulk-composition of exsolved mineral phases must be reconstructed from textural evidence, before correct igneous temperatures can be inferred as demonstrated exemplarily by MARKS & MARKL (2001). They combined image processing of back-scattered electron images of exsolved oxides with point analyses of exsolved ilmenite and broad beam analyses of exsolved magnetite. In most of the present Ferrar rocks, especially those of primitive composition, a recalculation of the original composition of Ti-magnetite was impossible because only ilmenite lamellae could be analysed, since the host Ti-magnetites were largely affected by alteration. Furthermore, the oxide phases represent rather the later crystallisation stages as deduced from petrographic observation and should thus not yield higher crystallisation temperatures than estimated by pyroxenes.

BROTZU et al. (1992) reported a maximum equilibration temperature of 870 °C and a maximum oxygen fugacity of $\log_{10}fO_2$ = -13.6 bars from a magnetite – ilmenite paragenesis in Ferrar low-Ti basaltic andesites using the oxygen barometer after ANDERSEN & LINDSLEY (1988). Similar values (T = 858 °C, $\log_{10}fO_2$ = -14.7 bars) have been estimated by ANTONINI et al. (1999) for homogeneous groundmass magnetite and ilmenite in Ferrar low-Ti sills from NVL. For the Dufek intrusive rocks, HIMMELBERG & FORD (1977) calculated a maximum fO_2 of $10^{-10.1}$ bars for primary oxide crystallisation at 1090 °C, a temperature inferred from a combination of pyroxene thermometry and reconstructed oxide composition. From calculations using the composition of ilmenite lamellae in Ti-magnetite hosts, HIMMELBERG & FORD also obtained much lower values confirming the widely observed subsolidus re-equilibration of oxides. These lower T and fO_2 values agree with those obtained for the newly analysed rocks.

The calculated systematic T and fO_2 variations do not exhibit significant differences for the analysed Fe-Ti oxides from different Ferrar low-Ti and high-Ti rocks. For both rock types, the obtained T – fO_2 relations are close to the conditions of the FMQ oxygen buffer indicating a relatively reducing environment during cooling and crystallisation of the Ferrar magmas. However, the estimates for oxides from high-Ti rocks show a slightly lower oxygen fugacity for a given temperature than those from the low-Ti rocks. This difference is not very significant, but it corresponds to the higher contents of

ulvöspinel in the Ti-magnetite$_{(SS)}$ and higher contents of ilmenite in the ilmenite-hematite$_{(SS)}$ corresponding to higher TiO_2 and lower Fe^{3+} concentrations in both solid solutions from high-Ti rocks.

In conclusion, the oxide composition in Ferrar low-Ti and high-Ti rocks cannot be applied to constrain crystallisation temperatures due to extensive exsolution at sub-solidus temperatures, but the estimates of fO_2 indicate that the Ferrar magmas evolved under rather reducing conditions corresponding to the FMQ oxygen buffer. A slightly lower oxygen fugacity is inferred for the high-Ti rocks than for the low-Ti rocks.

3.3   WHOLE-ROCK CHEMISTRY

Whole-rock chemical analyses of low-Ti and high-Ti samples from NVL and George V Land, including major and trace elements of the entire sample suite as well as rare earth element and platinum-group element concentrations of selected samples, are listed in the appendix **4**, **5** and **6**, respectively.

Since some of the recommended schemes for the classification of igneous rocks or the determination of magmatic affinities, like the total alkali − silica (TAS) diagram after LEMAITRE (1989), are partly based on concentrations of at least moderately mobile elements, the influence of alteration processes on magma composition of the analysed Ferrar rocks will be considered before classifying them.

3.3.1   Alteration

The petrography of the present rocks, especially the extrusive samples, indicates that they experienced a more or less pronounced alteration. During an alteration process, primary magmatic phases can be transformed into hydrated secondary phases increasing the volatile content of the magmatic rock. This volatile content can be estimated by its release during heating of the sample and is given as loss on ignition (LOI) in weight percent. Thereby, H_2O, CO_2, SO_2 and other volatile phases are not distinguished. Thus, this LOI value provides a semi-quantitative indicator of the amount of secondary alteration as demonstrated by FLEMING et al. (1992) for Ferrar lava flows from the Mesa Range.

Great variability of the LOI values and $H_2O + CO_2$ contents is shown by the new data set (Appendix **4**). Sills and dikes of the low-Ti series as well as all samples of the high-Ti series exhibit LOI values < 1 wt% and volatile contents between 0.6 and 1.7 wt%. In contrast, in lava flows of the low-Ti series, LOI varies between 1.3 and 7 wt%. These significantly higher values clearly correlate with the abundance of cavities and vesicles filled with secondary phases in these extrusive rocks. According to this, the very low values of LOI (0.01 – 0.6 wt%) analysed for the high-Ti unit from Litell Rocks might argue for an intrusive rather than an extrusive emplacement of magma. However, these low LOI values may result from a considerable weight gain due to oxidation of FeO to Fe_2O_3, consistent with the high iron contents of the high-Ti samples.

In view of variable iron contents and possible weight gain, sample alteration can thus not be identified satisfactorily by LOI alone. In figure **3.15**, the measured LOI is shown

in relation to selected mobile elements and to Zr, indicative for the immobile incompatible elements (Ti, Nb, REE). The variation of the immobile element Zr is inferred to represent original abundances, unmodified by alteration even in highly altered samples, which are characterised by high LOI values. As no significant variation of Zr exists within the low-Ti lava flow samples, their scatter of mobile element concentrations (e.g. K, Rb, Ba, Sr, as well as Na, Si, Al and Ca) indicates that they have been disturbed by post-magmatic alteration.
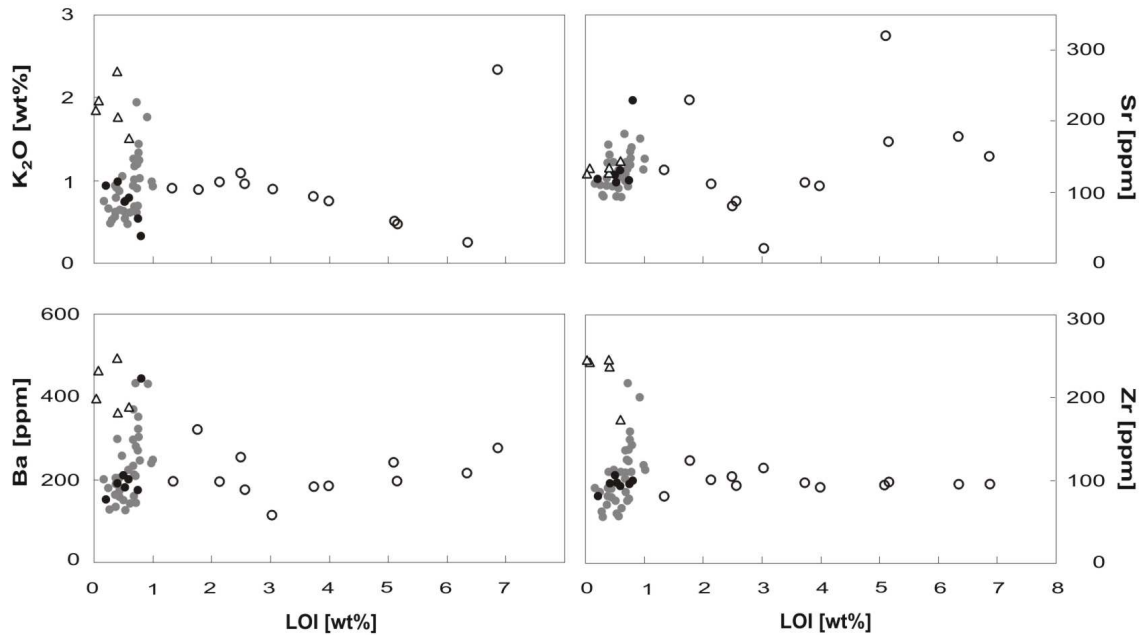
Fig. 3.15 - Variation of K_2O [wt%] and selected trace elements [ppm] with loss on ignition (LOI in wt%) of the studied Ferrar rocks. Not included are the few samples for which only H_2O and CO_2 contents have been analysed. All analyses have been recalculated loss-free to a total of 100 wt%. Symbols: black circles = chilled margins of low-Ti sills, grey circles = interior parts of low-Ti sills, open circles = low-Ti lava flows, triangles = high-Ti rocks.

Since nearly all extrusive low-Ti samples exhibit mobile element disturbances to various degrees, they would have to be excluded from the variation diagrams in the following figures. However, since many of the diagrams show variations of immobile elements and in order to allow comparison with the low-Ti intrusives they are not consistently excluded within this section, but indicated by a separate symbol. Nevertheless, they will largely be excluded from further petrogenetic discussions in order to interpret the geochemical data accurately.

3.3.2 Rock Types and Magma Series

According to the recommended classification scheme of LEMAITRE (1989), the TAS diagram, the analysed samples belong to a subalkalic magma series and can be classified as basaltic andesites and rare andesites on the basis of their total alkalis and silica contents (53 – 59 wt% SiO_2, Fig. **3.16**). Rare basaltic or dacitic compositions of samples from sills and dikes, reported by e.g. GUNN (1962, 1966) and BROTZU et al.

(1988), most likely represent evolved zones of differentiated units rather than true magma compositions, what will be discussed later on. Some of the scatter of data points in figure **3.16**, generally displaying positively correlated silica and total alkali contents, can be attributed to element disturbance by secondary alteration (see above), but does not significantly influence the classification of the analysed rock samples.
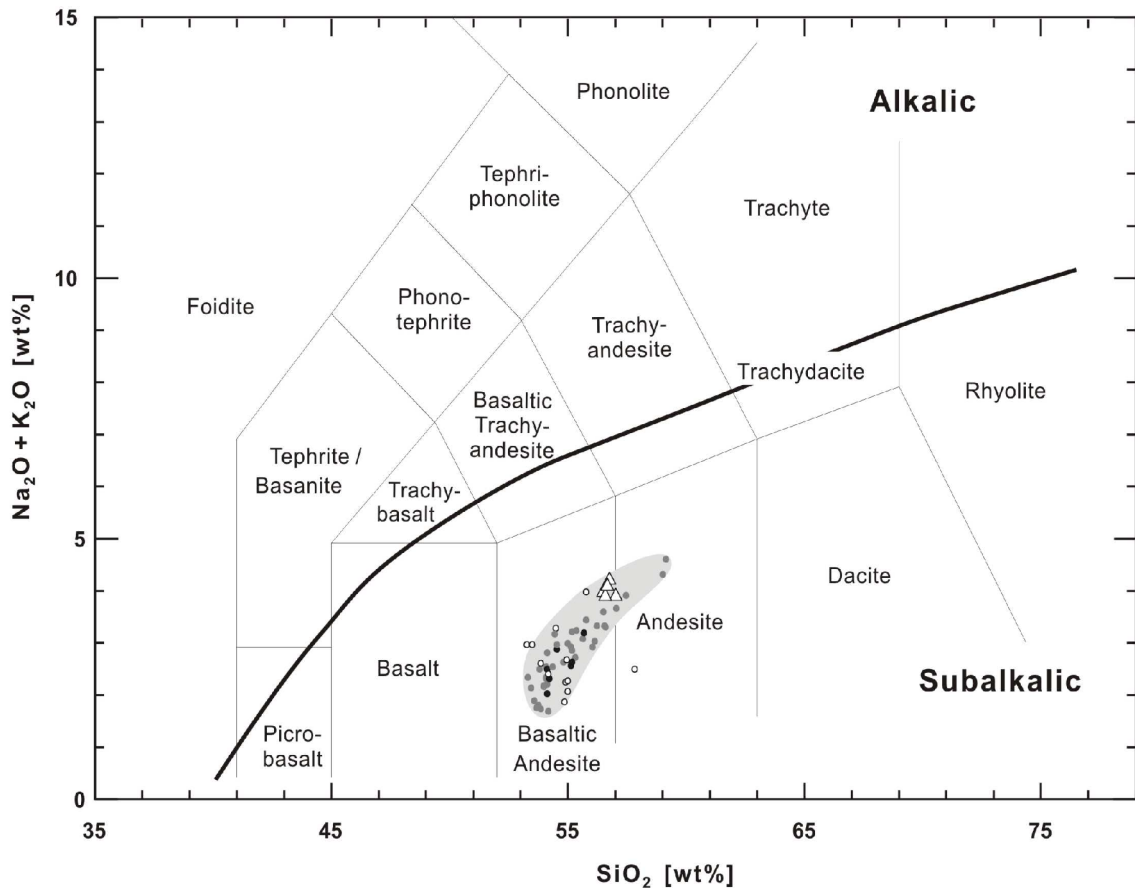
Fig. 3.16 – Classification of the studied Ferrar rocks in the TAS diagram (**t**otal **a**lkalis vs. **s**ilica) after LEMAITRE (1989). The solid curved line indicates the boundary between subalkalic and alkalic magma series after IRVINE & BARAGAR (1971). Symbols as in figure **3.15**.

Based on their major, trace and rare earth element abundances, the present rock samples can be attributed to the known Ferrar low-Ti and high-Ti magma series, referred to as Mount Fazio Chemical Type (MFCT) and Scarab Peak Chemical Type (SPCT), respectively, after FLEMING et al. (1992). As these terms imply, one main discriminating factor is the TiO_2 content, which is < 1.7 wt% and > 1.7 wt% in Ferrar low-Ti and high-Ti rocks, respectively. The highest TiO_2 content reported for Ferrar high-Ti rocks is 2.3 wt% (WILHELM & WÖRNER 1996).

A similar subdivision of magma series, mainly based on the TiO_2 content, has been proposed by COX (1980) for the Mesozoic Gondwana-related plateau basalts: by definition, tholeiitic rocks with TiO_2 values < 2 wt% belong to the 'Gondwana low-Ti province'. According to this, the use of the terms 'low- and high-Ti magma series' referring to the compositionally distinct groups of Ferrar rocks is contradictory since

nearly all Ferrar rocks belong to the 'Gondwana low-Ti province' by definition after COX (1980). However, BREWER et al. (1992) pointed out, that element ratios which are less sensitive to variable degrees of partial melting and fractional crystallisation are more relevant than absolute TiO_2 contents. In order to avoid confusion and to achieve consistency, the terms low-Ti and high-Ti series (LTS and HTS, respectively) will be used further on for the present Ferrar rock samples.

The majority of the analysed Ferrar samples from NVL and all samples from George V Land are of low-Ti chemistry with 0.4 – 1.2 wt% TiO_2. In addition to the reported high-Ti occurrences from Litell Rocks (SKINNER et al. 1981, HORNIG 1993), one newly sampled sill in the Alamein Range is identified to belong to the high-Ti suite (1.7 – 2.0 wt% TiO_2). All high-Ti samples can be distinguished by higher concentrations of incompatible major and trace elements than the low-Ti samples at a given SiO_2 content as exemplarily shown by the TiO_2 vs. SiO_2 diagram (Fig. **3.17**). The most distinctive features of both series are summarised further below in figure **4.8**
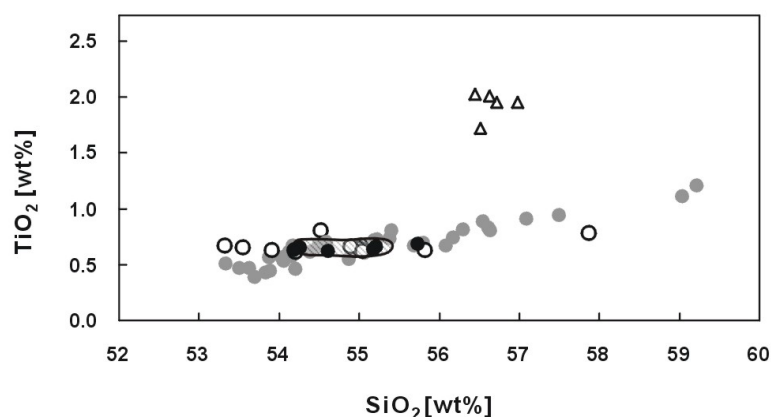
Fig. 3.17 – Concentrations of TiO_2 versus SiO_2 of the analysed Ferrar rock samples from NVL and George V Land showing the subdivision into the known low-Ti and high-Ti magma series, referred to as MFCT and SPCT, respectively (after FLEMING et al. 1992). Symbols as in figure **3.15**. For comparison, compositions of chilled margins of Tasmanian Ferrar sills after HERGT et al. (1989b) are included as shaded field.

3.3.3 Magmatic Affinities

As shown in the TAS diagram, all analysed Ferrar samples belong to the subalkalic magma series, which can further be subdivided into a calc-alkalic and a tholeiitic sub-group describing the magmatic affinity of a rock suite. The magmatic affinity is often determined by variations of the alkalis ($Na_2O + K_2O$), $FeO_{(T)}$ and MgO in the AFM ternary plot after IRVINE & BARAGAR (1971), which illustrates the variation trend a series of coherent igneous rocks follows during magmatic evolution.

In the AFM diagram (Fig. **3.18**), the investigated sample suite describes a trend typical for tholeiitic magma series that is characterised by a strong enrichment in $FeO_{(T)}$ with decreasing MgO content and only slightly increasing alkali contents. This increase of the Fe/Mg ratio indicates that the Ferrar magmas have experienced significant fractionation of mafic mineral phases during differentiation. On the other hand, Fe-

oxides have not been fractionated since they have not become a stable phase during most of the differentiation history. Comparing both magma series, the high-Ti samples show a slight but marked offset from the trend of the low-Ti series to higher $FeO_{(T)}$ concentrations.
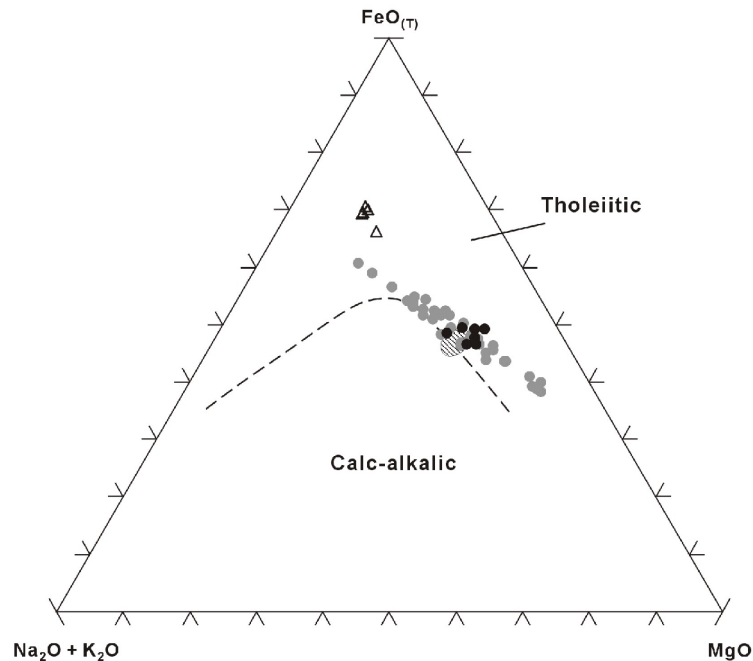
Fig. 3.18 – Ternary AFM diagram (**A** = Na_2O+K_2O, **F** = FeO, **M** = MgO) showing the magmatic affinity and the differentiation trend of the studied Ferrar samples from NVL and George V Land. Symbols as in figure **3.15**. Dashed line separates calc-alkalic and tholeiitic fields after IRVINE & BARAGAR (1971). Samples with LOI > 1 wt% are excluded. The chilled margins of Tasmanian Ferrar sills (HERGT et al. 1989b) are included as shaded field for comparison.
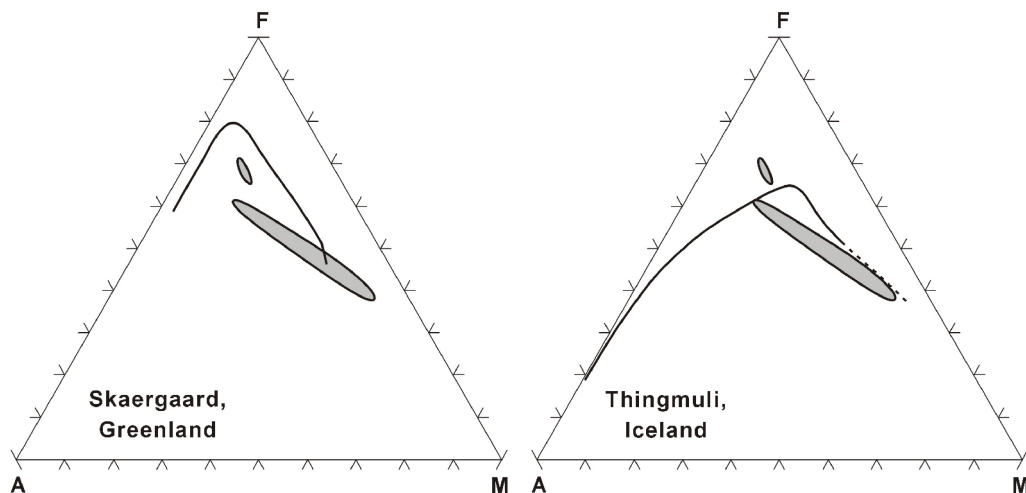
Fig. 3.19 – Ternary AFM diagrams comparing the differentiation trends of the analysed Ferrar samples from NVL and George V Land (grey fields) with those of the rock series of the Tertiary Skaergaard layered intrusion and the Thingmuli volcano (black lines) after WAGER (1960) and CARMICHAEL (1964), respectively. The dashed line, extending the Thingmuli trend in the right diagram to the Mg-rich corner, represents rocks of cumulus origin.

For comparison, figure **3.19** illustrates the AFM variation trends of the Tertiary Skaergaard layered intrusion, Greenland (WAGER 1960) and the rock series of the Tertiary Thingmuli volcano, Iceland (CARMICHAEL 1964). Both examples show an iron-enrichment trend similar to the one shown by the Ferrar tholeiites but with steeper gradients of enrichment in iron and a final abrupt decrease in iron contents. However, the obtained Ferrar trend corresponds rather to that of the Thingmuli rock series than to that of the Skaergaard intrusion. The trend displayed by the Skaergaard tholeiitic rocks is one of the most pronounced in respect of iron-enrichment reported from natural examples. This is noteworthy since the compositional variations within the Skaergaard intrusion are interpreted to result from a single intrusion of magma, which completely crystallised *in situ* in a closed magma chamber, a process of differentiation that will be discussed later on concerning the present Ferrar rock samples.

As already pointed out for the TAS diagram, the application of moderately mobile elements (like the alkalis) in the AFM diagram requires special care when determining the magmatic affinity of any rock suite. Therefore, another discrimination plot after MACLEAN & BARRETT (1993), applying immobile trace element concentrations, is exemplarily used (Fig. **3.20**) in which the analysed Ferrar rocks mainly plot within the tholeiitic field; some samples are transitional to the calk-alkalic magma series.
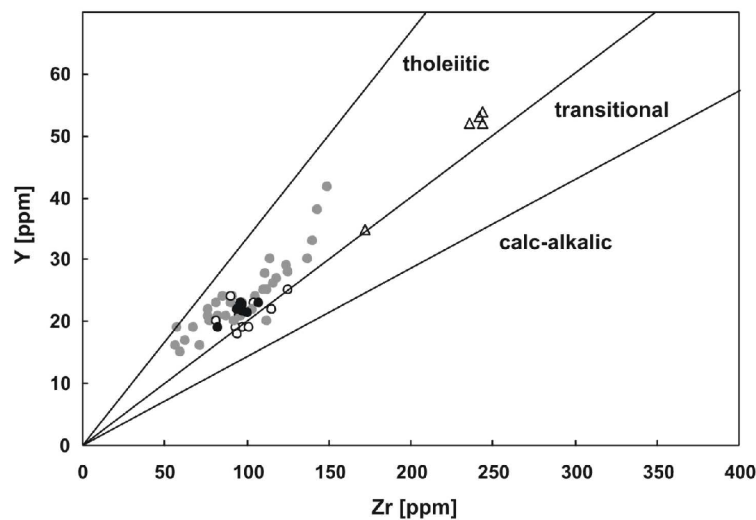
Fig. 3.20 – Magmatic affinity of the analysed Ferrar rocks displayed by variations of Y vs. Zr in the discrimination diagram after MACLEAN & BARRETT (1993) indicating the dominantly tholeiitic nature of the sample material. Symbols as in figure **3.15**.

Furthermore, some basaltic andesite samples have Al_2O_3 contents higher than 17 wt% and thus, match the criteria of high-alumina basalts (16 – 20 wt% Al_2O_3; MIDDLEMOST 1975) implying a calc-alkalic character rather than a tholeiitic given by the immobile trace element signatures. However, these rather high alumina contents might be explained by accumulation of plagioclase. Regardless of the transitional behaviour of some samples, the entire Ferrar rock suite is characterised by a clear tholeiitic affinity suggested by its iron-enrichment trend in the AFM diagram and by the immobile trace element systematics in the Zr – Y plot.

3.3.4 Geochemical Variations

Major and Trace Elements

In view of the large variations in petrographic characteristics and mineral compositions, a wide geochemical range has to be expected, as already indicated by the variations in the TAS and the AFM diagrams. The observed tholeiitic differentiation trend of the analysed Ferrar samples is displayed in detail by strongly varying major and trace element concentrations in figure **3.21** and **3.22** where they are plotted in relation to the Mg-number (Mg#) as differentiation index. Mg# has been calculated from the molar proportions of MgO and FeO from the XRF-analyses as Mg# = $100^*Mg / (Mg+Fe^{2+})$ assuming $Fe_2O_3/FeO = 0.15$.

Mg-numbers ranges from 33 to 74 and from 24 to 31 within the low-Ti and high-Ti series, respectively. Within both series, the decreasing Mg-numbers correlate with an increase of incompatible elements (e.g. FeO, TiO_2, P_2O_5, V, Y, Zr, Cu) whereas compatible elements decrease (e.g. MgO, CaO, Ni, Cr and partly Al_2O_3). The systematic variation trends displayed by most elements are characteristic for co-magmatic rock series developed by fractional crystallisation. The large range of element variations confirms that the magma, from which the investigated rocks were crystallised, has experienced fractionation of mafic phases to strongly varying degrees. A fractionation assemblage consisting of olivine, pyroxene and plagioclase is suggested from the different element variations, e.g. decreasing MgO, Ni, Cr, Ca and Al_2O_3 concentrations with decreasing Mg-number. Detailed interpretations will be discussed below in chapters **4.2** and **4.3**.

Considering the wide chemical variations within the low-Ti rocks, one significant observation is the narrow compositional range (Mg# 59 – 63) of those samples taken in proximity to the chilled margins of different sills and from thin dikes. Assuming that the intruding magma initially was homogeneous in composition, this can easily be attributed to the rapid cooling of magma emplaced into cold country rocks. As already mentioned, these samples referred to as 'chilled margins' do not represent the direct contacts with the host-rocks in order to avoid contamination and alteration. Thus, the small scatter of element abundances in these samples reflects probably the different distances to the contacts, from which the samples were taken. Mg-numbers of samples taken closest to the contacts are restricted to about 62. Their composition widely corresponds to the average composition of chilled margins of Tasmanian sills reported by HERGT et al. (1989b), which are included in some of the following variation plots for comparison.

Moreover, the compositional range shown by the present low-Ti intrusives from the rather restricted sampling area in NVL nearly reflects the entire variations of published data reported from low-Ti sills and dikes from widely separated occurrences within the FLIP (GUNN 1962, 1966, KYLE 1980, BROTZU et al. 1988, HERGT et al. 1989a, 1989b, 1991, HORNIG 1993, WILHELM & WÖRNER 1996, ANTONINI et al. 1999, DEMARCHI et al. 2001). Only a few samples reported in literature extend the observed range towards both directions of more mafic and of higher evolved bulk-rock compositions. Therefore, it is not surprising that the low-Ti samples from sills in George V Land cannot be

distinguished geochemically from those sampled in the Rennick Glacier area in northern Victorialand.
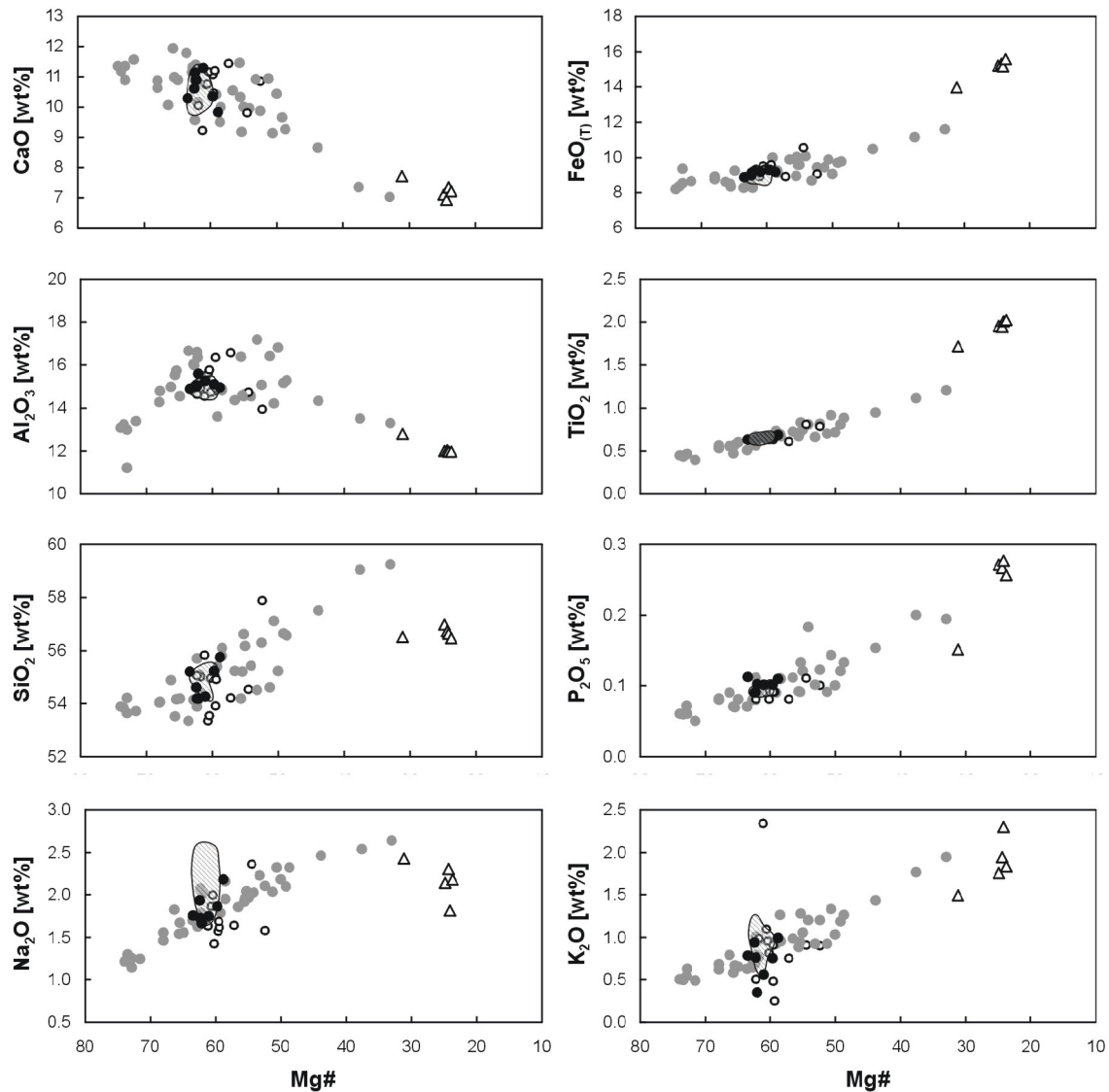
Fig. 3.21 – Variation of selected major elements with Mg# as differentiation index for the entire sample set. All analyses have been recalculated volatile and loss-free to a total of 100 wt%. Symbols as in figure **3.15**. Shaded fields represent compositions of chilled margins of Tasmanian Ferrar sills (HERGT et al. 1989b) included for comparison.

Within the suite of analysed samples, the extrusive low-Ti rocks fall within the compositional range of the low-Ti intrusives. Whereas mobile elements show some evidence of secondary mobilisation, immobile element concentrations in the extrusive low-Ti rocks largely resemble those of the intrusive counterparts at a comparable degree of differentiation. However, the extrusives exhibit no such wide variation in composition (Mg# 53 – 62) as the intrusives. This is in accordance with the homogeneous appearance of the extrusives with respect to crystallinity and modal rock composition compared to the wide petrographical range of the intrusives. This homogeneity results from the relatively rapid cooling of the subaerially extruded magmas. Furthermore,

besides differences in their secondary phase assemblage, no obvious geochemical differences are observable in the extrusives sampled in the two regionally distinct areas at Litell Rocks and at the Monument Nunataks. In general, the analysed compositions of low-Ti extrusives are in good accordance with those reported from the widely distributed lava flow sequences of the Mesa Range, NVL (e.g. MENSING et al. 1984, SIDERS & ELLIOT 1985, FLEMING et al. 1992, 1995, ELLIOT et al. 1995) as well as southern Victorialand (e.g. WILHELM & WÖRNER 1996, ANTONINI et al. 1999).
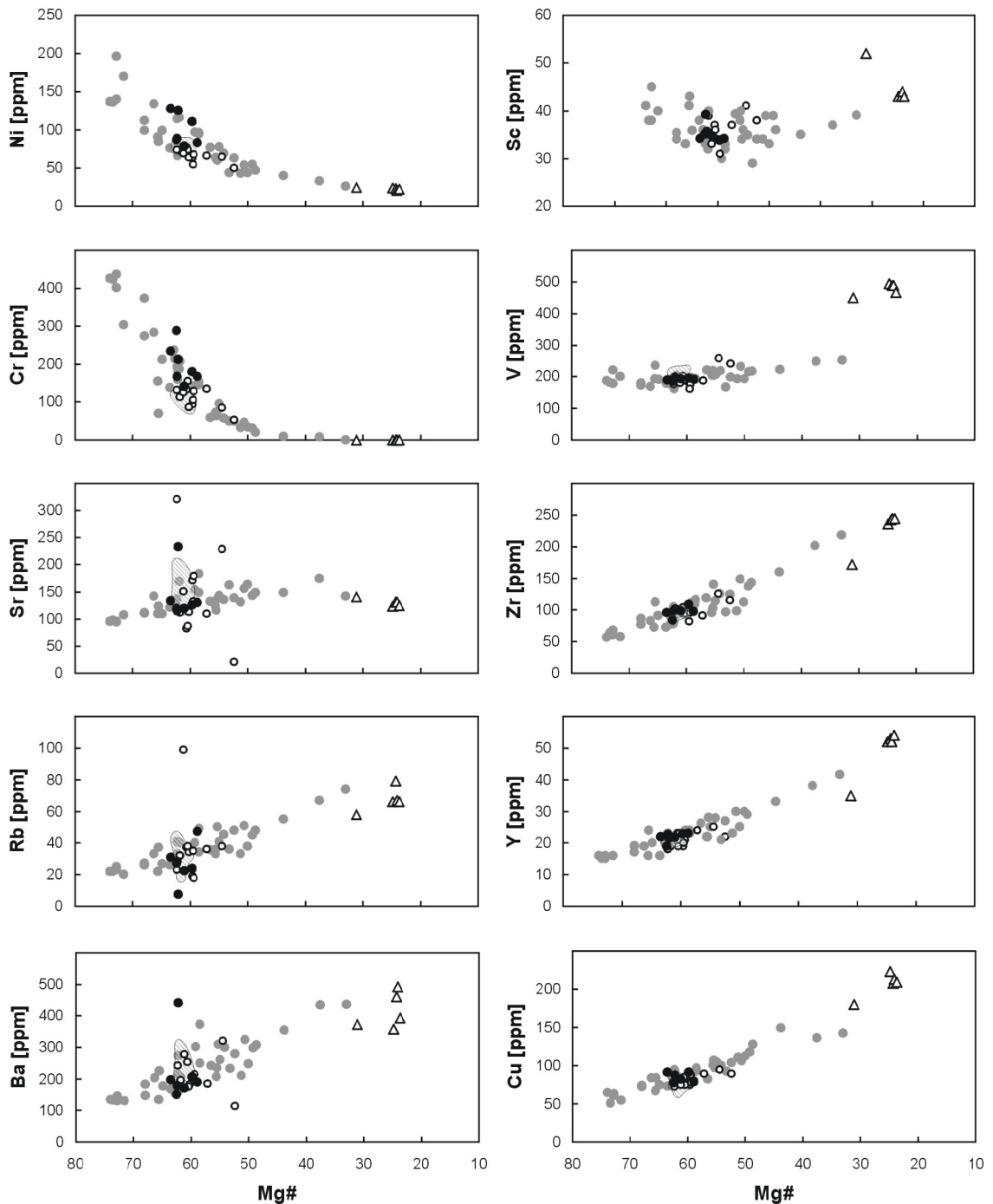
Fig. 3.22 – Variation of selected trace elements with Mg# as differentiation index for the entire sample set. Symbols as in figure **3.15**. Shaded fields represent compositions of chilled margins of Tasmanian Ferrar sills (HERGT et al. 1989b) included for comparison (except for Sc, since no data were available).

Compared to the wide geochemical range among the samples of the low-Ti series, the few high-Ti samples analysed are characterised by a more homogeneous composition, which is in agreement with the rather uniform petrography of the analysed samples, at least of the fine-crystalline high-Ti rocks from Litell Rocks. An exception is high-Ti rock sample RH24 that exhibits a notably coarser crystallinity and slightly deviating element concentrations in all Harker variation diagrams.

Taking the Mg# as differentiation index, the high-Ti rocks exhibit somewhat higher evolved compositions with lower Mg# than all low-Ti samples analysed. In the variation diagrams in figures **3.21** and **3.22**, the high-Ti samples often seem to extend the trends of the low-Ti samples, especially in those showing elements with compatible behaviour (e.g. Ni, Cr, Al_2O_3). However, in some of these plots (e.g. FeO, TiO_2, V), the high-Ti series shows a slight but marked off-set from the low-Ti series (like in the AFM diagram, Fig. **3.18**). Sample RH24 usually plots aside from the other high-Ti samples. Other elements (e.g. SiO_2, Na_2O) even show a contrary behaviour within the high-Ti series compared to the trends exhibited by the low-Ti samples.

It is worth mentioning that the high-Ti rocks are conspicuously homogeneous in composition compared to the low-Ti series, which may also be due to the small number of outcrops studied. For comparison, a compilation of the chemical variations of the present low-Ti and high-Ti samples from NVL and George V Land as well as available data from widely distributed occurrences within the FLIP that have been published over the last decades is given in figure **4.8**.

Compared to published data, the composition of the studied high-Ti rocks from the middle Rennick Glacier area in NVL matches those of high-Ti rocks from the few, widely scattered occurrences from NVL, SVL and the central Transantarctic Mountains (e.g. FLEMING et al. 1992, 1995, ELLIOT et al. 1995, 1999, WILHELM & WÖRNER 1996, ANTONINI et al. 1999). Most of these published data are from extrusive rocks of fine crystallinity, which partly may explain their striking compositional homogeneity. Reported variations for most elements are even within analytical precision (FLEMING & ELLIOT 1988) for these extrusives, but there are a few high-Ti rocks, which extend the narrow chemical range of this magma series, namely those from Brimstone Peak in the Prince Albert Mts., SVL (WILHELM & WÖRNER 1996, ANTONINI et al. 1999). WILHELM & WÖRNER described these samples as being taken from a single unit of about 150 m thickness and of unknown mode of emplacement.

Rare Earth Elements

Likewise major and trace elements, REE abundances cover a wide range (ΣREE 41 – 160 ppm) with a gradual increase of the total REE with decreasing Mg-number of the samples (Fig. **3.23**). The highest concentrations have been measured in the high-Ti sample RH6.

Both low-Ti and high-Ti rock samples show coherent chondrite-normalised REE patterns with enriched element abundances relative to chondritic values (La up to 27 – 106 times chondritic) and a generally smooth, negative slope from La to Yb. $(La/Yb)_N$ ratios vary between 2.8 and 4.0. Thereby, all patterns are characterised by enrichment

of the normalised light REE contents, with $(La/Sm)_{(N)}$ ranging from 2.2 to 2.6, over the heavy REE, which exhibit almost horizontal patterns with $(Gd/Yb)_{(N)}$ ranging from 1.06 to 1.25. These patterns agree with those published for both magma series (e.g. HERGT et al. 1989b, HORNIG 1993, ELLIOT et al. 1995, ANTONINI et al. 1999).

All samples exhibit a negative Eu-anomaly calculated as Eu/Eu*= Eu / √(Sm * Gd). Its magnitude correlates positively with the degree of REE-enrichment and thus, progressively increases with decreasing Mg# from Eu/Eu* = 0.89 in the most primitive low-Ti sample towards 0.71 in the most evolved low-Ti sample as well as in the high-Ti sample RH6.
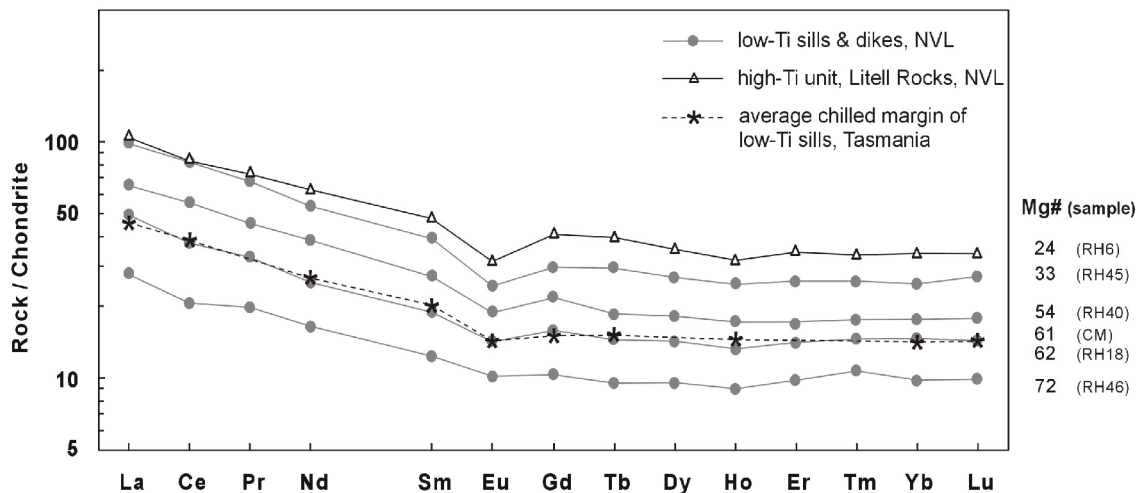
Fig. 3.23 – Chondrite-normalised REE patterns of selected Ferrar samples from the Rennick Glacier area, NVL. The average chilled margin (CM) composition of Tasmanian Ferrar sills (HERGT et al. 1989b) is included for comparison; it nearly matches the composition of a dike (RH18) from the Neall Massif, NVL. Normalisation values according to EVENSEN et al. (1978). Mg-numbers on the right underline the correlation of REE concentrations with bulk-rock chemistry of the distinctly evolved samples.

Platinum-Group Elements

For the Ferrar igneous province, only a few PGE analyses were previously reported, which are from the Dufek layered intrusion (FORD & HIMMELBERG 1991). However, the PGE behaviour in Ferrar rocks has not yet been investigated in more detail. Thus, in addition to the mineral and bulk-rock chemical characterisation of the Ferrar samples, PGE abundances in a subset of 24 samples have been analysed. The sample selection was based on the above outlined results with the purpose of excluding material with signs of strong secondary modification and of completely comprising the petrographic and geochemical variations.

The bulk-rock PGE analyses yield total concentrations reaching from ~ 4 to 40 ppb. In most of the analysed samples, the total PGE abundances correlate with their degree of differentiation: their PGE totals increase with decreasing Mg-numbers. A few samples of more evolved composition than that of the chilled margin samples follow an exceptional trend: their total PGE concentrations decrease with increasing degree of differentiation. In general, the PGE totals are largely a function of the elevated concen-

trations of Pt and Pd, since the concentrations of Ir, Ru and Rh do not vary significantly or are very low (< 1ppb), in some samples even below the limit of detection.

Since most of the PGE have a strong tendency to partition into iron-alloys, their variations are plotted against MgO instead of the Mg-number, which expresses the changes of MgO relative to FeO. The individual PGE show more or less systematic variations with the differentiation degree of the rocks (Fig. **3.24**). Ir consistently behaves as a compatible element with concentrations near the detection limit of 0.1 ppb within the most evolved samples. Ru (not shown) and Rh are rather invariant at very low abundances in the low-Ti rocks but are highly variable in the high-Ti rocks. In contrast to Ir, Pt and Pd show bimodal behaviour during differentiation: Relative to the chilled margin samples of low-Ti Sills (MgO ~ 6 – 7 wt%), the concentrations of these primarily siderophile elements decrease towards higher MgO (> 7 wt%). In more evolved samples (MgO < 7 wt%), two trends are indicated:

- an increase of Pt and Pd with decreasing MgO and
- a decrease of Pt and Pd with decreasing MgO.

For the high-Ti rocks, Pt and Pd (and Rh) exhibit large variations: the coarse-crystalline sample RH24 follows the depletion trend displayed by some low-Ti rocks and the other fine-crystalline high-Ti samples show strongly increased concentrations at almost unchanged MgO contents.
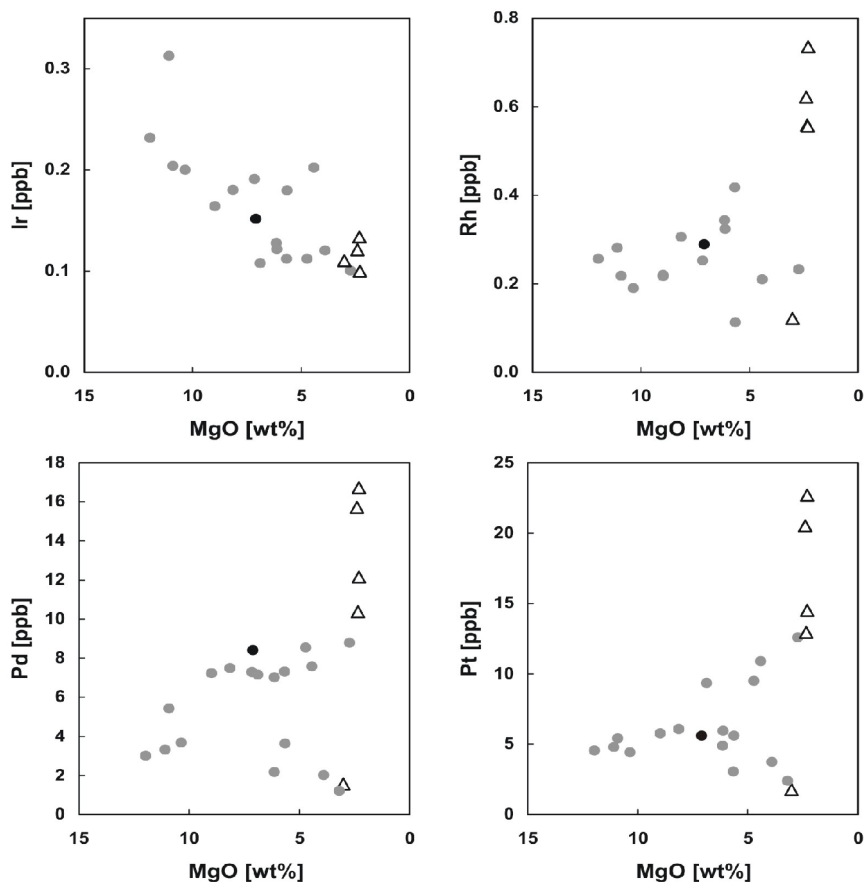
Fig. 3.24 – Variations of bulk-rock Ir, Rh, Pd and Pt concentrations [ppb] with MgO [wt%] as differentiation index for the analysed Ferrar low-Ti and high-Ti samples. Symbols as in figure **3.15**.

The distinct geochemical behaviour of the individual PGE results in a pronounced fractionation of the PGE from each other. This is clearly illustrated by the primitive mantle-normalised PGE patterns for the Ferrar igneous rocks in figure **3.25**, in which the PGE are plotted in the order of descending melting point. All samples exhibit an increase of normalised values from Ir to Pd indicating an appreciable enrichment of the PPGE over the IPGE regardless of increasing or decreasing Pt and Pd concentrations for more evolved samples. This fractionation between the PGE is more pronounced for high-Ti than for low-Ti samples (Fig. **3.26**). The Pd/Ir ratios vary from ~ 10 to ~ 170 for all samples, mostly according to the degree of differentiation (Fig. **3.27**).
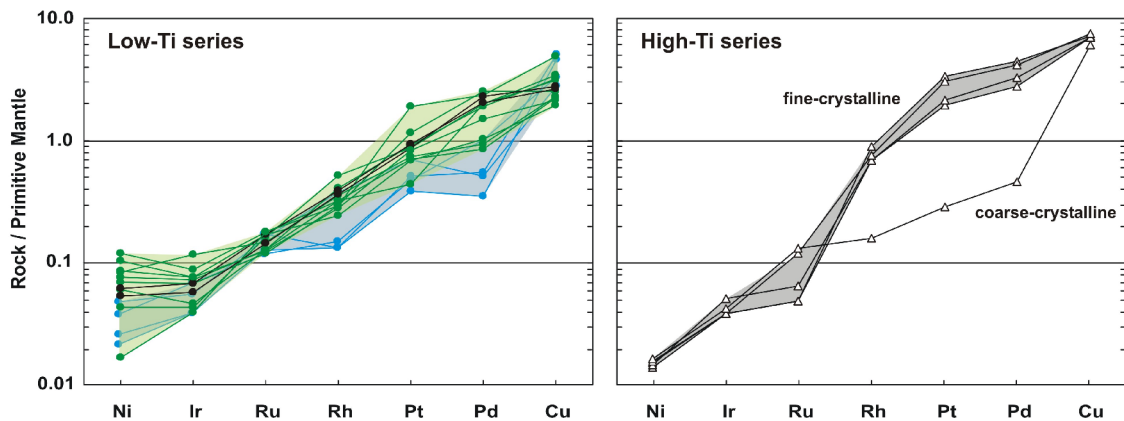
Fig. 3.25 – Primitive mantle-normalised Ni-PGE-Cu abundance patterns for the analysed Ferrar low-Ti and high-Ti samples showing the fractionation between the individual PGE. Normalisation values according to MCDONOUGH & SUN (1995). Differently coloured symbols in the left plot: black – fine-crystalline samples, green – increasing Pt + Pd at lower MgO, blue – decreasing Pt + Pd at lower MgO.
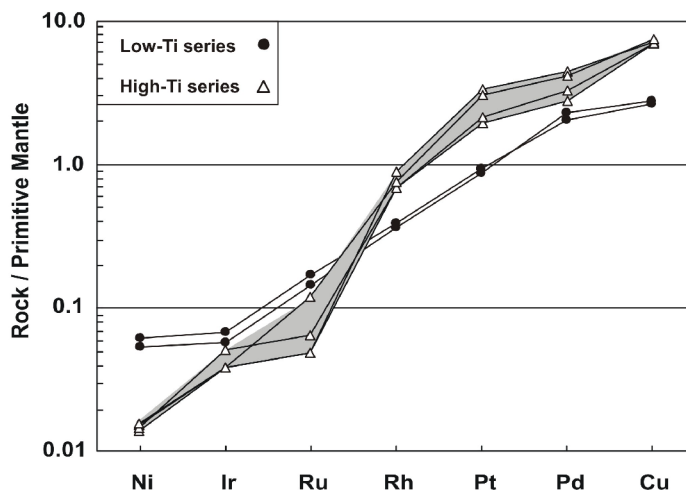
Fig. 3.26 – Comparison of primitive mantle-normalised Ni-PGE-Cu patterns for fine-crystalline low-Ti and high-Ti samples indicating the more pronounced PGE fractionation (steeper positive slope from Ni to Cu) for the high-Ti than the low-Ti samples.

For all low-Ti and high-Ti samples, concentrations of Ir, Ru and Rh are depleted relative to the primitive mantle composition. In most low-Ti samples, Pt and Pd have abundances similar to primitive mantle, but the most primitve and some of the more

evolved samples are slightly depleted in Pt and Pd, while low-Ti samples with most evolved whole-rock composition are enriched in both elements. In the coarse-crystalline high-Ti sample RH24 Pt and Pd are depleted relative to primitive mantle, but both elements are variably enriched in the homogeneous fine-crystalline high-Ti samples.
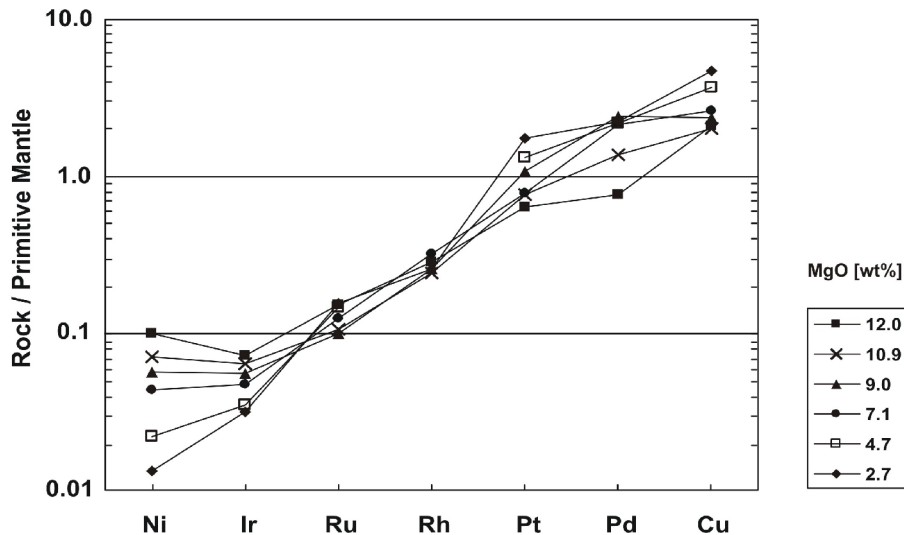
Fig. 3.27 – Primitive mantle-normalised Ni-PGE-Cu abundance patterns for selected Ferrar low-Ti samples emphasising the correlation of the degree of PGE fractionation with the bulk-rock chemistry of the variably evolved samples indicated by their MgO contents.

3.4   SUMMARY

The results of this study, including the petrographic observations as well as the compositions of primary mineral phases and whole rocks from NVL and George V Land, cover almost the entire range of compositional characteristics reported from previous investigations for widely separated occurrences from the entire Ferrar province.

Variations of mineral composition including iron-enrichment trends of low-Ca and high-Ca pyroxenes and an increase in Na_2O in plagioclase correlate with the bulk-rock chemical variations, which are displayed by decreasing concentrations of compatible elements and increasing concentrations of incompatible elements. These features suggest that the magma, from which the investigated rocks formed, underwent significant crystal fractionation during differentiation.

The systematic variations of mineral and whole-rock compositions as well as the estimated crystallisation parameters give evidence that the magmas experienced at least two periods of considerable differentiation, which probably took place under different conditions (e.g. higher and lower pressures). The two processes of fractional crystallisation that are to distinguish are 1) a differentiation process prior to ascent into the crust followed by 2) an *in situ* differentiation at lower pressures after magma emplacement in the upper crust or at the surface. Both processes will be described in more detail in the following chapters considering their influence on the compositional evolution of both magma series.

4   DISCUSSION

As outlined above, the newly investigated Ferrar rocks from NVL and George V Land display a wide range of petrographic, mineral and whole-rock chemical characteristics that are consistent with results previously published for Ferrar tholeiites from different areas in northern and southern Victorialand, the central Transantarctic Mountains (TAM) and Tasmania (e.g. GUNN 1962, 1965, 1966, KYLE 1980, SIDERS & ELLIOT 1985, BROTZU et al. 1988, HERGT et al. 1989a, 1989b, 1991, HORNIG 1993, ELLIOT et al. 1995, 1999, MOLZAHN et al. 1996, ANTONINI et al. 1999, DEMARCHI et al. 2001).

Aside from the general description of the petrogenesis of the Ferrar magmas, the main focus of this study is directed towards the distinct evolution of the low-Ti and high-Ti magma series. The compositional divergence of both series could reflect either differences in magma source composition, differences in conditions of melting or differentiation, differences in contamination by crustal rocks or any combination of these factors.

Based on the new data set and considering the published data, processes concerning the petrogenesis of the Ferrar magmas will be discussed in reverse chronological order as they modified the magma composition. Before magma source characteristics and effects of partial melting and crystal fractionation on magma composition can be adequately assessed, it is necessary to characterise processes that influenced the magma composition during and after its emplacement within crustal rocks or at the surface. Thus, post-magmatic alteration after cooling of the magma will be discussed at first, followed by the low-pressure *in situ* differentiation occurred during and immediately after magma emplacement.

4.1   ALTERATION

As indicated by the petrographic and the geochemical data, the present Ferrar rocks experienced a more or less pronounced secondary modification due to late stage hydrothermal activity. This alteration process mainly influenced the extrusive Ferrar rocks, whereas the composition of intrusives is not significantly affected. However, highly mobile elements are interpreted with caution.

Noteworthy are the secondary mineral phases formed by this hydrothermal alteration process in the extrusive rocks, because the observed secondary assemblages show distinct differences in rocks from Litell Rocks and from the Monument Nunataks. Rock samples from the latter exhibit an assemblage of several types of zeolites, calcite, smectite, chlorite, and smectite-chlorite mixed-layer minerals, which are characteristic for the metamorphic zeolite facies. In contrast to that and confirming published results of SKINNER et al. (1981), no zeolites were observed in the few examined samples from Litell Rocks more than 100 km to the north. Instead, the assemblage consists of quartz, chlorite, prehnite, pumpellyite, and epidote, which requires a higher metamorphic temperature. For Litell Rocks, estimated alteration temperatures of 300 – 400 °C were reported by HORNIG (1993) to indicate the transition from the zeolite to the greenschist facies. Even if this temperature range is slightly overestimated (FREY & ROBINSON

1999), a marked difference existed between the two regions with respect to the meta-morphic grade. Thus, a more elevated thermal gradient can be suggested in the vicinity of Litell Rocks during the alteration events.

Several workers already denoted the intense alteration of Ferrar extrusives. According to these studies, the geochemically and petrographically verified alteration of the new samples can be attributed to Cretaceous thermal events, which coincide with the separation of Australia from Antarctica (~ 95 – 135 Ma; DELISLE & FROMM 1984, 1989, FLEMING et al. 1992, MOLZAHN et al. 1999). Furthermore, this alteration event may be associated with the formation of the Rennick Graben as a failed rift arm (ROLAND & TESSENSOHN 1987). Alternatively, FLEMING et al. (1999) documented different $^{40}Ar/^{39}Ar$ ages for low-temperature apophyllite in lavas from the central TAM (114 – 133 Ma), southern Victorialand (95 – 114 Ma) and northern Victorialand (76 – 100 Ma), which were interpreted to reflect changes in the hydrologic regime related to the uplift of the TAM. Initial stages of the uplift in early Cretaceous times were supported by fission-track studies from FITZGERALD & STUMP (1997).

The diversity of secondary phase assemblages, their different formation ages and the distinct interpretations inferred for geographically widespread areas emphasise the complexity of these post-Jurassic alteration events. Thus, better-defined conditions of formation of secondary phases, attainable from detailed studies, may give more information about tectonothermal and hydrothermal activities in Cretaceous times. In particular, such a study may contribute to the evaluation of the formation of the Rennick Graben structure in NVL.

Nevertheless, the further discussion will not consider the present extrusive samples, since almost all of them experienced mobile element disturbances to various degrees. In spite of this observation, the literature data of low-Ti lava flows will partly be included in some of the further considerations for the purpose of comparison and compositional completeness.

4.2   IN SITU DIFFERENTIATION

In most of the variation diagrams shown, bulk-rock major and trace element concen-trations exhibit systematic trends as expected for a typical differentiation series formed by fractional crystallisation. There is evidence, that, to a certain extent, the Ferrar magmas experienced this fractionation during an *in situ* differentiation process after the magma emplacement within upper crustal levels or at the surface. A brief overview on some general characteristics of *in situ* differentiated magma bodies will be given before discussing the overall variations obtained from the studied Ferrar rock samples.

Over the last decades, a vast number of detailed investigations on *in situ* differentiation processes have been carried out by studying layered intrusions such as the Skaer-gaard intrusion (e.g. WAGER & BROWN 1967, MCBIRNEY & NOYES 1979, MCBIRNEY 1996) and numerous high-level sills (e.g. GUNN 1962, NASLUND 1989, GIBB & HENDERSON 1992, 1996, MARSH 1996, 1998, 2002, MARKL & WHITE 1999 and LATYPOV 2003a, 2003b) to mention a few amongst many others. Layered intrusions commonly exhibit a very complex internal stratification documented by subhorizontal rhythmic and

cryptic layering of different types of cumulates (e.g. gabbro, pyroxenite and anorthosite). These sequences reflect a long history of crystallisation characterised by compositional changes of mineral solid solutions in the order of decreasing liquidus temperature. As complex as these compositional variations in individual intrusions are the various models describing the solidification of the large batches of magma.

Some of the best insights into the processes producing (*in situ*) differentiated magma bodies are given by studies of basic-ultrabasic sills. They typically comprise complete rock sequences including distinctly evolved sections enclosed by a lower and an upper chilled contact zone. These chilled contacts form rather quickly for a magmatic body intruding relatively cold country rocks. Within the *in situ* crystallisation model, these rapidly cooled margins of intrusions are assumed to represent the magma composition at the time of emplacement. Since this magma has not experienced further fractionation, it provides evidence of the pre-emplacement magma composition. Nevertheless, numerous studies on sills and layered intrusions show that the chilled margins often exhibit higher evolved compositions than the bulk-intrusion (LATYPOV 2003a). This lack of mass-balance in most natural basic intrusions studied is not satisfactorily explainable in the context of the classic *in situ* crystallisation model; for alternative explanations see LATYPOV (2003a, 2003b).

An often discussed topic is the formation of different types of compositional profiles observed within various sheet-like intrusions (including some Ferrar low-Ti sills) of several hundred metres of thickness, which supposedly have been generated from a single injection of initially phenocryst-poor magma. Based on the shape of the variation of modal mineralogy or certain major and trace elements as function of stratigraphic height, three main types of compositional profiles are identified: S-, I- and D-shaped profiles (GIBB & HENDERSON 1992, MARSH 1996). Among these, the most extensively *in situ* differentiated magma bodies known are sills with well-developed "S-shaped" profiles (LATYPOV 2003b). These S-shaped crystal distribution and chemical variation patterns are classically ascribed to gravity settling since most of these intrusions are characterised by accumulation of early-crystallised mineral phases with primitive compositions in lower parts and by upward migration of evolved residual melts into higher, later crystallising parts. From the results of an increasing number of recent studies, many authors recognised that modifications of the very simplified model of gravity-induced crystal settling and convection are required.

LATYPOV (2003b) critically reviewed the effectiveness and importance of different mechanisms explaining the separation of crystals from the melt and hence the formation of the compositionally distinct profiles mentioned above. These processes include gravity-driven settling of crystals (already present in the magma prior to its emplacement or newly crystallising in the magma reservoir), flow differentiation (e.g. MARSH 1996, MARSH & PHILIPP 1996), multiple intrusions of chemically distinct magmas (e.g. GIBB & HENDERSON 1992) or convection of refractory components within the crystal-liquid mush during *in situ* differentiation (TAIT & JAUPART 1996). Irrespective of the detailed physical processes leading to extensively differentiated magma bodies, the following two sections discuss the variations of major and trace elements as well as platinum group elements in the framework of the *in situ* differentiation process

combined with the systematically changing mineralogical features observed for the studied Ferrar rocks.

4.2.1 Evidence of *In Situ* Differentiation from Major and Trace Elements

Low-Ti Series

The majority of the samples analysed within this study were taken from a number of sills at different stratigraphic heights, depending mainly on accessibility. Within this suite of samples, the bulk-rock major and trace element trends (Fig. **3.21** and **3.22**) are consistent with the determined variations of the petrographic and mineral chemical features. Although no systematic sampling throughout individual intrusions was performed during the fieldwork, the observed variations can be correlated with the stratigraphic position within the sills, where the field relations are unambiguous. These correlations will be discussed in the following in consideration of published geochemical data from occurrences of the entire Ferrar province, which are compiled in figure **4.1.**

One of the most evident features supporting a major influence of *in situ* differentiation on Ferrar magma evolution is the compositional homogeneity of very fine-crystalline rocks taken proximal to the chilled margins of sills and dikes as well as from thin lava flows. These samples exhibit a narrow compositional range (Mg# ~ 60 – 62, SiO_2 ~ 55 wt%) giving no evidence of further *in situ* differentiation. This observation is in good accordance with results from HERGT et al. (1989), who reported a similar chemical composition for chilled margins of Ferrar sills in Tasmania (see figures **3.21** and **3.22** for comparison). Although natural examples displaying similarity between the composition of the chilled margins and the bulk-intrusion are rare (LATYPOV 2003a), the chilled margin samples of low-Ti sills investigated within this study are assumed to represent the best approximation of composition of the pristine Ferrar magma, at least of the low-Ti series, since further differentiation was precluded by rapid cooling.

This assumption is furthermore supported by the fact that these chilled margin samples contain large phenocrysts of the most primitive compositions analysed, both ortho-pyroxene and plagioclase (Fig. **3.3, 3.4, 3.5, 3.7**). These euhedral to subhedral phenocrysts have a homogeneous composition, occur partly in glomerophyric clusters, do not contain inclusions of other minerals and are therefore believed as being crystallised slowly at depth prior to magma emplacement within the crust. Referring to this, LATYPOV (2003a) discusses the intratelluric versus *in situ* formation of phenocrysts and their general importance during the *in situ* differentiation process. He questions that size, morphology and composition provide unambiguous evidence for their intratelluric origin. However, the modal abundances of these phenocrysts in the chilled margin samples of Ferrar sills do not exceed a few percent indicating the predominantly phenocryst-poor nature of the Ferrar magma at the time of its emplacement. Due to their low amounts, these phenocrysts did not have significant impact on the evolution of the bulk-rock composition during *in situ* differentiation as the actually *in situ* crystallised minerals definitely did have. This furthermore explains why

the chilled margin samples do not exhibit the most primitive bulk-rock composition although they include the most primitive phenocrysts.
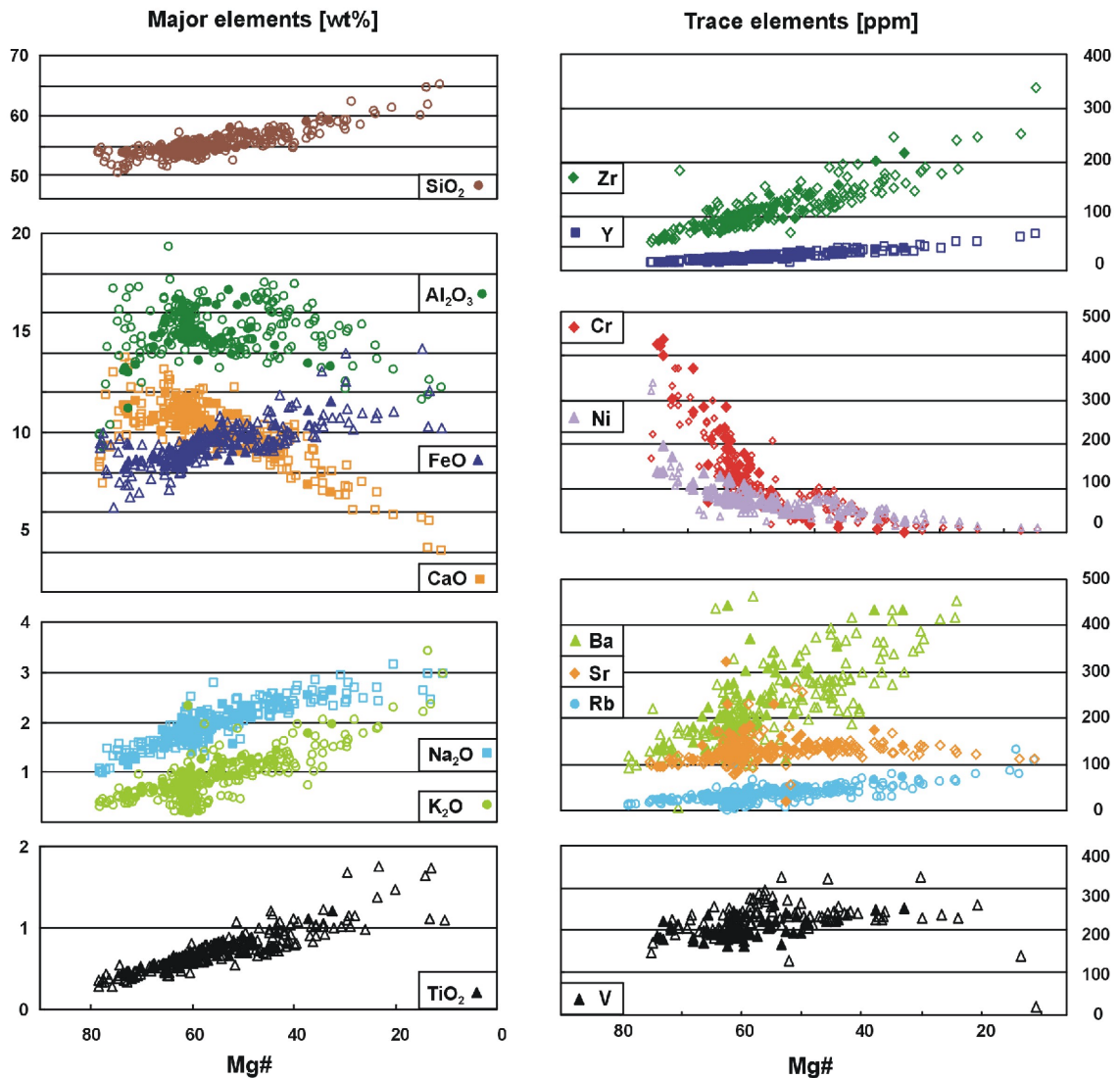
Fig. 4.1 – Variations of selected major and trace element concentrations with the Mg-number of the studied Ferrar low-Ti rocks (solid symbols) from northern Victorialand and George V Land as well as of published low-Ti rocks from widely separated Ferrar occurrences in northern and southern Victorialand, the Transantarctic Mountains and Tasmania. Literature data are from GUNN (1965, 1966), MENSING et al. (1984), SIDERS & ELLIOT (1985), BROTZU et al. (1988), HERGT et al. (1989a, 1989b, 1991), FLEMING et al. (1992, 1995), ELLIOT et al. (1995, 1999), WILHELM & WÖRNER (1996), ANTONINI et al. (1999), DEMARCHI et al. (2001). Note the different scales of concentrations. The scatter of concentrations of mobile elements (Na$_2$O, K$_2$O, Sr, Ba, and Rb) at Mg# ~ 60 can partly be attributed to secondary element mobilisation, since most of the extrusive rocks have Mg-numbers about 60.

Assuming the chilled margins represented the magma composition at the time of emplacement with Mg# ~ 60, the magma developed chemically into two opposite directions during the course of *in situ* differentiation: one of accumulation of early crystallised, primitive mineral phases and a second one formed by subsequent concentration of SiO$_2$ and incompatible elements. Certainly, this 'bimodal' evolution and the

causative physical processes in particular, e.g. the convection driving the separation of crystallising phases subsequently accumulating from the intercumulus liquid, are much more complex as demonstrated for different natural examples by e.g. PHILPOTTS et al. (1996), TAIT & JAUPART (1996), MARSH (2002) and LATYPOV (2003b). However, the obtained individual element variations within the suite of analysed Ferrar low-Ti rocks, as illustrated in figures **3.21** and **3.22**, are explainable as follows:

Geochemically primitive rocks, characterised by the presence of magnesian orthopyroxene, pigeonite and augite, calcic plagioclase and low contents of mesostasis, occur typically in lower parts of the sills. Due to the accumulation of variable amounts of these mineral phases, Mg# increases from ~ 60 in chilled margin samples to ~ 74 in cumulates. The most primitive Ferrar low-Ti rocks (Mg# ~ 79, MgO ~ 17 wt%, Fig. **4.1**) have been reported by GUNN (1965, 1966) and MARSH & PHILIPP (1996) from sills of a about few hundred metres in thickness in the Transantarctic Mts. They describe distinctly evolved zones in the vertical profile of ~ 350 m with concentrations of up to 70 vol% orthopyroxene of strongly zoned composition, which possibly can be interpreted to represent inverted pigeonite similar to the few observed in some samples of this study. However, the origin of these accumulated pyroxenes is unambiguous and the question, if they crystallised as phenocrysts under conditions of higher pressure, e.g. prior to or during magma ascent, or if they nucleated and grew *in situ* after the magma emplacement is not at all clear. The latter interpretation is favoured here.

The Mg# increase within the cumulates correlates with increasing concentrations of compatible elements such as MgO, Ni, Cr and CaO due to the high partition coefficients of these elements into the accumulated phases (pyroxenes, plagioclase), whereas concentrations of moderately compatible to incompatible elements (e.g. Na_2O, K_2O, TiO_2, P_2O_5, Y, Zr) decrease. It is noticeable that the most magnesian of the analysed rocks (Mg# ~ 74, MgO ~ 12 wt%) does not contain orthopyroxene but appreciable amounts of Mg-rich pigeonite, which either crystallised *in situ* or during magma transfer through the crust. Silica and iron are nearly unchanged and decrease only slightly towards the most magnesian rocks due to the similarity of the silica and iron concentrations of the accumulated mafic low-Ca pyroxenes and the residual liquid. CaO only faintly increases indicating the contemporaneous accumulation of calcic plagioclase and high-Ca clinopyroxene, both of which in turn are outbalanced by the high abundances of low-Ca pyroxenes. This dominance of low-Ca pyroxene fractionation during the cumulate stage of *in situ* differentiation is more significantly shown by the most mafic Ferrar low-Ti rocks reported by GUNN (1965, 1966) from sills in the Transantarctic Mts., which exhibit increasing Mg-numbers up to 79 correlating with a steep decrease in CaO (Fig. **4.1**). The predominant pyroxene accumulation compared to plagioclase furthermore explains the decrease of Al_2O_3 (Fig. **4.1**) and the increasing CaO/Al_2O_3 ratio (Fig. **4.2**) towards higher Mg-numbers. This is also shown by the variations of Sc and Y and the Sc/Y ratio, since Sc is extracted preferentially by clinopyroxenes due to a partition coefficient of $D_{Sc} > 1$ (e.g. EWART et al. 1973, ARTH 1976), whereas Y is incompatible in both pyroxenes and plagioclase (e.g. GREEN et al. 1989, BINDEMAN et al. 1998).
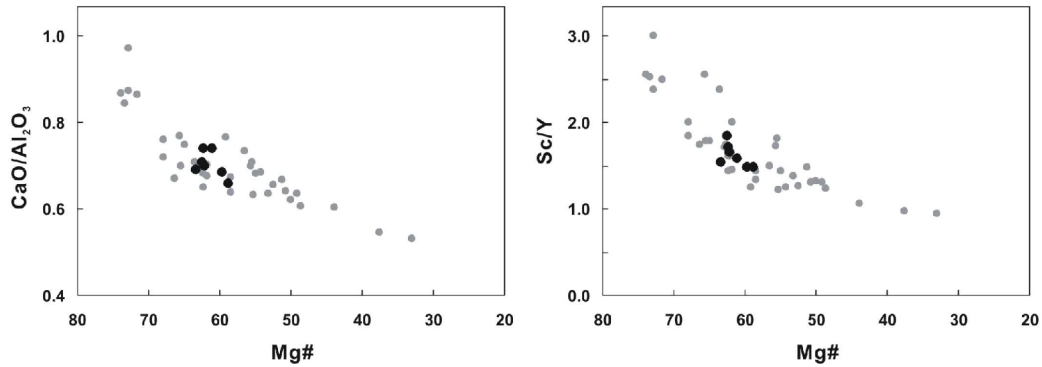
Fig. 4.2 – Variation of the CaO/Al$_2$O$_3$ and Sc/Y ratios with Mg# of the analysed Ferrar low-Ti rocks indicating the importance of high-Ca clinopyroxene fractionation during the *in situ* differentiation. Symbols as in figure **3.15**.

The proceeding magma evolution is characterised by crystallisation of clinopyroxenes and plagioclase which progressively become more iron-enriched and increasingly sodic, respectively, towards the later fractions and thus, in a simplified manner, upwards in the sequence. These progressive changes with increasing height in the intrusive profile resemble those exemplarily shown by the compositional variations within the Dufek intrusion (HIMMELBERG & FORD 1976, ABEL et al. 1979) and the Skaergaard intrusion (WAGER & BROWN 1967). Correspondingly, these higher differentiated rocks (Mg# < ~ 60) from upper sections of low-Ti sills exhibit a steady decrease of the Mg# to ~ 33 correlating with a further decrease of MgO, CaO, Al$_2$O$_3$, Ni, Cr and an increase of FeO, TiO$_2$, SiO$_2$, Na$_2$O, K$_2$O, Ba, Rb, Y, Zr and Cu. Towards the most differentiated composition, the trends of decreasing CaO/Al$_2$O$_3$ and Sc/Y ratios flatten, indicating an increased importance of crystallisation of plagioclase of more sodic composition in the later fractions. The role of plagioclase fractionation is further supported by the increasing Eu anomaly displayed by the most evolved samples (Fig. **3.23**) and the nearly unchanged Sr concentrations. This corresponds to the observation that the modal abundance of plagioclase slightly increases whereas those of pyroxenes decrease during the course of *in situ* differentiation.

The fact that the overall iron contents only moderately increase, can be attributed to the large abundance of Fe-poor pyroxenes accumulated during early fractionation stages, which is counterbalanced by the smaller amount of Fe-rich pyroxenes crystallised during later stages of progressive differentiation. This general increase of FeO correlates well with an increase of TiO$_2$, irrespective of the minor amounts of TiO$_2$ incorporated in the crystallising pyroxenes and plagioclase (< 0.8 wt% and < 0.1 wt%, respectively). The increasing bulk-rock TiO$_2$ contents are in accordance with Fe-Ti oxides occurring more frequently in rocks formed at advanced stages of differentiation. Similar to iron, vanadium concentrations only slightly increase during proceeding differentiation, since V substitutes in traces for Fe^{3+} in low-Ca and high-Ca pyroxenes (aside from oxides) according to the partition coefficients determined by REID (1983). As the pyroxenes become successively iron-enriched, V becomes enriched as well in rocks with higher amounts of iron-rich pyroxenes. Besides, the increasing bulk-rock V concentrations furthermore reflect its enrichment in the residual liquid. However, the

very few most evolved low-Ti Ferrar rocks of dacitic composition (Mg# ~ 11, MgO < 1 wt%), reported by GUNN (1962, 1966) and BROTZU et al. (1988), show decreasing TiO_2, FeO and V concentrations (Fig. **4.1**) indicating that Fe-Ti oxides have been fractionated leaving a slightly Fe-Ti-V depleted residual liquid at the very late stages of *in situ* differentiation.

Concomitantly, SiO_2 gradually increases correlating with an increase of the modal content of poorly crystallised silica- and alkali-rich mesostasis or graphically intergrown quartz and alkali feldspar. Such micropegmatite, derived from the last few percent of remaining melt fraction, sometimes segregated in so-called coarse pegmatitic schlieren as described for several Ferrar sills. After MARSH (2002), these subhorizontal veins and lenses of silicic or pegmatitic segregations, found at distinct horizons in the upper half of basaltic sills with bulk-compositions of 50 – 55 wt% SiO_2, show silica-enrichment over the host basalt of up to 60 – 65 wt%. Similar granophyric late-stage segregations have been described from several igneous provinces, for example from the 660 m thick Basistoppen Sill in East Greenland by NASLUND (1980) or from thick subaerial basalt flows in the Columbia River Basalt province by PUFFER & HORTER (1993), who discussed their main characteristics and origin.

In conclusion, the observations discussed above are comparable to the results obtained by detailed investigations on single Ferrar sills from e.g. the McMurdo Dry Valleys in the central Transantarctic Mountains (GUNN (1962, 1966, MARSH & WHEELOCK 1994, WHEELOCK & MARSH 1993, MARSH & PHILIPP 1996, MARSH 1996, 1998, 2002) and from the Prince Albert Mountains (SVL) (WILHELM & WÖRNER 1996, DEMARCHI et al. 2001). Their interpretation that the documented compositional variations and their stratigraphic correlations resulted from a considerable low-pressure *in situ* differentiation widely agrees with the petrographic, mineral and whole-rock chemical variations observed in the present Ferrar low-Ti sills from NVL. The *in situ* crystal fractionation model is furthermore supported by the parallel REE patterns and their correlation of absolute concentrations with the bulk-rock Mg-numbers, since closed-system fractionation can result in considerable fractionation of the REE (BERNSTEIN et al. 1998).

High-Ti Series

Taking into account the large variations within the low-Ti series, only minor petrographic and geochemical variations are observed for the investigated rocks of the high-Ti series that exhibit Mg-numbers between 31 and 24 and SiO_2 contents of 56.5 – 57 wt% (Fig. **3.21** and **3.22**). Considering only the fine-crystalline high-Ti rocks from Litell Rocks (Mg# ~ 24 – 25), no significant evidence of *in situ* differentiation is detectable indicating their rapid cooling after magma emplacement. This is in agreement with the smaller range of crystallisation temperatures estimated from the mineral chemistry compared to the larger temperature range for the low-Ti rocks. Furthermore, this uniformity widely corresponds to the majority of published results from high-Ti occurrences from elsewhere within the FLIP, since almost all of them are described as lava flows of generally homogeneous composition (e.g. FLEMING et al. 1992, 1995, ELLIOT et al. 1999).

However, the coarse-crystalline high-Ti sample RH24 from a sill in the Alamein Range shows a deviating, less evolved composition (Mg# ~31) with lower concentrations of iron, titanium and incompatible elements. In most variation diagrams, this sample RH24 seems to fill the compositional gap between the two magma series and thus to extend the well-defined fractionation trends displayed by the low-Ti series. The deviating composition of this intrusive high-Ti sample implies a greater influence of *in situ* differentiation on the high-Ti magma composition than assumed so far by considering almost exclusively extrusive high-Ti occurrences.

Due to the small number of high-Ti samples analysed within this study, the variation trends within the Ferrar high-Ti series are difficult to assess. Therefore, published data from previously studied high-Ti occurrences are included for comparison. The narrow compositional range obtained for extrusive high-Ti rocks is mainly extended by the rocks from a > 120 m thick high-Ti occurrence within the Prince Albert Mountains, southern Victorialand, studied by WILHELM & WÖRNER (1996) and ANTONINI et al. (1999). This is demonstrated by the variations of selected major and trace elements in figure **4.3**, which again emphasise that *in situ* differentiation influenced the composition of the high-Ti magmas as well as those of the low-Ti magmas, but is only pronounced enough to be identified in magma bodies of considerable thickness. Even if this process was not as significant as for the low-Ti magma series, there are some noteworthy characteristics.

Since there is no considerable variation of the Mg-numbers for the entire high-Ti series (partly due to the positive correlation of MgO and FeO), the major and trace element variations are plotted against SiO_2 as a measure of the degree of differentiation (Fig. **4.3**). The increase of SiO_2 from 55.7 to 59.1 wt% correlates with an increase in Al_2O_3 and decreasing contents of MgO, FeO, CaO, TiO_2 and V. Na_2O and most of the trace elements remain virtually unchanged or otherwise do not exhibit clear correlation with SiO_2. Some of the scatter of these elements, especially those of low concentrations, may partly be attributed to interlaboratory bias and to the different analytical techniques applied for determination. Abundances of mobile elements (e.g. Ba) may be modified by alteration to variable extents.

Since most authors have not reported variations of modal mineral abundances (which may be only moderate) for the distinctly evolved high-Ti rocks, the geochemical changes can poorly be constrained in detail. Nevertheless, the element variations indicate an *in situ* fractionation assemblage consisting of plagioclase, clinopyroxenes and oxides, which corresponds to the petrographic observations for the present high-Ti rocks. Comparable to the low-Ti series, the fine-crystalline high-Ti rocks (e.g. from Litell Rocks, NVL) can be interpreted to reflect the magma composition at the time of magma emplacement without further considerable changes during *in situ* differentiation. Assuming magma emplacement in a sheet-like magma body, whether a sill or a flow of considerable thickness, starting from the melt composition of the rapidly cooled margins, mineral phases crystallised with subsequently more evolved composition. Their subsequent accumulation in different stratigraphic heights caused the geochemical variation trends displayed by the entire suite of published high-Ti rocks (Fig. **4.3**).
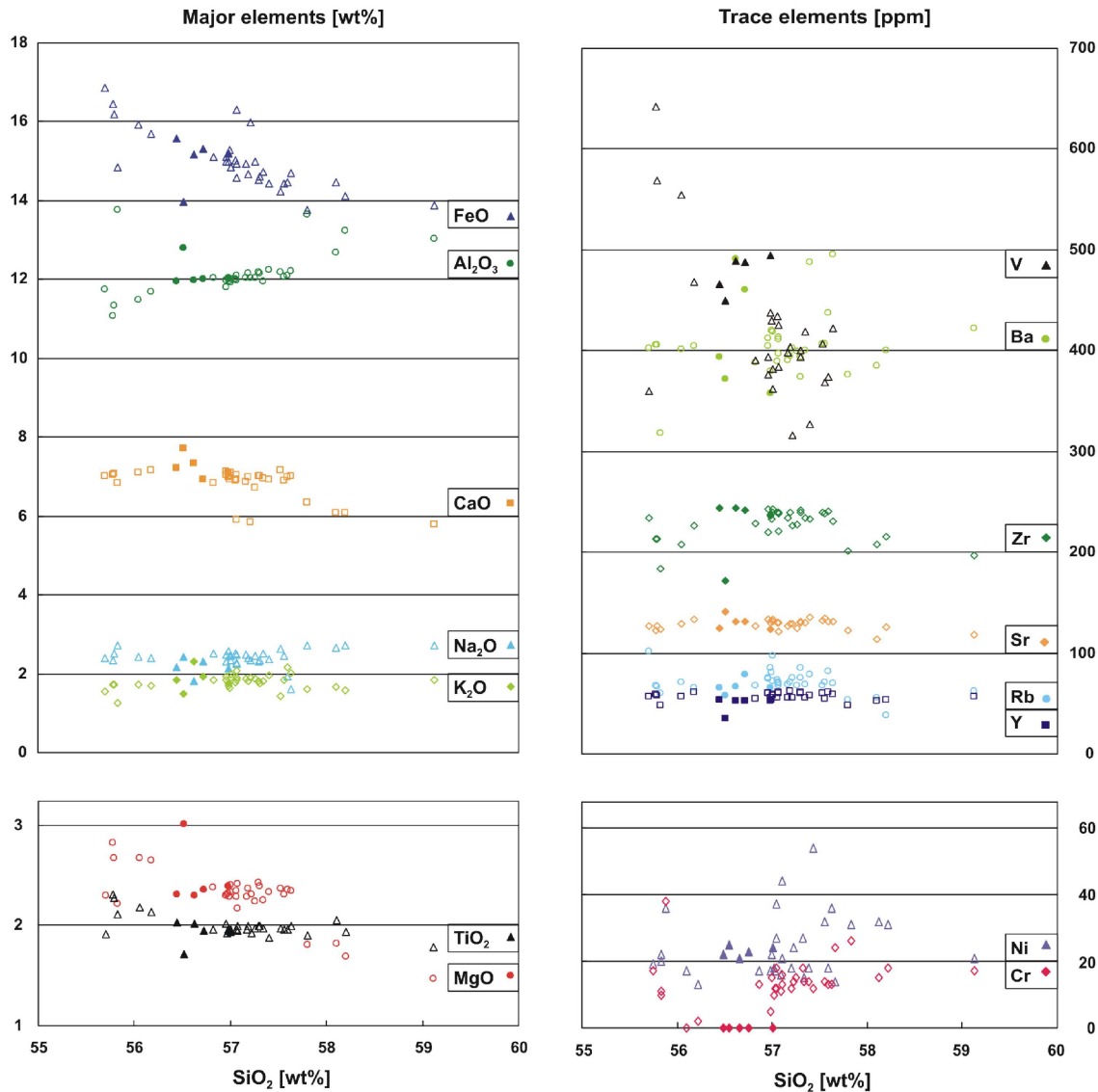
Fig. 4.3 – Variations of selected major and trace element concentrations with SiO_2 of the analysed (solid symbols) Ferrar high-Ti rocks from northern Victorialand as well as of published (open symbols) Ferrar high-Ti rocks from widely separated occurrences in northern and southern Victorialand and the Transantarctic Mountains. Literature data are from FLEMING et al. (1992, 1995), ELLIOT et al. (1995, 1999), WILHELM & WÖRNER (1996), ANTONINI et al. (1999).

However, one of the most distinctive features compared to the low-Ti magma series, is the considerable fractionation of Fe-Ti oxides, which is indicated by the throughout decreasing FeO, TiO_2 and V concentrations with increasing SiO_2. The very steep decrease of V for rocks with the lowest SiO_2 contents can be explained by the general observation of SCHUILING & FEENSTRA (1980) that early-fractionated oxides preferentially concentrate the highest V concentrations. Due to their accumulation, the residual liquid as well as the subsequently formed oxides became relatively depleted in V. This observation of highest V concentrations in early-crystallised oxide phases has also been described by HIMMELBERG & FORD (1977) for some low-Ti rocks from the Dufek intrusion.

The contents of SiO$_2$ and Al$_2$O$_3$ correlate positively and their throughout increase during *in situ* differentiation probably reflects the increasing amounts of residual liquid, which has been preserved as poorly crystallised mesostasis or patches of intergrown quartz and alkali-feldspar. This corresponds to the observation of WILHELM & WÖRNER (1996), who reported considerably varying modal abundances of mesostasis for the > 120 m thick high-Ti occurrence in southern Victorialand. The content of mesostasis increases upwards in the stratigraphic profile from ~ 25 vol% at the base up to 40 vol% at the top and correlates with a general decrease of the major mineral modes.

The significant increase in silica accompanying the Fe-Ti oxide fractionation is a characteristic feature of tholeiitic differentiation series and typically occurs at the very advanced differentiation stages, as discussed e.g. for the Kiglapait intrusion (MORSE 1981) or the Skaergaard intrusion (e.g. HUNTER & SPARKS 1987, 1990, MCBIRNEY & NASLUND 1990).

4.2.2   Evidence of *In situ* Differentiation from Platinum Group Elements

Similar to the major and trace elements, a noticeable fractionation of the PGE for the variably evolved Ferrar rocks is shown by the significantly varying bulk-rock PGE concentrations, which range from 4 to 40 ppb and correlate with the bulk-rock MgO contents as differentiation index. Since most of the observed major and trace element variations result from *in situ* differentiation as discussed above, the variation trends shown by the individual PGE against MgO (Fig. **3.24**) are interpreted to result from *in situ* differentiation as well.

To a certain degree, the considerable fractionation between the individual PGE, as shown by the higher concentrations of PPGE relative to IPGE, can be interpreted either to reflect a primary feature of the Ferrar magma source or to result from a differentiation process prior to magma emplacement or a combination of both. Thus, this issue will be discussed in the later chapters. Nevertheless, during the *in situ* differentiation the 'primary' PPGE/Ir ratio of ~ 94 for the low-Ti chilled margins changed to 27 for the accumulated and to 215 for the differentiated low-Ti rocks. Despite their conspicuously homogenous composition, the few high-Ti rocks exhibit a very wide range of PPGE/Ir ratios from 34 to 402. These strongly variable ratios can be ascribed to the steadily compatible behaviour of Ir and the bimodal, predominantly incompatible behaviour of Pd and Pt during low-pressure *in situ* differentiation of the Ferrar magmas (Fig. **3.24**). This observation indicates that Ir and partly Pd and Pt have been included in any of the fractionating mineral phases during the *in situ* differentiation.

The elements Ru and Rh do not show pronounced variation trends with MgO as differentiation index. This finding may either be attributed to their very low concentrations near the limit of detection or indicate that these elements have bulk-partition coefficients close to unity. Ir is consistently compatible during the *in situ* differentiation. Relative to the concentrations in chilled margins of low-Ti sills, Ir increases in rocks formed by accumulation. This indicates that Ir was either incorporated into a fractionating early-formed mineral phases or was trapped by small amounts of liquid between the solidifying silicates. Assuming the first case, it is difficult to determine

whether Ir was extracted from the melt by the formation of highly insoluble Ir metal alloys or monosulphide solid solutions (mss; BOCKRATH et al. 2004) that were incorporated into some early-segregated silicates or oxides (BARNES & NALDRETT 1987, WALKER et al. 1996, ANDREWS & BRENAN 2002) or if the Ir compatibility was crystal-chemically controlled and Ir was partitioned by true solid solution into the accumulated phases (MITCHELL & KEAYS 1981, BRÜGMANN et al. 1987). However, it is favoured that Ir did not substitute for metal ions into the crystal structure of the accumulated pyroxenes observed in the Ferrar cumulates, but either was included as separate phases in pyroxenes or remained in the trapped liquid until this liquid crystallised and enclosed micro-inclusions of Ir-bearing platinum group minerals. With enrichment of Ir in Ferrar cumulates, differentiates are left with low Ir abundances, which are in some cases even below the limit of detection.

In contrast to Ir, the elements Pt and Pd do have significantly higher concentrations and exhibit a more complex, bimodal fractionation behaviour during the *in situ* differentiation of the Ferrar magmas. Most of the low-Ti rocks follow a trend of increasing Pt and Pd concentrations with decreasing MgO, but some low-Ti rocks of more evolved compositions and the coarse-crystalline high-Ti sample RH24 exhibit a decrease of both elements. This bimodal behaviour of Pt and Pd will be examined in more detail considering some general basics controlling the fractionation of the PPGE.

As indicated by their high sulphide melt / silicate melt partition coefficients, $k_D^{sulphide/silicate\ melt} = 10^3 - 10^6$ (e.g. CAMPBELL et al. 1983, STONE et al. 1990, BEZMEN et al. 1994, FLEET et al. 1996, BARNES & MAIER 1999), the basically siderophile PPGE are recognised to have a strong chalcophile affinity as well. Confirmed by often observed high concentrations of PPGE in sulphides, it is widely accepted that sulphide fractionation is the main factor controlling the formation of distinct PGE distribution patterns documented in several magmatic profiles. Based on this general assumption, the PGE are removed from the silicate melt and concentrated in immiscible sulphidic liquids in the order of their different k_D values (e.g. CAMPBELL & NALDRETT 1979, NALDRETT & WILSON 1990, BARNES & PICARD 1993, MATHEZ 1999). During ongoing magma evolution, the PGE carrying sulphide liquids segregate from the silicate liquid at magmatic temperatures, when the maximum amount of sulphur that can be dissolved (sulphur-saturation) is reached. The PGE-bearing sulphide liquids either form immiscible droplets, which are disseminated in the crystallising matrix silicates, oxides or in the mesostasis or they subsequently form discrete noble metal minerals, which fractionate from the evolving magma by segregation and may concentrate in sulphide-rich layers. Such 'orthomagmatic' models have been emphasised as explaining the formation of stratiform noble metal mineralisations such as the Merensky Reef of the Bushveld Complex, South Africa (BARNES & MAIER 2002) or the Main Sulphide Zone of the Great Dyke, Zimbabwe (OBERTHÜR 2002).

In conclusion, the fractionation of the PPGE at magmatic temperatures is largely governed by their chalcophile tendency and thus, by their variable partition coefficients in the sulphide / silicate melt system. Based on this consensus, variations of the PPGE are often compared with those of other chalcophile elements such as Cu. A scheme, describing the fractionation of chalcophile elements in dependence on the sulphur-

saturation of tholeiitic magmas, is given by ANDERSEN et al. (2002, Fig. **4.4**). According to this scheme, the steadily negative correlation of Cu with a differentiation index such as MgO indicates its incompatibility and thus S-undersaturated conditions during *in situ* differentiation of the Ferrar magmas.
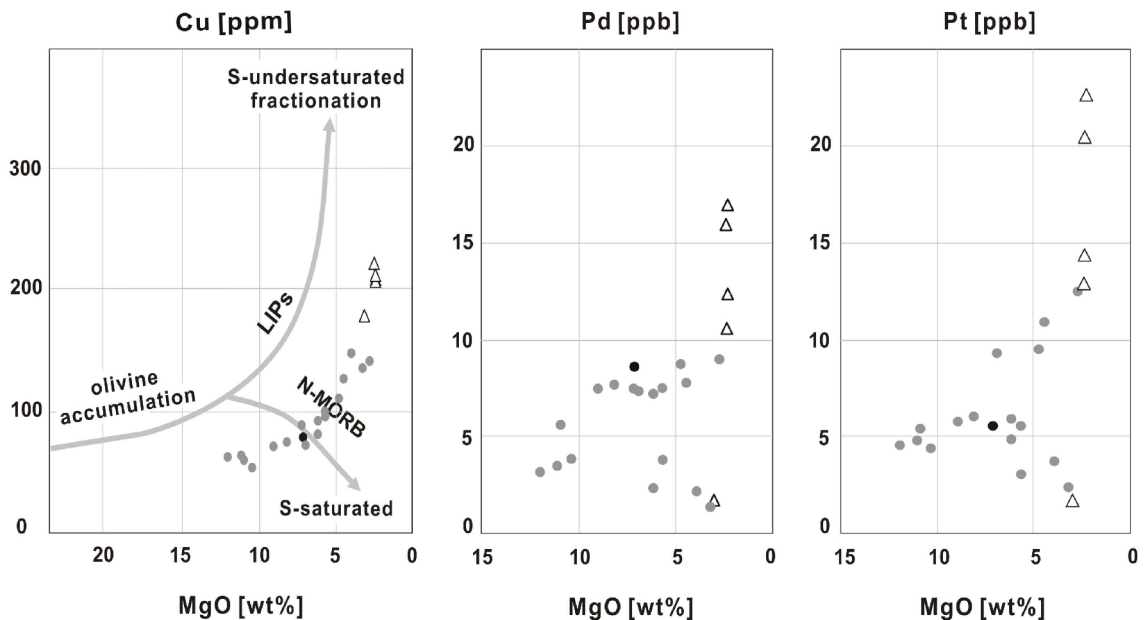
Fig. 4.4 – Variation of Cu, Pd and Pt with MgO of the analysed Ferrar low-Ti rocks (grey circles) and high-Ti rocks (open triangles) including the systematic of Cu fractionation depending on the sulphur-saturation during differentiation of tholeiitic magmas after ANDERSEN et al. (2002). The black circles represent the composition of a chilled margin of a low-Ti sill, from which cumulates and differentiates developed during *in situ* differentiation. Note the wide variations of PGE concentrations of the high-Ti samples despite their generally homogeneous composition.

However, in some of the evolved low-Ti rocks and one high-Ti rock, Pt and Pd are compatible and thus decoupled from Cu despite the inferred S-undersaturation of the Ferrar magmas. This suggests that during the *in situ* differentiation the Ferrar magmas achieved partly a degree of S-saturation, due to which at least the PPGE fractionated from the residual liquid. This is displayed more clearly by the Cu/Pd and the Cu/Pt ratios, which provide better indicators of S-saturation of magmatic liquids (VOGEL & KEAYS 1997, MOMME et al. 2002). These ratios are considered constant during fractionation of silicates under S-undersaturated conditions since all of these elements behave incompatible as long as no immiscible sulphide liquid is segregated from the magma. The almost constant Cu/PPGE ratios with varying MgO, shown by most of the present Ferrar low-Ti and high-Ti samples (Fig. **4.5**), confirm the mainly S-under-saturated nature of the Ferrar magmas. The partly elevated Cu/Pd and Cu/Pt ratios, however, indicate removal of the PPGE from the residual liquid. These may reflect a sudden increase in S-saturation in distinct sections of the *in situ* differentiated magmas that is large enough to at least fractionate the PPGE but not Cu. It is noteworthy that this feature is documented for both magma series, but it is more pronounced for the high-Ti rocks considering their very restricted range of MgO contents.
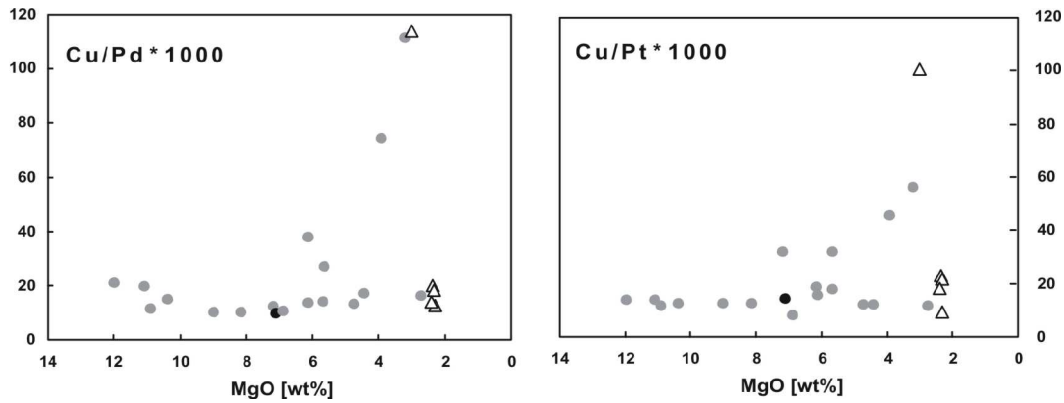
Fig. 4.5 – Variations of Cu/Pd and Cu/Pt ratios with MgO for the analysed Ferrar low-Ti (closed circles) and high-Ti (open triangles) rocks. The black circles represent the composition of a chilled margin of a low-Ti sill.

In order to constrain the petrogenetic significance of the distinct PPGE behaviour in the analysed Ferrar rocks, data presented here are compared with published data for tholeiitic rocks from mid-ocean ridges (MORB) as well as seaward dipping reflector sequences (SDRS) and plateau basalts from LIPs. In figure **4.6**, the variations of Cu, Pd and Pt are plotted against the bulk-rock MgO contents as differentiation index. The major element data have been recalculated to 100 wt% on a volatile-free basis.
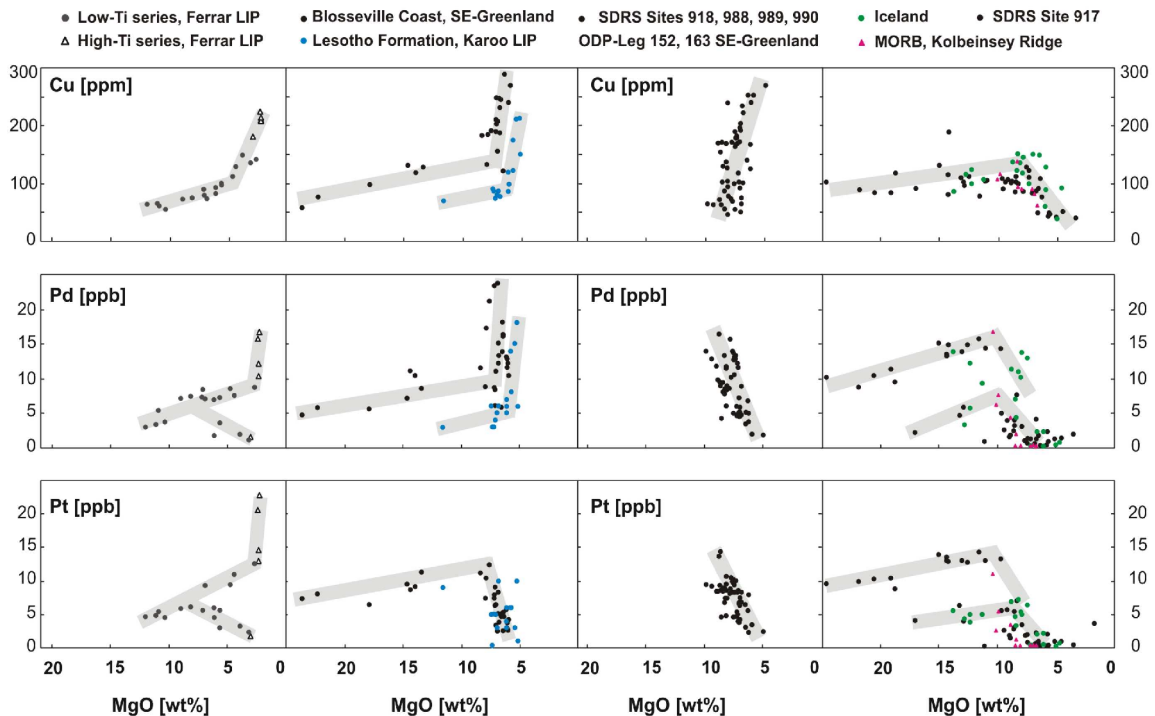
Fig. 4.6 – Comparison of variations of Cu, Pd and Pt with MgO for tholeiitic rocks from different magmatic settings emphasising the unique combination of variation trends of these elements for the analysed Ferrar rocks from Antarctica. Published data are from REHKÄMPER et al. (1999b), PHILIPP et al. (2001), ANDERSEN et al. (2002), MOMME et al. (2002, 2003) and MAIER et al. (2003).

All data records are nearly uniform in the range of MgO contents between 25 and 10 wt%, exhibiting increasing Cu, Pd and Pt concentrations with decreasing MgO. With further differentiation (MgO < 10 wt%), four different types of variation patterns of these elements can be distinguished:

Type A - coupled increase (incompatibility) of Cu, Pd and Pt (Ferrar LIP trend I)

Type B - coupled increase of Cu and Pd and decrease of Pt (Lesotho Formation, Karoo LIP, MAIER et al. 2003; Blosseville Coast E-Greenland, ANDERSEN et al. 2002, MOMME et al. 2002)

Type C - increase of Cu and coupled decrease of Pd and Pt (Ferrar LIP trend II, SDRS from SE-Greenland ODP Leg 152 und 163, PHILIPP et al. 2001)

Type D - coupled decrease (compatibility) of Cu, Pd and Pt (NE-Atlantic N-MORB, REHKÄMPER et al. 1999b; SDRS from ODP Leg 163 Site 917, PHILIPP et al. 2001; Iceland Neovolcanic Zone, MOMME et al. 2003)

Considering the high sulphide/silicate melt partition coefficients of Cu ($10^2 – 10^3$) and Pd and Pt ($10^3 – 10^5$) (BARNES & MAIER 2002 and references therein), the increasing Cu, Pd and Pt concentrations between 25 and 10 wt% MgO indicates a) their incompatibility due to S-undersaturation during olivine fractionation of primitive picritic magmas or b) dilution of these elements due to an increasing degree of partial melting of a peridotitic source, because sulphides are no longer residual phases at melting degrees higher than 20 % to 25 % (BARNES et al. 1985, KEAYS 1995, REHKÄMPER et al. 1999b).

The variable fractionation trends of Cu, Pd and Pt below MgO ~ 10 wt% for the individual magma provinces can be explained by different degrees of S-saturation achieved at distinct stages of the advancing differentiation of primarily S-undersaturated magmas (Fig. **4.7**). With respect to their S-saturation, the most contrary tholeiitic magmas are the Ferrar rocks analysed (Type A) and the MOR basalts (Type D). The asthenospheric N-MORB melts from the NE Atlantic and the plume-related magmas of the Iceland Neovolcanic Zone were S-saturated enough to fractionate Cu at MgO about 7 – 8 wt%. The variation pattern Type C (SDRS SE-Greenland; Ferrar LIP) is characterised by a steep increase of Cu and decreasing PPGE indicating that the level of S-saturation was only high enough to fractionate the PPGE. This is in accordance to the generally lower $D^{sulphide/silicate\ liquid}$ for Cu. In the Type B pattern (E-Greenland and Karoo LIP), Cu and Pd increase and only Pt decreases. The Type A pattern of some Ferrar rocks exhibits increasing concentrations of Cu, Pd and Pt indicating that the sulphur content was even too low to fractionate any of the chalcophile elements.

From the different types of element variation trends, it is evident that the PPGE are earlier fractionated than Cu, confirming that Cu has a lower k_D for sulphides, and that Pt fractionates earlier than Pd. Assuming that this fractionation is controlled mainly by the degree of sulphur-saturation of the evolving magma, the following model describing the fractionation behaviour of the chalcophile elements can be developed:
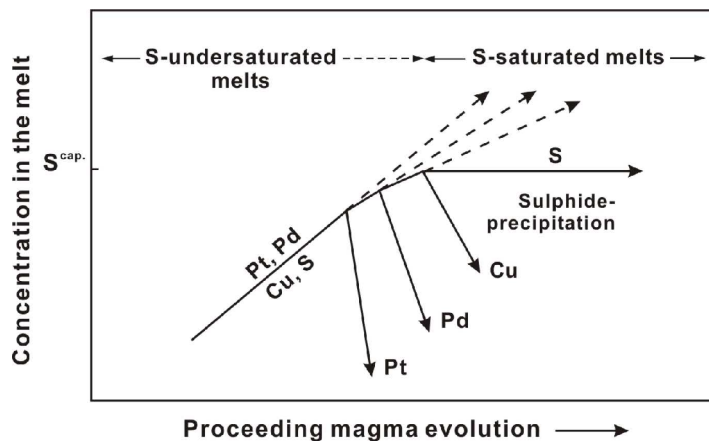
Fig. 4.7 – Schematic sketch illustrating the fractionation behaviour of Cu, Pd, Pt and S with proceeding magma evolution depending on the level of sulphur-saturation of tholeiitic magmas (modified after PHILIPP 1999, from KEAYS 1995) implying different partition coefficients between sulphide and silicate liquids for the individual elements.

The variations discussed above and the inferred conclusions summarised in figure **4.7** imply decreasing $k_D^{\text{sulphide/silicate liquids}}$ in the order Pt > Pd > Cu. This agrees with empirically estimated k_D values (e.g. HELZ & RAIT 1988, PHILIPP et al. 2001), but is inconsistent with some experimental determinations (e.g. STONE et al. 1990, FLEET et al. 1996, 1999a, 1999b) denoting higher k_D's for Pd than for Pt and hence a stronger affinity of Pd for sulphides. To some extent, differences of estimated k_D values may be attributed to considerably varying conditions applied during the experimental studies such as T, fO_2, fS and the liquid starting composition. This is in accordance to MATHEZ (1999), who emphasised that k_D values are not constant but depend strongly on physico-chemical conditions. Otherwise, this observed discrepancy of empirically and experimentally determined k_D values for sulphides may give evidence that the fractionation of Pt and Pd was not solely controlled by sulphides, but possibly by other phases such as metal alloys since the PGE are highly siderophile elements. Several authors (e.g. FLEET & STONE 1991, JANA & WALKER 1997, BARNES et al. 2001) determined distinctly different partition coefficients between alloys and sulphides for Pd and Pt: while $k_D^{\text{alloy/sulphide}}$ is ~ 1 – 2 for Pd that for Pt is in excess of 1000 (FLEET & STONE 1991). Thus, Pt is enriched in alloy phases whereas Pd is preferentially concentrated in sulphides.

These considerations indicate that the partitioning of PPGE in either sulphides or alloys could likely result in a fractionation between Pt and Pd during *in situ* differentiation of the Ferrar low-Ti and high-Ti magmas, as exemplarily displayed by the variation patterns of the continental flood basalts from the East Greenland volcanic rifted margin (MOMME et al. 2002) or the Karoo LIP (Maier et al. 2003). Instead, both elements show consistent fractionation behaviour for the analysed Ferrar rocks.

The inadequacy of the fractional sulphide or alloy segregation models suggests that other collectors of PPGE have to be considered as well (BARNES 1993), unless any combination of fractionating sulphides and alloys is assumed for the individual PPGE during the *in situ* differentiation of the Ferrar magmas. However, the coexistence of Pt-

alloys and sulphides at oxygen fugacities close to the FMQ buffer (which is typical during melting and differentiation processes of tholeiitic magmas) has been discussed controversially (e.g. ANDREWS & BRENAN 2002, PEREGOEDOVA et al. 2002, 2004). Hence, the depletion of Pd and Pt in some of the differentiated Ferrar low-Ti rocks and the coarse-crystalline high-Ti rock does not necessarily reflect the sole precipitation of minor amounts of sulphides and / or alloys.

Sulphur in figure **4.7** can be complemented by other oxy-anions available to form discrete platinum-group minerals (PGM); however, the origin of such PGM remains controversial. For example, HUTCHINSON & MCDONALD (2005) identified several discrete PGM such as arsenides, antimonides, bismuthides and tellurides besides sulphides within basal sections of the Bushveld Complex. They attributed the occurrence of these PGM to selective magma contamination by As, Sb, Bi and Te and subsequent formation of e.g. Pt-bearing arsenides and antimonides at magmatic temperatures. On the contrary, similar findings of discrete PGM in the Main Sulphide Zone of the Great Dyke layered intrusion (OBERTHÜR et al. 2003a, 2003b) have been ascribed to secondary re-distribution of the PPGE from primarily magmatic sulphide segregations. Possibly, a comparable post-magmatic process has to be considered as influencing the PGE characteristics of the Ferrar rocks as well.

This is in accordance to the recognition that the PGE, in spite of their chemical inertness, are variably mobile under metasomatic and hydrothermal conditions (e.g. BOUDREAU et al. 1986, BOUDREAU 1988, CROCKET 1990). This finding has been con-firmed by a number of recently reported thermodynamic data and several field studies (e.g. WATKINSON et al. 2002, WOOD 2002 and references therein). It has been recognised that the PPGE are more mobile than the other PGE. In this context, PEACH & MATHEZ (1996) for example emphasised that the distinct zonations of PPGE-enrichment and depletion found in several intrusions reflect significantly variable element mobilities for Pt and Pd during subsolidus re-distribution processes. Referring to this, Pd is more mobile than Pt (e.g. WOOD 2002, OBERTHÜR et al. 2003b). In contrast to this finding of distinct mobilities for individual PPGE during post-magmatic processes, no significant offset between both elements is observed for the analysed Ferrar rocks. The coupled decrease of Pd and Pt reported here disagrees with post-magmatic modification of the initial PGE abundance patterns. Moreover, the coupled decrease of the PPGE and MgO most likely is a primary igneous signature.

Consequently, the PPGE semi-compatibility is attributed to *in situ* differentiation at magmatic temperatures within the sheet-like magma reservoirs. During the advanced stages of cooling and solidification of these magma bodies, the PPGE are partly extracted from the residual silicate liquid by a fractionating phase(s) or the trapped liquid between them and are thus enriched or depleted in different horizons of these magmatic profiles.

It has been demonstrated that the bimodal PPGE fractionation behaviour with concurrent increase of Cu during *in situ* differentiation can be of quite different origins. However, no attempts have been made to identify the fractionating PGE phases so far. To better understand the fractionation behaviour of PGE during low-pressure differentiation, further detailed investigations of the stratigraphic distribution of the PGE

within massive intrusive units of the Ferrar LIP are required. For reasonable inter-
pretation of the whole-rock PGE variations, such a study would largely benefit from the
identification of the PGE-bearing mineral phases.

In conclusion, the comparison with tholeiitic rocks from different geodynamic
environments as well as large igneous provinces shows that the combination of PGE
variation trends in Ferrar rocks is unique, since the uniform increase of Cu and the
PPGE has not been documented by any of the other provinces. The significance of this
observation has to be discussed with respect to the source characteristics of the Ferrar
magmas; especially to what extent the enriched lithospheric mantle source may have
influenced the inferred very low degree of sulphur-saturation of the Ferrar magmas.

4.2.3   Comparison of *In Situ* Differentiation of the LTS and the HTS

The petrographic, mineralogical and geochemical variations of both the Ferrar low-Ti
and the high-Ti magma series (LTS and HTS, respectively) clearly indicate that the
evolving magmas experienced considerable *in situ* differentiation after emplacement.
The compositional variation trends of both magma series suggest fractionation
assemblages consisting of pyroxenes and plagioclase (and Fe-Ti oxides). On many
variation diagrams of the present Ferrar rocks (e.g. Fig. **3.21** and **3.22**), the high-Ti
compositions lie along the extensions of the well-defined major and trace element
trends of the low-Ti rocks. This observation implies that a continuation of the low-
pressure fractional crystallisation of the low-Ti magmas led to the formation of the high-
Ti magmas. The plausibility of this suggestion will be discussed briefly in the following.

Some authors performed mass balance calculations in order to model the
differentiation trends of the Ferrar magma series. For example, BROTZU et al. (1988,
1992) and ANTONINI et al. (1999) calculated the low-pressure fractional crystallisation of
the low-Ti magmas assuming distinct proportions of plagioclase, augite and pigeonite.
BROTZU et al. (1988) included minor amounts of fractionating Ti-magnetite. These
thermodynamic model calculations explained well the transition from basaltic andesites
to andesites and dacites of the LTS. Applying changed modal proportions of the same
fractionated mineral phases and of the same compositions, the model of BROTZU et al.
(1992) described even the evolution from the low-Ti to high-Ti basaltic andesites by
adding minor amounts of accumulated Ti-magnetite. However, some striking features
do not support the suggestion that the LTS and HTS magmas are directly related by
low-pressure *in situ* fractionation. This has already been emphasised by HABAN &
ELLIOT (1985) and ELLIOT et al. (1995). The former obtained satisfying results for major
element modelling only by assuming changes of the fractionation assemblage. The
modelling of ELLIOT et al. (1995), testing the derivation of the high-Ti from the low-Ti
magmas, produced only acceptable solutions when modified mineral compositions for
both magma series were applied. Nevertheless, in both cases, the trace element data
did not support the low-pressure fractionation models.

Therefore, the reliability of such *in situ* fractionation models for the generation of the
HTS will be tested by comparing the geochemical features of the LTS and HTS. In
figure **4.8**, the ranges of concentrations of individual major and trace elements, which

are inferred to result from low-pressure *in situ* differentiation, are summarised including the data of the present rocks from NVL as well as published data from the entire Ferrar province. The data points, which are suggested to represent the average compositions of the LTS and HTS at the time of magma emplacement, are averages of the chilled margins of the studied low-Ti sills and of the fine-crystalline high-Ti samples from Litell Rocks, respectively. It is noteworthy, that these compositions do not exactly correspond to the average compositions calculated from the entire chemical variations of the present and the published data. Nevertheless, the plotted estimates for the low-Ti series are widely in accordance to the average compositions of chilled margins of low-Ti sills from Tasmania (HERGT et al. 1989b) and from Portal Peak, central Transantarctic Mts. (HERGT et al. 1989a). The plotted high-Ti average concentrations correspond to the rapidly cooled, extrusive high-Ti occurrences reported from the Mesa Range and Litell Rocks (e.g. ELLIOT et al. 1995, HORNIG 1993).
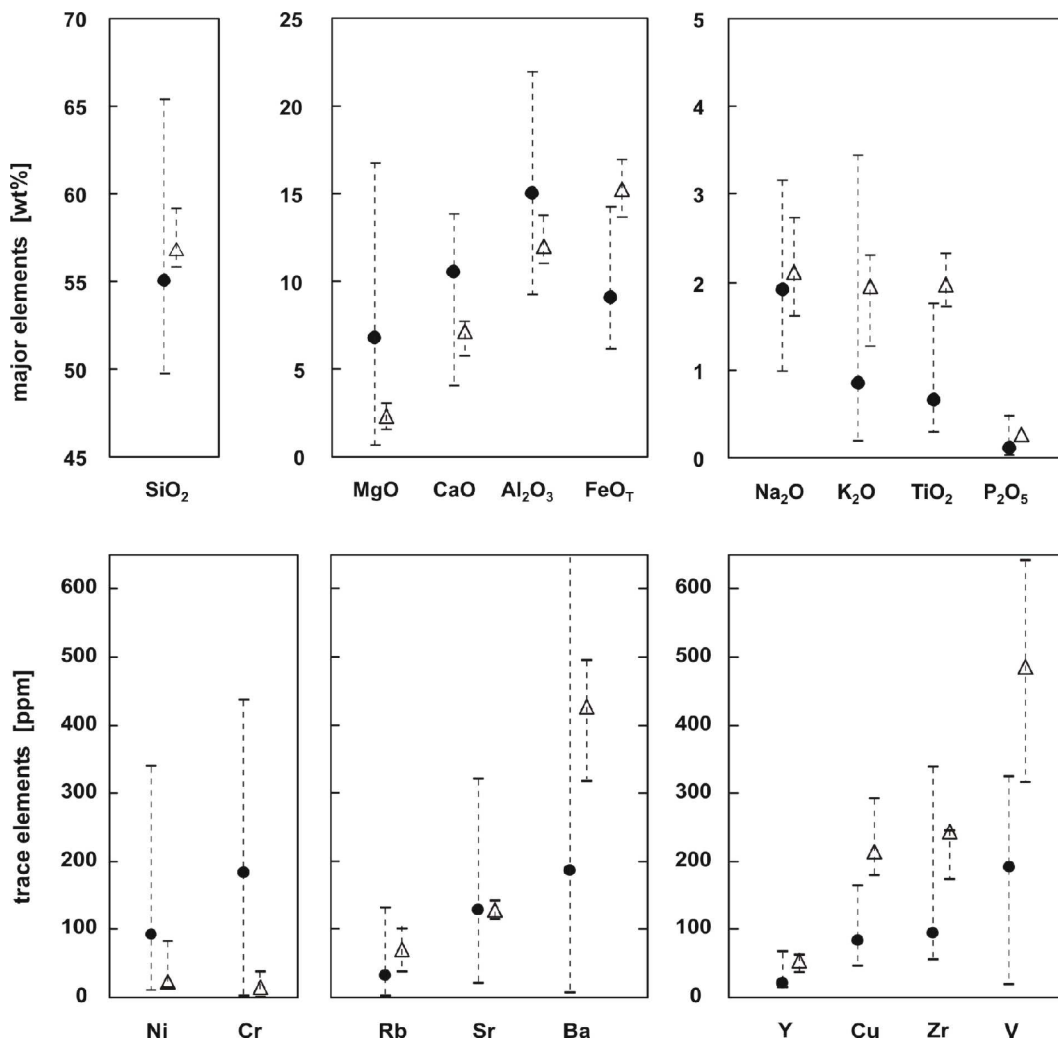
Fig. 4.8 – Comparison of whole-rock chemical variations of Ferrar low-Ti and high-Ti rocks. Black circles (LTS) and open triangles (HTS) represent the fine-crystalline samples of both magma series, which are assumed to represent the magma composition before magma emplacement. The dashed lines mark the range of variation of the different major and trace elements reflecting the chemical evolution by fractional crystallisation during low-pressure *in situ* differentiation. The published data included are those displayed in figures **4.1** and **4.3**.

Considering the geochemical variations of the LTS and HTS from the entire Ferrar province in figure **4.8**, the high-Ti rocks do not show the minimum or maximum concentrations of most of the compatible or incompatible elements, respectively, as expected if they simply continued the fractionation trends of the low-Ti magmas. Instead, the compositions of the high-Ti samples fall within the range of the LTS for most elements, except for e.g. FeO, TiO_2 and V (and the REE and PGE, not shown). Furthermore, the comparison of the variation trends of the LTS and HTS (Fig. **4.1** and **4.3**) clearly indicates slight but important differences in the *in situ* fractionation assemblages for both magma series. While Al_2O_3 contents decrease in the low-Ti differentiates, Al_2O_3 increases during the *in situ* differentiation of the HTS. Na_2O and K_2O steadily increase in the LTS but do not vary systematically in the HTS. In addition to the implication that different amounts of pyroxenes and plagioclase (of probably changed chemistry) have been fractionated during evolution of both series, one of the most striking differences is the fractionation of Fe-Ti oxides.

During the *in situ* differentiation of the LTS, concentrations of FeO and TiO_2 (and SiO_2) continuously increase towards more evolved samples because Fe-Ti oxides are not fractionated until considerable melt fractions have been crystallised. After significant enrichment in FeO and TiO_2, Fe-Ti oxides enter the fractionation assemblage. Thus, both elements decrease in the most evolved low-Ti rocks, which are transitional to dacites in composition and reach SiO_2 contents of up to ~ 65 wt%. In contrast, the entire suite of high-Ti rocks shows a steady decrease of FeO and TiO_2 concentrations indicating the fractionation of Fe-Ti oxides already at silica contents of about 56 wt%. Consequently, SiO_2 is enriched up to ~ 59 wt% in the residual high-Ti magma during the removal of oxides, but it does not reach the high concentrations observed for the most evolved low-Ti samples.

The distinctly different fractionation assemblages, in particular the difference of appearance of oxides as fractionating phases, are the most evident differences during the low-pressure differentiation of the two Ferrar magma series. In general, different factors control the point of oxide saturation of basaltic liquids. From experimental investigations on the phase relations in ferro-basaltic liquids, TOPLIS & CARROLL (1995) emphasised that the onset of oxide fractionation is largely governed by the oxygen fugacity, but the composition of the liquid itself (e.g. FeO and TiO_2 contents, Fe^{2+}/Fe^{3+} ratio) as well as its temperature are important factors, too.

In conclusion, the discussed differences in the geochemical variation trends (and the inferred differences in mineral assemblages and chemistries) indicate that the generation of the high-Ti magma series can not be ascribed to proceeding *in situ* fractionation of the low-Ti magmas as modelled by e.g. BROTZU et al. (1992), at least not if unchanged conditions are assumed for both series. However, appreciable variations of differentiation conditions (e.g. oxygen fugacity, temperature or pressure) are difficult to explain considering the apparently short interval of emplacement of both magma series and their close spatial relationship. Thus, it is concluded that the compositional differences of the LTS and the HTS reflect pre-emplacement characteristics inherited from a process prior to the *in situ* differentiation. Therefore, the following chapter discusses the evolution of both magma series during differentiation

prior to emplacement in upper crustal levels considering only the fine-crystalline low-Ti and high-Ti rocks. These are suggested as being least modified by processes taking place during and after the magma emplacement.

4.3   PRE-EMPLACEMENT DIFFERENTIATION

In order to describe the evolution of the two Ferrar magma series during pre-emplacement differentiation, the most evident features for this process will initially be given by means of major and trace elements as well as platinum group elements of the present Ferrar samples. Afterwards, the differentiation history will be evaluated in more detail considering especially the differences of the evolutionary paths of both series.

4.3.1   Evidence of Differentiation from Major and Trace Elements

A powerful tool to understand the differentiation process of magma series is the Mg-number since it is highly sensitive to the amount of fractional crystallisation of mafic mineral phases but is insensitive to the degree of partial melting. Compared to average continental tholeiitic rocks, the fine-crystalline Ferrar rocks are characterised by generally low Mg-numbers of ~ 62 and ~ 24 for the LTS and the HTS, respectively. Since primary mantle melts have Mg# > 70, the value expected for magmas formed in equilibrium with ~ Fo_{90} olivine (ROEDER & EMSLIE 1970), the lower Mg# of the Ferrar rocks give evidence that they do not represent primary magma compositions, which have been formed by partial melting in equilibrium with normal upper mantle mineral assemblages (COX 1980). Furthermore, the low Mg# of the Ferrar rocks are combined with generally low FeO, TiO_2, Na_2O, P_2O_5 contents and high SiO_2 contents.

These characteristics of the Ferrar magmas have been discussed as being derived from fractional crystallisation accompanied by substantial assimilation of crustal material. Such coupled assimilation-fractional crystallisation processes (AFC after DEPAOLO 1981) have been modelled successfully by e.g. FAURE et al. (1974) and ANTONINI et al. (1999). However, for several reasons, HERGT et al. (1989b, 1991), FLEMING et al. (1995), MOLZAHN et al. (1996) and BRAUNS et al. (2000) argued against an essential influence of crustal contamination on the Ferrar magmas *en route* to the surface. The fact that the Ferrar magmas are of non-primary composition rather implies that they experienced extensive differentiation by fractional crystallisation prior to and during their ascent from the mantle source, but before they entered the upper continental crust. The question to which extent a compositionally exceptional magma source or the melt generation from this source influenced the Ferrar magmas will be evaluated later on.

Nevertheless, the Mg/Fe ratios of the Ferrar rocks (especially those of the high-Ti series) are far too low for credible mantle melts and hence require the removal of considerable amounts of mafic mineral phases such as forsteritic olivine and / or enstatitic orthopyroxene. This differentiation process is further supported by the general absence of Mg-rich olivine and low Ni and Cr concentrations of the present Ferrar rocks (Fig. **4.1** and **4.3**) compared to primary melts. The latter typically have Ni and Cr

concentrations of > 400 – 500 ppm and > 1000 ppm, respectively, and their SiO_2 contents do not exceed ~ 50 wt% (WILSON 1989). In contrast, the fine-crystalline Ferrar low-Ti and high-Ti samples exhibit clearly higher SiO_2 contents with ~ 54.5 wt% and 56.5 – 57 wt%, respectively.

Corresponding to their lower Mg#, the rapidly cooled high-Ti rocks have elevated concentrations of incompatible major and trace elements relative to the low-Ti chilled margins as summarised in figure **4.8**. These data indicate a more evolved composition and hence an elevated degree of differentiation of the high-Ti rocks, a feature that is confirmed by higher abundances of REE and PGE. The behaviour of the latter element group during differentiation will be considered in the following in more detail.

4.3.2   Evidence of Differentiation from Platinum Group Elements

The fact that the Ferrar rocks are of fairly evolved composition compared to primary mantle melts is indicated by the characteristics of the PGE as well. The most obvious feature is the marked fractionation between the individual PGE causing the positive slope of the chondrite-normalised PGE patterns (Fig. **3.25**), which is characteristic for all analysed Ferrar samples. The Pd/Ir ratios obtained are about ~ 55 for the low-Ti chilled margin samples; for the fine-crystalline high-Ti samples, the Pd/Ir ratios are highly variable but at least twice as high as for the low-Ti chilled margins. The Pd/Ir ratios correspond to those given for other continental flood basalts (e.g. BRÜGMANN et al. 1993, PHILIPP et al. 2001, MOMME et al. 2002), whereas the Pd/Ir ratios of mantle rocks are typically much lower with values about 1.3 (BARNES & MAIER 1999).

The observed enrichment of the PPGE over the IPGE can mainly be attributed to the low concentrations of the latter element group. Assuming that the Ferrar magma source was not notably depleted in IPGE, this gives evidence for an early differentiation event prior to magma emplacement and *in situ* differentiation. A number of studies have shown that during early fractionation episodes, the IPGE are preferentially extracted from the primary magma concurrently to the removal of appreciable amounts of (near-) liquidus phases (e.g. Cr-spinel or olivine, BARNES & NALDRETT 1987, GREENOUGH & OWEN 1992, BARNES & PICARD 1993, RIGHTER et al. 2004). One example favouring this mechanism of segregation of early magmatic phases including IPGE-compounds has been given by OBERTHÜR et al. (2002), who found elevated IPGE/PPGE ratios at the base of the Main Sulphide Zone of the Great Dyke; increased amounts of e.g. laurite (RuS_2) in the basal sections confirmed their interpretation. This highly compatible behaviour of the IPGE during early magma differentiation is in accordance to their experimentally determined high spinel and olivine / silicate melt partition coefficients (e.g. CAPOBIANCO & DRAKE 1990, RIGHTER et al. 2004). Irrespective to the question, if a real crystal-chemical control on IPGE distribution exists (BRÜGMANN et al. 1987) or if IPGE micro-inclusions have been scavenged by early magmatic phases (BARNES et al. 1985, KEAYS 1995, BARNES et al. 2001), the observation of their elevated compatibility is widely confirmed by the PGE abundances in typical mantle rocks. For example, mantle-derived lherzolitic xenoliths exhibit clearly higher concentrations of the IPGE (MITCHELL & KEAYS 1981, LORAND & ALARD 2001), which

are partly in the range of the PPGE or even higher than the latter. Furthermore, early-precipitated chromitites from various ophiolites have been reported with Ir contents clearly dominating over Pd (PARRY 1984, BARNES et al. 1985, AHMED & ARAI 2002 and references therein). Nevertheless, the lack of olivine or Cr-spinel in the present Ferrar rocks as well as the overall rare presence of olivine in Ferrar rocks indicate that possibly orthopyroxene as major liquidus phase included the IPGE (e.g. as Ir-alloys or mss). This corresponds to observations of GREENOUGH & FRYER (1995), who described elevated IPGE concentrations in orthopyroxene-enriched basalts, which have been taken from accumulation zones of thick lava flows from Nova Scotia, North America. They concluded that orthopyroxene (aside from olivine or spinel) is able to separate noble-metal-bearing micro-inclusions from the evolving magmatic liquid as well.

Aside from the interpretation of removal of IPGE-bearing phases during early fractional crystallisation, the IPGE depletion of the Ferrar rocks compared to the PPGE could be interpreted as reflecting their different behaviour during the melt generation considering the higher melting points of the IPGE (BARNES et al. 1985). Due to lower degrees of partial melting, the IPGE could be retained because of incomplete solution of sulphides or alloys in the magma source, as discussed by e.g. BARNES et al. (1985) or PUCHTEL et al. (2004). The interpretation of early fractionation of the IPGE is favoured here because of the positive correlation of Ir contents with the differentiation index of the analysed fine-crystalline Ferrar low-Ti and high-Ti samples.

Additionally, the fractionation between IPGE and PPGE is influenced by the enrichment of the latter during differentiation of the Ferrar magmas as indicated by their higher abundances in high-Ti than in low-Ti rocks. As already discussed, increasing PPGE during magma evolution can be interpreted as reflecting sulphur-undersaturated conditions, at which sulphides do not become stable phases and hence PPGE are enriched in the residual liquid. From experimental investigations, MAVROGENES & O'NEILL (1999) concluded that the sulphur content at S-saturation (SCSS) of basaltic and picritic melts is rather unaffected by the temperature or oxygen and sulphur fugacities prevailing during differentiation as proposed in several previous studies (e.g. WALLACE & CARMICHAEL 1992). Instead, the SCSS is rather sensitive to changes in pressure: it exponentially increases with decreasing pressure (MAVROGENES & O'NEILL 1999). Thus, adiabatic decompression due to magma ascent can cause an initially S-saturated magma to become undersaturated in sulphur and appreciable crystallisation is required to reach S-saturation to fractionate sulphides and consequently the PPGE. This mechanism of increased SCSS due to magma ascent could also explain the S-undersaturated nature of the Ferrar magmas during differentiation. Otherwise, this S-undersaturation could reflect a primary feature of the Ferrar magma source suggesting that the low level of S-saturation of the Ferrar magmas reflect their derivation from an S-poor mantle source being depleted in sulphur (and the PGE) due to former melting events. Furthermore, the degree of partial melting may have controlled the initial content of sulphur (and the PGE) in the primary Ferrar magma.

However, a differentiation-induced difference is favoured and hence, the elevated Pd/Ir ratios of high-Ti rocks relative to those of low-Ti chilled margins again underline the more evolved composition of the HTS and thus their higher degree of differentiation.

4.3.3   Comparison of the Differentiation Paths of the LTS and HTS

Before comparing the pre-emplacement differentiation of the Ferrar low-Ti and high-Ti magma series, some theoretical considerations on differentiation processes required in this discussion will be given.

For describing the differentiation history of magmatic rock series, it is of great importance to characterise the composition of the primary magma, from which the rocks derived. It can be estimated by several computer models, which have been developed based on (and restricted by) the results of experimental investigations during the last decades. These models simulate numerically the crystallisation paths of cogenetic magmatic rocks by calculating their liquid lines of descent. For example, FRAM & LESHER (1997) computed the liquid lines of descent of the tholeiitic Tertiary East Greenland flood basalts and estimated their primary magma composition using the fractional crystallisation program of LONGHI (1991). The composition of the primary melt calculated (e.g. SiO_2 48 wt%, TiO_2 1.6 wt%, FeO 11.5 wt% and MgO 16 wt%) is largely in accordance to picritic rocks reported from various continental flood basalt provinces, for example, from the Deccan province (KRISHNAMURTHY & COX 1977) and the Karoo province (COX & JAMIESON 1974). Therefore, such picrites with forsteritic olivine have been discussed controversially as being representative for the parental magma composition, from which the tholeiitic flood basalts derived by fractional crystallisation, since their average compositions are obviously lower in MgO.

From these observations, a general scenario of magma evolution of continental flood basalts has been established by COX (1980), which can be adopted for the Ferrar rocks as well. After their melt generation in the mantle and their buoyancy-driven ascent, picritic magmas of high density are trapped at the base of the continental crust or at any level within the crust because the magma density is intermediate between that of the crust and the underlying mantle. In these temporary magma reservoirs, the MgO-rich picritic magmas differentiate under high-pressure conditions, and dense cumulates and less dense differentiated liquids are produced until the density contrast to the surrounding crust is appropriate to allow the differentiated melts to ascend. Further periods of stagnation during magma ascent are possible, and these may result in a very complex, polybaric differentiation history like those presented for the Karoo (COX 1980) or the East Greenland flood basalts (FRAM & LESHER 1997). Another example that individual batches of magma experienced more than one episode of differentiation have been reported from the British Tertiary Volcanic Province by MORRISON et al. (1985). They described multiple magmatic plumbing systems for the volcanic complexes on the Skye and Mull islands in order to explain the presence of different magma series and their evolutionary paths through the crust. A similar polybaric differentiation model can be developed for the Ferrar tholeiitic rocks as indicated by the whole-rock textural and mineral chemical features described, which imply two stages of differentiation at least.

The latest of these differentiation processes, the post-emplacement fractional crystallisation under low-pressure conditions, has been discussed already. By comparing the (polybaric?) pre-emplacement differentiation of the two Ferrar magma series, it will be discussed to which extent this process can explain their distinct compositions. For this

purpose, the most obvious compositional differences of the fine-crystalline low-Ti and the high-Ti rocks can be summarised as follows: Only the low-Ti chilled margins contain phenocrysts of orthopyroxene; low-Ca and high-Ca pyroxenes are notedly higher in MgO and plagioclase is more calcic in low-Ti than in high-Ti rocks. This corresponds to the difference in the average whole-rock MgO content, which is about 4.5 wt% lower in the HTS. The resulting lower Mg-numbers of the HTS are accompanied by lower concentrations of compatible elements (Ni, Cr, CaO, Al_2O_3, IPGE) and increased incompatible element abundances (FeO, TiO_2, V, Y, Zr, REE, PPGE) as displayed mainly in figure **4.8**. This more evolved composition of high-Ti compared to low-Ti samples indicates a more pronounced influence of differentiation on the high-Ti magma composition. Based on the systematic mineral and whole-rock chemical variations presented and based on data of numerous previous studies, the fine-crystalline low-Ti and high-Ti Ferrar rocks seem to be genetically linked by fractional crystallisation of pyroxenes and plagioclase. This suggestion is confirmed by the parallel chondrite-normalised REE-patterns of low-Ti and high-Ti rocks (Fig. **3.23**) with higher absolute REE concentrations and an increased Eu-anomaly of the latter.

These observations imply the possibility that the high-Ti magma series evolved by progressive differentiation of the low-Ti magmas prior to their emplacement. HABAN & ELLIOT (1985) and SIDERS & ELLIOT (1985) have already mentioned this genetic relationship of the Ferrar low-Ti and high-Ti magmas by fractional crystallisation. In the following, it will be evaluated if the two magma series differentiated along the same evolutionary path from a less evolved parental magma assuming only variable degrees of differentiation or if they followed separate evolutionary paths from a more primitive parental magma as shown below in figure **4.9**. The latter model has been suggested by e.g. FLEMING et al. (1995). For discussing these two possibilities by means of the compositional differences summarised above, it is necessary to characterise the composition of the primary magma, from which the Ferrar rocks derived, a task that is difficult to establish considering their generally low MgO contents. In a first assumption, the parental magma composition is suggested to be uniform for both magma series and not to distinguish due to differences in the partial melting degree or the source composition; both preconditions will be tested in detail afterwards.

In order to explain the derivation of the Ferrar rocks by differentiation from normal picritic mantle melts as given above, the Mg-depleted composition of the fine-crystalline Ferrar rocks has to be corrected for the highly efficient removal of Mg-rich phases prior to *in situ* differentiation. Due to the lack of olivine in the present samples and its generally rare presence in Ferrar rocks, the formation of olivine cumulates alone to explain the Mg-poor composition of the Ferrar magmas seems questionable. Instead, orthopyroxene is assumed as being the dominating early-segregated Mg-rich phase as indicated by its presence as phenocryst phase in chilled margins of low-Ti sills. This has already been denoted by ELLIOT (1972) and was confirmed later by DEMARCHI et al. (2001), who calculated orthopyroxene as liquidus phase using the program MELTS of GHIORSO & SACK (1991). The possibility that orthopyroxene crystallised as first stable phase at elevated pressure conditions, preferentially to olivine, can probably be attributed to a non-typically high silica content of the primary Ferrar magmas compared

to 'normal' primary magma compositions given above with SiO_2 < 50 wt% (WILSON 1989).

As Mg-rich orthopyroxene has been analysed to contain ~ 56 wt% SiO_2, its removal as single fractionating phase from a supposedly silica-poorer primary magma would further decrease the SiO_2 content of the residual liquid. Since the derivative low-Ti rocks have SiO_2 contents of ~ 54.5 wt%, it is required that the primary magma had initial silica contents comparable to those of orthopyroxene. However, this seems to be a most unlikely primary magma composition for tholeiitic flood basalts. In order to counterbalance this SiO_2 decrease expected by orthopyroxene fractionation alone, an additionally fractionating phase with lower SiO_2 contents has to be assumed such as anorthitic plagioclase. This corresponds to its presence as further phenocryst phase in the low-Ti chilled margin samples and its SiO_2 contents analysed with ~ 47 wt%.

This suggested early gabbro fractionation has been modelled by HERGT et al. (1989b) for the generation of the low-Ti rocks by adding orthopyroxene and plagioclase in roughly equal proportions to the average composition of the chilled margins of low-Ti sills from Tasmania. To the resulting melt composition, they furthermore added small amounts of olivine of Fo_{87} to raise the melt Mg content and hence to obtain a magma composition that is theoretically capable to crystallise olivine of Fo_{89}, which represents an equilibrium crystallisation phase with normal mantle (ROEDER & EMSLIE 1970). However, the obtained SiO_2 content (53.4 wt%) of this primary Ferrar magma is still high compared to mantle melts. The recalculation of an even more pronounced gabbro fractionation to obtain a more typical primary magma composition would yield unrealistically low contents of incompatible elements. For example, the FeO and TiO_2 contents modelled by HERGT et al. (1989b) with 8.1 wt% and 0.48 wt%, respectively, are very low compared to those of parental magmas modelled for the East Greenland tholeiitic rocks with 11.5 wt% FeO and 1.6 wt% TiO_2 (FRAM & LESHER 1997). The low FeO and TiO_2 concentrations of the Ferrar magmas could be explained by the assumption that appreciable amounts of Fe-Ti bearing phases have been fractionated during the early differentiation. However, this seems rather implausible since oxides are not found as early phenocryst phases in any of the fine-crystalline low-Ti rocks studied. Thus, the low iron and titanium concentrations as well as the high SiO_2 content can be interpreted as reflecting source characteristics.

The composition of this 'near'-primary Ferrar magma from HERGT et al. (1989b) will be used to constrain the differentiation paths of the two Ferrar magma series. It is thus included as starting composition in the major element variation diagrams in figures **4.9** and **4.10** together with the average compositions of the derivative fine-crystalline rocks of the LTS and the HTS. For the gabbro fractionation suggested above, a simplified fractionation scheme can be drawn as shown in figure **4.9**. It displays the compositional evolution of residual liquids during differentiation from basaltic to andesitic magmas controlled by fractionation of the given phases. According to this scheme, the removal of Mg-rich olivine and/or orthopyroxene causes decreasing Mg-numbers at nearly constant CaO/Al_2O_3 ratios, whereas plagioclase fractionation leads to increasing CaO/Al_2O_3 ratios at unchanged Mg#. A fractionation dominated by high-Ca clino-pyroxene causes a decrease in both the Mg# and the CaO/Al_2O_3 ratio in residual melts.
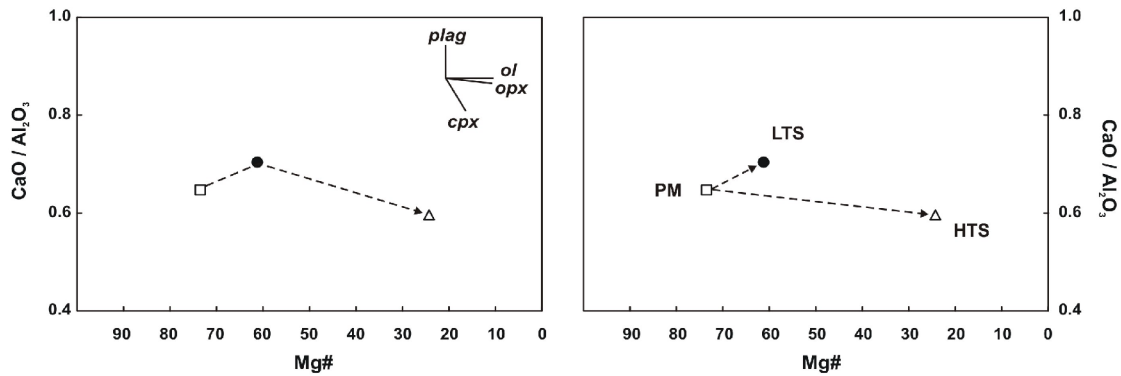
Fig. 4.9 – Variations of the CaO/Al$_2$O$_3$ ratios with Mg# of the average composition of chilled margins of low-Ti sills – **LTS** and the fine-crystalline high-Ti samples – **HTS** from Litell Rocks as well as the composition of their 'near'-parental magma – **PM** calculated by HERGT et al. (1989b). Vectors in the upper right corner of the left diagram indicate schematically the compositional evolution of residual liquids caused by removal of ol – olivine, opx – orthopyroxene, cpx – clinopyroxene and plag – plagioclase. Dashed lines indicate the two possible evolution paths of the HTS via the LTS (left) or along a separate differentiation path (right).

The individual element variations in figures **4.9** and **4.10** indicate that a gabbro fractionation, as modelled for the LTS by HERGT et al. (1989b), can be inferred for the HTS as well, but some important differences between both series are obvious. For the LTS, the increasing CaO/Al$_2$O$_3$ ratio with decreasing Mg# starting from the 'near'-primary magma composition is controlled by increasing CaO and nearly unchanged Al$_2$O$_3$ contents, which clearly reflect the modelled fractionation of ol + opx + plag. For the HTS, decreasing CaO and Al$_2$O$_3$ contents indicate that high-Ca clinopyroxene appeared in the phase assemblage instead of orthopyroxene and that the fractionation of plagioclase was more pronounced than for the LTS. The elevated Eu-anomaly of the high-Ti rocks supports this implication of more effective plagioclase removal during differentiation of the HTS. The decreasing CaO/Al$_2$O$_3$ ratio does not necessarily imply that augite fractionation was more effective than that of plagioclase, since both phases analysed have considerably different CaO/A$_2$O$_3$ ratios (plagioclase < 0.5, augite > 10) and thus removal of augite has a larger effect on this element ratio in residual melts.

The two possibilities to obtain the composition of the HTS by differentiation from the suggested 'near'-primary magma are shown exemplarily by the dashed lines in the two diagrams in figure **4.9**. Both types of evolutionary trends could be drawn for each of the element variations in figure **4.10**, as the inferred conclusions do not change whether the evolution of the HTS via the LTS or along a separate path is assumed. However, the latter model is favoured since orthopyroxene, which played a major role during the differentiation of the LTS, has not been found in any of the present high-Ti samples. Thus, only the trend lines describing the separate evolution of both magma series are shown in the variation diagrams in figure **4.10**. The distinct trends of CaO, Al$_2$O$_3$ and CaO/Al$_2$O$_3$, the distinctly different Mg-numbers as well as the less pronounced increase of SiO$_2$ and Na$_2$O contents and the steeper increase of FeO and TiO$_2$ contents for the HTS than for the LTS give evidence that 1) different pyroxenes have been fractionated, 2) different amounts of pyroxenes and plagioclase have been fractionated, and 3)

pyroxenes and plagioclase have been of different composition for both magma series. These implications are confirmed by the mineralogical and mineral chemical compositions obtained for the analysed rocks. For example, fractionation of plagioclase of more albitic composition, such as analysed in the high-Ti samples with > 54 wt% SiO_2 and > 4 wt% Na_2O, yields a less pronounced enrichment of these two elements in the residual magma compared to fractionation of anorthitic plagioclase, which has been analysed in low-Ti chilled margins with 47 wt% SiO_2 and < 1.5 wt% Na_2O. However, different amounts of fractionating phases, especially different pyroxene / plagioclase ratios, may have played an even more important role on the melt evolution. A lower pyroxene / plagioclase ratio being fractionated during evolution of the HTS can explain the fact that FeO and TiO_2 increase more significantly while SiO_2 and Na_2O increase less significantly in residual high-Ti melts than in low-Ti magmas. This furthermore explains the higher FeO and TiO_2 contents in pyroxenes analysed in high-Ti rocks.
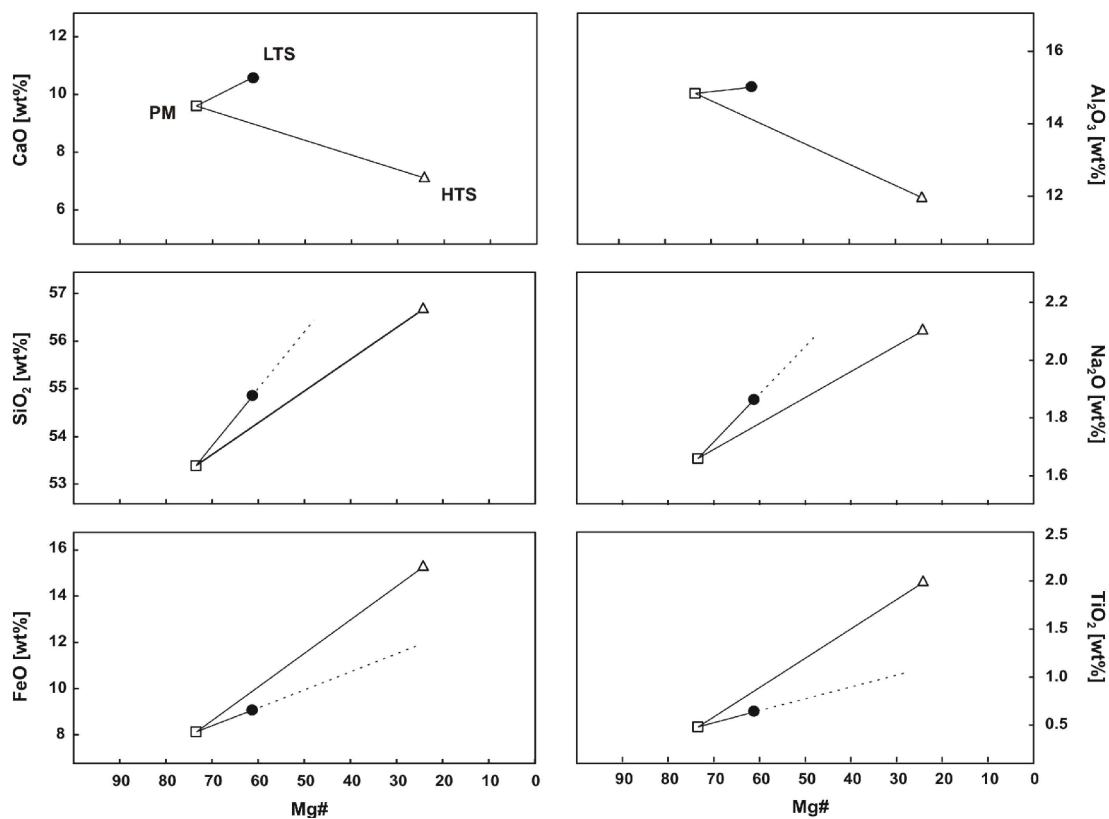
Fig. 4.10 – Variations of selected major elements with Mg# of the average compositions of fine-crystalline low-Ti and high-Ti rocks as well as the composition of the 'near'-primary Ferrar magma from HERGT et al. (1989b). Solid lines mark the evolutionary trends from the primary magma composition; dashed lines mark the suggested continuation of differentiation of the low-Ti magma series under unchanged conditions with the purpose of indicating the differences to the HTS. Symbols as in figure **4.9**.

In conclusion, the distinct trends inferred for the pre-emplacement differentiation of the two Ferrar magma series indicate that a simple continuation of the gabbro fractionation proposed for the LTS cannot explain the evolution of the HTS and its distinct composition. This conclusion is in accordance to interpretations of HABAN & ELLIOT

(1985), FLEMING & ELLIOT (1988), FLEMING et al. (1992) and MENSING & FAURE (1996), who emphasised that other factors must have been involved.

From the considerations above, it is concluded that both magma series experienced the pre-emplacement differentiation under different physico-chemical conditions prevailing during differentiation (e.g. T, P and fO_2), since they have been accepted to largely control the stability of crystallising phases and their compositions. This suggestion is in agreement with the relative differences of intensive crystallisation parameters emphasised for both magma series in chapter **3.2.5**. Other physical parameters may have played an important role as well, such as the densities of the crystals and the magmatic liquid or the rate of magma movement. Some of these parameters, suggested as having influenced the generation of the two Ferrar magma series, will be considered in more detail afterwards.

However, to constrain, if solely the differentiation history of both magma series caused their distinct geochemical evolution, in the following the before-mentioned assumptions of negligible differences in melt generation and magma source composition will be tested.

4.4   PARTIAL MELTING

For understanding the process of partial melting and its influence on primary magma composition, it is necessary to evaluate the complex relations of several factors such as the mineralogical and chemical composition of the melting source, the conditions during the melting process (pressure, temperature, volatile contents), the degree of melting as well as the mechanism of the melting process itself (equilibrium or fractional melting). Reliable evidence on the chemical composition and mineralogy of the upper mantle can be inferred from kimberlite- or basalt-hosted xenoliths of presumed mantle origin. Based on comprehensive data about the nature of such xenoliths, it is now generally accepted that partial melting of peridotite in the upper mantle plays an important role in the generation of basaltic melts. During the last decades, a large number of melting experiments at high-pressure conditions have been performed to constrain the effects of source peridotite composition and the degree of melting under variable conditions on the partial melt composition (e.g. JAQUES & GREEN 1980, TAKAHASHI & KUSHIRO 1983, HIROSE & KUSHIRO 1993, FALLOON et al. 2001). Compared to alkali basalts, which are believed to be generated by relatively small degrees of partial melting at high pressures (within ascending plumes from a deep-seated mantle reservoir), tholeiitic flood basalts are widely suggested to be derived by larger melting degrees at lower pressures (e.g. YODER & TILLEY 1962, JAQUES & GREEN 1980). The relatively high melting degrees are in accordance to the large volumes of magma produced during LIP magmatism.

The site and nature of melting sources as well as their composition have been discussed controversially, but some consensus seems to exist concerning the importance of the subcontinental lithosphere in continental LIP generation (in addition to the asthenosphere) (e.g. ELLAM & COX 1989, 1991, LIGHTFOOT et al. 1993, LASSITER & DEPAOLO 1997). For the Paraná-Etendeka province, for example, GALLAGHER &

HAWKESWORTH (1992) proposed melt generation entirely in the subcontinental lithosphere that has partly been affected by the presence of small amounts of volatiles. They emphasised that a hydrous peridotitic source (compared to anhydrous peridotite) with a depressed solidus increases the feasibility of partial melting of lithospheric mantle. TURNER & HAWKESWORTH (1995) reviewed the major element characteristics of continental flood basalts and suggested their derivation from melting of a hydrated, depleted peridotitic source within the lithospheric mantle that previously experienced episodes of melt extraction as well as enrichment in incompatible elements and volatiles. HARRY & LEEMAN (1995) proposed a similar model; they also favoured partial melting of metasomatised subcontinental lithospheric mantle.

For the Ferrar province, the option of derivation of the primary magmas from a crustal source (inferred by their crust-like geochemical signatures) has been considered most unlikely for several reasons as summarised, for example, by HERGT et al. (1989b). Instead, according to the models proposed for some other continental flood basalt provinces, the melting source for generation of the Ferrar magmas has been established to be a primarily melt-depleted lithospheric mantle that has been enriched by crustal components during Palaeozoic subduction processes at the continental margin of Gondwana (e.g. KYLE 1980, HERGT 1989b, 1991, FLEMING et al. 1992, 1995, MOLZAHN et al. 1996). Evidence for this conclusion will be reviewed in more detail in the next chapter considering the composition of the Ferrar source.

While the estimation of absolute values of the different factors influencing melting processes is largely subject to some uncertainties due to model-sensitive parameters, relative differences between related magma series (e.g. the extent of partial melting) can be more easily constrained (HARGRAVES 1980). For this reason, the purpose of the following considerations will not be a quantitative characterisation of all these factors but rather an evaluation if significant differences in these factors controlled the generation of the two Ferrar magma series.

For many flood basalt provinces, the presence of a wide diversity of basaltic magma compositions has been described, and they are distinguishable from each other by their distinct concentrations and ratios of incompatible trace elements. For some of them, the main arguments for the presence of these distinct magma series and their spatial and / or temporal separation have been variable degrees of partial melting and changing conditions during melt generation rather than significant magma source heterogeneities. A few examples will briefly be given before testing the option of different melting degrees and conditions for the genesis of the present Ferrar rocks.

An often suggested explanation for different melting degrees is the apparent relation between the chemical signatures of the magma series and their distance from a proposed mantle plume. This implication has mainly been inferred from the geographical separation of distribution areas of these series. For example, for the Caribbean-Colombian oceanic plateau, KERR et al. (1997) described both tholeiitic and mildly alkaline basalts of which the latter exhibit higher Ti/Y and Nb/Zr ratios as well as steeper slopes of distinct parts of the chondrite-normalised REE patterns (see figure **4.13**). These features have been suggested to represent lower degrees of melting in the cooler outer zones of the plume head or a later melting episode during cooling-

down of the plume. COX & ELLAM (1991) as well explained the geochemical provinciality within the Karoo province to some extent by distinct geographical positions relative to the plume axis. An analogue explanation has been given by FODOR (1987) for the low-Ti and high-Ti magma series (TiO$_2$ ~ 1 wt% and > 3 wt%, respectively) of the Paraná province of southern Brazil. Assuming an essentially homogeneous magma source across the entire province, the higher incompatible element concentrations of the high-Ti rocks are ascribed to lower melting degrees caused by a larger distance to the early Tristan da Cunha hotspot. Different rates of melt production for the high- and low-Ti basalts of the Paraná-Etendeka province have also been suggested by HAWKESWORTH et al. (2000). However, after their model, initially produced lithosphere-derived melts from a hydrous peridotite are followed by asthenosphere-derived melts generated from an anhydrous peridotite. In contrast to FODOR (1987), HAWKESWORTH et al. (2000) related the inferred changes in the melting degrees, the source regions and the resulting magma compositions to changes in the extension history at the continental rift margins during the break-up of Gondwana.

Another example suggesting that differences in the melting process controlled the generation of 'low-Ti' and 'high-Ti' magma types in continental flood basalts has been given by ARNDT et al. (1993), who attributed the assumed differences to varying lithospheric thicknesses. They concluded that where the lithosphere is thick the melt is generated at higher pressures in the garnet stability field and at lower melting degrees resulting in higher abundances of incompatible trace elements as typical for high-Ti magma types. The opposite is proposed assuming thin lithosphere, where the melt generation proceeded under lower pressure and by an elevated melting degree. The generated melts rather correspond to the low-Ti magma type with characteristically lower concentrations of incompatible trace elements compared to those of the high-Ti magmas.

As evident from the previous considerations, the conclusion of different melting degrees has partly been inferred from the observation of systematic differences in overall absolute abundances of incompatible elements, since their concentrations are inversely correlated to the extent of partial melting. Thus, the generally higher abundances of incompatible major and trace elements of the Ferrar HTS compared to the LTS imply different degrees of partial melting as possible explanation of the distinct composition of both magma series. Therefore, according to the model of FODOR (1987) for the Paraná Province, a somewhat lower melting degree for the Ferrar HTS (15 – 20 %) compared to the LTS (~ 25 %) has been proposed by HORNIG (1993). This range of melting degree corresponds to that suggested for the LTS (~ 20%) by ANTONINI et al. (1999) and to the high melting degree of > 25% modelled for the LTS by DEMARCHI et al. (2001). Nevertheless, the conclusion of different melting degrees based on incompatible element contents is only appropriate as long as a significant influence of variable differentiation degrees on the composition of the co-genetic magma series can be ruled out. This context is exemplarily shown in figure **4.11** by the variations of TiO$_2$ against Zr of the present Ferrar rocks including schematic variation trends that illustrate the compositional evolution of magma during fractional crystallisation as well as partial melting.
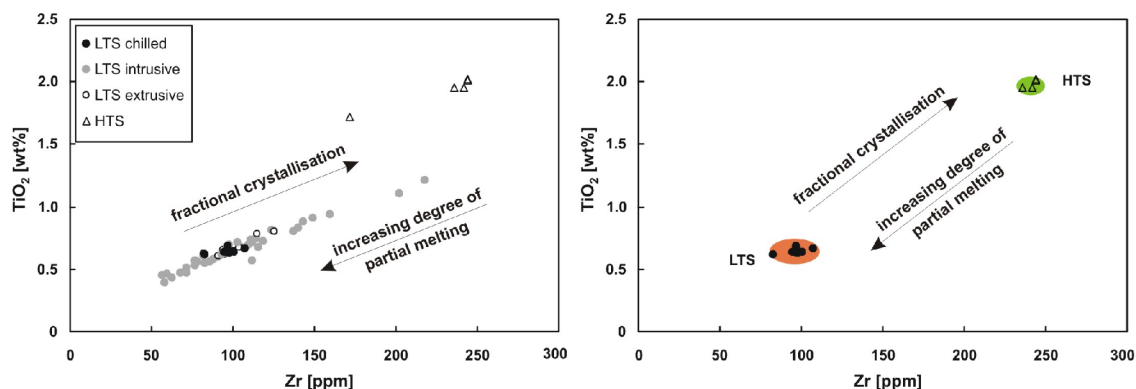
Fig. 4.11 – Variations of TiO$_2$ vs. Zr of the analysed Ferrar rocks. The left plot shows the entire element variations of both magma series attributable to *in situ* differentiation. The right plot shows only the compositional differences of the fine-crystalline low-Ti and high-Ti samples attributable either to fractional crystallisation during pre-emplacement differentiation or to different degrees of partial melting.

The systematically increasing TiO$_2$ and Zr concentrations displayed by the present low-Ti and high-Ti rocks (left diagram) can clearly be ascribed to *in situ* differentiation by fractional crystallisation under low-pressure conditions as discussed in chapter **4.2**. For comparison, the right diagram shows only the compositional differences between the fine-crystalline low-Ti and high-Ti rocks. The elevated concentrations of the two incompatible elements of the high-Ti rocks are consistent with both subsequent fractional crystallisation from the low-Ti to the high-Ti magmas and lower degrees of partial melting for the generation of the high-Ti compared to the low-Ti magmas. This example shows the inadequacy of establishing different melting degrees for related magma series solely by incompatible element concentrations. Instead, ratios of incompatible trace elements such as Zr and Y or individual REE provide tools that are more independent to assess the depth and the extent of melt generation.

For example, FRAM & LESHER (1997) obtained largely variable Zr/Y ratios and Zr concentrations for different tholeiitic rock series within the East Greenland Tertiary flood basalts and related these differences to mantle melting systematics (and source compositions). Nevertheless, BERNSTEIN (1994) interpreted increasing Zr/Y ratios with decreasing MgO for tholeiitic basalts from the Faeroe Islands to result from high-pressure crystal fractionation involving garnet at the base of the continental crust. Comparatively, increasing Zr/Y ratios with increasing Zr (and decreasing MgO) are also displayed by the Ferrar low-Ti rocks (Fig. **4.12**), but can clearly be ascribed to low-pressure *in situ* differentiation with Y being less incompatible than Zr due to its slightly higher partition coefficient for the fractionating pyroxenes (e.g. FUJIMAKI et al. 1984, GREEN 1989). However, the present fine-crystalline Ferrar low-Ti and high-Ti rocks do not exhibit markedly different Zr/Y ratios (Fig. **4.12**), although significantly elevated concentrations of both elements are characteristic for the high-Ti rocks. These different absolute concentrations of Zr and Y clearly reflect the variable degrees of differentiation of the low-Ti and high-Ti rocks, but the homogeneous Zr/Y ratios may imply that no significant differences in the melting degree (and magma source compositions) have to be assumed.
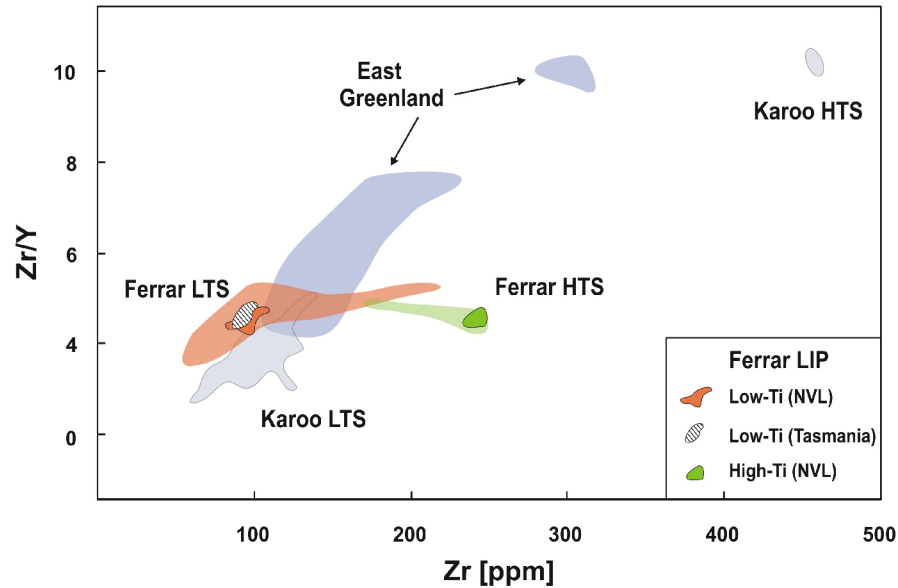
Figure 4.12 – Variations of Zr/Y ratios with Zr of the analysed Ferrar low-Ti and high-Ti rocks from northern Victorialand; stronger coloured fields mark the compositions of the fine-crystalline rocks, light-coloured fields mark the entire variation range. For comparison, data for chilled margins of low-Ti sills from Tasmania (HERGT et al. 1989b) as well as low-Ti and high-Ti Karoo basalts from Lesotho (MARSH et al. 1997) and East Greenland flood basalts (FRAM & LESHER 1997) are included.

The lack of evidence of differences in the melting degree, inferred from the comparable Zr/Y ratios of the present fine-crystalline Ferrar low-Ti and high-Ti rocks, will further be tested by some REE characteristics. Although the REE are known to behave as largely incompatible element group, solid/melt partition coefficients of the individual REE have been determined to be systematically different for distinct mantle minerals (e.g. NICHOLLS & HARRIS 1980, JOHNSON 1984). Thus, partial melting of mantle material consequently results in a fractionation between the individual REE in the mantle residua and in the generated melt. The extent of this fractionation of light REE from heavy REE largely depends on the degree of melting and the phase assemblage of the source material. Since the partitioning of HREE for garnet and spinel peridotite largely differs and since the stability of these phases strongly depends on pressure, chondrite-normalised REE patterns are important tools to constrain relative differences in melting degrees and in source compositions and hence in depth of the melting source.

Irrespective whether garnet or spinel is present in peridotite, partial melting will enrich the LREE due to their higher incompatibility in most mantle phases compared to those of the MREE. Consequently, LREE/MREE ratios (e.g. La/Sm) indicate relative differences of melting extents. Furthermore, the slope between MREE and HREE (e.g. Sm/Yb) gives evidence about the presence of residual garnet in the melting source, since garnet preferentially accommodates the HREE due to their elevated garnet/melt partition coefficients. These values systematically increase from the MREE towards the HREE (e.g. JOHNSON 1994), and thus a markedly negative slope in this section of REE patterns indicates residual garnet. These relations are displayed in figure **4.13**, which has been modified after LASSITER & DEPAOLO (1997). One main advantage using REE

ratios is that they are only little influenced by fractional crystallisation, while changes in melting extents or source compositions markedly change these element ratios.

The large variations of REE ratios displayed in figure **4.13** for compositionally distinct magma series from various flood basalt provinces are mostly well explained by difference in melt fractions and / or source mineral assemblages. For the Siberian Traps, for example, SHARMA (1997) observed variations of REE ratios with stratigraphic heights and ascribed them to changes in the melting environment with temporal evolution of the LIP. Contrary, the present Ferrar rocks (and the data from literature) exhibit an overall homogeneous composition with rather limited variations of REE fractionation between individual rocks (see also figure **3.23**). Since increasing melt fraction lowers the difference between La and Sm enrichment in the melt, the moderate La/Sm ratios shown for all Ferrar rocks indicate rather moderate to high degrees of partial melting. Nevertheless, elevated La/Sm ratios may also be evidence of considerable contribution of crustal material, whether indicating crustal assimilation or source characteristics (see next chapter). Hence, the Ferrar magmas were generated possibly at even greater melting degrees, which are obscured by crust-like signatures. Furthermore, the characteristically low Sm/Yb ratios imply the absence of residual garnet in the melting source, and thus may give evidence of lower pressure conditions during melt generation. However, it is also possible that garnet has been a stable phase in the mantle residua, but has been entirely consumed due to the high melting degree proposed.
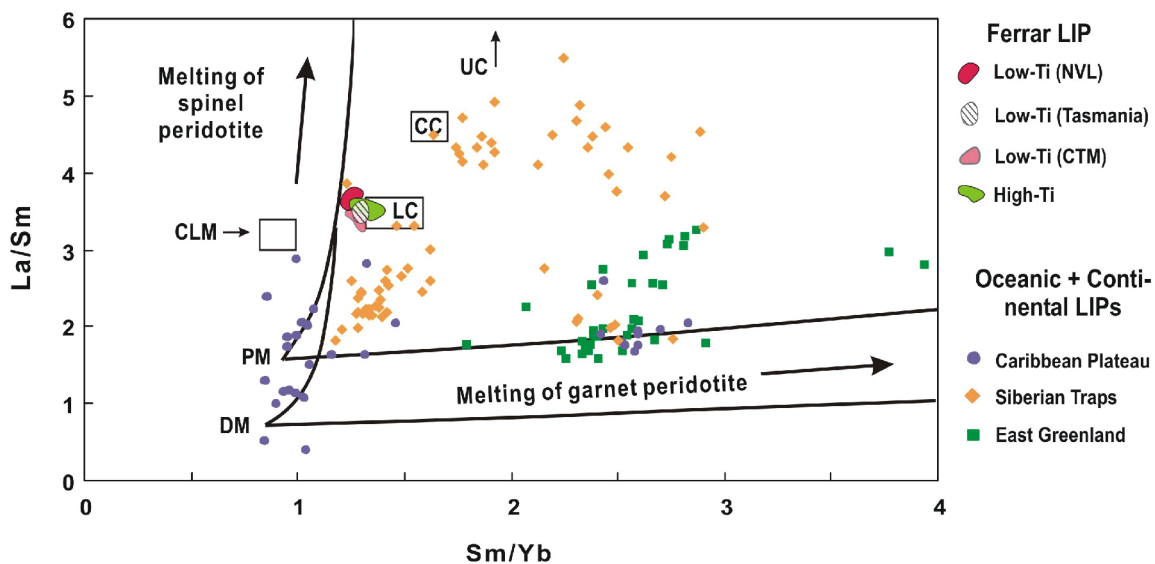
Fig. 4.13 – Melting relations from La/Sm vs. Sm/Yb for the analysed Ferrar low-Ti and high-Ti rocks from NVL. Arrows show the effect of decreasing melting extent. Further Ferrar data include low-Ti sills from Tasmania (HERGT et al. 1989b), a low-Ti sill from the central Transantarctic Mts. (CTM) (HERGT et al. 1989a) and high-Ti rocks from the Mesa Range and the CTM (ELLIOT et al. 1995, 1999). East Greenland flood basalts are from FRAM & LESHER (1997); Siberian Traps from LIGHTFOOT et al. (1993) and WOODEN et al. (1993); Caribbean Plateau from DONNELLY et al. (1973), SEN et al. (1988) and KERR et al. (1996). The solid lines mark the calculated trends of batch melting of spinel and garnet peridotite taken from LASSITER & DEPAOLO (1997), see references therein for compositions of primitive (PM), depleted (DM) and continental lithospheric (CLM) mantle as well as upper (UC), lower (LC) and bulk continental (CC) crust.

Nevertheless, the main point inferred from the observed signatures for Ferrar rocks in figures **4.12** and **4.13** is that there exists no obvious difference between the fine-crystalline rocks of the low-Ti and the high-Ti magma series, and thus similar extents and depths of melting (and similar magma source compositions) are concluded. Of course, the effect of only slightly varying degrees of partial melting on compositions of two coexisting magma series is less sensitive at higher than at lower melting degrees. Since higher melting degrees are deduced for the Ferrar magmas, it is possible that even though the REE patterns of the Ferrar LTS and HTS do not vary significantly there was a (small) difference in their melting degree. Even so, it remains questionable if a small difference in the melting degree was adequate to obtain the distinct compositions of the two magma series. However, an interpretation of the very small differences in any REE or trace element ratio for the two Ferrar magma series as resulting from different melting histories may be overrated. Instead, such small differences could partly be ascribed to analytical uncertainty due to interlaboratory bias, since the various authors applied largely different analytical techniques.

Aside from the use of trace element and REE ratios, the depth and extent of partial melting of mantle sources can be estimated from the major elements as well. After FRAM & LESHER (1993), the FeO content of a primary partial melt correlates positively with the melting pressure, corresponding to the experimental results from HIROSE & KUSHIRO (1993). Furthermore, the contents of (moderately) incompatible elements (e.g. TiO_2, Na_2O) of a melt decrease with increasing degree of partial melting as mentioned above. These findings confirm the observations of KLEIN & LANGMUIR (1987), who noted a strong negative correlation of FeO and Na_2O for average MORB compositions, which have been corrected for low-pressure gabbro fractionation to MgO contents of 8 wt%. This correlation was interpreted as resulting from increasing melting degrees at increasing pressure. In contrast to this global average correlation, KLEIN & LANGMUIR (1989) observed local variations, often showing positively correlated corrected FeO and Na_2O contents, which are attributed to lower melting pressures and increasing melting degrees. This feature of generally low FeO and Na_2O contents is exhibited by a large number of continental flood basalts such as those of the Ferrar LIP. Additionally, JAQUES & GREEN (1980) emphasised from melting experiments that partial melting at low pressure produces melts that are more silica saturated than those generated at higher pressure and furthermore, that high degrees of melting at lower pressure generate silica-rich olivine-poor tholeiites (like the Ferrar rocks). TURNER & HAWKESWORTH (1995) summarised the melting systematics of peridotite by reviewing the experimental results from anhydrous peridotite melting from e.g. FALLOON et al. (1988) and hydrous partial melting from e.g. GREEN (1973). They pointed out that melting of hydrous peridotite, where the solidus is markedly depressed below the anhydrous solidus, results in silica-richer melts than obtained by anhydrous studies and thus confirmed the findings reported by JAQUES & GREEN (1980). In conclusion, TURNER & HAWKESWORTH (1995) explained these major element systematics, which are typical for many tholeiitic flood basalts, with melt generation from a hydrated, melt-depleted peridotitic mantle in the subcontinental lithosphere.

In respect of these considerations, the generally low FeO, TiO_2, Na_2O and elevated SiO_2 concentrations characteristic for the Ferrar tholeiites (compared to many oceanic tholeiites at similar Mg#) support the high degree of partial melting as inferred from the REE ratios. Additionally, these features indicate rather lower pressure conditions during the melt generation corresponding to the missing garnet signature as previously discussed and emphasise the depleted and hydrous nature of the Ferrar melting source. The latter implications have also been favoured by HERGT et al. (1991) and DEMARCHI et al. (2001); in both studies it is emphasised that the elevated SiO_2 contents observed in the Ferrar rocks can be reached only if the melt was generated from a hydrous peridotite. Certainly, the above considered characteristics of the Ferrar rocks have to be discussed in conjunction with the composition of the magma source, which may be atypical to a certain extent (see next chapter).

A further argument supporting the deduced high degrees of melting is the S-under-saturated nature of the present Ferrar rocks that has been inferred previously from the PGE characteristics. While magmas generated at low to moderate melting degrees are S-saturated due to the retention of PGE-rich sulphides in the source residue (HAMLYN et al. 1985, HAMLYN & KEAYS 1986), at elevated melting degrees of 20 % to 25 %, sulphides may have been entirely exhausted in the melting residue (e.g. BARNES et al. 1985, HAMLYN et al. 1985, KEAYS 1995, REHKÄMPER et al. 1999b). Thus, the produced melts are S-undersaturated. In consideration of these findings, MAIER et al. (2003) inferred different melting extents from PGE characteristics of southern African flood-type basalts from various geographical regions and geological ages. Based on strongly varying Cu/Pd ratios, they emphasised increasingly lower extents of mantle melting throughout geological time. In contrast, PHILLIP et al. (2001) and MOMME et al. (2002, 2003) observed also variations of Cu/Pd ratios (albeit less pronounced) for distinct stratigraphic units of tholeiites from Greenland and Iceland, but ascribed them to silicate fractionation with subordinate, concurrent segregation of sulphides. Neverthe-less, no significant differences in the Cu/Pd ratios have been obtained for most of the analysed Ferrar rocks (Fig. **4.5**), except for those that are attributed to the changed fractionation behaviour of Pd during *in situ* differentiation. In general, further implications for the Ferrar melt generation such as differences in the melting extent are difficult to assess by means of PGE characteristics, since the obtained differences in absolute concentrations and ratios between individual PGE and between individual samples can be well explained by differentiation processes (see chapters **4.2** and **4.3**).

In conclusion, the only moderate LREE/MREE fractionation, the absence of a marked MREE/HREE fractionation and the unchanged ratios of incompatible trace elements as well as certain major element features obtained for the fine-crystalline low-Ti and high-Ti Ferrar rocks indicate 1) similar, moderate to high melting degrees for both magma series, 2) melt generation at lower pressures without garnet as stable mantle phase and 3) possibly a derivation from a hydrous peridotitic source depleted by earlier melt extraction. From these considerations, it is favoured that no significant differences are required for the melt generation of the two Ferrar magma series implying the same depth and degree of melt generation and moreover, an indistinguishable composition of

the melting source. The last implication suggesting a homogeneous magma source for both Ferrar magma series will be discussed in the next chapter.

4.5   MAGMA SOURCE

One of the favoured models explaining the presence of compositionally distinct magma types within individual large igneous provinces has been the assumption of magma derivation from different sources within the asthenospheric and / or the lithospheric mantle. In such complex models, suggesting lithospheric-asthenospheric interaction, variable amounts of contribution from both source regions are proposed to be responsible for the generation of distinct magma types (e.g. GIBSON et al. 1995, PEATE & HAWKESWORTH 1996, LASSITER & DEPAOLO 1997, PEATE 1997, MARZOLI et al. 2000). As outlined beforehand, there has been general agreement about the importance of the subcontinental lithospheric mantle for the generation of the Ferrar magmas and furthermore, about a noticeable continental crustal signature of the resulting tholeiitic rocks.

In the following, the Ferrar magma source will be characterised based on the major and trace element composition of the present Ferrar rocks from NVL and George V Land. Beyond the present state of knowledge about the Ferrar magma source, the discussion of the obtained data is mainly directed towards possible differences in source composition for the two magma series. Afterwards, a brief comparison with previously published results from isotope studies from the whole Ferrar province will be given in order to emphasise the origin of the characteristic crust-like component. Finally, the obtained PGE systematics will be discussed with respect to magma source characteristics and a possible mantle plume involvement in the generation of the Ferrar magmas.

4.5.1   Evidence for magma source composition from major and trace elements

Aside from trace element and isotope characteristics, mostly applied to constrain the nature of mantle sources of continental flood basalts, their major element compositions provide powerful tools as well. As denoted in chapter **4.4**, TURNER & HAWKESWORTH (1995) reviewed the most characteristic features that are typical for many continental LIPs and distinguish them from their oceanic counterparts such as mid-ocean ridge or ocean island basalts (MORB and OIB, respectively). Hence, they emphasised the subcontinental lithospheric mantle as one of the main source regions of melt generation for continental flood basalts. Their crucial arguments of comparably low FeO, TiO_2, Na_2O and elevated SiO_2 contents, indicating lithospheric mantle sources, are exhibited by the present Ferrar magmatic rocks as well. The refractory nature of the subcontinental lithospheric mantle is explainable by previous events of melt extraction.

Further evidence on the composition of this lithospheric source can be deduced from trace element characteristics. The present Ferrar rocks exhibit, for example, enrichment of LREE relative to MREE and HREE causing the negative slope of the chondrite-normalised REE patterns (Fig. **3.23**). This is well expressed by the La/Sm

ratios in figure **4.13**, in which both the fine-crystalline low-Ti and high-Ti rocks show elevated La/Sm ratios relative to primitive mantle or depleted mantle composition. The composition of the Ferrar rocks is shifted towards La/Sm and Sm/Yb ratios that are close to those of the lower crust.

Besides REE systematics, indicating chemical similarities to crustal rocks, further evidence of crustal influence on the Ferrar magma composition is given by its enriched concentrations of incompatible elements. This is well demonstrated by the multi-element spider diagram in figure **4.14**, in which the element abundances are plotted normalised to primitive mantle composition. The incompatible elements in this plot are ordered 1) according to their mobility with the mobile element group to the left (except Sr) and 2) according to their relative incompatibilities generally decreasing from the left to the right.
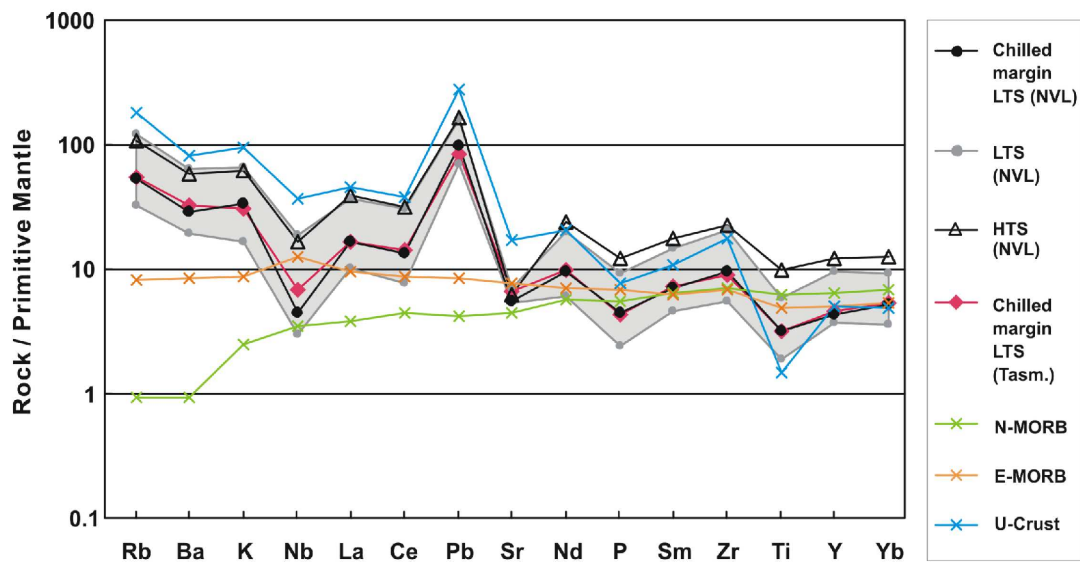
Fig. 4.14 – Primitive mantle-normalised multi-element patterns for the analysed Ferrar low-Ti and high-Ti rocks from NVL and George V Land. The grey field encloses the patterns of most primitive and most evolved low-Ti samples analysed. The pattern of the average chilled margin composition for Tasmanian Ferrar low-Ti sills (HERGT et al. 1989b) as well as those of normal-type (N-) and enriched-type (E-) MORB (SUN & MCDONOUGH 1989) and of the average upper continental crust (TAYLOR & MCLENNAN 1985) are included for comparison. Normalisation values of primitive mantle are from MCDONOUGH & SUN (1995).

These multi-element variations show that all present Ferrar rocks are characterised by enriched element concentrations relative to primitive mantle. They feature strong enrichment of the large-ion lithophile elements (LILE: Rb, Ba, K, LREE) as well as pronounced troughs at Nb, P and Ti and a strongly positive Pb anomaly. By comparison, it is noteworthy that there are no obvious differences for the low-Ti and high-Ti rocks; both exhibit very homogeneous multi-element patterns and REE patterns resulting in almost undistinguishable REE ratios. Certainly, there are differences in the extent of element enrichment, but since absolute concentrations of trace elements can be largely influenced by differentiation processes, trace element ratios provide more useful tools to constrain differences in mantle source compositions of cogenetic

magmatic rocks. One example has been shown in figure **4.12**, where the fine-crystalline low-Ti and high-Ti rocks do not show differences in the Zr/Y ratios, although both elements are significantly enriched in the high-Ti relative to the low-Ti samples. These variably enriched element concentrations (e.g. Zr, Y, TiO_2, REE) and different magnitudes of the anomalies in the mantle-normalised patterns for individual samples are clearly explainable by variable degrees of differentiation of the distinctly evolved rocks of the LTS and HTS as discussed in the previous chapters. However, the agreement of trace element characteristics of both magma series emphasises that significant differences in the magma source composition are not required to explain their genesis. It is rather suggested that both series derived by melt generation from the same source region.

Nevertheless, the multi-element patterns presented are characteristic for all Ferrar tholeiitic rocks (e.g. HERGT et al. 1991, MOLZAHN et al. 1996, ANTONINI et al. 1999) and are shown similarly by other continental flood basalts, for example from the Karoo province (COX et al. 1984), the Columbia River Plateau (HOOPER 1997) or by the Jurassic dolerites from Coats Land and Dronning Maud Land, Antarctica (BREWER & CLARKSON 1987). These patterns largely differ from those of oceanic basalts, which in contrast do not show decoupling of LILE and high-field strength elements (HFSE) as exemplarily displayed by the patterns of normal-type and enriched-type MORB. The fractionation of HFSE from LILE is rather typical of subduction related magmas and almost all rocks in the continental crust (e.g. ARNDT et al. 1993). This is demonstrated in figure **4.14** by the composition of the terrestrial shale from TAYLOR & MCLENNAN (1985), representing the average composition of the upper continental crust. The apparent agreement between this remarkable crustal pattern and those of the Ferrar rocks confirms the widely accepted implication that the major and trace element composition of the Ferrar rocks does not agree with an origin in typical mantle, but rather reflects the contribution of some crustal component. In general, a LILE/HFSE decoupling of mantle derived magmas could have been inherited either through contamination of basaltic magma by crustal assimilation during its ascent to the surface or by partial melting of an atypical mantle source, a subcontinental lithospheric mantle wedge that experienced enrichment in LILE by slab-derived fluids during earlier subduction processes (e.g. PEARCE 1983).

To summarise, the crust-like trace elemental features for the present Ferrar tholeiitic rocks from NVL and George V Land are largely comparable to those reported from previously studied Ferrar rocks from southern Victorialand, the Transantarctic Mountains, Tasmania and Southeast Australia as well as from the Dufek Intrusion. Considering such a large distribution area of occurrences of Ferrar magmatic rocks, the conspicuous agreement of their crustal signatures is difficult to explain by contamination with crustal material during passage of the magma through the continental crust. Thus, a large number of authors emphasised the probability of derivation of the Ferrar magmas and their unique compositional features from a uniformly enriched mantle source region. This topic has been discussed controversially based on comprehensive studies of the isotopic composition of the Ferrar rocks. The main points of argumentation will be summarised briefly in the following.

4.5.2   Comparison with magma source constraints from isotope studies

Over the last decades, a large data set describing the isotope composition of the Ferrar rocks from Antarctica and Tasmania has been acquired including O, Sr, Nd, Pb and Os isotope data. All analysed rocks from the entire Ferrar province exhibit considerably elevated initial $^{87}Sr/^{86}Sr$ ratios (> 7.08) and slightly depleted $^{143}Nd/^{144}Nd$ ratios (ε_{Nd} < -3) compared to the composition of the bulk-silicate earth. Comparable values are typically shown by crustal rocks rather than by magmatic rocks derived from the upper mantle. Hence, similar to the crust-like trace element signatures, these uniform isotope features have been interpreted contrarily and debate was centred on the origin of such radiogenic Sr isotope compositions with models advocating either hydration of mantle material from subducted slab components or interaction with the crust.

Particularly, some of the earlier published Sr and O isotope data of Ferrar basaltic andesites such as from the Queen Alexandra Range, central TAM (FAURE et al. 1974, HOEFS et al. 1980) or the Mesa Range, NVL (MENSING et al. 1984) have been interpreted as resulting from combined assimilation and fractional crystallisation processes (AFC, DePAOLO 1981). HOEFS et al. (1980) for example, attributed positive correlations between $\delta^{18}O$ and the initial $^{87}Sr/^{86}Sr$ ratios and major elements to wall-rock assimilation during the magma ascent to the surface. Such AFC processes causing the unusual isotope composition of the Ferrar rocks have been confirmed more recently by isotope chemical modelling by ANTONINI et al. (1999), but there have been some critical objections to this model by HERGT (2000). Meanwhile, it had been widely recognised that contamination of basaltic melts with crustal material causes an increase in $\delta^{18}O$ with increasing contribution of the crustal component. However, FLEMING et al. (1992, 1995) denoted that Ferrar rocks with anomalously high initial Sr and low Nd isotope ratios have $\delta^{18}O$ values (+ 5.6 ‰) that are not significantly elevated but rather typical of mantle rocks. These findings indicated that involvement of high $\delta^{18}O$ crustal material possibly did not have a major impact on the Ferrar magma composition and hence their isotope signatures were suggested to reflect an inherent feature of the uncontaminated primary Ferrar magmas.

Additionally, large variations of the $^{87}Sr/^{86}Sr$ ratios ranging from 0.708 to 0.718 have been reported for the Ferrar rocks indicating that their isotope composition is not at all homogeneous. Based on this observation, KYLE (1980) discussed the possibility that these variations reflect small-scale source heterogeneities. However, the assumption of compositional differences of the underlying magma source for spatially separated Ferrar occurrences is difficult to assess based solely on Sr isotope variations, since the Sr isotope system is known to be easily disturbed by post-magmatic processes such as alteration or weathering. Indeed, from correlations of the Sr isotope data with alteration-sensitive parameters such as the loss on ignition, FLEMING et al. (1992) emphasised that much of the Sr isotope variation shown by the extensively studied lava flow sequences from the Mesa Range may have been caused by low-temperature, hydrothermal alteration. Moreover, the homogeneity of the ε_{Nd} values (–5.04 to –5.36) reported by HERGT et al. (1989b) for Tasmanian Ferrar dolerites supports the interpretation that much of the variability of Sr isotopes can be attributed to secondary alteration rather than to differences in source composition or AFC processes.

In general, the distinction whether the Ferrar magmas experienced contamination by crustal assimilation or if they derived from a compositionally atypical mantle source is not recorded or observed through the use of only O, Sr, Nd and Pb isotope data. In contrast, osmium isotopes have the potential to distinguish between subduction-related (SCLM) and crustal components in continental flood basalts. While continental crust has high Re/Os ratios and thus is characterised by extremely radiogenic Os isotopes (markedly higher than mantle values), the continental lithospheric mantle has been shown to possess subchondritic γ_{Os} values (e.g. WALKER et al. 1989, ELLAM et al. 1992, CARLSON & IRVING 1994). According to this, contributions of crustal components and continental lithospheric mantle will affect the Os isotopes oppositionally.

For testing the model of crustal assimilation, proposed mainly in earlier Ferrar studies, MOLZAHN et al. (1996) investigated the Os, Sr, Nd, Pb and O isotope composition of whole-rocks and partly of mineral separates from Ferrar occurrences in Victorialand. On the basis of Sr-O and Sr-Os isotope mixing calculations between depleted mantle peridotite and crustal material using geochemical data from the TAM, they confined the amount of added crustal material to 2 – 3 % at most, confirming the results of an earlier study by HERGT et al. (1989b). This conclusion has been confirmed by BRAUNS et al. (2000) and HERGT & BRAUNS (2001), who carried out Os isotope studies on oxides separated from Ferrar basaltic andesites from Tasmanian. The obtained unradiogenic initial $^{187}Os/^{188}Os$ ratios (0.145 ± 0.045 2σ, comparable to those from MOLZAHN et al. 1996) have been interpreted as being inconsistent with assimilation of crustal rocks by mantle-derived magmas. Instead, the model is favoured that suggests a melt-depleted mantle source that has been subsequently re-enriched by the introduction of upper-crustal materials before the melt generation from this source.

A further potential role for Re-Os isotope characteristics lies in their ability to distinguish between shallow (lithospheric) and deep (asthenospheric) mantle source regions. While mantle xenoliths representing the subcontinental mantle lithosphere have been demonstrated to exhibit very low, mainly negative γ_{Os} values, ocean-island (plume) magmas generally feature γ_{Os} values greater than zero (see data compilation by BRAUNS et al. 2000). As demonstrated, the crust-like trace element and Sr-isotope compositions described for the Ferrar rocks obscure the involvement of a possible mantle plume, but the combination of these features with the lack of radiogenic Os isotope ratios corresponds to a secondarily enriched magma source within the SCLM rather than a deeper asthenospheric source. This last implication will be evaluated below by considering some of the PGE characteristics outlined in the previous chapters.

4.5.3   Evidence for magma source composition from PGE

Similar to other element groups, variations of PGE concentrations in basaltic rocks are affected by differences in source mineralogy, depth and degree of melting and the extent of earlier melting events. These factors fundamentally determining PGE characteristics are discussed in detail by e.g. FRYER & GREENOUGH (1992). Aside from conditions during melt generation, the behaviour of PGE during subsequent magma

evolution is largely predicted by their initial concentrations in the magma source. The strongly variable PGE characteristics observed for magmatic rock suites from different settings (e.g. MORB, OIB, oceanic and continental LIPs) can thus be attributed in part to differences in noble metal abundances in their source regions.

In this context, especially the non-chondritic PGE abundances, exhibited by numerous mantle rocks, have been a main point of discussion (e.g. PATTOU et al. 1996, LORAND et al. 1999, 2000) aiming to decipher the origin of elevated PGE concentrations and of the generally strongly variable composition of mantle source regions with respect to PGE. Various models have been proposed such as incomplete mixing of meteorite material added to the mantle by heterogeneous meteorite bombardment after the core formation ('late-veneer hypothesis', e.g. KIMURA et al. 1974) or incomplete incorporation of the highly siderophile PGE into the earth's core during its separation from the mantle (TREDOUX et al. 1989). Another explanation has been the subsequent introduction of PGE-enriched core material into the convecting lower mantle, from which via mantle plume activity portions of deep mantle material can be brought to higher mantle levels. The favoured argument for the latter model is its ability to explain the significantly elevated PGE concentrations of many ocean island basalts (FRYER & GREENOUGH 1992), which largely contrast with the low concentrations in typical mid-ocean ridge basalts. Based on these considerations, PGE systematics are thought to represent powerful geochemical tracers to establish plume involvement in LIP magmatism.

Similar to any other continental flood basalt province, the long-standing debate about the origin of the Ferrar province has focussed on the question of any mantle plume involvement. If any plume source existed, special interest was (and still is) directed towards the question whether its involvement was confined to conductive heat transfer to the lithospheric mantle or if there has been active contribution of plume-derived material. In order to evaluate this problem, the determined PGE concentrations of the Ferrar low-Ti and high-Ti rocks have been compared to those of other tholeiitic rocks series from different geodynamic settings in a primitive mantle-normalised plot (Fig. **4.15**). The PGE patterns shown for selected Ferrar samples are characterised by a considerable PGE fractionation with enrichment of PPGE over IPGE. They are rather comparable to tholeiitic rocks from other LIPs and OIB but are markedly distinguishable from MORB-type patterns, which show much greater depletion of IPGE relative to Ni and of PPGE relative to Cu and generally lower PGE abundances. Such features are expected for magmas that sustained PGE loss due to sulphide precipitation indicating that the melt achieved sulphur-saturated conditions (e.g. HAMLYN et al.1985, CROCKET 2002).

However, considering the large influence of changing conditions during subsequent magma evolution on the PGE fractionation (e.g. during differentiation), it remains questionable to what extent the mantle-normalised patterns give reasonable information on mantle source characteristics. Even if the tholeiitic rocks from different geodynamic settings (Fig. **4.15**) are originated from significantly varying mantle sources (asthenospheric and lithospheric mantle), there are no apparent differences in their PGE patterns (except from the MORB pattern). Thus, it has to be emphasised that the

features of these patterns do not represent only source characteristics. Therefore, the similarity of the present Ferrar PGE patterns with those of rocks with proven plume influence during their generation does not necessarily indicate a plume involvement for the Ferrar LIP. The largely contrasting major and trace element as well as isotope signatures of the Ferrar rocks and of plume-derived magmas (e.g. from the oceanic environment) are more striking arguments that do not support any active plume contribution for the petrogenesis of the Ferrar magmas.
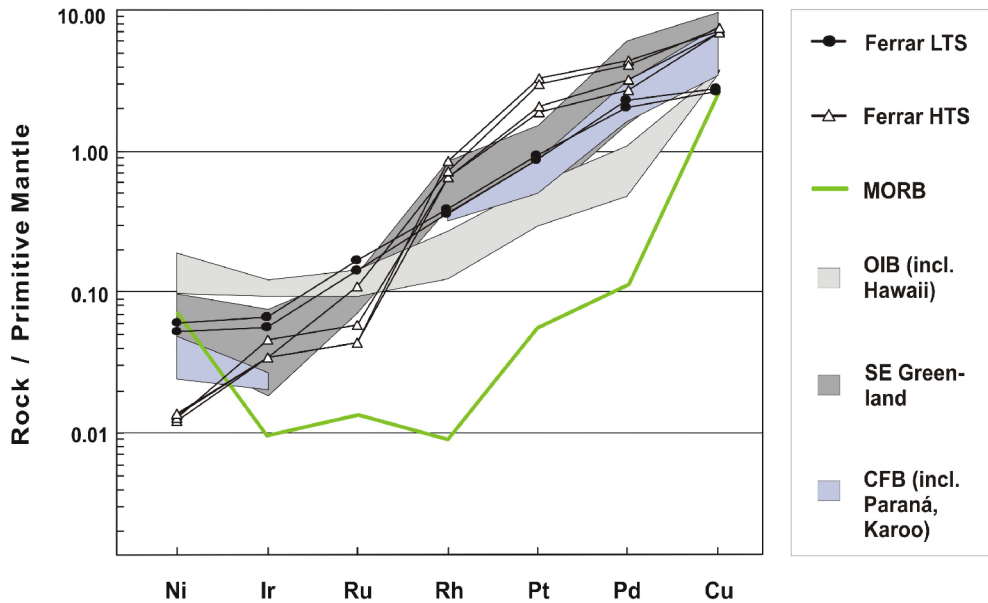
Fig. 4.15 – Primitive mantle-normalised PGE patterns of selected Ferrar rocks in comparison with tholeiitic rocks from different geodynamic settings. CFB – continental flood basalts, MORB – mid ocean ridge basalts, OIB – ocean island basalts. Data compilation from CROCKET (2002); normalisation values from MCDONOUGH & SUN (1995).

Nevertheless, further evidence of Ferrar source characteristics from the behaviour of PGE is deduced from the sulphur-undersaturated differentiation, which has been inferred consistently for all of the analysed Ferrar rocks. This feature can be attributed to a sulphur-poor magma source resulting from previous melt extractions as suggested by RUDASHEVSKIY (1987) from analyses of mantle residues. This finding confirms the refractory nature of the Ferrar magma source region, a melt-depleted, secondarily enriched subcontinental lithospheric mantle, as indicated by major and trace element signatures of the present Ferrar rocks. This subduction-related enrichment process of the Ferrar source region may additionally obscure source characteristics detectable from PGE, since their inherent concentrations can be highly affected by mantle metasomatism events, as discussed for example by HANDLER & BENNETT (1999).

Relative differences in source characteristics are often discussed using PGE ratios (e.g. Pd/Ir, Cu/Pd) instead of absolute element concentrations. To a certain extent, these ratios represent a measure of PGE fractionation caused by differentiation, but in some cases, variations in certain PGE ratios do not obviously correlate with differentiation parameters and are hence ascribed rather to differences in source

compositions. MOMME et al. (2002), for example, determined elevated Cu/Pd ratios in some basaltic rocks from the East Greenland rifted margin and attributed them to initially variable element ratios of their parental magmas. Similarly, VOGEL & KEAYS (1997) observed variable PGE ratios for distinct basaltic magma suites of the Tertiary to Quaternary Newer Volcanic Province from Victoria, Australia. They suggested differences in the fractionation behaviour of Pt and Pd due to variable amounts of sulphide precipitation predicted by relative differences in initial sulphur concentrations of the respective mantle sources. Thus, they proposed distinct, more or less refractory mantle materials for the different magma suites. In a comparative study, MAIER & BARNES (2004) reviewed PGE ratios of mantle-derived magmas, including tholeiites, komatiites and alkaline magmas from continental as well as oceanic settings. They obtained differences in Pt/Pd and Pd/Ir ratios over few orders of magnitude at comparable whole-rock MgO contents. Their interpretation that these features reflect differences in the conditions during melt generation of "dry" and fluid-enriched, metasomatised mantle source regions indirectly also emphasises differences in source composition. Considering the wide variations of PGE ratios summarised by MAIER & BARNES (2004), the PGE ratios of all present Ferrar samples fall in the range of the continental tholeiites, but no obvious differences exist between the fine-crystalline Ferrar low-Ti and high-Ti rocks (e.g. Cu/Pd, Fig. **4.5**). The more pronounced PPGE/IPGE fractionation, e.g. the higher Pd/Ir ratios of the fine-crystalline high-Ti rocks can be attributed to their more evolved whole-rock composition acquired during differentiation prior to final magma emplacement. In general, the differentiation processes heavily modified the primary magma composition with respect to PGE and may to a certain extent obscure source characteristics. However, the overall agreement in isotope and trace element signatures of both magma series, including the fractionated PGE patterns, do not give any reason for an origin from different magma sources.

In summary, the high degree of PGE fractionation of all analysed Ferrar rocks is in agreement with their generally evolved whole-rock composition indicating that the Ferrar magmas have experienced extensive differentiation. Irrespective of the absolute concentrations of the individual PGE, the present Ferrar low-Ti and high-Ti rocks do not exhibit significantly different PGE abundance patterns when normalised against primitive mantle composition. Small differences in the slope of PGE patterns observed both within the two magma series and between them can be well explained by differences in their degree of differentiation. However, the conspicuous similarity of these patterns implies that there is no significant difference of magma source composition for both Ferrar magma series. Furthermore, the implications deduced from the PGE systematics agree with the refractory nature of the proposed SCLM source, but give no evidence for active plume contribution during Ferrar magmatism. These findings are in accordance to the conclusions inferred from the major and trace element features as well as from the isotope data above discussed.

In conclusion, PGE systematics are very sensitive to changes in conditions during magmatic processes such as partial melting, differentiation or post-magmatic

mobilisation as outlined before in the respective chapters. Thus, PGE definitely provide valuable tools for describing the petrogenesis of igneous rock series. Nevertheless, since their concentrations and consequently their ratios are very prone to modifications by any petrogenetic process, PGE are in contrast to incompatible lithophile trace elements probably not well suited as indicators of magma source compositions as pointed out by REHKÄMPER et al. (1999b).

4.5.4   Summary of magma source characteristics

In conclusion, by means of the major and trace element features obtained for the present Ferrar rocks, the source of the Ferrar rocks is interpreted to be a subcontinental lithospheric mantle characterised by subduction-related enrichment in some crustal component. However, there is no substantial evidence that the evolution of the low-Ti and high-Ti magma series was controlled by significant differences in their magma source composition. They rather derived by similar degrees of partial melting from a homogeneous source and experienced considerable crystal fractionation during differentiation before and after magma emplacement as deduced in the previous chapters.

Furthermore, there is no evidence of contribution of deep asthenospheric mantle material in the Ferrar magma generation, neither by major and trace element nor by PGE characteristics, supporting the results of previous isotope studies.

4.6   PROPOSED DIFFERENTIATION MODEL

As discussed in the previous chapters, the petrogenesis of the two compositionally distinct Ferrar magma sources can not be ascribed to differences during their melt generation from a uniform subcontinental lithospheric mantle source. As evident from their generally evolved nature, the Ferrar rocks do not represent compositions of normal mantle melts indicating that the Ferrar magmas underwent an extensive polybaric differentiation history. This finding requires that the mantle-derived magmas have been stored after their melt generation in the SCLM in temporary magma reservoirs between the base of the crust and the upper crust for some period of time prior to their final ascent and emplacement in upper crustal levels. In consideration of the compositional differences of the fine-crystalline low-Ti and high-Ti rocks, which have not experienced further modifications by *in situ* fractional crystallisation at low-pressure conditions, a model is proposed after which the two magma series experienced the pre-emplacement differentiation independently from each other.

For reasons outlined before, the proposed differentiation model is based solely on the compositional differences of the present fine-crystalline Ferrar samples as exemplarily shown by their $SiO_2 - TiO_2$ characteristics in figure **4.16**. The compositions of these rapidly cooled Ferrar rocks from NVL have been demonstrated to resemble those published for widely distributed occurrences from the entire Ferrar province in Antarctica and Tasmania.
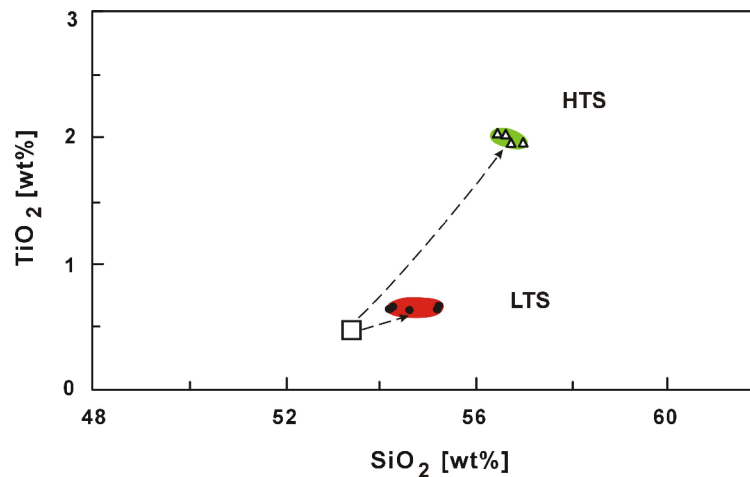
Fig. 4.16 – Concentrations of TiO_2 vs. SiO_2 of the analysed fine-crystalline low-Ti and high-Ti samples from NVL representing the Ferrar magma composition unaffected by *in situ* differentiation. The open square represents the primary magma composition estimated by HERGT et al. (1989b) by recalculating the effect of early gabbro fractionation from the average composition of chilled margins of a low-Ti sill from Tasmania.

In accordance to the more elevated composition of the fine-crystalline high-Ti rocks, indicated by their significantly lower Mg-numbers, they exhibit noticeably higher TiO_2 contents but only slightly elevated SiO_2 contents compared to the low-Ti rocks. A similarly unproportional enrichment of certain major elements of the HTS relative to the LTS, as discussed and displayed in chapter **4.3**, has been observed for Na_2O that is less enriched and for FeO that is more enriched in the high-Ti samples than expected for continued differentiation from the low-Ti magmas under unchanged conditions. From these findings, the two magma series are supposed to have experienced differentiation under different physico-chemical conditions.

From a large number of experimental and theoretical approaches it is now well understood that, besides the importance of the primary composition of magma, its differentiation is largely controlled by pressure and temperature conditions but is also strongly affected by its volatile content and the prevailing oxygen fugacity. The following sections briefly discuss the general influence various intensive parameters have on differentiation paths of basaltic magmas. The developed systematics will be applied to the data obtained for the present Ferrar rocks. The acquired conclusions are summarised afterwards in a preliminary differentiation model for the two Ferrar magma series.

4.6.1 Oxygen Fugacity

The oxidation state of a silicate melt, expressed as oxygen fugacity (fO_2), has an important influence on many geochemical processes. Since the fO_2 controls for example, the ratios of multi-valent metal ions such as iron in silicate liquids (e.g. Fe^{3+}/Fe^{2+} ratios, SACK et al. 1980, KILINC et al. 1983), it has widely been recognised to play a major role on the stability and composition of iron-bearing mineral phases. Thus, changes in the redox conditions can considerably change the order of mineral phases

crystallising from the liquid during fractional crystallisation. Therefore, the fO_2 influences the compositional path a residual liquid follows, described as 'the liquid line of descent'. Consequently, the oxidation state affects the type and composition of mineral phases that are finally accumulated at the site of magma cooling.

This relation between oxygen fugacity and differentiation trends of mafic magmas due to different fractionating mineral assemblages is illustrated in an AFM diagram (Fig. **4.17**). It allows the discrimination between magmatic rock series characterised by tholeiitic and calc-alkaline affinities. The fractionation trend of a calk-alkaline magma series typically shows an initial increase of iron, which soon decreases in favour of the alkalis. OSBORN (1959) ascribed this early removal of significant amounts of iron from the residual liquid to the appearance of Fe-Ti oxides in the fractionation assemblage, which is favoured by oxidising conditions. HAMILTON et al. (1964) confirmed experimentally that precipitation of oxides as first phase is only possible at conditions of elevated fO_2, while under more reducing conditions the stability of oxides is not reached due to lower Fe^{3+}/Fe^{2+} ratios of the magma. This non-appearance of oxides under lower fO_2 and the concomitant separation of initially Mg-rich mafic mineral phases (e.g. olivine, pyroxenes) cause an increase of the Fe/Mg ratios in the liquid phase during the early stages of closed-system fractionation. One of the most pronounced Fe-enrichment trends, producing a ferro-basaltic liquid, is exhibited by the magmas of the Skaergaard layered intrusion (WAGER 1960, Fig. **4.17**). It represents the classic example of tholeiitic magma differentiation with oxide precipitation only at advanced stages of differentiation. After calculations of WAGER & BROWN (1968), the original Skaergaard magma was more than 98 % solidified before the stability of oxide minerals was reached. The sudden oxide precipitation caused the sharp bend in the AFM diagram reflecting the decrease in total iron, which leads subsequently to a SiO_2 increase in the melt phase (e.g. TOPLIS & CARROLL 1995). Nevertheless, at the onset of oxide fractionation the Skaergaard residual liquid was still very basic with $SiO_2 < 50$ wt%. In general, such strong Fe-enrichment trends require the assumption that the magmatic systems evolve under conditions closed to oxygen (TOPLIS & CARROLL 1996) and that replenishment of original magma, as suggested periodically for other large intrusive magma bodies (e.g. Muskox Intrusion, Bushveld Complex), is negligible.

While most of the earlier experimental studies were conducted at atmospheric pressure conditions, meanwhile, an increasing number of experimental data obtained at elevated pressures have been published for a wide range of magma composition highlighting the general importance of the oxidation state of silicate liquids on their Fe-Ti oxide saturation. More recently, FREISE (2004) as well as FEIG et al. (2004b) and BERNDT et al. (2005) performed crystallisation experiments under pressure conditions up to five kbar using basaltic melt compositions typical of the Kerguelen LIP and of mid-ocean ridges, respectively. They confirmed the absence of magnetite at reducing fO_2 corresponding to the FMQ oxygen buffer (see figure **4.18**), consequently causing a tholeiitic differentiation trend of the residual liquids. In contrast, at more oxidising fO_2, they observed the early fractionation of magnetite and hence decreasing Fe/Mg ratios in the residual liquid describing a typical calc-alkaline differentiation trend.
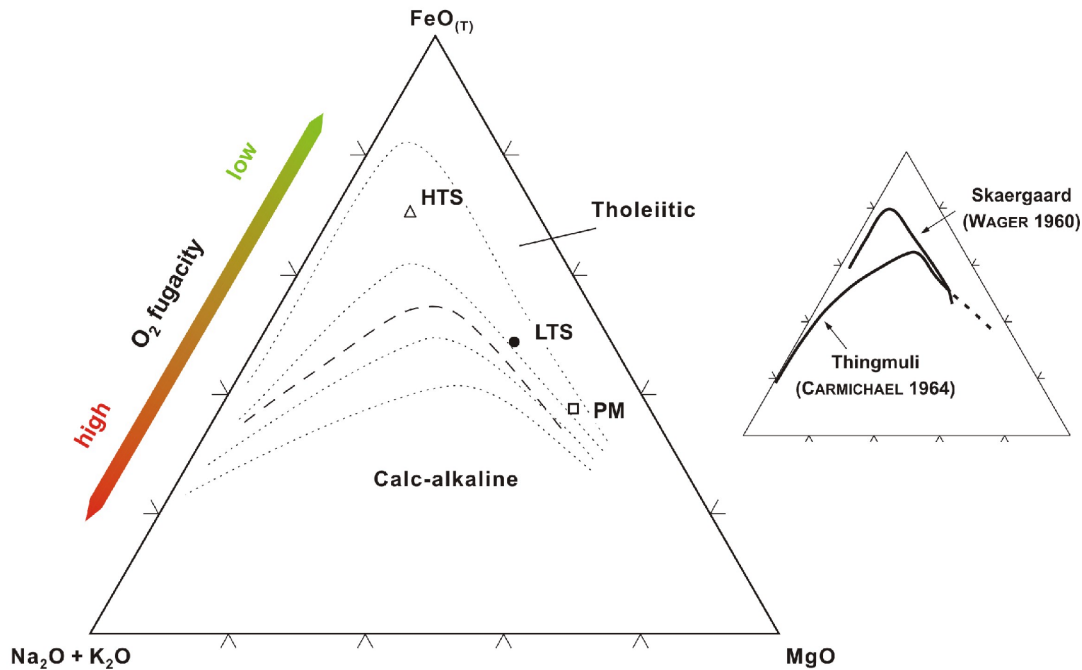
Fig. 4.17 – AFM-diagram showing the average composition of analysed fine-crystalline low-Ti (**LTS** l) and high-Ti (**HTS** r) Ferrar rocks and the fractionation-corrected composition of the primary Ferrar magma (**PM** ¨) from HERGT et al. (1989b) suggested as starting composition for the differentiation of both magma series. Dashed line separates calc-alkaline and tholeiitic fields after IRVINE & BARAGAR (1971). Dotted lines are schematic trends of magma evolution by fractional crystallisation; note their relation to variable oxygen fugacities. In the right diagram, the compositional trends of the evolving liquids of the Skaergaard layered intrusion and the Thingmuli volcanoe are shown.

The AFM diagram in figure **4.17** shows the average compositions of the present fine-crystalline Ferrar rocks from both magma series, which are suggested to be derived by differentiation from a uniform, more primitive primary magma. Its composition, which has been re-calculated by HERGT et al. (1989b), as well as those of the present low-Ti and high-Ti rocks plot above the separation line defining the calc-alkaline and tholeiitic fields after IRVINE & BARAGAR (1971). This observation that both magma series follow rather the tholeiitic than the calc-alkaline differentiation trend indicates a generally low oxygen fugacity prevailing during their differentiation agreeing with the estimated fO_2 values around the FMQ oxygen buffer. However, the high-Ti magma displays a considerably stronger enrichment in iron than the low-Ti magma. This could simply be explained by a more pronounced fractional crystallisation of the high-Ti magma according to its elevated differentiation degree. However, as inferred from the systematics in figure **4.10,** this iron enrichment is more pronounced than expected by simple continuation of the low-Ti magma differentiation trend. Considering the relation between oxidation state and distinct differentiation trends schematically drawn in figure **4.17**, the stronger Fe-enrichment may give evidence that the high-Ti magma evolved under more reducing conditions compared to the low-Ti magma. This implication confirms the small differences of the T-fO_2 estimates (Fig. **3.14**) calculated from the composition of the Fe-Ti oxides analysed in the present Ferrar rocks, whereby slightly lower fO_2 values were obtained for the high-Ti rocks at given temperature.

Since there is textural evidence that the oxides in both the low-Ti and high-Ti rocks crystallised mainly during low-pressure *in situ* differentiation, it is questionable to which extent the fO_2 values estimated from the present oxides can be used to assess differences in magma oxidation state prior to final ascent and emplacement at upper crustal levels. This general problem of redox conditions possibly changing during magma ascent is focus of a long-standing debate considering the significance of the present oxidation state of mafic magmas with respect to their pre-eruption history and their source regions.

Based on studies on mantle xenoliths, the oxidation state of the mantle has been recognised to be largely heterogeneous, both vertically and laterally corresponding to different depths and geodynamic environments, respectively (e.g. ARCULUS 1985, BALLHAUS 1993, BRANDON & DRAPER 1996, WOODLAND & KOCH 2003). However, the origin of differences in fO_2 in mantle regions in oceanic settings, below cratons, in subduction milieus or in the subcontinental lithospheric mantle has been discussed quite controversially and remains a complex issue that is by no means thoroughly understood. Considerable debate exists about the question if the present redox state of a magmatic rock reflects an inherent feature of its mantle source, as a wide range of processes may alter the initial oxidation state of a mantle-derived melt relative to its source, such as changes in Fe^{3+}/Fe^{2+} ratios upon decompression or low-pressure volatile degassing (BALLHAUS 1993).

In an earlier study, SATO (1978) postulated that the ascent of basic magmas includes the thermal dissociation of H_2O to H_2, which is lost subsequently causing oxidation of ascending magmas. This hydrogen degassing is one of the most commonly invoked mechanisms to explain the discrepancy observed between the rather reduced nature of mantle source regions of basalts and their far more oxidised state at the site of eruption. In contrast, CARMICHAEL (1991) and BALLHAUS (1993) emphasised that the effect of diffusive volatile loss causing oxidation is only minimal. For further understanding, KRESS & CARMICHAEL (1991) studied the relations of temperature, pressure and fO_2 by determining the compressibility of Fe_2O_3-bearing silicate liquids. They obtained a small change in fO_2 with melt decompression amounting to < 0.5 log units over a range of 30 kbar for a magma ascending as an oxygen-closed system. Hence, the ΔFMQ (difference of fO_2 to the FMQ oxygen buffer) representing the oxidation state of a mantle melt ascending closed to oxygen is approximately pressure-independent and reflects the redox conditions of its source region confirming the results of CARMICHAEL (1991). However, after FROST & LINDSLEY (1992) this conclusion is only valid assuming that a batch of magma experienced only little or no differentiation, since they demonstrated for the Skaergaard magmas that the iron enrichment during differentiation must involve relative reduction in fO_2.

In another study investigating the pressure dependence of fO_2, MO et al. (1982) determined the partial molar volumes of oxide components from density measurements of Fe_2O_3-containing silicate liquids. Based on the results, they developed a thermodynamic approach, which suggests a positive correlation between pressure and fO_2 under the assumption that during ascent the magma composition remains constant (including its Fe^{3+}/Fe^{2+} ratio). Thus, for isochemically ascending magmas, they propose

a decrease in fO_2 of about one log unit for 10 kbar pressure decrease. This finding implies that, in contrast to e.g. SATO (1978) and KRESS & CARMICHAEL (1991), the fO_2 in source regions of basic magmas must be greater than on the surface. Considering this pressure-fO_2 relation, the slightly lower oxidation state inferred for the Ferrar high-Ti magmas would agree with somewhat lower pressure conditions during their pre-emplacement differentiation compared to the low-Ti magmas.

However, a more reduced fO_2 for the HTS seems to be inconsistent with the elevated amounts of oxides typically present in the fine-crystalline high-Ti samples, but it is not since the precipitation of Fe-Ti oxides is not only controlled by the prevailing fO_2 as reported by TOPLIS & CARROLL (1995). They emphasised the importance of temperature and liquid composition itself, especially its FeO and TiO_2 concentrations, and denoted that the ferric-iron content of magnetite-saturated magmas is a nearly fO_2-independent function of temperature. Hence, a melt that became strongly enriched in FeO and TiO_2 during pre-emplacement differentiation without Fe-Ti oxide fractionation (such as the Ferrar high-Ti magmas) can eventually reach the point of oxide saturation during ascent to the upper crust and further cooling. Consequently, oxides crystallise in large abundance at the site of magma cooling, but their crystallisation does not require obviously changed redox conditions.

Aside from the widely accepted influence of fO_2 on oxide saturation, silicate phases are demonstrated to be affected by variations in the melt oxidation state as well. For example, FEIG et al. (2004b) experimentally examined phase relations in a tholeiitic basaltic system and obtained a reduced field of stability for the crystallisation of orthopyroxene at reducing compared to oxidising conditions (Fig. **4.18**), confirming results of previous studies (GROVE & BAKER 1984, GROVE & JUSTER 1989). In the studied Ferrar sample suite, orthopyroxene phenocrysts are present only in low-Ti rocks and generally absent in high-Ti rocks, an observation that may further indicate more reduced redox conditions during differentiation of the latter magma series.
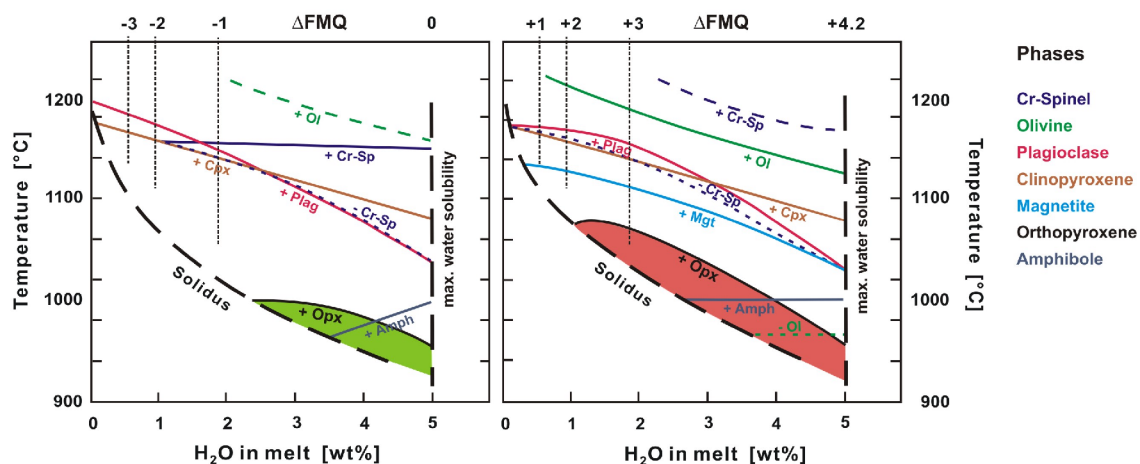
Fig. 4.18 – Phase relations for a tholeiitic basaltic melt obtained from crystallisation experiments performed in internally heated pressure vessels at 2 kbar and variable melt water contents under reducing (left) and oxidising (right) conditions after FEIG et al. (2004b). Phase boundaries reflect the appearance (+) and disappearance (–) of phases. Note the increased stability field for orthopyroxene at elevated fO_2 as well as the non-appearance of magnetite at reduced fO_2.

In addition to effects on phase relations, the fO_2 furthermore influences the composition of silicate minerals fractionating from mafic silicate liquids. In contrast to TOPLIS & CARROLL (1995), who denoted only a subordinated influence of fO_2 on compositions of silicate phases and on element partitioning between coexisting mineral – melt pairs in general, FREISE (2004) obtained systematically higher Fe/Mg ratios for residual melts and the corresponding clinopyroxenes synthesised at lower fO_2. A correspondingly lower Fe^{3+}/Fe^{2+} ratio in the melt and thus an elevated partitioning of Fe^{2+} into pyroxene may explain this observation. In consideration of this finding, the obviously higher Fe/Mg ratios obtained for the pyroxenes in the present Ferrar high-Ti rocks could be further evidence of lower fO_2 during the differentiation of the high-Ti compared to the low-Ti magma series.

4.6.2 Water Activity

Aside from the redox conditions, the water activity of silicate liquids has been recognised to be a further important intensive parameter during magmatic processes. One of the most important consequences of water present during melting of mantle material is lowering the melting temperature (KUSHIRO 1990, HIROSE & KAWAMOTO 1995, GAETANI & GROVE 1998). Furthermore, water dissolved in silicate liquids has been demonstrated to affect the phase relations during magma differentiation, since it depresses the appearance temperature of silicate minerals (e.g. SISSON & GROVE 1993). This shift in phase stabilities to lower temperatures, observed in several experimental studies during the last decades, does not only affect water-bearing phases (e.g. amphibole), but also nominally anhydrous mineral phases. Even small changes in the water contents can cause significant variations in the crystallisation sequence and hence control the evolutionary path followed by the residual liquids (GAETANI et al. 1993) as well as the mineral assemblage finally crystallising during solidification.

For example, MÜNTENER et al. (2001) performed experimental studies on arc magmas under uppermost mantle conditions and observed that plagioclase is an early-stabilised phase at low water contents, whereas higher water contents suppress plagioclase crystallisation. FEIG et al. (2004a) reported a similar finding from crystallisation experiments on gabbroic melts at two kbar. They observed clinopyroxene crystallising before plagioclase at elevated water activities and the opposite at reduced water activities (see figures **4.18** and **4.19**). These results confirm the destabilisation of plagioclase as early crystallising phase under increasingly hydrous conditions that has been denoted by SISSON & GROVE (1993). Consequently, this change in the near-liquidus mineral phase appearance causes an increase of the amounts of mafic silicates crystallising as early phases. Since plagioclase, crystallising from (near-) primary mantle melts, is rather anorthitic than albitic (i.e. CaO-rich, SiO_2-poor and Na_2O-poor), the fractionation of elevated amounts of mafic (initially Mg-rich) silicates accompanying the lesser amounts of Ca-rich plagioclase causes the residual liquid to evolve along a path of decreasing MgO, increasing SiO_2 and alkalis and only slight enrichment in FeO. In contrast, under rather anhydrous conditions, plagioclase is preferentially fractionated relative to mafic mineral phases. Of course, the residual liquid is also depleted in MgO,

but the enrichment in silica and alkalis is not as pronounced as under hydrous conditions and iron is more significantly enriched since lower proportions of mafic minerals are fractionated.

This suppression of silica and sodium enrichment under dry compared to hydrous conditions is furthermore enhanced by the influence water has on the composition of plagioclase as exemplarily demonstrated in the plagioclase phase diagram after JOHANNES (1978) (Fig. **3.13**). A large number of experimental studies confirmed that the system anorthite – albite is very prone to variations of the water pressures prevailing during crystallisation. While higher amounts of anorthite are typically observed at elevated melt water contents, more albitic plagioclase is obtained at anhydrous conditions (e.g. SISSON & GROVE 1993, PANJASAWATWONG et al. 1995, MARTEL et al. 1998, SCAILLET & EVANS 1999, BERNDT 2002, BERNDT et al. 2005). In a more recent study, FEIG et al. (2006) emphasised that this Ca-enrichment trend in plagioclase with increasing water activity at given temperature and pressure can cause a difference in the anorthite content of up to 25 mol% between runs with a moderate water content and water-saturated conditions.

However, the composition of plagioclase analysed for the present Ferrar low-Ti and high-Ti rocks is apparently different. Core compositions of plagioclase phenocrysts in the chilled margin samples of low-Ti sills exhibit the highest anorthite contents with up to 88 mol%. In contrast, plagioclase in the fine-crystalline high-Ti rocks reaches anorthite contents of 60 mol% at most. This difference can be interpreted either to reflect simply distinct degrees of differentiation or to indicate different water activities during the pre-emplacement differentiation of the two magma series or a combination of both aspects. In consideration of the facts outlined above, this finding could explain the distinctly developed SiO_2 and Na_2O enrichment trends for the fine-crystalline Ferrar low-Ti and high-Ti rocks from the primary Ferrar magma (Fig. **4.10**). The stronger enrichment of SiO_2 and Na_2O obtained for the low-Ti rocks indicates both fractionation of plagioclase of more anorthitic composition and suppressed fractionation of plagioclase relative to pyroxenes that give evidence of higher contents of dissolved water during differentiation of the low-Ti magmas.

This influence increasing water activity has on the stability and composition of plagioclase is more pronounced at elevated pressure as shown by FEIG et al. (2006), an observation that can mainly be attributed to the higher water solubility in silicate melts with increasing pressure (e.g. HAMILTON et al. 1964, see next chapter). According to this finding, the higher melt water contents deduced for the Ferrar low-Ti magmas (similar to the higher oxygen fugacity) could be evidence of elevated pressure conditions during their differentiation compared to the high-Ti magmas.

Aside from the water dependence of plagioclase stability and composition, it has been recognised from recent experimental investigations that water affects the composition of mafic nominally water-free silicates as well. BERNDT et al. (2005) and FEIG et al. (2006), for example, reported higher Fe/Mg ratios in olivine and pyroxene produced at lower melt water contents during crystallisation experiments on tholeiitic magmas. They emphasised that increasing water activity of magmatic liquids directly shifts their oxygen fugacity and hence their Fe^{3+}/Fe^{2+} ratio to higher values, whereas MOORE et al.

(1995) denoted that dissolved water does not measurably influence the oxidation state of iron in natural silicate liquids. However, as discussed before, according to the influence of fO_2 on Fe/Mg ratios of crystallising minerals (FREISE 2004) increasing water indirectly shifts the composition of e.g. pyroxenes to lower Fe/Mg ratios. Thus, the considerably higher contents of MgO in low-Ca and high-Ca pyroxenes in the Ferrar low-Ti samples compared to those analysed in the high-Ti samples may be further evidence of higher water contents for the low-Ti magmas.

Another argument supporting a higher water activity during differentiation of the low-Ti Ferrar magmas is the presence of large, nearly unzoned orthopyroxene phenocrysts, which are generally absent in high-Ti rocks. Corresponding to results from DEMARCHI et al. (2001), who modelled the crystallisation assemblage in primitive Ferrar magmas from the Prince Albert Mountains (Victorialand) using the program MELTS, the appearance of orthopyroxene is preferred at hydrous compared to anhydrous conditions. Since the presence of water changes the redox conditions of silicate liquids, which in turn affects the stability of orthopyroxene (e.g. FEIG et al. 2004b, Fig. **4.18**), increasing water contents indirectly support the saturation of orthopyroxene as well.

4.6.3   Pressure

In addition to oxygen fugacity and water activity, pressure is a further intensive parameter that controls the evolution of mantle-derived melts, since it affects the phase relations and hence the evolving melt compositions. Recently, VILLIGER et al. (2007) performed anhydrous crystallisation experiments at 7 kbar and 10 kbar to estimate the influence of changing pressure on the evolution of liquid lines of descent by fractional crystallisation in tholeiitic systems using primitive mantle-derived tholeiitic basalt. They obtained systematic variation trends of the major element composition of the residual liquids showing increasing concentrations of FeO, TiO_2, SiO_2 and Na_2O. However, FeO and TiO_2 followed a steeper enrichment trend at lower compared to higher pressure, while SiO_2 and Na_2O are increasing to higher concentrations at higher pressure. Concerning the compositional variations for the fine-crystalline Ferrar low-Ti and high-Ti rocks (Fig. **4.10** and **4.16**), derived by fractional crystallisation from a common primary magma, the more pronounced enrichment in SiO_2 and Na_2O obtained for the low-Ti rocks imply higher pressure conditions than for the high-Ti magma differentiation. In contrast, the high-Ti magmas exhibit stronger enrichment in FeO and TiO_2 indicating lower pressure conditions during pre-emplacement differentiation according to the results of VILLIGER et al. (2007).

Changes in pressure conditions also affect phase relations as exemplarily demonstrated by FEIG et al. (2006), who studied experimentally the phase relations in a primitive tholeiitic magma system. For pressures ranging from one to five kbar, they reported a shift of the orthopyroxene saturation temperature of about 100 °C to higher temperatures at low water contents. The resulting increased stability field of orthopyroxene with increasing pressure is illustrated in figure **4.19**. This correlation is in agreement with observations of HERMANN et al. (2001), who described a gabbro complex in the Eastern Central Alps (Italy) that intruded the transition zone between

the lowermost continental crust and the subcontinental upper mantle. The mainly occurring gabbro-norites are characterised by large amounts of cumulus clino- and orthopyroxene, but contain only small amounts of olivine being interpreted as evidence of crystallisation at high pressure (~ 10 kbar). Since olivine has not been identified in any of the studied Ferrar samples and since orthopyroxene phenocrysts are only present in low-Ti samples, the before mentioned findings indicate higher pressure conditions during the differentiation of the LTS compared to the HTS magmas.
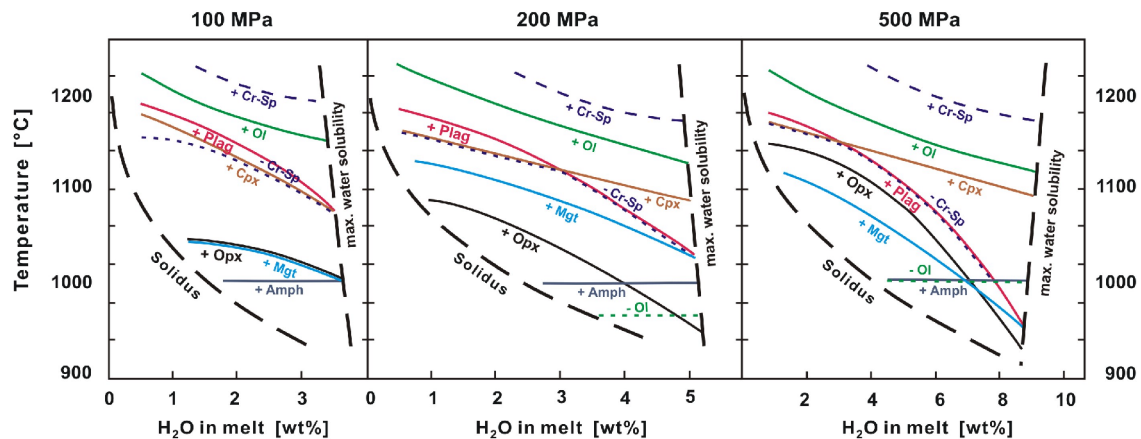
Fig. 4.19 – Phase relations in a tholeiitic melt system from FEIG et al. (2006) obtained from crystallisation experiments conducted in internally heated pressure vessels at different pressures at oxidising conditions (ΔFMQ +1 to +4). Note the increased stability field for orthopyroxene and the suppression of plagioclase relative to clinopyroxene with increasing pressure. For abbreviations of mineral phases see figure **4.18**.

Moreover, the displayed phase relations in figure **4.19** indicate that with increasing pressure the plagioclase saturation temperature is markedly depressed at water-saturated conditions. This effect may indirectly reflect the marked influence water activity has on the plagioclase stability (e.g. MÜNTENER et al. 2001, FEIG et al. 2006), since the water solubility in silicate liquids increases significantly with pressure (e.g. HAMILTON et al. 1964, HOLTZ et al. 1995). In contrast, at nominally water-free conditions, the plagioclase saturation temperature does not exhibit obvious variations with changing pressure from one to five kbar (FEIG et al. 2004b). However, VILLIGER et al. (2004) conducted anhydrous fractional crystallisation experiments at 10 kbar on mantle-derived tholeiitic liquids and obtained ultramafic cumulates. Their formation has been ascribed to the suppression of plagioclase crystallisation relative to pyroxenes at high pressures, while the fractionation of tholeiitic liquids at low-pressure conditions favours the early stabilisation of plagioclase. The consequence of this pressure-dependent change in the crystallisation order of plagioclase and pyroxenes is comparable to the effect of different water contents described in the previous chapter, which may explain the distinct enrichment trends of silica and the alkalis that differ from those of iron and titanium (MÜNTENER et al. 2001). Hence, in addition to the higher water activity inferred for the Ferrar low-Ti magmas, a higher pressure may explain their more pronounced SiO_2 and Na_2O enrichment agreeing with the differences in liquid evolution at different pressures reported by VILLIGER et al. (2007).

Compared to the pressure sensitivity of liquid composition and phase relations, the compositions of mineral phases synthesised in several experimental studies are recognised to be less significantly influenced by pressure variations. For example, the partitioning of Ca and Na into plagioclase is almost unaffected by pressure changes at dry conditions and given temperature, at least unless very large differences in pressure are considered (e.g. SMITH & BROWN 1988, SISSON & GROVE 1993) that are rather unrealistic for the generation of the two Ferrar magma series. Moreover, the influence of water on plagioclase composition dominates its pressure dependence as described before. In contrast to plagioclase, the well-known pressure- (and temperature-) sensitive equilibrium between clinopyroxene and the coexisting melt is often used to calculate the magma crystallisation depth (e.g. NIMIS 1995, PUTIRKA et al. 1996, 2003, and references therein). However, discrepancies of pressures calculated from clino-pyroxene – melt pairs, which were experimentally synthesised at given pressure (e.g. FREISE 2004), are partly ascribed to the fact that the application of these commonly used geothermobarometers is mainly restricted to anhydrous conditions. Nevertheless, elevated Al_2O_3 contents in clinopyroxene are often regarded as evidence for crystallisation at high pressure, since Al-rich clinopyroxene is typically observed as one of the major constituents of mantle-xenoliths, mafic cumulates or basaltic rocks that crystallised near the crust-mantle transition zone (e.g. MCGUIRE & MUKASA 1997, DAMASCENO et al. 2002). Recently, FEIG et al. (2006) confirmed experimentally the positive correlation of Al_2O_3 contents with pressure between one and five kbar at anhydrous conditions, but denoted that at higher water contents the trends of increasing Al_2O_3 with increasing pressure could not be reproduced. Concerning the Ferrar rocks, there are small differences in the Al_2O_3 content of high-Ca clinopyroxenes determined for the present fine-crystalline low-Ti and high-Ti rocks with tendentially lower values for the latter. Due to the ambiguous influence of water, this small difference may not be a very convincing argument; however, it supports the com-parably higher pressure during differentiation of the low-Ti magmas that has been inferred from the lack of orthopyroxene in high-Ti rocks.

Recapitulating the enlarged orthopyroxene stability field, the suppressed plagioclase saturation and the steeper enrichment of SiO_2 and Na_2O with increasing pressure, the obtained compositional differences of the Ferrar low-Ti and high-Ti rocks can be attributed to higher pressure during differentiation of the low-Ti magma series. Higher pressure in turn is in agreement with comparably higher water contents and oxygen fugacities also inferred for the LTS.

4.6.4 Differentiation Model

The considerations discussed above emphasise the complexity of the relations of various intensive crystallisation parameters and that the influence of the individual parameters on evolving silicate liquids is hardly to constrain separately. However, even if the interplay of temperature, oxygen fugacity, water content and pressure is probably not understood in all details, there is evidence of systematic differences of the physico-chemical conditions during the pre-emplacement differentiation of the two Ferrar magma series. As a result, a differentiation model describing these differences is

established according to the arguments outlined above. This schematic model (Fig. **4.20**) is based on the SiO_2 – TiO_2 variations of the fine-crystalline low-Ti and high-Ti rocks, suggesting their derivation from the same primary magma, which has been generated by comparable degrees of partial melting of a single magma source. The suggested conditions during proceeding differentiation of the high-Ti magma series are comparably lower oxygen fugacity and water activity at lower pressure relative to the low-Ti magma series.
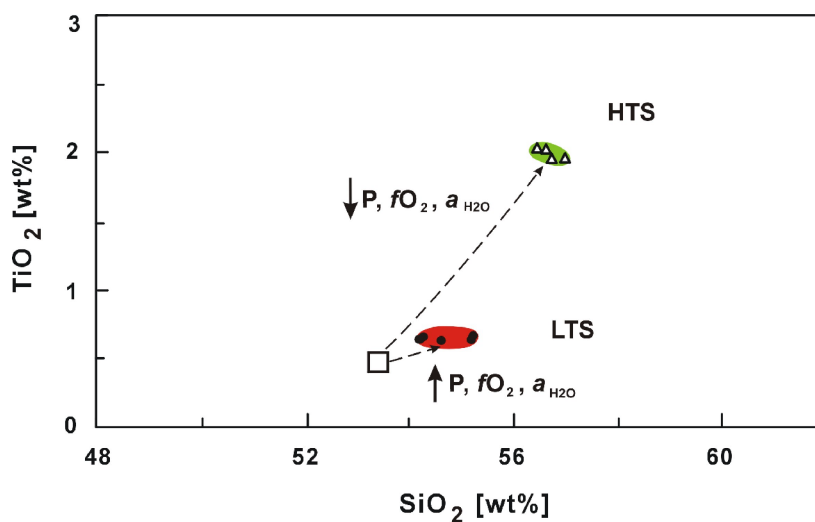
Fig. 4.20 – Proposed differentiation model for the distinct genesis of the two Ferrar magma series demonstrated by the SiO_2 – TiO_2 characteristics for the fine-crystalline Ferrar low-Ti (**LTS** l) and high-Ti (**HTS** r) rocks. The differences in their chemical evolution from a uniform primary magma (**PM** ¨) are suggested to be controlled by different conditions of pressure – P, oxygen fugacity – fO_2 and water activity – a_{H2O} during pre-emplacement differentiation.

In order to test this preliminary model of the distinct differentiation history of the two magma series, crystallisation experiments were performed to evaluate the influence of some of the intensive parameters on the evolution of the Ferrar magmas as described in the next chapter.

5 EXPERIMENTAL TEST OF THE DIFFERENTIATION MODEL

As mentioned above, the differentiation history of basaltic magma depends on its primary composition, its volatile content and composition, pressure and temperature as well as the prevailing oxygen fugacity. In order to review the above developed differentiation model to explain the distinct petrogenesis of the two Ferrar magma series, crystallisation experiments were performed using internally heated pressure vessels in the experimental petrology laboratory at the Institute of Mineralogy at the University of Hannover. This technique allows a systematic variation of different intensive crystallisation parameters. The aim of this experimental study was to estimate the influence of oxygen fugacity and water activity on the differentiation of the Ferrar magmas using a low-Ti sample as starting material.

5.1 EXPERIMENTAL TECHNIQUES AND ANALYSES

5.1.1 Internally Heated Pressure Vessel

The setup of the internally heated pressure vessels (IHPV) used for this study was specially designed to realise high-pressure crystallisation experiments on low-viscosity, volatile- and Fe-bearing basaltic systems in order to investigate the effects of pressure, temperature, oxygen fugacity (fO_2) and water activity (a_{H2O}) on phase relations of such systems. This setup combines two established experimental techniques:

the Shaw membrane technique using a hydrogen sensor membrane allowing accurate determination and control of the partial pressure of hydrogen and hence the hydrogen and oxygen fugacities (SHAW 1963, SCAILLET et al. 1992, SCHMIDT et al. 1995) and

the quench-wire technique to prevent non-equilibrium quench effects such as the formation of quench crystals during rapid cooling of low-viscosity melts (HOLLOWAY et al. 1992, ROUX & LEFEVRE 1992).

A detailed description of the vertically mounted furnace apparatus and the sample holder including the H_2-membrane and the rapid-quench device is given by BERNDT (2002) and BERNDT et al. (2002).

The experiments were conducted in large-volume IHPV pressurised with pure Ar at the intrinsic oxygen fugacity of the vessels, which was estimated by BERNDT (2002) to lie along the MnO-Mn_3O_4 solid oxygen buffer curve (based on the equation of CHOU 1978) between 900 and 1200 °C at water saturated conditions. In order to run experiments at more reduced conditions, a defined Ar-H_2 mixture is used as pressure medium that enables the adjustment of specific oxygen fugacities. The temperature was measured and controlled continuously by two pairs of thermocouples, which were integrated in the system to allow exact determination of both the furnace temperature and the sample temperature. Total pressure was controlled by a Burster Type 8221 transducer. Temperature and pressure are accurate to within ± 5 °C and ± 0.01 kbar, respectively.

At the end of the experiment, the rapid quench is achieved by the quench-wire technique. The Pt-wire holding the sample capsules in the hot spot of the furnace is

fused electrically and the sample charges are quenched isobarically as the capsules drop down from their fixed position in the furnace hot spot to the cold-quench area (20 – 25 °C) of the vessel chamber. At this point, no reaction takes place within the capsules because the temperature is far below the glass transition temperature (BERNDT et al. 2002). The quench rate is estimated to be hundreds of degrees per second (HOLLOWAY et al. 1992). A successful rapid quench is indicated by a small temperature increase in the cold zone recorded by a thermocouple placed on the bottom of the quench area as well as a small change in the Ar pressure in the vessel.

5.1.2   Synthesis and Pre-equilibration of the Starting Material

As starting material, the natural sample RH36 from a chilled margin of a Ferrar low-Ti sill was chosen. Even though its chemistry does not directly reflect the primary magma composition of the low-Ti series, it represents one of the least modified samples after magma emplacement in the upper crust. It does not exhibit obvious evidence of secondary alteration, and it is not affected by *in-situ* differentiation due to its rapid cooling after intrusion.

Sample RH36 was ground in an agate swing mill to ~ 100 µm grain size. The sample powder was fused twice (with grinding in between) in a Pt-crucible at 1600 °C and 1-atm to obtain a homogeneous, bubble- and crystal-free, dry glass. The melting time was limited to about one hour to avoid loss of alkalis from the glass. Thin sections of pieces from the upper, middle and lower part of the synthesised glass were prepared for analysis by electron microprobe in order to prove its major element composition and its homogeneity. The results listed in table **5.1** show that the composition of the synthetic glass is widely in agreement with the composition of the natural sample RH36. The low values of standard deviation of the single element oxides indicate the homogeneity of the synthesised glass. After this synthesis, the starting glass was crushed in a steel mortar and sieved to obtain the < 150 µm fraction. The small grain size of the starting material enables a better homogenisation of the sample powder with the later added water and silver oxalate ($Ag_2C_2O_4$).

Tab. 5.1 – Major element composition of the natural Ferrar low-Ti sample RH36 from XRF-analysis and of the synthetic glass from microprobe analysis used as starting material in the crystallisation experiments. All concentrations are normalised to 100 wt% with all Fe as $FeO_{(T)}$ (total iron). Numbers in parentheses are standard deviations * 100 of the 40 replicate analyses of the synthetic glass.

	SiO_2	TiO_2	Al_2O_3	$FeO_{(T)}$	MnO	MgO	CaO	Na_2O	K_2O	P_2O_5
natural RH36	54.18	0.63	15.02	9.12	0.18	7.17	11.12	1.73	0.76	0.09
synthetic glass	54.65 (41)	0.65 (3)	15.00 (23)	8.91 (32)	0.16 (9)	7.19 (17)	10.83 (25)	1.79 (15)	0.70 (5)	0.12 (13)

To avoid disequilibrium effects during experiments under reducing conditions, the starting glass was pre-equilibrated in a gas mixing furnace (H_2/H_2O). The sample powder was loaded in a ceramic crucible and fused at 1250 °C for 2 hours at the desired oxygen fugacity of the experiments. In earlier studies, electron microprobe analyses generally showed a marginal contamination of 2 – 3 mm of the glass. Thus, a glass cylinder was cored from the interior of the glass to remove the contaminated rims. The obtained pre-equilibrated glass was ground to < 150 µm grain size.

5.1.3 Capsule preparation

Presaturation of the Capsules

During high-temperature phase equilibrium crystallisation experiments in basaltic systems the loss of iron from the sample charge to the sample container is a general problem (e.g. FORD 1978, GROVE 1981, RATAJESKI & SISSON 1999). To minimise this potential Fe-diffusion into the capsule walls during the experiments, an $Au_{80}Pd_{20}$ alloy was used as capsule material due to the lower solubility of iron in this alloy than in pure Pt-capsules and due to the higher melting point of $Au_{80}Pd_{20}$ than of pure Au-capsules (KAWAMOTO & HIROSE 1994). Using these alloys, BERNDT et al. (2002) demonstrated that at oxidising conditions the loss of iron is negligible. Nevertheless, for experiments at reducing redox conditions the capsules have to be presaturated in iron at an oxygen fugacity similar to the desired redox conditions in the experiments (BERNDT et al. 2002). This was performed following the method of FORD (1978). A ceramic crucible containing the capsule material and a basaltic glass of similar composition as the sample material was placed into a 1-atm gas mixing furnace (H_2/H_2O) for 3 days at 1250 °C and at an oxygen fugacity equivalent to the FMQ buffer at 200 MPa. Afterwards, the surrounding basaltic glass was completely removed by dissolution with hydrofluoric acid to recover the presaturated capsule material.

Preparation of the Capsules

The capsules were made of $Au_{80}Pd_{20}$ tubes with an inner diameter of ~ 3 mm, which were cut into ~ 15 mm long pieces, cleaned with pure acetone and afterwards sealed on one end by arc welding. Capsules for the experiments at reducing conditions were presaturated in Fe as described above. All experiments were performed fluid-saturated except the nominally dry. In order to run the experiments at different water activities, the capsules were filled with a well-defined mixture of H_2O and CO_2. The initial fluid weight X_{H2Oin} [molar X_{H2O} / (X_{H2O} + X_{CO2})] was varied from ~ 0.5 to 0.0. The required amount of distilled and deionised water was added to the bottom of the capsule using a micro syringe. As source of CO_2 silver oxalate ($Ag_2C_2O_4$) was added, which dissociates during heating with a reactivity of ~ 93% as estimated by FREISE (2004) after the method of BOHLEN et al. (1982). Finally, after loading 30 mg of dry sample powder, the capsules were sealed at the open end while the welded end was cooled by liquid nitrogen to avoid an early volatilisation of the added water. Before being loaded into the pressure vessel, the filled capsules were heated up to 120 °C for 2 hours to check the capsules for leaks and additionally, to enhance the homogenisation of the fluid phases

(H_2O and partly CO_2) throughout the charge (the complete dissociation of the silver oxalate occurs at ~ 200 °C during the experiment). A final weighing of the capsules showed them to be impermeable.

5.1.4   Experimental Conditions and Procedure

The temperature and oxygen fugacity conditions applied during the equilibrium crystallisation experiments were selected according to the intensive crystallisation parameters, which were estimated from the mineral chemical data obtained from the analysed Ferrar samples. Hence, two experimental runs were conducted at 1100 °C in internally heated pressure vessels under crustal pressure (2 kbar) at two different oxygen fugacities: one run corresponding to the estimated FMQ buffer and a second one, more oxidising at the intrinsic fO_2 of the vessel, which corresponds to the MnO-Mn_3O_4 buffer (log fO_2 ~ ΔFMQ + 4) at water saturation. The two different fO_2 ranges were adjusted by using different pressure media in the vessel, an Ar-H_2 mixture and a pure Ar pressure medium for reducing and oxidising conditions, respectively. For both runs, four capsules with different bulk water contents were prepared and tight together. The sample charges were fixed to a Pt-wire inside the rapid-quench-device of the IHPV and heated directly to the desired run temperature of 1100 °C at 2 kbar. The experimental run under oxidising conditions was performed for 22 hours, while the run duration at reducing conditions was limited to 4 hours in order to minimise the diffusive Fe-loss to the capsule material. After the quench, all capsules were weighed separately to prove for leaks and then punctured to control the presence of a fluid phase. Finally, polished sections were prepared from the synthesised solid material of each sample charge for electron microprobe analysis.

Table **5.2** summarises the conditions prevailing during the single experiments. As the oxygen fugacity of a system is influenced by its preset X_{H2O} and hence by its water activity, fO_2 is distinct in each of the four capsules of the two experimental runs at constant P-T-conditions. In general, higher water content in an experimental charge increases the oxygen fugacity. The exact values of fO_2 of each charge have been calculated using the water activities, which were determined after the model of BURNHAM (1979) based on the estimated water contents of the residual melts (see below). Using the water activities and the equation of PITZER & STERNER (1994), the water fugacities were calculated. They were required to obtain the fO_2 using the water dissociation constant after ROBIE et al. (1978) and the H_2 fugacities, which are determined from the H_2 fugacity coefficients from SHAW & WONES (1964) and the H_2 partial pressure imposed by the vessel. Equations of calculations are given in detail in BERNDT (2002) and FREISE (2004).

In the following, the oxygen fugacity of the experimental runs will be given as ΔFMQ, which indicates the displacement of the fO_2 in the experiments relative to the FMQ oxygen buffer at 1100 °C after SCHWAB & KÜSTNER (1981). As the calculated values show, fO_2 for the two experimental runs are about ΔFMQ - 1 and ΔFMQ + 3 representing the desired reducing and oxidising conditions, respectively. Furthermore,

fO$_2$ of the single charges of the two different runs slightly vary in dependence on the preset X_{H2O} and hence the water activities, which range from 0.19 to 0.39.

5.1.5 Characterisation and Analysis of the Experimental Products

Electron Microprobe

The crystalline mineral phases were identified using back-scattered electron images based on their form and contrast, since the 'brightness' depends on the mean atomic number of the phases. Hence, plagioclase, iron-bearing pyroxenes and residual melts could easily be distinguished. The major element compositions of the experimental phases (as well as of the starting glass) were analysed by wavelength-dispersive technique using a Cameca SX-100 electron microprobe. In general, the phase compositions, listed in the appendix **A7**, are means of replicate analyses measured throughout the sample. Instrumental conditions for the analysis of these phases were 15 kV accelerating voltage, 15 nA beam current, focussed beam (~ 1 µm) and counting times of 5 s for Na and K and 10 s for all other elements. To minimise the loss of alkalis, the composition of quenched melt pools was determined with a defocussed beam of 5 to 10 µm depending on the crystallinity of the sample, with reduced counting times (2 s for Na and K, 5 s for the other elements) and a beam current of 4 nA. During previous investigations, no significant alkali migration was noticed with these analytical conditions (FREISE et al. 2003). In order to monitor instrument drift, standard minerals were analysed prior to and interspersed between the analyses of the experimental products. Due to different water contents, all glass analyses have been recalculated to 100 wt% prior to comparison of the data from different runs as well as the calculation of modal proportions for reasons of internal consistency.

Estimation of the water contents of the experimental glasses

For calculating the water activity that is required to calculate the exact oxygen fugacity, it is necessary to know the water content of the quenched residual melts. These melt water contents were estimated using the "by-difference" method, which is an often applied method in experimental studies (e.g. DEVINE et al. 1995, KOEPKE 1997, FREISE et al. 2003). It is based on the calculated difference from 100 wt% of the microprobe analysis of the experimental residual melts. This difference was calibrated against the water contents in specially prepared hydrous standard glasses of MORB composition. Their water contents were determined by Fourier-transform infrared spectroscopy (FTIR) and Karl-Fischer-titration (KFT) (see BERNDT et al. 2002, FREISE 2004). These standard glasses with known H$_2$O contents were analysed together with the quenched glasses from the experiments during the same microprobe session. Thus, a calibration curve is obtained plotting the known H$_2$O contents of the standard glasses against their H$_2$O contents determined by differences from 100 wt% of the microprobe analyses.

The final bulk water contents of the residual glasses were estimated to vary between 1.36 and 2.00 wt% and between 1.88 and 2.16 wt% for the oxidising and reducing runs, respectively. For comparison, the water content at water saturation (defined as a_{H2O} = 1) in basaltic melts has been determined by BERNDT et al. (2005) for a primitive

MORB to be about 5 wt% at 2 kbar pressure and a temperature of 1100 °C; hence, the present experiments were run at low to moderate water activities (a_{H2O} = 0.19 – 0.39).

Reasons for the difficulties reaching "nominally dry" conditions, even at preset X_{H2O} = 0.0, have been discussed in detail by FEIG et al. (2006). In addition to a certain amount of air in the capsules, FEIG et al. assume increased water contents due to the hygroscopic nature of the silver oxalate absorbing additional water. In general, the experiments are performed as 'closed systems', however, hydrogen is added to the Ar pressure medium to adjust more reducing redox conditions than given by the intrinsic oxygen fugacity of the vessel. Due to H_2 diffusion through the capsule walls, the water contents are increased in the capsules. The experimental setup may explain the observation that higher bulk-water contents were reached in the sample capsules of the reducing experimental run irrespective of similar X_{H2O} preset for both the oxidising and the reducing experiments. Moreover, since the prevailing fO_2 during the reducing run is slightly lower than during the synthesis of the starting material, the reduction of certain amounts of Fe^{3+} to Fe^{2+} results in further release of oxygen. This oxygen increases the H_2O content in the charges of the reducing experiment due to its reaction with the available H_2 of the buffer.

Estimation of Phase Proportions in the Experimental Runs

The modal phase proportions of each experimental product were determined by mass balance calculations following the principle of least-squares linear regression using the PETMIX program of WRIGHT & DOHERTY (1970). These calculations balance the major elemental composition of the bulk starting material against the averages of all synthesised phases in each charge (all recalculated to 100 wt%) with the purpose of approaching the best fit mineralogical composition. This is expressed by the sum of the residuals squared (ΣR^2). The results are listed below in table **5.2** together with the experimental conditions applied. In addition to the determination of the modal composition of the run products, the residuals from the mass balance calculations give evidence of element disturbances or disequilibrium reactions (see below).

5.2   RESULTS AND INTERPRETATION

5.2.1   Achievement of Equilibrium

In comparison to melting experiments, crystallisation experiments are recognised to be the most appropriate method to attain phase equilibrium conditions (PICHAVANT 1987). During previous studies using the same IHPV, similar conditions and comparable starting materials, BERNDT et al. (2005) showed that equilibrium conditions are achieved after 2 – 5 hours at temperatures above 1000 °C. Additionally, the use of extremely fine-grained sample powder as starting material favours a fast homogenisation of water through the charge and hence an attainment of equilibrium within short run times. However, the following characteristics are evidence of near-equilibrium conditions during the present experiments: 1) The synthesised mineral phases are ± euhedral and distributed homogeneously throughout all charges. 2) They

do not show disequilibrium features such as complex mineral zonation but are chemically homogeneous within analytical error. 3) Residual melts exhibit homogeneous composition as well, irrespective of location within the charges. 4) The rapid quench technique successfully avoided the formation of disequilibrium quench crystals during cooling the charges. 5) The phase relations and compositions exhibit systematic variations with changing experimental conditions within the two run series. 6) These variations, i.e. the correlation of compositional parameters such as Mg# of pyroxenes or anorthite contents of plagioclase with Mg# of the residual melts (Fig. **5.1**), are in agreement with expected variation trends.
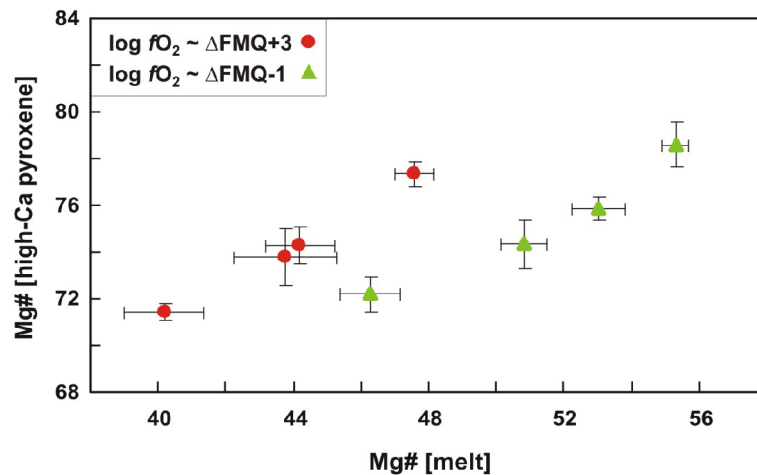
Fig. 5.1 – Variation of Mg# of high-Ca pyroxene vs. Mg# of residual melts synthesised at 1100 °C and 2 kbar under variable redox conditions and water activities. Mg# = 100*Mg / [Mg+Fe], molar. The distinctly positive correlations of pyroxene and melt compositions emphasise the approach of (near-)equilibrium conditions for both the oxidising and reducing experiments. Error bars indicate standard deviation of average pyroxene and melt compositions from replicate electron microprobe analyses.

Further evidence of successful attainment of equilibrium conditions during the experiments is provided by the quality of mass balance calculations estimating the phase proportions; it is given by the sum of the residuals squared (ΣR^2) (Tab. **5.2**). For the experiments at oxidising conditions, these calculations yield values of $\Sigma R^2 < 1$ indicating that near equilibrium conditions have been approached and that no significant element disturbance occurred during the experiments. In contrast, the calculations for the experiments at reducing conditions yield higher residuals varying between 0.3 and 2.5 reflecting a poor fit to the data. The residuals of the individual elements show the highest values for iron indicating that despite the efforts made to minimise any iron exchange between the sample charges and the precious metal capsules some changes in the bulk composition occurred.

Several authors denoted that outer zones of experimental charges are affected most intensely by disequilibrium conditions. Hence, analyses close to capsule walls were widely avoided. Within the single charges, noticeable spatial variations in compositions of the synthesised minerals and quenched liquids could not be observed considering the reasonable values of standard deviation of replicate analyses (see Appendix **7**).

Therefore, a significant loss of iron to the capsules during the experiments may be excluded. However, at similar water activities, quenched liquids synthesised at reducing conditions exhibit slightly lower iron contents than those obtained under oxidising conditions (Fig. **5.6**). This observation is largely inconsistent with results from previous studies (e.g. TOPLIS & CARROLL 1995, FREISE 2004) and may rather be evidence of iron loss from the starting material before performing the reducing experiments. The loss in iron possibly occurred during pre-equilibrating the starting glass to the desired redox condition. Whatever process caused the element disturbance noticed for the experiments at lower oxygen fugacity, three different ways of modelling have been tested for the entire data set in order to adjust this loss of iron:

- adding small amounts of iron to the synthesised Fe-bearing phases
- reducing the iron content of the starting glass
- omitting all iron from all synthesised phases as well as from the starting glass

Irrespective of the applied recalculation method, the mass balance calculations using modified contents of iron are significantly improved with residuals that are reduced to values lower than 1 without significant consequences for modal phase proportions. The general systematics of changing phase abundances with varying experimental conditions remain unaffected.

However, since the magnitude of iron loss is unknown and the rates of adjustment of iron loss from the starting material may differ for pyroxenes and quenched liquids, a meaningful examination of the Fe-Mg partitioning between these phases from the two experimental runs is hampered and will be evaluated carefully.

5.2.2   Phase relations

In all experimental runs, the produced phase assemblage is composed of quenched residual melt and homogeneously distributed mineral phases. The modal compositions of these synthesised products, obtained from mass balance calculations, exhibit systematic variations with changing experimental conditions (Tab. **5.2**). The back-scattered electron images in figure **5.2** illustrate the inverse correlation of the crystallinity of the charges with the prevailing water activity within both run series. It is obvious that the modal abundances of the mineral phases crystallised within the same run time decrease with increasing a_{H2O}, because the addition of water to a dry system shifts the solidus drastically to lower temperatures. As a consequence of increasing a_{H2O}, the melt proportions increase from 39 to 64 vol% at oxidising and from 50 to 80 vol% at reducing conditions. The difference of melt contents under higher and lower fO_2 can partly be attributed to the considerably different run durations of the two run series (22 h vs. 4 h, respectively). In addition, at similar initial X_{H2O}, the water content and thus the water activity in the single capsules are found to be systematically higher under reducing conditions than under oxidising conditions for reasons outlined before. These somewhat higher melt water contents in the experimental charges at lower fO_2 additionally support lower contents of crystalline phases when compared to the oxidising experiments.
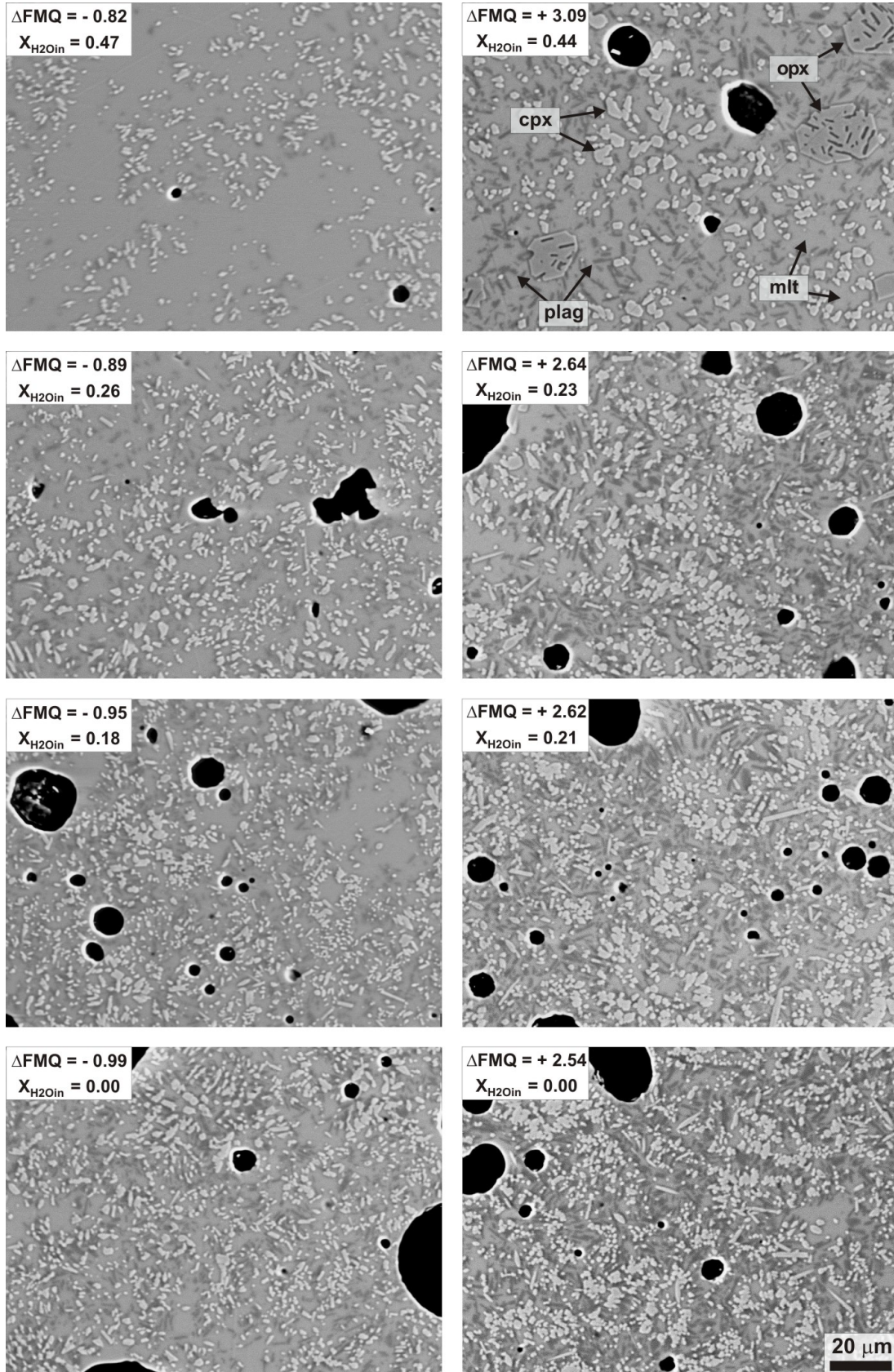
Fig. 5.2 – Back scattered electron images of experimental products obtained at 1100 °C and 2 kbar. Images show variations in modal compositions with varying fO_2 and bulk water content and thus a_{H2O} of the charges. Left row: ΔFMQ ~ -1, right row: ΔFMQ ~ +3; from top to bottom: decreasing $X_{H2O\ in}$ from ~ 0.5 to 0.0. Abbreviations of phases: mlt - melt, opx – orthopyroxene, cpx – clinopyroxene, plag – plagioclase.

The phase assemblage in all experimental products consists of pyroxenes and plagioclase of systematically varying modal proportions within the two run series. While high-Ca pyroxene (augite) is present in all experiments, orthopyroxene as low-Ca pyroxene is present only at the highest water activity under oxidising conditions. It is substituted by pigeonite in all other experiments except the one with the highest water activity at reducing conditions. According to the decrease of melt proportion with decreasing water activity, the modal abundances of all mineral phases increase. However, contents of low-Ca and high-Ca pyroxenes increase moderately with decreasing water, while the increase in plagioclase fraction is slightly more significant. This finding confirms the sensitivity of plagioclase stability to changing water contents that has been reported by a large number of studies (e.g. SISSON & GROVE 1993, MÜNTENER et al. 2001, FEIG et al. 2004a).

While the absolute abundances of the single mineral phases vary significantly in both run series, the ratios between them do not vary markedly under oxidising conditions, where the pyroxene / plagioclase ratio is steadily about unity. On the contrary, under reducing fO_2 this ratio decreases from ~ 2 to ~ 1 with decreasing water content. Comparing both run series, high-Ca clinopyroxene was synthesised with slightly higher amounts under reducing fO_2, whereas low-Ca pyroxenes and plagioclase have higher proportions at oxidising fO_2.

Tab. 5.2 – Experimental run conditions as well as phase proportions of the runs J1 to J8 performed at 1100 °C and two kbar.

Exp. No.	$X_{H2O\ in}$ [a]	H_2O [wt%] [b]	a_{H2O} [c]	log fO_2 [bar] [d]	ΔFMQ [bar] [e]	Phase proportions [wt%] [f]	ΣR^2
J4	0.44	2.00	0.35	-6.27	3.09	mlt (63.5), aug (11.0), opx (7.4), plag (18.1)	0.31
J1	0.23	1.46	0.21	-6.71	2.64	mlt (49.3), aug (14.8), pig (10.0), plag (25.8)	0.33
J2	0.21	1.44	0.20	-6.73	2.62	mlt (48.6), aug (14.5), pig (11.3), plag (25.6)	0.41
J3	0.00	1.36	0.19	-6.81	2.54	mlt (38.5), aug (15.8), pig (14.1), plag (31.5)	0.28
J5	0.47	2.16	0.39	-10.17	-0.82	mlt (80.3), aug (13.1), plag (6.6)	2.37 [g]
J6	0.26	2.06	0.36	-10.24	-0.89	mlt (60.1), aug (14.5), pig (6.4), plag (19.0)	2.51 [g]
J7	0.18	1.97	0.33	-10.30	-0.95	mlt (56.7), aug (17.9), pig (5.8), plag (19.6)	1.70 [g]
J8	0.00	1.88	0.32	-10.35	-0.99	mlt (50.3), aug (18.8), pig (6.5), plag (24.4)	0.33

[a] initial water contents in the charges: $X_{H2O\ in}$ = H_2O / H_2O + CO_2 [mol]

[b] water contents of experimental glasses estimated using the "by-difference" method

[c] calculated after BURNHAM (1979)

[d] log fO_2 calculated based on the MnO-Mn$_3$O$_4$ buffer after SCHWAB & KÜSTNER (1981) and HUEBNER & SATO (1970) using the water dissociation constant K_w after ROBIE et al. (1978), fH_2 calculated after SHAW & WONES (1964) and fH_2O after PITZER & STERNER (1994)

[e] ΔFMQ = log fO_2 (experiment) – log fO_2 (FMQ buffer) after SCHWAB & KÜSTNER (1981)

[f] modal phase proportions calculated by mass balance based on least square regressions with ΣR^2 indicating the quality of the regression; abbreviations: mlt = glass, opx = orthopyroxene, aug = augite, pig = pigeonite, plag = plagioclase

[g] residuals are significantly improved to values below 1, if mass balance calculations are repeated with corrected iron contents for all iron-bearing phases or the starting glass to compensate the iron-loss of the starting glass

5.2.3 Phase chemistry

Plagioclase

Plagioclase, which is synthesised in all experimental samples with significant variations in modal abundance, exhibits small but systematic compositional variations with intensive variables. At both oxidising and reducing conditions, the anorthite content of synthesised plagioclase continuously increases with increasing water content of the residual melt (Fig. **5.3**). The increasing CaO concentrations are accompanied by decreasing SiO_2, Na_2O and K_2O concentrations. This anorthite enrichment trend with increasing a_{H2O} is in agreement with results from previous investigations (e.g. PANJASAWATWONG et al. 1995, MARTEL et al. 1998, SCAILLET & EVANS 1999, BERNDT 2002, FREISE 2004, BERNDT et al. 2005).

The observation of PANJASAWATWONG et al. (1995) that the increase of anorthite is more pronounced in H_2O-saturated than in H_2O-undersaturated melts has been confirmed recently by FEIG et al. (2006). The latter obtained experimentally an increase of ~ 25 mol% An between runs with moderate bulk-water contents (2.8 wt% H_2O) and runs with water-saturated conditions (~ 5 wt% H_2O) at 2 kbar. Since the range of varying a_{H2O} applied in the present study is rather narrow, the observed changes in the anorthite content for synthesised plagioclase are comparably small; however, the correlation of anorthite with a_{H2O} is unambiguously positive.
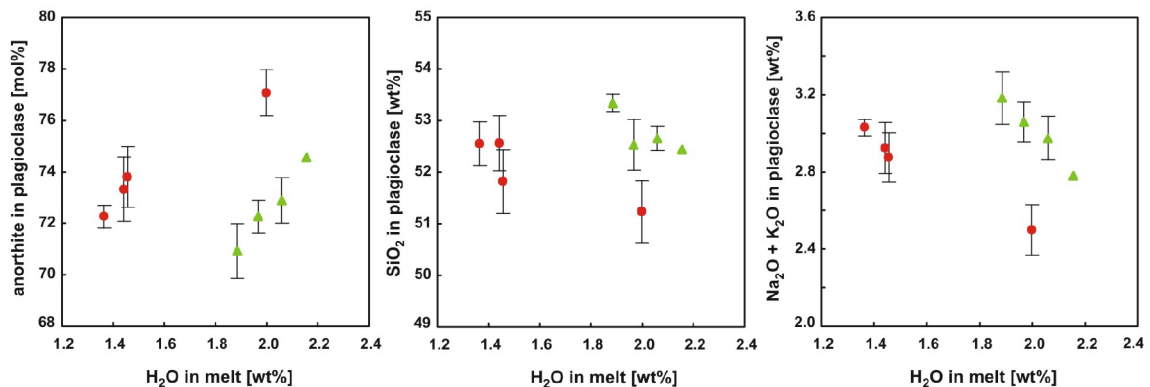
Fig. **5.3** – Compositional variations of experimental plagioclase with changing water contents in residual melts synthesised at 1100 °C, 2 kbar and oxidising (● = ΔFMQ ~ +3) and reducing (▲ = ΔFMQ ~ -1) oxygen fugacity. Error bars indicate standard deviation of average plagioclase compositions from replicate electron microprobe analyses.

The influence of melt water content on plagioclase composition is slightly more efficient in the oxidising (ΔAn ~ 5 mol%) than in the reducing experiments (ΔAn ~ 3 mol%). This observation may partly be attributed to the fact that the water content and hence a_{H2O} vary more significantly in the sample charges under oxidising conditions (a_{H2O} = 0.19 – 0.35) than under reducing conditions (a_{H2O} = 0.32 – 0.39). However, the comparison of plagioclase compositions from the two experimental runs indicates that despite the higher water activities during the reducing run, the anorthite contents are tendentially higher in plagioclase synthesised under oxidising redox conditions. At melt water

contents of about 2 wt% the anorthite content in plagioclase crystallised at ΔFMQ ~ +3 is almost 5 mol% higher than at ΔFMQ ~ -1.

Pyroxene

All experimental products contain pyroxene not only of systematically varying modal proportions but also of systematically changing compositions depending on the run conditions. Low-Ca and high-Ca pyroxenes have been synthesised, which are present in the natural Ferrar samples as well.

Orthopyroxene, which only occurs at high water activity under oxidising conditions, is the most mafic mineral phase (Mg# ~ 79.1) crystallised during the experiments. It is substituted by pigeonite in all other charges except of the reducing one with the highest melt water content, which contains only augitic clinopyroxene.

At oxidising conditions, low-Ca pyroxenes exhibit decreasing FeO, TiO_2, MnO, CaO, Na_2O and increasing MgO and SiO_2 contents with increasing melt water content (Fig. **5.4**). At lower oxygen fugacity, FeO, TiO_2 and SiO_2 decrease while CaO and Na_2O behave invariable and MgO and MnO increase. Hence, in both experimental runs, low-Ca pyroxenes with the highest Mg# crystallised in the charges with the highest melt water contents, whereby Mg# is higher under oxidising fO_2 at similar a_{H2O}. The wollastonite component is rather invariant under reducing fO_2, but decreases markedly with increasing a_{H2O} at oxidising fO_2.
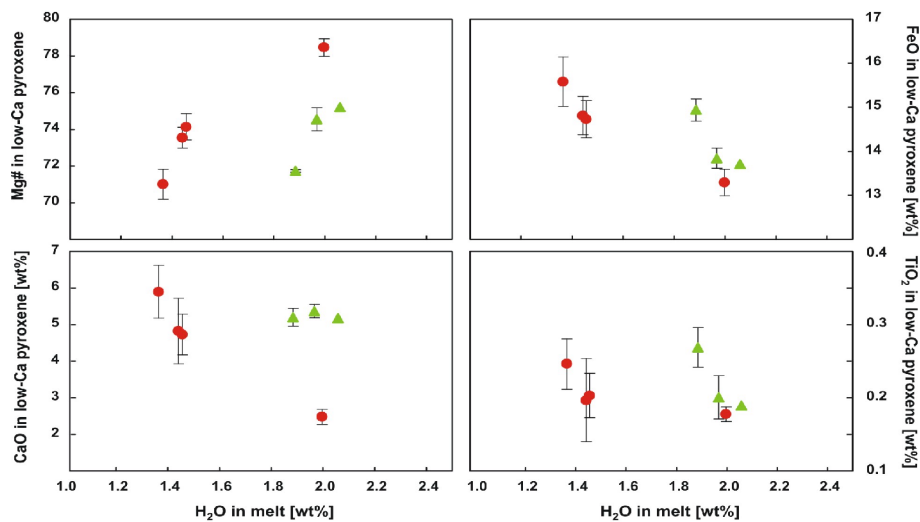
Fig. 5.4 – Compositional variations of experimental low-Ca pyroxenes (orthopyroxene, pigeonite) with changing water contents in residual melts synthesised at 1100 °C, 2 kbar and oxidising (● = ΔFMQ ~ +3) and reducing (▲ = ΔFMQ ~ -1) fO_2. Error bars indicate standard deviation of average low-Ca pyroxene compositions from replicate electron microprobe analyses.

Augitic clinopyroxene exhibits decreasing FeO, TiO_2 and MnO contents as well as increasing CaO contents with increasing melt water contents at both oxidising and reducing conditions (Fig. **5.5**). At higher fO_2, MgO slightly increases, while SiO_2 and Na_2O are almost invariant with rather unsystematic variations. At lower fO_2, SiO_2

increases with water activity, while MgO and Na_2O vary only slightly but unsystematically.

However, while the enstatite (MgO) component is nearly unaffected by increasing melt water contents, the values of Mg# obviously increase with increasing a_{H2O} for both the oxidising and reducing experimental runs. This finding can mainly be attributed to the strongly decreasing ferrosilite (FeO) component in augite from the individual charges, which is accompanied by a significant increase in wollastonite (CaO).
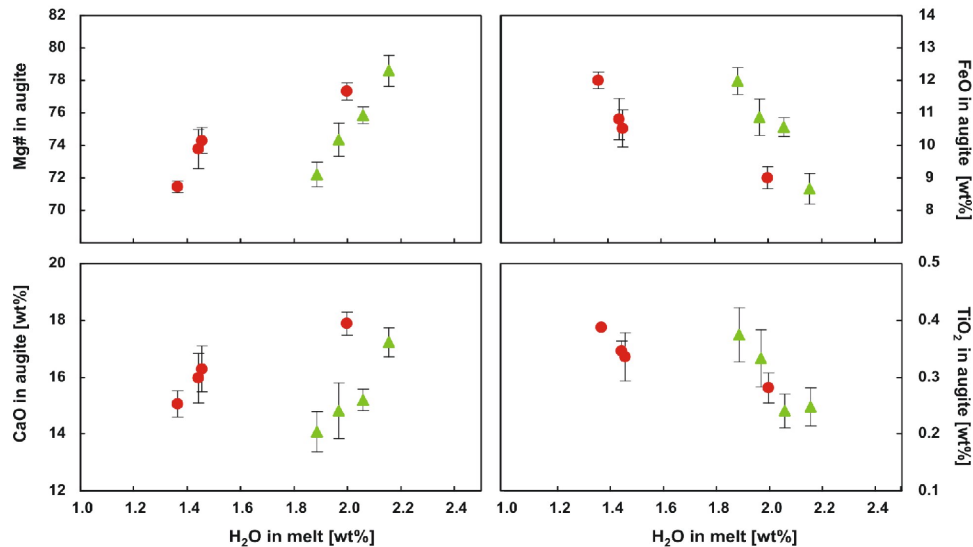
Fig. 5.5 – Compositional variations of experimental high-Ca pyroxene (augite) with changing water contents in residual melts synthesised at 1100 °C, 2 kbar and oxidising (● = ΔFMQ ~ +3) and reducing (▲ = ΔFMQ ~ -1) fO_2. Error bars indicate standard deviation of average augite compositions from replicate electron microprobe analyses.

Similar to the low-Ca pyroxenes, augites synthesised at similar melt water contents (~ 2 wt%) exhibit higher Mg# under oxidising relative to reducing conditions. This obtained difference in Mg/Fe ratio between augite crystallised at oxidising and reducing fO_2 would probably be even more significant considering the fact that some iron has been lost from the starting material used in the reducing experiments.

The Ca-enrichment and Fe-depletion trends observed for augitic clinopyroxene with increasing a_{H2O}, which are slightly more pronounced under reducing redox conditions, are in agreement with previous results from e.g. GAETANI et al. (1993) and FREISE (2004).

Residual Melt

Similar to the crystallised minerals, the residual melts exhibit systematic changes of their major element composition with varying run conditions within both experimental run series; however, the interpretation of the evolution trends of residual melts is very complex due to the interaction of different effects. In general, the presence of water largely influences the crystal / melt ratio due to its effect of shifting the saturation curves of crystallising phases to markedly lower temperatures. Consequently,

variations of modal abundances of synthesised minerals influence the compositional evolution of residual melts. Additionally, water not only determines the crystallisation order of minerals but also their compositions and thus, those of the evolving coexisting melts. Moreover, water increases the oxygen fugacity, which affects the MgO/FeO ratios of residual liquids as well as the stability of ferromagnesian phases and their compositions.

The diagrams in figure **5.6** demonstrate the key features of changing melt compositions depending on melt water contents by means of major elemental variations of the quenched glasses. Since the chemical variations follow generally expected differentiation trends for tholeiitic magmas with decreasing water contents, they are in contrast to the mineral phases described and interpreted with respect to decreasing melt water contents. SiO_2, TiO_2 and K_2O increase and MgO, CaO and Al_2O_3 decrease in concentration with decreasing water contents. FeO is rather invariable in the oxidising experiments, while it increases markedly in the reducing run series. On the contrary, Na_2O does not show significant variation under reducing conditions and varies only about 0.2 wt% under oxidising conditions at lower water contents.
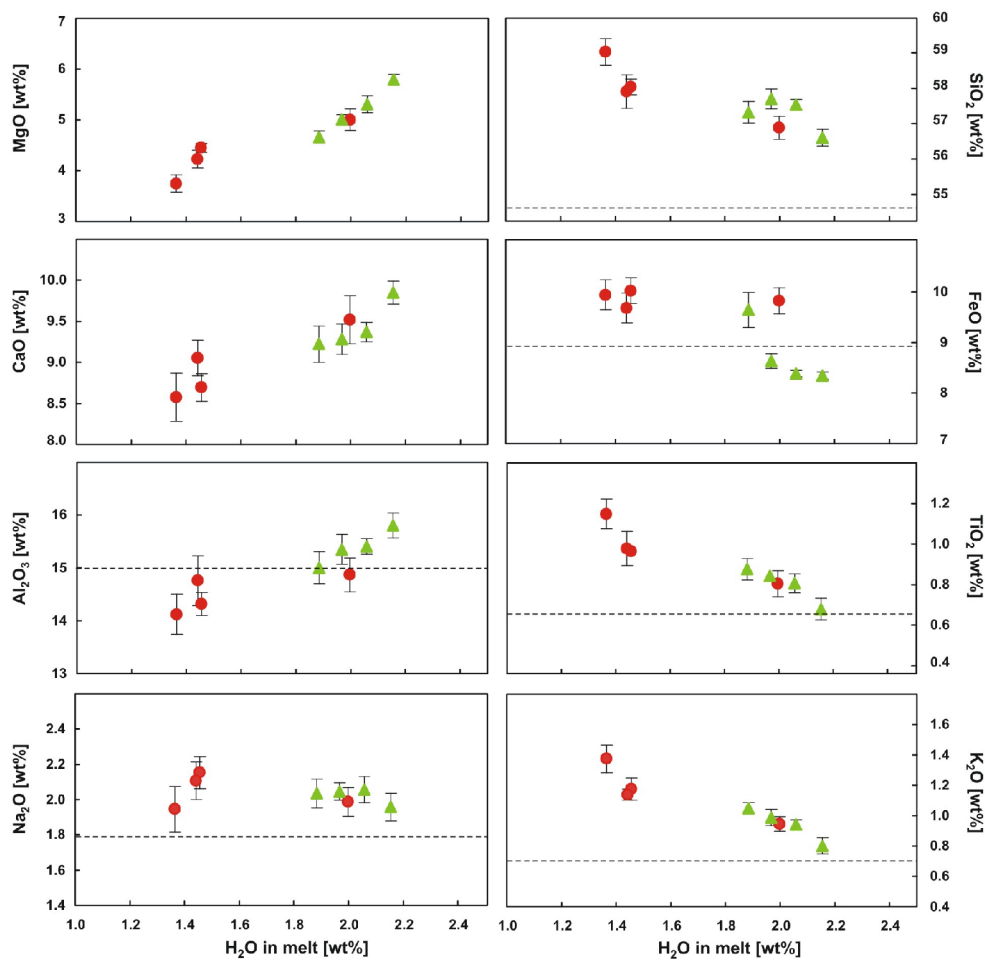
Fig. 5.6 – Influence of dissolved water on the chemical composition of residual melts synthesised at 1100 °C, 2 kbar and oxidising (● = ΔFMQ ~ +3) and reducing (▲ = ΔFMQ ~ -1) fO_2. Error bars indicate standard deviation of average melt compositions from replicate electron microprobe analyses. The dashed horizontal lines mark the element concentrations in the starting glass except for MgO (7.2 wt%) and CaO (10.8 wt%).

Most of the chemical variations observed for the present residual melts can be attributed to changes in the modal phase proportions affected by differences in the water activity. The decrease in MgO, CaO and Al_2O_3 in residual melts with decreasing water contents within both run series can be related to the increasing number of crystallising low-Ca and high-Ca pyroxenes as well as plagioclase. These changes in melt composition in turn influence the chemistry of minerals crystallising from these melts as described above: with decreasing melt MgO content, for example, MgO contents in low-Ca and high-Ca pyroxenes decrease as well (e.g. Fig. **5.1**).

In a similar manner, the SiO_2 contents in residual melts increase with decreasing melt fraction due to increasing abundances of crystallising pyroxenes and plagioclase, which contain lower SiO_2 contents than the bulk composition of the starting glass. Since K_2O and TiO_2 are only minor constituents in the observed phase assemblage, they become enriched in the residual melt with decreasing water due to the advancing crystallisation of pyroxenes and plagioclase.

The variations of FeO and Na_2O are more complex. The invariability of iron under oxidising and of sodium under reducing conditions indicates that the 'normally' expected enrichment of these elements during differentiation was counterbalanced by increasing amounts of synthesised pyroxenes and plagioclase, respectively. Under oxidising fO_2, sodium is even depleted in melts with low water contents reflecting the highest fraction of plagioclase crystallised in the present experiments. The increasing iron concentrations with decreasing water contents under reducing fO_2 can be explained by the effect that lower water contents stabilise plagioclase, which in turn decreases the ratio of crystallising pyroxenes to plagioclase as observed in the reducing experiments. This shift in the mafic silicates / plagioclase ratio to lower values with decreasing melt water contents has been described similarly by BERNDT (2002) agreeing with results of e.g. SISSON & GROVE (1993), GAETANI et al. (1993) and MÜNTENER et al. (2001). Under oxidising conditions, iron does not vary significantly being consistent with the almost invariant pyroxene / plagioclase ratios obtained despite changing water contents.

For evaluating the influence of oxygen fugacity on evolving residual melts, the chemical differences of the quenched glasses synthesised under different fO_2 have to be compared. However, a direct comparison of the two run series is hampered by following factors: the difference in the absolute water activities, the difference in the run duration and the loss of iron detected for the reducing run series.

- water activity

Despite the effort to adjust the same initial water contents within the sample capsules for the two experimental runs, the water activities are analysed to be higher for the reducing than for the oxidising experiments for reasons described already. Therefore, a direct evaluation of the effect of fO_2 on melt compositions is difficult, but possible considering only experiments with similar melt water contents. However, for most elements there are only small differences in concentrations between both run series; for rather incompatible elements with low absolute concentrations no difference is observed. Moreover, these small differences are often within analytical precision of the replicate analyses.

- run duration

In general, the run duration influences the crystallinity and the average size of the crystallising minerals. Due to the distinctly different run durations, 22 h and 4 h for the oxidising and the reducing experiments, respectively, the mineral modes vary considerably between both run series with markedly higher mineral fractions under oxidising conditions. Consequently, the enrichment of incompatible elements in the melt phase and the concomitant depletion of compatible elements are suggested to be more pronounced in crystallisation products with higher crystallinity. This effect possibly obscures differences in the melt evolution for the two experimental runs performed under different fO_2. This problem was denoted similarly by SCAILLET & MCDONALD (2003) or FREISE (2004), who also question the significance of compositional variations of residual melts that are largely affected by their crystallinity, which strongly depends on the melt water contents and the run duration. Hence, the only slightly varying concentrations of most element oxides in quenched glasses obtained at oxidising and reducing conditions can not be compared conclusively.

- loss of iron

The lower iron concentrations determined for residual melts in the reducing relative to the oxidising experiments do not agree with the expected systematic of iron enrichment under lower fO_2. This finding can be attributed to the above-mentioned loss of an indefinable amount of iron from the starting material for the reducing experiments. Hence, the differences in FeO and consequently in Mg# of the residual melts at similar water activity can not be interpreted reasonably.

To sum up, the influence of different oxygen fugacities on melt composition is hardly to constrain considering the mentioned factors. However, there is evidence that the water activity has a stronger influence on the compositional variation of residual liquids than the oxygen fugacity, at least for the experimental conditions applied during the described experiments.

5.3   DISCUSSION

The importance of the experimental results to the evolution of the Ferrar magmas will be discussed briefly by comparing the mineralogical and mineral chemical data of the experimental products with the distinct characteristics of the natural Ferrar low-Ti and high-Ti samples examined.

In all experiments, a mineral assemblage consisting of pyroxenes, plagioclase and residual melts has been synthesised, which agrees with the fractionation assemblage inferred for the natural Ferrar samples. One of the most important results is the synthesis of orthopyroxene only at oxidising conditions and moderate melt water contents of ~ 2 wt%. Since only low-Ti chilled margin samples and some low-Ti cumulates contain orthopyroxene, its appearance in experiments at higher fO_2 and a_{H2O} defines the conditions during pre-emplacement differentiation of the low-Ti magmas. This implication is further supported by the mineral chemical results. As demonstrated in the diagrams in the last chapter, anorthite contents in synthesised plagioclase and Mg-numbers of low-Ca and high-Ca pyroxenes increase with increasing melt water

contents (Fig. **5.3**, **5.4**, **5.5**). Additionally, at similar water contents of ~ 2 wt%, anorthite and Mg# are higher when these phases crystallised under higher oxygen fugacity. Within the suite of analysed Ferrar rocks, the highest An-contents in plagioclase (An_{88}) and the most magnesian pyroxenes (Mg# ~ 85) are observed within the chilled margins of low-Ti sills. On the contrary, natural Ferrar high-Ti samples contain plagioclase with significantly more albitic composition (An_{60}) as well as considerably iron-richer augite and pigeonite (Mg# ~ 54), but no orthopyroxene. These compositional characteristics of the high-Ti rocks may indicate that the high-Ti magmas experienced differentiation under lower water activity and oxygen fugacity relative to the low-Ti magmas.

Another important experimental result is the strong dependence of phase relations on changing intensive variables including the systematic increase of modal abundances of crystallising phases with decreasing water activity. The present experiments showed a slightly more significant increase of plagioclase modes than of pyroxene modes with decreasing melt water contents. Since the water contents in the present experiments varied only slightly, the shift of the pyroxene / plagioclase ratio with decreasing melt water content is not that significant as in other studies (e.g. MÜNTENER et al. 2001, BERNDT 2002). However, a decrease of the ratio between crystallising mafic phases and plagioclase due to enhanced stabilisation of the latter with decreasing water activity and concomitantly increasing albite content of plagioclase may explain the less pronounced enrichment of SiO_2 and Na_2O that has been inferred for the differentiation of the Ferrar high-Ti magmas (Fig. **4.10**). Associated with this diminished enrichment of silica and sodium in evolving melts, the decreased abundances of crystallising mafic minerals relative to plagioclase cause a steeper increase in iron, which also agrees with the elevated iron contents typical for high-Ti rocks. This implication is important, since it indicates that iron-enrichment trends in early differentiation stages of evolving tholeiitic liquids are not predominantly governed by the non-appearance of Fe-Ti oxides, but are largely affected by the proportions of fractionating plagioclase and ferro-magnesian minerals. This finding gives evidence that the influence of changing water activity on phase relations and compositions is more significant than variations of the oxygen fugacity, at least in terms of the conditions applied for this study.

As already mentioned, similar trends of liquid lines of descent for tholeiitic magmas with suppressed silica and sodium enrichment and more pronounced iron (and titanium) enrichment have been described by VILLIGER et al. (2007) for experiments performed at lower pressure (7 kbar) compared to higher pressure (10 kbar), where the opposite trends are observed. Therefore, in addition to the lower water activity and oxygen fugacity inferred for the differentiation of the Ferrar high-Ti magmas, lower pressure conditions are indicated as well. This conclusion is again supported by the lack of orthopyroxene in all studied high-Ti samples, since its stability has been demonstrated to correlate positively with pressure (e.g. BAKER & GROVE 1984, FEIG et al. 2004b).

In conclusion, the experimental results obtained from the present study on Ferrar magmas are widely in agreement with previous experimental investigations. The implications for the distinct evolution of the two Ferrar magma series drawn from the presented and from published experimental data confirm the differences in conditions that have been proposed in the preliminary differentiation model in figure **4.20.**

6   PETROGENETIC MODEL AND CONCLUDING REMARKS

Based on the considerations above, a petrogenetic model explaining the evolutionary differences between both Ferrar magma series is developed as displayed schematically in figure **6.1**. After melt generation from an identical magma source within the subcontinental lithospheric mantle, the primary Ferrar magma ascended from the mantle to the continental crust in response to buoyancy forces. At the base of the crust, the majority of primary magma was retained, since its density was intermediate between those of the mantle and the crust. This batch of magma evolved in a plumbing system under low-crustal conditions forming the low-Ti magma series. On the contrary, another batch of primary magma, generating the high-Ti magma series, possibly stagnated after immediate ascent at shallower crustal level and differentiated at lower pressure, lower water activity and lower oxygen fugacity than the low-Ti magma series. The complex interplay of the distinctly different conditions during magma differentiation in these two independent temporary magma reservoirs largely influenced the fractionating mineral phases and hence the compositionally distinct evolution of the Ferrar magma series.
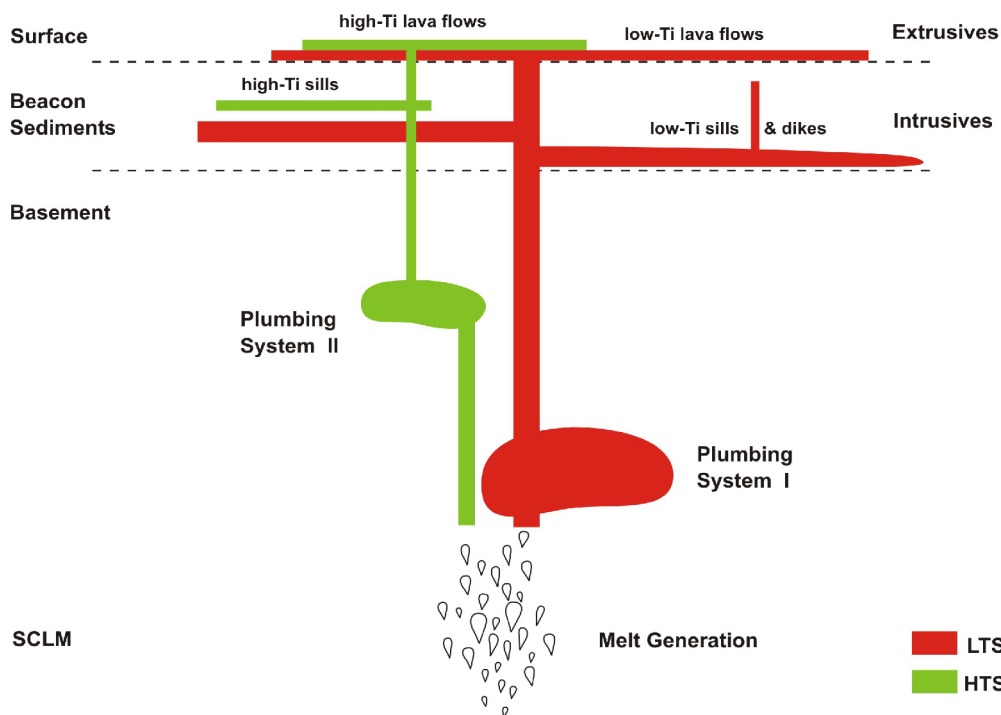
Fig. 6.1 – Schematic petrogenetic model illustrating the evolution of the Ferrar low-Ti and high-Ti magma series suggesting melt generation in the subcontinental lithospheric mantle (SCLM) and proceeding polybaric differentiation during magma storage in temporary magma reservoirs under distinctly different conditions prior to and during magma emplacement in the upper crust and at the surface.

With advancing degree of differentiation, the density of the residual low-Ti magma decreased until it reached a density that was low enough to allow ascent of the moderately evolved low-Ti magma to upper-crustal levels and the surface. The higher

water contents of the low-Ti magma (relative to the high-Ti magma) further influenced its lower density and viscosity supporting a rapid magma ascent. After emplacement as sills, dikes and lava flow sequences, the low-Ti magma further differentiated in the course of an extensive *in situ* fractional crystallisation under low-pressure conditions.

In contrast to the low-Ti magmas, a higher density contrast to the surrounding rocks at shallower crustal depth can be assumed for the high-Ti magmas, which depressed their buoyancy and thus increased the magma residence time explaining the higher degree of differentiation of the high-Ti compared to the low-Ti magmas. With a certain delay, the density of the evolving high-Ti magma decreased also below that of the overlying crust (now including an indefinable volume of low-Ti magma). Due to the increasing lithostatic pressure, the highly evolved residual high-Ti magma was forced to the surface as well. This suggested model is in agreement with the general temporal relationship of the two magma series, since the rocks of the high-Ti series always cover sequences of low-Ti rocks, wherever both series are present as extrusive occurrences.

This proposed model is a very simplified implication of what a magma plumbing system for the Ferrar magmas might look like; additional stages of stagnation, fractional crystallisation and magma ascent may have been included making the polybaric differentiation history much more complex.

The essential control of the transfer of magmas to the surface is a complex problem as well, and a large number of mechanisms have been discussed. The different episodes of magma ascent proposed here for the polybaric differentiation history of the Ferrar magmas may have been controlled by major changes in the tectonic environment, which allowed rapid ascent of magma without significant loss of heat due to the propagation of zones of structural weakness. These changes can be related to rifting processes associated with the initial break-up of the Gondwana supercontinent.

No geochemical evidence of the contribution of a deep-seated mantle plume is given based on the presented data; nevertheless, it is not excluded that the thermal anomaly of a mantle plume acted at least as heat source initiating melt generation in the SCLM. However, as proposed by ANDERSON (1994b) and KING & ANDERSON (1995), lithospheric pull-apart tectonics at cratonic boundaries causing convective partial melting may be the main factors triggering extensive continental magmatism. This suggestion is strongly supported by the recognition that all large continental flood basalt provinces occur on the edges of thick cratonic lithosphere (e.g. ANDERSON et al. 1992), such as the Ferrar LIP exposed at the cratonic margin of Gondwana. The unusual distribution of Ferrar rocks implies a strong relation of magma emplacement and pre-existing lithospheric discontinuities such as deep rift or fractures zones.

In this context, a model of long-distance crustal magma transport has been proposed by ELLIOT et al. (1999) suggesting a single site of magma origin within the Weddell Sea region to explain the almost contemporaneous emplacement of the compositionally uniform Ferrar high-Ti magmas over a few thousands of kilometres. A review of this issue based only on geochemical data is far beyond the scope of this thesis; however, the presented model for the distinct petrogenesis of the two Ferrar magma series represents valuable fundamentals for discussing this outstanding problem in a more interdisciplinary context.

7   REFERENCES

Abel K.D., Himmelberg G.R. & Ford A.B., 1979. Petrologic studies of the Dufek intrusion: plagioclase variation. Antarctic Journal of the U.S., 14, 6-8.

Ahmed A.H. & Arai S., 2002. Unexpectedly high-PGE chromitite from the deeper mantle section of the northern Oman ophiolite and its tectonic implications. Contributions to Mineralogy and Petrology, 143, 263-278.

Alard O., Griffin W.L., Lorand J.P., Jackson S.E. & O'Reilly S.Y., 2000. Non-chondritic distribution of the highly siderophile elements in mantle sulfides. Nature, 407, 891-894.

Andersen D.J. & Lindsley D.H., 1985. New (and final!) models for the Ti-magnetite/ilmenite geothermometer and oxygen barometer. Abstract AGU 1985 Spring Meeting Eos Transactions, 66, 416.

Andersen D.J. & Lindsley D.H., 1988. Internally consistent solution models for Fe-Mg-Mn-Ti oxides: Fe- Ti oxides. American Mineralogist, 73, 714-726.

Andersen D.J., Lindsley D.H. & Davidson P.M., 1993. QUILF: A pascal program to assess equilibria among Fe-Mg-Mn-Ti Oxides, Pyroxenes, Olivine and Quarz. Computers & Geosciences, 19, 1333-1350.

Andersen J.C.Ø., Power M.R. & Momme P., 2002. Platinum-Group Elements in the Palaeogene North Atlantic Igneous Province. In: Cabri L.J. (ed), The Geology, Geochemistry, Mineralogy and Mineral Beneficiation of Platinum-Group Elements, Geological Society of Canadian Institute of Mining, Metallurgy and Petroleum, 54, 637-667.

Anderson, A.T., 1968. Oxidation of the La Blanche Lake titaniferous magnetite deposit, Quebec. Journal of Geology, 76, 528-547.

Anderson D.L., 1994a. Superplumes or supercontinents? Geology, 22, 39-42.

Anderson D.L., 1994b. The sublithospheric mantle as the source of continental flood basalts; the case against the continental lithosphere and plume head reservoirs. Earth and Planetary Science Letters, 123, 269-280.

Anderson D.L., Tanimoto T. & Zhang Y.-S., 1992. Plate tectonics and hotspots: The third dimension. Science, 256,1645-1651.

Andrews D.R.A. & Brenan J.M., 2002. Phase-equilibrium constraints on the magmatic origin of laurite + Ru-Os-Ir alloy. Canadian Mineralogist, 40, 1705-1716.

Antonini P., Piccirillo E.M., Petrini R., Civetta L., D'Antonio M. & Orsi G., 1999. Enriched mantle - Dupal signature in the genesis of the Jurassic Ferrar tholeiites from Prince Albert Mountains (Victoria Land, Antarctica). Contributions to Mineralogy and Petrology, 136, 1-19.

Arculus R.J., 1985. Oxidation status of the mantle: Past and present, Annual Reviews of Earth and Planetary Sciences, 13, 75-95.

Armstrong J.T., 1991. Quantitative elemental analysis of individual microparticles with electron beam instruments. In: Heinrich K.F.J. & Newbury D.E. (eds), Electron probe quantitation, Plenum Press, New York, 261-315.

Arndt N.T. & Christensen U., 1992. The Role of Lithospheric Mantle in Continental Flood Volcanism: Thermal and Geochemical Constraints. Journal of Geophysical Research, 97, 10.967-10.981.

Arndt N.T., Czamanske G.K., Wooden J.L. & Fedorenko V.A., 1993. Mantle and crustal contributions to continental flood volcanism. Tectonophysics, 223, 39-52.

Arth J.G., 1976. Behaviour of trace elements during magmatic processes - a summary of theoretical models and their applications. Journal of Research of the U.S. Geological Survey, 4, 41-47.

Atkins F.B., 1969. Pyroxenes of the Bushveld Intrusion, South Africa. Journal of Petrology, 10, 222-249.

Baksi A.K., 1987. Critical evaluation of the age of the Deccan Traps, India: Implications for flood-basalt volcanism and faunal extinctions. Geology, 15, 147-150.

Ballhaus C., 1993. Redox states of lithospheric and asthenospheric upper mantle. Contributions to Mineralogy and Petrology, 114, 331-348.

Ballhaus C., Berry R.F. & Green D.H., 1991. High pressure experimental calibration of the olivine-ortho-pyroxene-spinel oxygen geobarometer: implications for the oxidation state of the upper mantle. Contributions to Mineralogy and Petrology, 107, 27-40.

Baragar W.R.A., Ernst R.E., Hulbert L. & Peterson T., 1996. Longitudinal Petrochemical Variation in the Mackenzie Dyke Swarm, Northwestern Canadian Shield. Journal of Petrology, 37, 317-359.

Barnes S.J., 1993. Partitioning of the platinum group elements and gold between silicate and sulfide magmas in the Munni Munni Complex, Western Australia. Geochimica et Cosmochimica Acta, 57, 1277-1290.

Barnes S.-J., Achterbergh van E., Makovicky E. & Li C., 2001. Proton microprobe results for the partitioning of platinum-group elements between monosulphide solid solution and sulphide liquid. South African Journal of Geology, 104, 275-286.

Barnes S.-J. & Maier W.D., 1999. The fractionation of Ni, Cu and the noble metals in silicate and sulfide liquids. In: Keays R.R., Lesher C.M., Lightfoot P.C. & Farrow C.E.G. (eds), Dynamic Processes in Magmatic Ore Deposits and their application in mineral exploration, Geological Association of Canada, Short Course Notes, 13, 69-106.

Barnes S.-J. & Maier W.D., 2002. Platinum-group Elements and Microstructures of Normal Merensky Reef from Impala Platinum Mines, Bushveld Complex. Journal of Petrology, 43, 103-128.

Barnes S.-J., Naldrett A.J. & Gorton M.P., 1985. The Origin of the Fractionation of Platinum-Group Elements in Terrestrial Magmas. Chemical Geology, 53, 303-323.

Barnes S.-J. & Naldrett A.J., 1987. Fractionation of the platinum-group elements and gold in some komatiites of the Abitibi greenstone belt, northern Ontario. Econ. Geology, 82, 165-183.

Barnes S.-J. & Picard C.P., 1993. The behaviour of platinum-group elements during partial melting, crystal fractionation, and sulphide segregation: An example from the Cape Smith Fold Belt, northern Quebec. Geochimica et Cosmochimica Acta, 57, 79-87.

Barrett P.J., 1991. The Devonian to Jurassic Beacon Supergroup of the Transantarctic Mountains and correlatives in other parts of Antarctica. In: Tingey R.J. (ed), The Geology of Antarctica, Clarendon Press Oxford, 120-152.

Barrett P.J., Elliot D.H. & Lindsay J.F., 1986. The Beacon Supergroup (Devonian-Triassic) and Ferrar Group (Jurassic) in the Beardmore Glacier area, Antarctica. In: Turner M.D. & Splettstoesser J.F. (eds), Geology of the Transantarctic Mountains, AGU Antarctic Research Series, 36, 339-428.

Behrendt J.C., Drewry D.J., Jankowski E. & Grim M.S., 1981. Aeromagnetic and radio echo ice-sounding measurements over the Dufek intrusion, Antarctica. Journal of Geophysical Research, 86, 3014-3020.

Behrendt J.C., Henderson J.R., Meister L. & Rambo W.L., 1974. Geophysical investigations of the Pensacola Mountains and adjacent glacierized areas of Antarctica. United States Geological Survey Professional Paper, 844.

Berndt J., 2002. Differentiation of MOR Basalt at 200 MPa: Experimental Techniques and Influence of H_2O and fO_2 on Phase Relations and Liquid Line of Descent. Ph.D. Thesis, Universität Hannover, 118 pp.

Berndt J., Koepke J. & Holtz F., 2005. An Experimental Investigation on the Influence of Water and Oxygen Fugacity on Differentiation of MORB at 200 MPa. Journal of Petrology, 46, 135-167.

Berndt J., Liebske C., Holtz F., Freise M., Nowak M., Ziegenbein D., Hurkuck W. & Koepke J., 2002. A combined rapid-quench and H_2-membrane setup for internally heated pressure vessels: Description and application for water solubility in basaltic melts. American Mineralogist, 87, 1717-1726.

Bernstein S., 1994. High-pressure fractionation in rift-related basaltic magmatism: Faeroe plateau basalts. Geology, 22, 815-818.

Bernstein, S., Kelemen, P.B., Tegner, C., Kurz, M.D., Blusztajn, J., Kent Brooks, C., 1998. Post-breakup basaltic magmatism along the East Greenland Tertiary rifted margin. Earth and Planetary Science Letters, 160, 845-862.

Bezmen N.I., Asif M., Brügmann G.E., Romanenko I.M. & Naldrett A.J., 1994. Distribution of Pd, Rh, Ru, Ir, Os, and Au between sulfide and silicate metals. Geochimica et Cosmochimica Acta, 58, 1251-1260.

Bindeman I.N., Davis A.M. & Drake M.J., 1998. Ion microprobe study of plagioclase-basalt partition experiments at natural concentration levels of trace elements. Geochimica et Cosmochimica Acta, 62, 1175-1193.

Bockrath C., Ballhaus C. & Holzheid A., 2004a. Fractionation of the Platinum-Group Elements During Mantle Melting. Science, 24, 1951- 1953.

Bohlen S.R. & Boetcher A.L., 1981. Experimental investigations and geological applications of orthopyroxene geobarometry. American Mineralogist, 66, 951-964.

Bohlen S.R., Boettcher A.L. & Wall V.J., 1982. The system albite-H_2O-CO_2: a model for melting and activities of water at high pressures. American Mineralogist, 67, 451-462.

Borg S.G., 1984. Granitoids of northern Victoria Land, Antarctica. Ph.D. Thesis, Arizona State University, Tempe, AZ, 356 pp.

Borg S.G. & De Paolo D.J., 1991. A tectonic model of the Antarctic Gondwana margin with implications for southern Australia: isotopic and geochemical evidence. Tectonophysics, 196, 339-358.

Borg S.G. & Stump E., 1987. Paleozoic magmatism and associated tectonic problems of Northern Victoria Land, Antarctica. In: McKenzie G.D. (ed.), Gondwana Six: Structure, Tectonics and Geophysics. AGU Geophysical Monograph Series, 40, 67-75.

Borg S.G., Stump E., Chappell B.W., McCulloch M.T., Wyborn D., Armstrong R.L. & Holloway J.R., 1987. Granitoids of northern Victoria Land: implications of chemical and isotopic variations to regional structure and tectonics. American Journal of Science, 287, 127-169.

Boudreau A.E., 1988. Investigations of the Stillwater Complex. IV. The role of volatiles in the petrogenesis of the J-M reef, Minneapolis adit section. Canadian Mineralogist, 26, 193-208.

Boudreau A.E., Mathez E.A. & McCallum I.S., 1986. Halogen geochemistry of the Stillwater and Bushveld Complexes: evidence for transport of the platinum-group elements by Cl-rich fluids. Journal of Petrology, 27, 967-986.

Bradshaw J.D., 1987a. Terrane boundaries and terrane displacement in northern Victoria Land, Antarctica: some problems and constraints. In: Leitch E. & Scheibner E. (eds), Terrane Accretion and Orogenic Belts, AGU Geodynamics Series, 19, 199-206.

Bradshaw M.A., 1987b. Additional field interpretation of the Jurassic sequence at Carapace Nunatak and Coombs Hills, south Victoria Land, Antarctica. New Zealand Journal of Geology and Geophysics, 30, 37-49.

Brandon A.D. & Draper D.S., 1996. Constraints on the origin of the oxidation state of mantle overlying subduction zones: An example from Simcoe, Washington, USA. Geochimica et Cosmochimica Acta, 60, 1739-1749.

Brauns C.M., Hergt J.M., Woodhead J.D. & Maas R., 2000. Os Isotopes and the Origin of the Tasmanian Dolerites. Journal of Petrology, 41, 905-918.

Brewer T.S., 1989. Mesozoic dolerites from Whichaway Nunataks. Antarctic Science, 1, 151-155.

Brewer T.S. & Clarkson P.D., 1987. Mesozoic magmatism in Greater Antarctica: implications for Precambrian plate tectonics. In: Thomson M.R.A., Crame J.A. & Thomson J.W. (eds), Geological Evolution of Antarctica, Cambridge University Press, Cambridge, 117-121.

Brewer T.S., Hergt J.M., Hawkesworth C.J., Rex D. & Storey B.C., 1992. Coats Land dolerites and the generation of Antarctic continental flood basalts. In: Storey B.C., Alabaster T. & Pankhurst R.J. (eds), Magmatism and the Causes of Continental Break-Up, Geological Society of London, Special Publication, 68, 185-208.

Brey G.P. & Köhler T., 1990. Geothermobarometry on four-phase lherzolites II. New thermobarometers, and practical assessment of existing thermobarometers. Journal of Petrology, 31, 1353-1378.

Brotzu P., Capaldi G., Civetta L., Melluso L. & Orsi G., 1988. Jurassic Ferrar Dolerites and Kirkpatrick Basalts from Northern Victoria Land (Antarctica): Stratigraphy, Geochronology and Petrology. Memorie della Società Geologica Italiana, 43, 97-116.

Brotzu P., Capaldi G., Civetta L., Orsi G., Gallo G. & Melluso L., 1992. Geochronology and geochemistry of Ferrar rocks from North Victoria Land, Antarctica. European Journal of Mineralogy, 4, 605-617.

Brown G.M. & Vincent E.A., 1963. Pyroxenes from the Late Stages of Fractionation of the Skaergaard Intrusion, East Greenland. Journal of Petrology, 4, 175-197.

Brügmann G.E., Arndt N.T., Hofmann A.W. & Tobschall H.J., 1987. Noble metal abundances in komatiite suites from Alexo, Ontario, and Gorgona Island, Colombia. Geochimica et Cosmochimica Acta, 51, 2159-2169.

Brügmann G.E., Naldrett A.J., Asif M., Lightfoot P.C., Gorbachev N.S. & Fedorenko V.A., 1993. Siderophile and chalcophile metals as tracers of the evolution of the Siberian Trap in the Noril'sk region, Russia. Geochimica et Cosmochimica Acta, 57, 2001-2018.

Buddington A.F. & Lindsley D.H., 1964. Iron-titanium oxide minerals and synthetic equivalents. Journal of Petrology, 5, 310-357.

Burnham C.W., 1979. The importance of volatile constituents, The evolution of the igneous rocks, 16., Princeton University Press, 439-482.

Campbell I.H. & Griffiths R.W., 1990. Implications of mantle plume structure for the evolution of flood basalts. Earth and Planetary Science Letters, 99, 79-93.

Campbell I.H. & Naldrett A.J., 1979. The influence of silicate:sulfide ratios on the geochemistry of magmatic sulfides. Economic Geology, 74, 1503-1505.

Campbell I.H., Naldrett A.J. & Barnes S.J., 1983. A model for the origin of the platinum-rich sulphide horizons in the Bushveld and Stillwater Complexes. Journal of Petrology, 24, 133-185.

Capobianco C.J. & Drake M.J., 1990. Partitioning of ruthenium, rhodium, and palladium between spinel and silicate melt and implications for platinum group element fractionation trends. Geochimica et Cosmochimica Acta, 54, 869-874.

Capobianco C.J., Hervig R.L. & Drake M.J., 1994. Experiments on crystal/liquid partitioning of Ru, Rh and Pd for magnetite and hematite solid solutions crystallized from silicate melt. Chemical Geology, 113, 23-43.

Carlson R.W. & Irving A.J., 1994. Depletion and enrichment history of subcontinental lithospheric mantle: An Os, Sr, Nd and Pb isotopic study of ultramafic xenoliths from the northwestern Wyoming Craton. Earth and Planetary Science Letters, 126, 457-472.

Carmichael I.S.E., 1964. The Petrology of Thingmuli, a Tertiary Volcano in Eastern Iceland. Journal of Petrology, 5, 435-460.

Carmichael I.S.E., 1967. The Iron-Titanium Oxides of Salic Volcanic Rocks and their Associated Ferro-magnesian Silicate. Contributions to Mineralogy and Petrology, 14, 36-64.

Carmichael I.S.E.,1991. The redox states of basic and silicic magmas: a reflection of their source regions? Contributions to Mineralogy and Petrology, 106, 129-141.

Carmichael I.S.E., Turner F.J. & Verhoogen J., 1974. Igneous Petrology. McGraw Hill, New York, 739 pp.

Chou I.-M., 1978. Calibration of oxygen buffers at elevated P and T using the hydrogen fugacity sensor. American Mineralogist, 63, 690-703.

Coffin M.F. & Eldholm O., 1992. Volcanism and continental break-up: A global compilation of large igneous provinces. In: Storey B.C., Alabaster T. & Pankhurst R.J. (eds), Magmatism and the Causes of Continental Break-Up, Geological Society of London, Special Publication, 68, 21-34.

Coffin M.F. & Eldholm O., 1993. Scratching the surface: estimating dimensions of large igneous provinces. Geology, 21, 515-518.

Coffin M.F. & Eldholm O., 1994. Large Igneous Provinces: Crustal Structure, Dimensions, and External Consequences. Reviews of Geophysics, 32, 1-36.

Collinson J.W., Isbell J.L., Elliot D.H., Miller M.F. & Miller J.M.G., 1994. Permian-Triassic Transantarctic basin. In: Veevers J.J. & Powell C.M. (eds), Permian-Triassic Pangean Basins and Foldbelts Along the Panthalassan Margin of Gondwanaland, Boulder, Colorado, Geological Society of America Memoir, 184, 173-221.

Collinson J.W., Pennington D.C. & Kemp N.R., 1986. Stratigraphy and Petrology of Permian and Triassic Fluvial Deposits in Northern Victoria Land, Antarctica. In: Stump E. (ed), Geological Investigations in Northern Victoria Land, AGU Antarctic Research Series, 46, 211-242.

Compston W., McDougall I. & Heier K.S., 1968. Geochemical comparison of the mesozoic basaltic rocks of Antarctica, South Africa, South America and Tasmania. Geochemica et Cosmochimica Acta, 32, 129-149.

Courtillot V., Besse J., Vandamme D., Montigny R., Jaeger J.J. & Cappetta H., 1986. Deccan flood basalts at the Cretaceous/Tertiary boundary? Earth and Planetary Science Letters, 80, 361-374.

Courtillot V., Jaupart C., Manighetti I., Tapponnier P. & Besse J., 1999. On causal links between flood basalts and continental breakup. Earth and Planetary Science Letters, 166, 177-195.

Cox K.G., 1980. A Model for Flood Basalt Vulcanism. Journal of Petrology, 21, 629-650.

Cox K.G., 1988. The Karoo Province. In: Macdougall J.D. (ed), Continental flood basalts, Kluwer Academic Publishers, Boston, 239-272.

Cox K.G., Duncan A.R., Bristow J.W., Taylor S.R. & Erlank A.J., 1984. Petrogenesis of the basic rocks of the Lebombo. Geological Society of South Africa, Special Publications, 13, 149-169.

Cox K.G. & Jamieson B.G., 1974. The Olivine-rich Lavas of Nuanetsi: a Study of Polybaric Magmatic Evolution. Journal of Petrology, 15, 269-301.

Craig J.R., 2001. Ore-Mineral textures and the tales they tell. The Canadian Mineralogist, 39, 937-956.

Crocket J.H., 1990. Noble metals in seafloor hydrothermal mineralizations from Juan de Fuca and Mid-Atlantic ridges: A fractionation of gold from platinum metals in hydrothermal fluids. Canadian Mineralogist, 28, 639-648.

Crocket J.H., 2002. Platinum-Group Element Geochemistry of Mafic and Ultramafic Rocks. In: Cabri L.J. (ed), The Geology, Geochemistry, Mineralogy and Mineral Beneficiation of Platinum-Group Elements, Geological Society of Canadian Institute of Mining, Metallurgy and Petroleum, Special Volume, 54, 177-210.

Dalziel I.W.D., Lawver L.A. & Murphy J.B., 2000. Plumes, orogenesis, and supercontinental fragmentation. Earth and Planetary Science Letters, 178, 1-11.

Damasceno D., Scoates J.S., Weis D., Frey F.A. & Giret A., 2002. Mineral Chemistry of Mildly Alkalic Basalts from the 25 Ma Mont Crozier Section, Kerguelen Archipelago: Constraints on Phenocryst Crystallization Environments. Journal of Petrology, 43, 1389-1413.

Delisle G. & Fromm K., 1984. Paleomagnetic investigation of Ferrar Supergroup Rocks, North Victoria Land, Antarctica. Geologisches Jahrbuch, B60, 41-55.

Delisle G. & Fromm K., 1989. Further evidence for a Cretaceous thermal event in North Victoria Land. Geologisches Jahrbuch, E38, 143-151.

Demarchi G., Antonini P., Piccirillo E.M., Orsi G., Civetta L. & D'Antonio M., 2001. Significance of ortho-pyroxene and major element constraints on the petrogenesis of Ferrar tholeiites from southern Prince Albert Mountains, Victoria Land, Antarctica. Contributions to Mineralogy and Petrology, 142, 127-146.

DePaolo D.J., 1981. Trace element and isotopic effects of combined wallrock assimilation and fractional crystallization. Earth and Planetary Science Letters, 53, 189-202.

Devine J.D., Gardener J.E., Brack H.P., Layne G.D. & Rutherford M.J., 1995. Comparison of micro-analytical methods for estimating H_2O contents of silicic volcanic glasses. American Mineralogist, 80, 319-328.

Devine J.D., Rutherford M.J., Norton G.E. & Young S.R., 2003. Magma Storage Region Processes Inferred from Geochemistry of Fe-Ti Oxides in Andesitic Magma, Soufrière Hills Volcano, Montserrat, W.I. Journal of Petrology, 44, 1375-1400.

Donnelly T.W., Melson W.G., Kay R.W. & Rogers J.J.W., 1973. Basalts and dolerites of late Cretaceous age from the central Caribbean. Initial Reports of the Deep Sea Drilling Project, 15, 989-1012.

Droop G.T.R., 1987. A general equation for estimating Fe^{3+} concentrations in ferromagnesian silicates and oxides from microprobe analyses, using stoichiometric criteria. Mineralogical Magazine, 51, 431-435.

Duncan A.R., Hooper P.R., Rehacek J., Marsh J.S. & Duncan A.R., 1997. The timing and duration of the Karoo igneous event, southern Gondwana. Journal of Geophysical Research, 102, 18,127-18,138.

Duncan R.A. & Pyle D.G., 1988. Rapid eruption of the Deccan flood basalts at the Cretaceous/Tertiary boundary. Nature, 333, 841-843.

Duncan R.A. & Richards M.A., 1991. Hotspots, mantle plumes, flood basalts, and true polar wander. Reviews of Geophysics, 29, 31-50.

Elkins L.T. & Grove T.L., 1990. Ternary feldspar experiments and thermodynamic models. American Mineralogist, 75, 544-559.

Ellam R.M., Carlson R.W. & Shirey S.B., 1992. Evidence from Re-Os isotopes for plume-lithosphere mixing in Karoo flood basalt genesis. Nature, 359, 718-721.

Ellam R.M. & Cox K.G., 1989. A Proterozoic lithospheric source for Karoo magmatism: evidence from the Nuanetsi picrites. Earth and Planetary Science Letters, 92, 207-218.

Ellam R.M. & Cox K.G., 1991. An interpretation of Karoo picrite basalts in terms of interaction between asthenospheric magmas and the mantle lithosphere. Earth and Planetary Science Letters, 105, 330-342.

Elliot D.H., 1992. Jurassic magmatism and tectonism associated with Gondwanaland break-up: an Antarctic perspective. In: Storey B.C., Alabaster T. & Pankhurst R.J. (eds), Magmatism and the Causes of Continental Break-Up, Geological Society of London, Special Publication, 68, 165-184.

Elliot D.H., 1996. The Hanson Formation: a new stratigraphical unit in the Transantarctic Mountains, Antarctica. Antarctic Science, 8, 389-394.

Elliot D.H., 1999. Paleovolcanological Setting of the Middle Jurassic Mawson Formation: Evidence from the Prince Albert Mountains, Victoria Land. Abstract Antarctica Meeting Wellington, 97.

Elliot D.H., 2000. Stratigraphy of Jurassic pyroclastic rocks in the Transantarctic Mountains. Journal of African Earth Sciences, 31, 77-89.

Elliot D.H., Fleck R.J. & Sutter J.F., 1985. Potassium-argon age determination of Ferrar Group rocks, central Transantarctic Mountains. In: Turner M.D. & Splettstoesser J.F. (eds), Geology of the Central Transantarctic Mountains, AGU Antarctic Research Series, 36, 197-224.

Elliot D.H. & Fleming T.H., 2000. Weddell triple junction: The principal focus of Ferrar and Karoo magmatism during initial breakup of Gondwana. Geology, 28, 539-542.

Elliot D.H. & Fleming T.H., 2004. Occurrence and Dispersal of magmas in the Jurassic Ferrar Large Igneous Province. Gondwana Research, 7, 223-237.

Elliot D.H., Fleming T.H., Haban M.A. & Siders M.A., 1995. Petrology and mineralogy of the Kirkpatrick Basalt and Ferrar Dolerite, Mesa Range Region, North Victoria Land, Antarctica. In: Elliot D.H. & Blaisdell L.L. (eds), Contribution to Antarctic Research IV, AGU Antarctic Research Series, 67, 103-141.

Elliot D.H., Fleming T.H., Kyle P.R. & Foland K.A., 1999. Long-distance transport of magmas in the Jurassic Ferrar Large Igneous Province, Antarctica. Earth and Planetary Science Letters, 167, 89-104.

Elliot D.H., Fleming T.H. & Larsen D., 1986a. Ferrar and the uppermost Beacon rocks, Beardmore Glacier region. Antarctic Journal of the U.S., 21, 22-23.

Elliot D.H., Haban M.A. & Siders M.A., 1986b. The Exposure Hill Formation, Mesa Range. In: Stump E. (ed), Geological Investigations in Northern Victoria Land, AGU Antarctic Research Series, 46, 267-278.

Elliot D.H. & Hanson R.E., 2001. Origin of widespread, exceptionally thick basaltic phreatomagmatic tuff breccia in the Middle Jurassic Prebble and Mawson Formations, Antarctica. Journal of Volcanology and Geothermal Research, 111,183-201.

Elliot D.H. & Larsen D., 1993. Mesozoic volcanism in the central Transantarctic Mountains, Antarctica: depositional environment and tectonic setting. In: Findlay R.H., Unrug R., Banks M.R. & Veevers J.J. (eds), Gondwana eight: assembly, evolution and dispersal. Balkema, Rotterdam, 397-410.

Elliot D.H., Siders M.A. & Haban M.A., 1986c. Jurassic Tholeiites in the Region of the Upper Rennick Glacier, North Victoria Land. In: Stump E. (ed), Geological Investigations in Northern Victoria Land, AGU Antarctic Research Series, 46, 249-265.

Encarnación J., Fleming T.H., Elliot D.H. & Eales H.V., 1996. Synchronous emplacement of Ferrar and Karoo dolerites and the early breakup of Gondwana. Geology, 24, 535-538.

Evensen N.M., Hamilton P.J. & O'Nions R.K., 1978. Rare earth abundances in chondritic meteorites. Geochimica et Cosmochimica Acta, 42, 1199-1212.

Ewart A., Bryan W.B. & Gill J.B., 1973. Mineralogy and Geochemistry of the Younger Volcanic Islands of Tonga, S.W. Pacific. Journal of Petrology, 14, 429-465.

Falloon T.J., Green D.H., Hatton C.J. & Harris K.L., 1988. Anhydrous partial melting of a fertile and depleted peridotite from 2 to 30 kb and application to basalt petrogenesis. Journal of Petrology, 29, 1257-1282.

Falloon T.J., Danyushevsky L.V. & Green D.H., 2001. Peridotite Melting at 1 GPa: Reversal Experiments on Partial Melt Compositions Produced by Peridotite-Basalt Sandwich Experiments. Journal of Petrology, 42, 2363-2390.

Faure G., Bowman J.R., Elliot D.H. & Jones L.M., 1974. Strontium Isotope Composition and Petrogenesis of the Kirkpatrick Basalt, Queen Alexandra Range, Antarctica. Contributions to Mineralogy and Petrology, 48, 153-169.

Faure G. & Mensing T.M., 1993. K-Ar dates and paleomagnetic evidence for Cretaceous alteration of Mesozoic basaltic lava flows, Mesa Range, northern Victoria Land, Antarctica. Chemical Geology, 109, 305-315.

Feig S.T., Koepke J. & Snow J.E., 2004a. Experiments on the effect of water on the phase equilibria in a gabbroic system. Berichte der Deutschen Mineralogischen Gesellschaft, Beihefte zum European Journal of Mineralogy, 16, 35.

Feig S.T., Koepke J. & Snow J.E., 2004b. The effect of oxygen fugacity on the phase equilibria in a gabbroic system: An experimental study. Berichte der Deutschen Mineralogischen Gesellschaft, Beihefte zum European Journal of Mineralogy, 16, 36.

Feig S.T., Koepke J. & Snow J.E., 2006. Effect of water on tholeiitic basalt phase equilibria: an experimental study under oxidizing conditions. Contributions to Mineralogy and Petrology, 152, 611-638.

Ferris J., Johnson A. & Storey B., 1998. Form and extent of the Dufek intrusion, Antarctica, from newly compiled aeromagnetic data. Earth and Planetary Science Letters, 154, 185-202.

Ferris J.K., Vaughan A.P.M. & Storey B.C., 2000. Relics of a complex triple junction in the Weddell Sea embayment, Antarctica. Earth and Planetary Science Letters, 178, 215-230.

Fitzgerald P.G. & Stump E., 1997. Cretaceous and Cenozoic episodic denudation of the Transantarctic Mountains, Antarctica: New constraints from apatite fission track thermochronology in the Scott Glacier region. Journal of Geophysical Research, 102, 7747-7765.

Fleet M.E. & Stone W.E., 1991. Partitioning of platinum-group elements in the Fe-Ni-S system and their fractionation in nature. Geochimica et Cosmochimica Acta, 55, 245-253.

Fleet M.E., Chryssoulis S.L., Stone W.E. & Weisener C.G., 1993. Partitioning of platinum-group elements and Au in the Fe - Ni - Cu - S system: experiments on the fractional crystallization of sulfide melt. Contributions to Mineralogy and Petrology, 115, 36-44.

Fleet M.E., Crocket J.H., Liu M. & Stone W.E., 1999a. Laboratory partitioning of platinum-group elements (PGE) and gold with applications to magmatic sulfide-PGE deposits. Lithos, 47, 127-142.

Fleet M.E., Crocket J.H. & Stone W.E., 1996. Partitioning of platinum-group elements (Os, Ir, Ru, Pt, Pd) and gold between sulfide liquid and basalt melt. Geochimica et Cosmochimica Acta, 60, 2397-2412.

Fleet M.E., Liu M. & Crocket J.H., 1999b. Partitioning of trace amounts of highly siderophile elements in the Fe-Ni-S system and their fractionation in nature. Geochimica et Cosmochimica Acta, 63, 2611-2622.

Fleet M.E., Stone W.E. & Crocket J.H., 1991. Partitioning of palladium, iridium, and platinum between sulfide liquid and basalt melt: Effects of melt composition, concentration, and oxygen fugacity. Geochimica et Cosmochimica Acta, 55, 2545-2554.

Fleming T.H. & Elliot D.H., 1988. Iron-rich tholeiitic rocks of the Kirkpatrick Basalt, Beardmore Glacier region. Antarctic Journal of the U.S., 23, 15-17.

Fleming T.H., Elliot D.H., Jones L.M., Bowman J.R. & Siders M.A., 1992. Chemical and isotopic variations in an iron-rich lava flow of the Kirkpatrick Basalt, North Victoria Land, Antarctica: implications for low-temperature alteration. Contributions to Mineralogy and Petrology, 111, 440-457.

Fleming T.H., Foland K.A. & Elliot D.H., 1995. Isotopic and chemical constraints on the crustal evolution and source signature of Ferrar magmas, north Victoria Land, Antarctica. Contributions to Mineralogy and Petrology, 121, 217-236.

Fleming T.H., Foland K.A. & Elliot D.H., 1999. Apophyllite ^{40}Ar/^{39}Ar and Rb-Sr geochronology: Potential utility and application to the timing of secondary mineralization of the Kirkpatrick Basalt, Antarctica. Journal of Geophysical Research, 104 (B9), 20,081-20,096.

Fleming T.H., Heimann A., Foland K.A. & Elliot D.H., 1997. ^{40}Ar/^{39}Ar geochronology of Ferrar Dolerite sills from the Transantarctic Mountains, Antarctica: Implications for the age and origin of the Ferrar magmatic province. Geological Society of America Bulletin, 109, 533-546.

Fodor R.V., 1987. Low- and high-TiO$_2$ flood basalts of southern Brazil: origin from picritic parentage and a common mantle source. Earth and Planetary Science Letters, 84, 423-430.

Foland K.A., Fleming T.H., Heimann A. & Elliot D.H., 1993. Potassium-argon dating of fine-grained basalts with massive Ar loss: Application of the ^{40}Ar/^{39}Ar technique to plagioclase and glass from the Kirkpatrick Basalt, Antarctica. Chemical Geology, 107, 173-190.

Ford A.B. & Himmelberg G.R., 1991. Geology and crystallization of the Dufek Intrusion. In: Tingey R.J. (ed), The Geology of Antarctica, Clarendon Press, Oxford, 175-214.

Ford A.B. & Kistler R.W., 1980. K-Ar age, composition, and origin of Mesozoic mafic rocks related to Ferrar Group, Pensacola Mountains, Antarctica. New Zealand Journal of Geology and Geophysics, 23, 371-390.

Ford C.E., 1978. Platinum-iron alloy sample containers for melting experiments on iron bearing rocks, minerals, and related systems. Mineralogical Magazine, 42, 271-275.

Fram M.S. & Lesher C.E., 1993. Geochemical constraints on mantle melting during creation of the North Atlantic basin. Nature, 363, 712-715.

Fram M.S. & Lesher C.E., 1997. Generation and Polybaric Differentiation of East Greenland Early Tertiary Flood Basalts. Journal of Petrology, 38, 231-275.

Freise M., 2004. Differenzierung von Basalten einer "Large Igneous Province" am Beispiel des Kerguelen Plateaus. Eine experimentelle Studie. Ph.D. Thesis, Universität Hannover, 99 pp.

Freise M., Holtz F., Koepke J., Scoates J. & Leyrit H., 2003. Experimental constraints on the storage conditions of phonolites from the Kerguelen Archipelago. Contributions to Mineralogy and Petrology, 145, 659-672.

Frey M. & Robinson D., 1999. Low-Grade Metamorphism. Blackwell Science Publications, Oxford, 313 pp.

Frost B.R. & Lindsley D.H., 1992. Equilibria among Fe-Ti oxides, pyroxenes, olivine, and quartz: Part II. Application. American Mineralogist, 77, 1004-1020.

Fryer B.J. & J.D. Greenough, 1992. Evidence for mantle heterogeneity from platinum-group-element abundances in Indian Ocean basalts. Canadian Journal of Earth Sciences, 29, 2329-2340.

Fuhrman M.L. & Lindsley D.H., 1988. Ternary-feldspar modeling and thermometry. American Mineralogist, 73, 201-215.

Fujimaki H., Tatsumoto M. & Aoki K.-i., 1984. Partition coefficients of Hf, Zr, and REE between phenocrysts and groundmasses. Journal of Geophysical Research, 89, 662-672.

Gaetani G.A. & Grove T.L., 1998. The influence of water on melting of mantle peridotite. Contributions to Mineralogy and Petrology, 131, 323-346.

Gaetani G.A., Grove T.L. & Bryan W.B., 1993. The influence of water on the petrogenesis of subduction-related igneous rocks. Nature, 365, 332-334.

Gallagher K. & Hawkesworth C., 1992. Dehydration melting and the generation of continental flood basalts. Nature, 358, 57-59.

GANOVEX-TEAM, 1987. Geological map of north Victoria Land, Antarctica, 1:500.000 – Explanatory notes. Geologisches Jahrbuch, B66, 7-79.

Ghiorso M.S. & Sack R.O., 1991. Fe-Ti oxide geothermometry: thermodynamic formulation and the estimation of intensive variables in silicic magmas. Contributions to Mineralogy and Petrology, 108, 485-510.

Ghiorso M.S. & Sack R.O., 1995. Chemical mass transfer in magmatic processes IV. A revised and internally consistent thermodynamic model for the interpolation and extrapolation of liquid-solid equilibria in magmatic systems at elevated temperatures and pressures. Contributions to Mineralogy and Petrology, 119, 197-212.

Gibb F.G.F. & Henderson C.M.B., 1992. Convection and crystal settling in sills. Contributions to Mineralogy and Petrology, 109, 538-545.

Gibb F.G.F. & Henderson C.M.B., 1996. The Shiant Isles Main Sill: structure and mineral fractionation trends. Mineralogical Magazine, 60, 67-97.

Gibson S.A., Thompson R.N., Dickin A.P. & Leonardos O.H., 1995. High-Ti and low-Ti mafic potassic magmas: Key to plume-lithosphere interactions and continental flood-basalt genesis. Earth and Planetary Science Letters, 136, 149-165.

Gill J.B., 1981. Orogenic andesites and plate tectonics. Springer-Verlag, Berlin, 390 pp.

Goldsmith J.R., 1980. The melting and breakdown reactions of anorthite at high pressures and temperatures. American Mineralogist, 65, 272-284.

Green D.H., 1973. Experimental melting studies on a model upper mantle composition at high pressure under water-saturated and water-undersaturated conditions. Earth and Planetary Science Letters, 19, 37-53.

Green T.H., Sie S.H., Ryan C.G. & Cousens D.R., 1989. Proton microprobe-determined partitioning of Nb, Ta, Zr, Sr and Y between garnet, clinopyroxene and basaltic magma at high pressure and temperature. Chemical Geology, 74, 201-216.

Greenough J.D. & Fryer B.J., 1995. Behavior of the Platinum-Group Elements during Differentiation of the North Mountain Basalt, Nova Scotia. Canadian Mineralogist, 33, 153-163.

Greenough J.D. & Owen J.V., 1992. Platinum-group element geochemistry of continental tholeiites: Analysis of the Long Range dyke swarm, Newfoundland, Canada. Chemical Geology, 98, 203-219.

Grew E.S., Kleinschmidt G. & Schubert W., 1984. Contrasted metamorphic belts in north Victoria Land. Geologisches Jahrbuch, B60, 253-263.

Grindley G.W., 1963. The Geology of the Queen Alexandra Range, Beardmore Glacier, Ross Dependency, Antarctica; with notes on the correlation of Gondwana sequences. New Zealand Journal of Geology and Geophysics, 7, 307-347.

Grove T.L. & Baker M.B., 1984. Phase-equilibrium controls on the tholeiitic versus calc-alkaline differentiation trends. Journal of Geophysical Research, 89, 3253-3274.

Grove T.L. & Juster T.C., 1989. Experimental investigations of low-Ca pyroxene stability and olivine pyroxene liquid equilibria at 1-atm in natural basaltic and andesitic liquids. Contributions to Mineralogy and Petrology, 103, 287-305.

Gunn B.M., 1962. Differentiation in Ferrar Dolerites, Antarctica. New Zealand Journal of Geology and Geophysics, 5, 820-863.

Gunn B.M., 1965. K/Rb and K/Ba ratios in Antarctic and New Zealand tholeiitic and alkali basalts. Journal of Geophysical Research, 70, 6241-6247.

Gunn B.M., 1966. Modal and element variations in Antarctic tholeiites. Geochimica et Cosmochimica Acta, 30, 881-920.

Haban M.A. & Elliot D.H., 1985. Mineral chemistry of the Kirkpatrick Basalt, northern Victoria Land. Antarctic Journal of the U.S., 20, 30-31.

Haensel J.M., Himmelberg G.R. & Ford A.B., 1986. Plagioclase compositional variations in anorthosites of the lower part of the Dufek intrusion. Antarctic Journal of the U.S., 21, 61-63.

Haggerty S.E., 1991. Oxide textures - a mini atlas. In: Lindsley D.H. (ed), Oxide Minerals: Petrologic and Magnetic Significance, Reviews in Mineralogy, 25, 129-219.

Hamilton D.L., Burnham C.W. & Osborn E.F., 1964. The Solubility of Water and Effects of Oxygen Fugacity and Water Content on Crystallization. Journal of Petrology, 5, 21-39.

Hamlyn P.R., Keays R.R., Cameron W.E., Crawford A.J. & Waldron H.M., 1985. Precious metals in magnesian low-Ti lavas: Implications for metallogenesis and sulfur saturation in primary magmas. Geochimica et Cosmochimica Acta, 49, 1797-1811.

Hamlyn P.R. & Keays R.R., 1986. Sulfur saturation and second stage melts: application to the Bushveld platinum metal deposits. Economic Geology, 81, 1431-1445.

Handler M.R. & Bennett V.C., 1999. Behaviour of Platinum-group elements in the subcontinental mantle of eastern Australia during variable metasomatism and melt depletion. Geochimica et Cosmochimica Acta, 63, 3597-3618.

Hanson R.E. & Elliot D.H., 1996. Rift-related Jurassic basaltic phreatomagmatic volcanism in the central Transantarctic Mountains: precursory stage to flood-basalt effusion. Bulletin of Volcanology, 58, 327-347.

Hargraves R.B., 1980. Physics of Magmatic Processes. Princeton University Press, Princeton, NJ, 585 pp.

Harrington H.J., 1958. Nomenclature of rock units in the Ross Sea region, Antarctica. Nature, 182, 290.

Harry D.L. & Leeman W.P., 1995. Partial melting of melt metasomatized subcontinental mantle and the magma source potential of the lower lithosphere. Journal of Geophysical Research, 100, 10,255-10,270.

Hawkesworth C.J., Gallagher K., Kirstein L., Mantovani M.S.M., Peate D.W. & Turner J.S., 2000. Tectonic controls on magmatism associated with continental break-up: an example from the Paraná-Etendeka Province. Earth and Planetary Science Letters, 179, 335-349.

Heimann A., Fleming T.H., Elliot D.H. & Foland K.A., 1994. A short interval of Jurassic continental flood basalt volcanism in Antarctica as demonstrated by $^{40}Ar/^{39}Ar$ geochronology. Earth and Planetary Science Letters, 121, 19-41.

Helz R.T. & Rait N., 1988. Behavior of Pt and Pd in Kilauea Iki lava lake. V.M. Goldschmidt Conference Abstract, Baltimore, p. 47.

Hergt J., 2000. Comment on: ``Enriched mantle - Dupal signature in the genesis of the Jurassic Ferrar tholeiites from Prince Albert Mountains (Victoria Land, Antarctica)" by Antonini P. et al. (Contributions to Mineralogy and Petrology 136, 1-19; 1999)". Contributions to Mineralogy and Petrology, 139, 240-244.

Hergt J. & Brauns C.M., 2001. On the origin of Tasmanian dolerites. Australian Journal of Earth Sciences, 48, 543-549.

Hergt J.M., Chappell B.W., Faure G. & Mensing T.M., 1989a. The geochemistry of Jurassic dolerites from Portal Peak, Antarctica. Contributions to Mineralogy and Petrology, 102, 298-305.

Hergt J.M., Chappell B.W., Mc Culloch M.T., Mc Dougall I. & Chivas A.R., 1989b. Geochemical and Isotopic Constraints on the Origin of the Jurassic Dolerites of Tasmania. Journal of Petrology, 30, 841-883.

Hergt J.M., Peate D.W. & Hawkesworth C.J., 1991. The petrogenesis of Mesozoic Gondwana low-Ti flood basalts. Earth and Planetary Science Letters, 105, 134-148.

Hermann J., Müntner O. & Günther D., 2001. Differentiation of Mafic Magma in a Continental Crust-to-Mantle Transition Zone. Journal of Petrology, 42, 189-206.

Hill R.I., 1991. Starting plumes and continental break-up. Earth and Planetary Science Letters, 104, 398-416.

Himmelberg G.R. & Ford A.B., 1976. Pyroxenes of the Dufek Intrusion, Antarctica. Journal of Petrology, 17, 219-243.

Himmelberg G.R. & Ford A.B., 1977. Iron-titanium oxides of the Dufek intrusion, Antarctica. American Mineralogist, 62, 622-633.

Hirose K. & Kawamato T., 1995. Hydrous partial melting of lherzolite at 1GPa: The effect of H_2O on the genesis of basaltic magmas. Earth and Planetary Science Letters, 133, 463-473.

Hirose K. & Kushiro I., 1993. Partial melting of dry peridotites at high pressures: Determination of compositions of melts segregated from peridotite using aggregates of diamond. Earth and Planetary Science Letters, 114, 477-489.

Hoefs J., Faure G. & Elliot D.H., 1980. Correlation of $\delta^{18}O$ and Initial $^{87}Sr/^{86}Sr$ Ratios in Kirkpatrick Basalt on Mt. Falla, Transantarctic Mountains. Contributions to Mineralogy and Petrology, 75, 199-203.

Holloway J.R., Dixon.J.E. & Pawley A.R., 1992. An internally heated, rapid-quench, high-pressure vessel. American Mineralogist, 77, 643-646.

Holtz F., Behrens H., Dingwell D.B. & Johannes W., 1995. H_2O solubility in haplogranitic melts - compositional, pressure, and temperature dependence. American Mineralogist, 80, 94-108.

Holzheid A., Sylvester P., O'Neill H.S.C., Rubie D.C. & Palme H., 2000. Evidence for a late chondritic veneer in the Earth's mantle from high-pressure partitioning of palladium and platinum. Nature, 406, 396-399.

Hooper P.R., 1990. The timing of crustal extension and the eruption of continental flood basalts. Nature 345, 246-249.

Hooper P.R., 1997. The Columbia River Flood Basalt Province: Current Status. In: Mahoney J.J. & Coffin M.F. (eds), Large Igneous Provinces: Continental, Oceanic, and Planetary Flood Volcanism, AGU Geophysical Monograph Series, 100, 1-27.

Hornig I., 1993. High-Ti and Low-Ti Tholeites in the Jurassic Ferrar Group, Antarctica. Geologisches Jahrbuch, E47, 335-369.

Housh T.B. & Luhr J.F., 1991. Plagioclase-melt equilibria in hydrous systems. American Mineralogist, 76, 477-492.

Huebner J.S. & Sato M., 1970. Oxygen fugacity-temperature relationships of manganese oxide and nickel oxide buffers. American Mineralogist, 55, 934-952.

Hunter R. H. & Sparks R. S. J., 1987. The differentiation of the Skaergaard Intrusion. Contributions to Mineralogy and Petrology, 95, 451-161

Hunter R. H. & Sparks R. S. J., 1990. The differentiation of the Skaergaard Intrusion. Reply to McBimey and Naslund. Contributions to Mineralogy and Petrology, 106, 248-254.

Hutchinson D. & McDonald I., 2005. Breaking the rules. Divergent behaviour of platinum and palladium in the Northern Limb of Bushveld Complex, R.S.A. In: Törmänen T.O. & Alapieti T.T. (eds), Extended Abstracts, 10th International Platinum Symposium, Oulu Finland, 118-121.

Irvine T.N. & Baragar W.R.A., 1971. A guide to the chemical classification of the common volcanic rocks. Canadian Journal of Earth Sciences, 8, 523-548.

Jackson S.E., Fryer B.J., Gosse W., Healey D.C., Longerich H.P. & Strong D.F., 1990. Determination of the precious metals in geological materials by inductively coupled plasma - mass spectrometry (ICP-MS) with nickel sulphide fire-assay collection and tellurium coprecipitation. Chemical Geology, 83, 119-132.

Jana D. & Walker D., 1997. The influence of sulfur on partitioning of siderophile elements. Geochimica et Cosmochimica Acta, 61, 5255-5277.

Jaques A.L. & Green D.H., 1980. Anhydrous Melting of Peridotite at 0-15 Kb Pressure and the Genesis of Tholeiitic Basalts. Contributions to Mineralogy and Petrology, 73, 287-310.

Johannes W., 1978. Melting of plagioclase in the system Ab-An-H_2O and Qz-Ab-An-H_2O at P_{H2O} = 5 kbars, an equilibrium problem. Contributions to Mineralogy and Petrology, 66, 295-303.

Johnson K.T.M., 1994. Experimental cpx/ and garnet/melt partitioning of REE and other trace elements at high pressures; petrogenetic implications. Mineralogical Magazine, 58, 454-455.

Kawamoto T. & Hirose K., 1994. Au-Pd sample containers for melting experiments on iron and water bearing systems. European Journal of Mineralogy, 6, 381-385.

Keays R.R., 1995. The role of komatiitic and picritic magmatism and S-saturation in the formation of ore deposits. Lithos, 34, 1-18.

Kerr A.C., Tarney J., Marriner G.F., Klaver G.Th., Saunders A.D. & Thirlwall M.F., 1996. The geochemistry and petrogenesis of the late-Cretaceous picrites and basalts of Curacao, Netherlands Antilles: a remnant of an oceanic plateau. Contributions to Mineralogy and Petrology, 124, 29-43.

Kerr A.C., Tarney J., Marriner G.F., Nivia A. & Saunders A.D., 1997. The Caribbean-Colombian Cretaceous Igneous Province: The Internal Anatomy of an Oceanic Plateau. In: Mahoney J.J. & Coffin M.F. (eds), Large Igneous Provinces: Continental, Oceanic, and Planetary Flood Volcanism, AGU Geophysical Monograph Series, 100, 123-144.

Kilinc A., Carmichael I.S.E., Rivers M.L. & Sack R.O., 1983. The Ferric-Ferrous Ratio of Natural Silicate Liquids Equilibrated in Air. Contributions to Mineralogy and Petrology, 83, 136-140.

King S.D. & Anderson D.L., 1995. An alternative mechanism of flood basalt formation. Earth and Planetary Science Letters, 136, 269-279.

Klein E. M. & Langmuir C. H., 1987. Global correlations of ocean ridge basalt chemistry with axial depth and crustal thickness. Journal of Geophysical Research, 92, 8089-8115.

Klein E.M. & Langmuir C.H., 1989. Local versus global correlations in ocean ridge basalt composition: a reply. Journal of Geophysical Research, 94, 4241-4252.

Kleinschmidt G. & Tessensohn F., 1987. Early Paleozoic Westward Directed Subduction at the Pacific Margin of Antarctica. In: McKenzie G.D. (ed), Gondwana Six: Structure, Tectonics and geophysics, AGU Geophysical Monograph Series, 40, 89-105.

Koepke J., 1997. Analyse von wasserhaltigen silikatischen Gläsern mit der Mikrosonde: Wassergehalte und Alkaliverluste. Beihefte zum European Journal of Mineralogy, 9, 200.

Kress V.C. & Carmichael I.S.E., 1991. The compressibility of silicate liquids containing Fe_2O_3 and the effect of composition, temperature, oxygen fugacity and pressure on their redox states. Contributions to Mineralogy and Petrology, 108, 82-92.

Kreuzer H., Höhndorf A., Lenz H., Vetter U., Tessensohn F., Müller P., Jordan H., Harre W. & Besang C., 1981. K/Ar and Rb/Sr dating of igneous rocks from North Victoria Land, Antarctica. Geologisches Jahrbuch, B41, 267-273.

Krishnamurthy P. & Cox K. G., 1977. Picrite basalts and related lavas from the Deccan Traps of western India. Contributions to Mineralogy and Petrology, 62, 53-75.

Kudo A.M. & Weill D.F., 1970. An Igneous Plagioclase Thermometer. Contributions to Mineralogy and Petrology, 25, 52-65.

Kushiro I., 1990. Partial melting of mantle wedge and evolution of island arc crust. Journal of Geophysical Research, 95, 15,929-15,939.

Kyle P.R., 1980. Development of Heterogeneities in the Subcontinental Mantle: Evidence From the Ferrar Group. Contributions to Mineralogy and Petrology, 73, 89-104.

Kyle P.R., 1990. McMurdo Volcanic Group, Western Ross embayment. In: LeMasurier W.E. & Thomson J.W. (eds), Volcanoes of the Antarctic plate and southern Oceans, AGU Antarctic Research Series, 48, 19-25.

Kyle P.R., Elliot D.H. & Sutter J.F., 1981. Jurassic Ferrar Supergroup tholeiites from the Transantarctic Mountains, Antarctica, and their relationship to the initial fragmentation of Gondwana. In: Cresswell M.M. & Vella P. (eds), Gondwana V, A.A. Balkema, Rotterdam, 283-287.

Läufer A.L. & Rossetti F., 2001. Brittle deformation features in the Rennick Glacier-Yule Bay area, northern Victoria Land, Antarctica. Terra Antartica Reports, 5, 77-80.

Lassiter J. & DePaolo D.J., 1997. Plume/Lithosphere Interaction in the Generation of Continental and Oceanic Flood Basalts: Chemical and Isotopic Constraints. In: Mahoney J.J. & Coffin M.F. (eds), Large Igneous Provinces: Continental, Oceanic, and Planetary Flood Volcanism, AGU Geophysical Monograph Series, 100, 335-355.

Lattard D., Sauerzapf U. & Käsemann M., 2005. New calibration data for the Fe–Ti oxide thermo-oxybarometers from experiments in the Fe–Ti–O system at 1 bar, 1,000–1,300°C and a large range of oxygen fugacities. Contributions to Mineralogy and Petrology, 149, 735-754.

Latypov R.M., 2003a. The Origin of Marginal Compositional Reversals in Basic-Ultrabasic Sills and Layered Intrusions by Soret Fractionation. Journal of Petrology, 44, 1579-1618.

Latypov R.M., 2003b. The Origin of Basic-Ultrabasic Sills with S-. D-, and I-shaped Compositional Profiles by in Situ Crystallization of a Single Input of Phenocryst-poor Parental Magma. Journal of Petrology, 44, 1619-1656.

Le Maitre R.W., 1989. A Classification of Igneous Rocks and Glossary of Terms. Blackwell Scientific Publications, Oxford.

Leat P.T., Luttinen A.V., Storey B.C. & Millar I.L., 2006. Sills of the Theron Mountains, Antarctica: evidence for long distance transport of mafic magmas during Gondwana break-up. In: Hanski E., Mertanen S., Ramo T. & Vuollo J. (eds), Dyke Swarms: Time Markers of Crustal Evolution. Taylor & Francis Group, London, 183-199.

Leat P.T., Riley T.R., Storey B.C., Kelley S.P. & Millar I.L., 2000. Middle Jurassic ultramafic lamprophyre dyke within the Ferrar magmatic province, Pensacola Mountains, Antarctica. Mineralogical Magazine, 64, 95-111.

Lepage L.D., 2003. ILMAT: An Excel worksheet for ilmenite-magnetite geothermometry and geobarometry. Computers and Geosciences, 29, 673-678.

Li C., Barnes S.-J., Makovicky E., Rose-Hansen J. & Makovicky M., 1996. Partitioning of Ni, Cu, Ir, Rh, Pt, and Pd between monosulfide solid solution and sulfid liquid: effect of composition and temperature. Geochimica et Cosmochimica Acta, 60, 1231-1238.

Lightfoot P.C., Hawkesworth C.J., Hergt J.M., Naldrett A.J., Gorbachev N.S., Fedorenko V.A. & Doherty W., 1993. Remobilisation of the continental lithosphere by a mantle plume: major-, trace-element, and Sr-, Nd-, and Pb-isotope evidence from picritic and tholeiitic lavas of the Noril'sk District, Siberian Trap, Russia. Contributions to Mineralogy and Petrology, 114, 171-188.

Lindsley D.H., 1983. Pyroxene thermometry. American Mineralogist, 68, 477-493.

Lindsley D.H. & Frost B.R., 1992. Equilibria among Fe-Ti oxides, pyroxenes, olivine, and quartz: Part I. Theory. American Mineralogist, 77, 987-1003.

Lindsley D.H. & Spencer K.J., 1982. Fe–Ti oxide geothermometry: Reducing analyses of coexisting Ti-magnetite (Mt) and ilmenite (Ilm). Abstract AGU 1982 Spring Meeting Eos Transactions, 63 , 471.

Lisker F., 2002. Review of fission track studies in northern Victoria Land, Antarctica -- passive margin evolution versus uplift of the Transantarctic Mountains. Tectonophysics, 349, 57-73.

Longhi J., 1991. Comparative liquidus equilibria of hypersthene-normative basalts at low pressure. American Mineralogist, 76, 785-800.

Lorand J.P., Pattou L. & Gros M., 1999. Fractionation of Platinum-group Elements and Gold in the Upper Mantle: a Detailed Study in Pyrenean Orogenic Lherzolites. Journal of Petrology, 40, 957-981.

Lorand J.P., Schmidt G., Palme H. & Kratz K.L., 2000. Highly siderophile element geochemistry of the Earth's mantle: New data for the Lanzo (Italy) and Ronda (Spain) orogenic peridotite bodies. Lithos 53, 149-164.

Lorand J.-P. & Alard O., 2001. Platinum-group element abundances in the upper mantle: New constraints from in situ and whole-rock analyses of Massif Central xenoliths (France). Geochimica et Cosmochimica Acta, 65, 2789-2806.

MacLean W.H. & Barrett T.J., 1993. Lithogeochemical techniques using immobile elements. Journal of Geochemical Exploration, 48, 109-133.

Maier W.D. & Barnes S.-J., 2004. Pt/Pd and Pd/Ir ratios in mantle-derived magmas: A possible role for mantle metasomatism. South African Journal of Geology, 107, 333-340.

Maier W.D., Barnes S.-J. & Marsh J.S., 2003. The concentrations of the noble metals in Southern African flood-type basalts and MORB: implications for petrogenesis and magmatic sulphide exploration. Contributions to Mineralogy and Petrology, 146, 44-61.

Markl G. & White C., 1999. Complex zoning between super-calcic pigeonite and augite from the Graveyard Point sill, Oregon: a record of the interplay between bulk and interstitial liquid fractionation. Contributions to Mineralogy and Petrology, 137, 170-183.

Marks M. & Markl G., 2001. Fractionation and Assimilation Processes in the Alkaline Augite Syenite Unit of the Ilímaussaq Intrusion, South Greenland, as Deduced from Phase Equilibria. Journal of Petrology, 42, 1947-1969.

Marsh B.D., 1996. Solidification fronts and magmatic evolution. Mineralogical Magazine, 60, 5-40.

Marsh B.D., 1998. On the Interpretation of Crystal Size Distributions in Magmatic Systems. Journal of Petrology, 39, 553-599.

Marsh B.D., 2002. On bimodal differentiation by solidification front instability in basaltic magmas, part 1: Basic mechanics. Geochimica et Cosmochimica Acta, 66, 2211-2229.

Marsh B.D. & Philipp J.R., 1996. Three-dimensional magmatic filling of Basement sill revealed by unusual crystal concentration. Antarctic Journal of the U.S., 31, 39-41.

Marsh B.D. & Wheelock M.M., 1994. The vertical variation of composition in the Peneplain sill and Basement sills of the Dry Valleys: the null hypothesis. Antarctic Journal of the U.S., 29, 25-26.

Marsh J.S., Hooper P.R., Rehacek J., Duncan R.A. & Duncan A.R., 1997. Stratigraphy and Age of Karoo Basalts of Lesotho and Implications for Correlations Within the Karoo Igneous Province. In: Mahoney J.J. & Coffin M.F. (eds), Large Igneous Provinces: Continental, Oceanic, and Planetary Flood Volcanism, AGU Geophysical Monograph Series, 100, 247-272.

Martel C., Pichavant M., Holtz F. & Scaillet B., 1999. Effects of fO_2 and H_2O on andesite phase relations between 2 and 4 kbar. Journal of Geophysical Research, 104, 29,453-29,470.

Marzoli A., E.M. P., Renne P.R., Bellieni G., Iacumin M., Nyobe J.B. & Tongwa A.T., 2000. Petrogenesis of Continental Basaltic Magmas from Lithospheric and Asthenospheric Mantle Sources. Journal of Petrology, 41, 87-109.

Mathez E.A., 1973. Refinement of the Kudo-Weill Plagioclase Thermometer and Its Application to Basaltic Rocks. Contributions to Mineralogy and Petrology, 41, 61-72.

Mathez E.A., 1999. On factors controlling the concentrations of platinum group elements in layered intrusions and chromitites. In: Keays R.R., Lesher C.M., Lightfoot P.C. & Farrow C.E.G. (eds), Dynamic Processes in Magmatic Ore Deposits and their application in mineral exploration, Geological Association of Canada, Short Course Notes, 13, 251-285.

Mavrogenes J.A. & O`Neill H.S.C., 1999. The relative effects of pressure, temperature and oxygen fugacity on the solubility of sulfide in mafic magmas. Geochimica et Cosmochimica Acta, 63, 1173-1180.

McBirney A.R., 1996. The Skaergaard Intrusion. In: Cawthorn R.G. (ed), Layered Intrusions, Elsevier, Amsterdam, 147-180.

McBirney A.R. & Noyes R.M., 1979. Crystallization and Layering of the Skaergaard Intrusion. Journal of Petrology, 20, 487-554.

McBirney A. R. & Naslund H. R., 1990. The differentiation of the Skaergaard Intrusion. A discussion of Hunter and Sparks. Contributions to Mineralogy and Petrology, 104, 235-240.

McClintock M. & White J.D.L., 2006. Large phreatomagmatic vent complex at Coombs Hills, Antarctica: Wet, explosive initiation of flood basalt volcanism in the Ferrar-Karoo LIP. Bulletin of Volcanology, 68, 215-239.

McDonough W.F. & Sun S.-s., 1995. The composition of the Earth. Chemical Geology, 120, 223-253.

McGuire A.V. & Mukasa S.B., 1997. Magmatic modification of the uppermost mantle beneath the Basin and Range to Colorado Plateau Transition Zone; Evidence from xenoliths, Wikieup, Arizona. Contribution to Mineralogy and Petrology, 128, 52-65.

McKenzie D. & Bickle M.J., 1988. The Volume and Composition of Melt Generated by Extension of the Lithosphere. Journal of Petrology, 29, 623-679.

Mensing T.M., Faure G., Jones L.M., Bowman J.R. & Hoefs J., 1984. Petrogenesis of the Kirkpatrick Basalt, Solo Nunatak, Northern Victoria Land, Antarctica, based on isotopic compositions of strontium, oxygen and sulfur. Contributions to Mineralogy and Petrology, 87, 101-108.

Middlemost E.A.K., 1975. The basalt clan. Earth Science Reviews, 11, 337-364.

Milnes A.R., Cooper B.J. & Cooper J.A., 1982. The Jurassic Nisanger Basalt of Kangaroo Island, South Australia. Transactions of the Royal Society of South Australia, 106, 1-13.

Minor D.R. & Mukasa S.B., 1997. Zircon U-Pb and hornblende [40]Ar-[39]Ar ages for the Dufek layered mafic intrusion, Antarctica: Implications for the age of the Ferrar large igneous province. Geochimica et Cosmochimica Acta, 61, 2497-2504.

Mitchell R.H. & Keays R.R., 1981. Abundance and distribution of gold, palladium and iridium in some spinel and garnet Iherzolites: implications for the nature and origin of precious metal-rich intergranular components in the upper mantle. Geochimica et Cosmochimica Acta, 45, 2425-2442.

Mo X., Carmichael I.S.E., Rivers M. & Stebbins J., 1982. The partial molar volume of Fe_2O_3 in multicomponent silicate liquids and the pressure dependence of oxygen fugacity in magmas. Mineralogical Magazine, 45, 237-245.

Molzahn M., Reisberg L. & Wörner G., 1996. Os, Sr, Nd, Pb, O isotope and trace element data from the Ferrar flood basalts, Antarctica: evidence for an enriched subcontinental lithospheric source. Earth and Planetary Science Letters, 144, 529-546.

Molzahn M., Wörner G., Henjes-Kunst F. & Rocholl A., 1999. Constraints on the Cretaceous thermal event in the Transantarctic Mountains from alteration processes in Ferrar flood basalts. Global and Planetary Change, 23, 45-60.

Momme P., Oskarsson N. & Keays R.R., 2003. Platinum-group elements in the Icelandic rift system: melting processes and mantle sources beneath Iceland. Chemical Geology, 196, 209-234.

Momme P., Tegner C., Brooks C.K. & Keays R.R., 2002. The behaviour of platinum-group elements in basalts from the East Greenland rifted margin. Contributions to Mineralogy and Petrology, 143, 133-153.

Moore G., Righter K. & Carmichael I.S.E., 1995. The effect of dissolved water on the oxidation state of iron in natural silicate liquids. Contributions to Mineralogy and Petrology, 120, 170-179.

Morimoto N., 1989. Nomenclature of Pyroxenes. Canadian Mineralogist, 27, 143-156.

Morrison M.A., Thompson R.N. & Dickin A.P., 1985. Geochemical evidence for complex magmatic plumbing during development of a continental volcanic center. Geology, 13, 581-584.

Morse S. A., 1981. Kiglapait geochemistry IV: The major elements. Geochimica et Cosmochimica Acta, 45, 461-479.

Mortimer N., Parkinson D., Raine J.I., Adams C.J., Graham I.J., Oliver P.J. & Palmer K., 1995. Ferrar magmatic province rocks discovered in New Zealand: Implications for Mesozoic Gondwana geology. Geology, 23, 185-188.

Müntener O., Kelemen P.B. & Grove T.L., 2001. The role of H_2O during crystallization of primitive arc magmas under uppermost mantle conditions and genesis of igneous pyroxenites: an experimental study. Contributions to Mineralogy and Petrology, 141, 643-658.

Myers J. & Eugster H.P., 1983. The System Fe-Si-O: Oxygen Buffer Calibrations to 1,500K. Contributions to Mineralogy and Petrology, 82, 75-90.

Naldrett A.J. & Wilson A.H., 1990. Horizontal and vertical variations in noble-metal distribution in the Great Dyke of Zimbabwe: A model for the origin of the PGE mineralization by fractional segregation of sulfide. Chemical Geology, 88, 279-300.

Naslund H.R., 1989. Petrology of the Basistoppen Sill, East Greenland: A Calculated Magma Differentiation Trend. Journal of Petrology, 30, 299-319.

Neal C.R., Mahoney J.J., Kroenke L.W., Duncan R.A. & Petterson M.G., 1997. The Ontong Java Plateau. In: Mahoney J.J. & Coffin M.F. (eds), Large Igneous Provinces: Continental, Oceanic, and Planetary Flood Volcanism, AGU Geophysical Monograph Series, 100, 183-216.

Nicholls I.A. & Harris K.L., 1980. Experimental rare earth element partition coefficients for garnet, clinopyroxene and amphibole coexisting with andesitic and basaltic liquids. Geochimica et Cosmochimica Acta, 44, 287-308.

Nielsen R.L. & Drake M.J., 1979. Pyroxene-melt equilibria. Geochimica et Cosmochimica Acta, 43, 1259-1272.

Nimis P., 1995. A clinopyroxene geobarometer for basaltic systems based on crystal-structure modeling. Contributions to Mineralogy and Petrology, 121, 115-125.

Oberthür T., 2002. Platinum-group element mineralization of the Great Dyke, Zimbabwe. In: Cabri L.J. (ed), The Geology, Geochemistry, Mineralogy and Mineral Beneficiation of Platinum-Group Elements, Geological Society of Canadian Institute of Mining, Metallurgy and Petroleum, 54, 483-506.

Oberthür T., Weiser T.W., Gast L. & Kojonen K., 2003a. Geochemistry and mineralogy of platinum-group elements at Hartley Platinum Mine, Zimbabwe. Part 1. Primary distribution patterns in pristine ores of the Main Sulfide Zone of the Great Dyke. Mineralium Deposita, 38, 327-343.

Oberthür T., Weiser T.W. & Gast L., 2003b. Geochemistry and mineralogy of platinum-group elements at Hartley Platinum Mine, Zimbabwe. Part 2. Supergene redistribution in the oxidized Main Sulfide Zone of the Great Dyke, and alluvial platinum-group minerals. Mineralium Deposita, 38, 344-355.

Oberthür T., Weiser T.W. & Kojonen K., 2002. Local Variations and Regional Trends in PGE Geochemistry and Mineralogy in the Main Sulfide Zone of the Great Dyke, Zimbabwe. In: Boudreau A. (ed), 9th International Platinum Symposium, Abstracts with Programme, Billings, Montana, USA, 337-340.

Oguri K., Shimoda G. & Tatsumi Y., 1999. Quantitative determination of gold and the platinum-group elements in geological samples using improved NiS fire-assay and tellurium coprecipitation with inductively coupled plasma-mass spectrometry ICP-MS. Chemical Geology, 157, 189-197.

Olsen P.E., 1999. Giant Lava Flows, Mass Extinctions, and Mantle Plumes. Science, 284, 604-605.

Osborn E.F., 1959. Role of oxygen pressure in the crystallization and differentiation of basaltic magma. American Journal of Science, 257, 609-647.

Pálfy J. & Smith L., 2000. Synchrony between early Jurassic extinction, oceanic anoxic event, and the Karoo – Ferrar flood basalt volcanism. Geology, 28, 747-750.

Panjasawatwong Y., Danyushevsky L.V., Crawford A.J. & Harris K.L., 1995. An experimental study of the effects of melt composition on plagioclase - melt equilibria at 5 and 10 kbar: implications for the origin of magmatic high-An plagioclase. Contributions to Mineralogy and Petrology, 118, 420-432.

Parry S.J., 1984. Abundance and distribution of palladium, platinum, iridium and gold in some oxide minerals. Chemical Geology, 43, 115-125.

Pattou L., Lorand J.P. & Gros M., 1996. Non-chondritic PGE ratios in the terrestrial upper mantle. Nature, 379, 712-715.

Peach C.L., Mathez E.A. & Keays R.R., 1990. Sulfide melt-silicate melt distribution coefficients for noble metals and other chalcophile elements as deduced from MORB: Implications for partial melting. Geochimica et Cosmochimica Acta, 54, 3319-3389.

Peach C.L. & Mathez E.A. 1996. Constraints on the formation of platinum-group element deposits in igneous rocks. Economic Geology, 91, 439-450.

Peach C.L., Mathez E.A., Keays R.R. & Reeves S.J., 1994. Experimentally determined sulfide melt-silicate melt partition coefficients for iridium and palladium. Chemical Geology, 117, 361-377.

Pearce J.A., 1983. Role of the subcontinental lithosphere in magma genesis at active continental margins. In: Hawkesworth C.J. & Norry M.J. (eds), Continental basalts and mantle xenoliths. Nantwick, Shiva Press, Ltd., 230-249.

Peate D.W., 1997. The Paraná Province. In: Mahoney J.J. & Coffin M.F. (eds), Large Igneous Provinces: Continental, Oceanic, and Planetary Flood Volcanism, AGU Geophysical Monograph Series, 100, 217-245.

Peate D.W. & Hawkesworth C.J., 1996. Lithospheric to asthenospheric transition in Low-Ti flood basalts from southern Paraná, Brazil. Chemical Geology, 127, 1-24.

Peregoedova A., Barnes S.-J. & Baker D., 2002. The formation of Pt and Ir minerals in base metal sulfides: effect of sulfur fugacity and composition. In: Boudreau A. (ed), 9th International Platinum Symposium, Abstracts with Programme, Billings, Montana, USA, 363-366.

Peregoedova A., Barnes S.-J. & Baker D., 2004. The formation of Pt–Ir alloys and Cu–Pd-rich sulfide melts by partial desulfurization of Fe–Ni–Cu sulfides: results of experiments and implications for natural systems. Chemical Geology, 208, 247-264.

Philipp H., 1999. The behaviour of PGE during petrogenetic processes: a case study of basalts of the seaward dipping reflector sequences (SE-Greenland coast). Karlsruher Geochemische Hefte, Ph.D. thesis, 14, 155 pp.

Philipp H., Eckhardt J.D. & Puchelt H., 2001. Platinum-Group Elements (PGE) in Basalts of the Seaward-Dipping Reflector Sequences, SE Greenland Coast. Journal of Petrology, 42, 407-432.

Philpotts A.R., Carroll M.R. & Hill J.M., 1996. Crystal-Mush Compaction and the Origin of Pegmatitic Segregation Sheets in a Thick Flood-Basalt Flow in the Mesozoic Hartford Basin, Connecticut. Journal of Petrology, 37, 811-836.

Pichavant M., 1987. Effects of B and H_2O on liquidus phase relations in the haplogranite system at 1 kbar. American Mineralogist, 72, 11-12.

Pitzer K.S. & Sterner S.M., 1994. Equation of state valid continuously from zero to extreme pressures for H_2O and CO_2. Journal of Chemical Physics, 102, 3111-3116.

Price G.D., 1982. Exsolution in titanomagnetites as an indicator of cooling rates. Mineralogical Magazine, 46, 19-25.

Puchtel I.S., Humayun M., Campbell A.J., Sproule R.A. & Lesher C.M., 2004. Platinum group element geochemistry of komatiites from the Alexo and Pyke Hill areas, Ontario, Canada. Geochimica et Cosmochimica Acta, 68, 1361-1383.

Puffer J.H. & Horter D.L., 1993. Origin of pegmatitic segregation veins within flood basalts. Geological Society of America Bulletin, 105, 738-748.

Putirka K., 2005. Igneous thermometers and barometers based on plagioclase + liquid equilibria: Tests of some existing models and new calibrations. American Mineralogist, 90, 336-349.

Putirka K., Johnson M., Kinzler R., Longhi J. & Walker D., 1996. Thermobarometry of mafic igneous rocks based on clinopyroxene-liquid equilibria, 0-30 kbar. Contributions to Mineralogy and Petrology, 123, 92-108.

Putika K.D., Mikaelian H., Ryerson F. & Shaw H., 2003. New clinopyroxene-liquid thermobarometers for mafic, evolved, and volatile-bearing lava compositions, with applications to lavas from Tibet and the Snake River Plain, Idaho. American Mineralogist, 88, 1542-1554.

Ratajeski K. & Sisson T.W., 1999. Loss of iron to gold capsules in rock-melting experiments. American Mineralogist, 84, 1521-1527.

Rehkämper M., 2000. Tracing the Earth's evolution. Nature 407, 848-849.

Rehkämper M., Halliday A.N., Alt J., Fitton J.G., Zipfel J. & Takazawa E., 1999a. Non-chondritic platinum-group element ratios in oceanic mantle lithosphere; petrogenetic signature of melt percolation? Earth and Planetary Science Letters, 172, 65-81.

Rehkämper M., Halliday A.N., Fitton J.G., Lee D.-C., Wieneke M. & Arndt N.T., 1999b. Ir, Ru, Pt and Pd in basalts and komatiites: New constraints for the geochemical behavior of the platinum-group elements in the mantle. Geochimica et Cosmochimica Acta, 63, 3915-3934.

Reid F., 1983. Origin of the Rhyolitic Rocks of the Taupo Volcanic Zone, New-Zealand. Journal of Volcanology and Geothermal Research, 15, 315-338.

Renne P.R., Deino A.L., Walter R.C., Turrin B.D., Swisher C.C., Becker T.A., Curtis G.H., Sharp W.D. & Jaouni A.-R., 1994. Intercalibration of astronomical and radioisotopic time. Geology, 22, 783-786.

Renne P.R., Zichao Z., Richards M.A., Black M.T. & Basu A.R., 1995. Synchrony and causal relations between Permian-Triassic boundary crises and Siberian flood volcanism. Science, 269, 1413-1416.

Richards M.A., Duncan R.A. & Courtillot V., 1989. Flood basalts and hot spot tracks: Plume heads and tails. Science, 246, 103-107.

Rietmeijer F.J.M. & Champness P.E., 1982. Exsolution structures in calcic pyroxenes from the Bjerkreim-Sokndal lopolith, SW Norway. Mineralogical Magazine, 45, 11-24.

Righter K., Campbell A.J., Humayun M. & Hervig R.L., 2004. Partitioning of Ru, Rh, Pd, Re, Ir, and Au between Cr-bearing spinel, olivine, pyroxene and silicate melts. Geochimica et Cosmochimica Acta, 68, 867-880.

Riley T.R. & Knight K.B., 2001. Age of Pre-Break-Up Gondwana Magmatism. Antarctic Sciences, 13. 99-110.

Riley T.R., Leat P.T., Storey B.C., Parkinson I.J. & Millar I.L., 2003. Ultramafic lamprophyres of the Ferrar large igneous province: evidence for a HIMU mantle component. Lithos, 66, 63-76.

Robie R.A., Hemingway B.S. & Fisher J.R., 1978. Thermodynamic properties of minerals and related substances at 298.15 K and 1 bar (10^5 Pascals) pressure and at higher temperatures. Geological Survey Bulletin, 1452, 456.

Roeder P.L. & Emslie R.F., 1970. Olivine-liquid equilibrium. Contributions to Mineralogy and Petrology, 29, 275-289.

Roland N.W., Laeufer A.L. & Rossetti F., 2004. Revision of the Terrane Model of Northern Victoria Land. Terra Antartica, 11, 55-65.

Roland, N.W. and Tessensohn, F., 1987. Rennick faulting – an early phase of Ross Sea rifting. Geologisches Jahrbuch, B66: 203-229.

Roland N.W. & Wörner G., 1996. Kirkpatrick Flows and Associated Pyroclastics: New Occurrences, Definition, and Aspects of a Jurassic Transantarctic Rift. Geologisches Jahrbuch, B89, 97-121.

Roux J. & Lefèvre A., 1992. A fast-quench device for internally heated pressure vessels. European Journal of Mineralogy, 4, 279-281.

Rudashevskiy N.S., 1987. Origin of the various types of platinoid mineralization in ultramafic rocks. International Geology Review, 29, 465-480.

Sack R.O., Carmichael I.S.E., Rivers M.L. & Ghiorso M.S., 1980. Ferric-ferrous equilibria in natural silicate liquids at 1 bar. Contributions to Mineralogy and Petrology, 75, 369-376.

Sato M., 1978. Oxygen fugacity of basaltic magmas and the role of gas-forming elements. Geophysical Research Letters, 5, 447-449.

Scaillet B. & Evans B.W., 1999. The 15 June 1991 Eruption of Mount Pinatubo. I. Phase Equilibria and Pre-eruption P-T-fO_2-fH_2O Conditions of the Dacite Magma. Journal of Petrology, 40, 381-411.

Scaillet B. & McDonald R., 2003. Experimental Constraints on the Relationships between Peralkaline Rhyolites of the Kenya Rift Valley. Journal of Petrology, 44, 1867-1894.

Scaillet B., Pichavant M., Roux J., Humbert G. & Lefèvre A., 1992. Improvements of the Shaw membrane technique for measurement and control of fH_2 at high temperatures and pressures. American Mineralogist, 77, 647-655.

Scheibner B., 2003. Das geochemische Verhalten der Platingruppenelemente bei der Entstehung und Differenzierung der Magmen der Kerguelen-Flutbasaltprovinz (Indischer Ozean). Karlsruher Mineralogische und Geochemische Hefte, 24, Ph.D. thesis, Universität Karlsruhe, 193 pp.

Schmidt B.C., Scaillet B. & Holtz F., 1995. Accurate control of fH_2 in cold-seal pressure vessels with the Shaw membrane technique. European Journal of Mineralogy, 7, 893-903.

Schuiling R.D. & Feenstra A., 1980. Geochemical behaviour of vanadium in iron-titanium oxides. Chemical Geology, 30, 143-150.

Schwab R.G. & Küstner D., 1981. Die Gleichgewichtsfugazitäten technologisch und petrologisch wichtiger Sauerstoffpuffer. Neues Jahrbuch der Mineralogie, Abhandlungen, 140, 111-142.

Sen G., Hickey-Vargas R., Waggoner D.G. & Maurrasse F., 1988. Geochemistry of basalts from the Dumisseau Formation, southern Haiti: implications for the origin of the Caribbean Sea crust. Earth and Planetary Science Letters, 87, 423-437.

Sharma M., 1997. Siberian Traps. In: Mahoney J.J. & Coffin M.F. (eds), Large Igneous Provinces: Continental, Oceanic, and Planetary Flood Volcanism, AGU Geophysical Monograph Series, 100, 273-295.

Shaw H.R., 1963. Hydrogen-Water Vapor Mixtures: Control of Hydrothermal Atmospheres by Hydrogen Osmosis. Science, 139, 1220-1222.

Shaw H.R. & Wones D.R., 1964. Fugacity coefficients for hydrogen gas between 0°C and 1000°C for pressures to 3000 atm. American Journal of Science, 262, 918-929.

Siders M.A. & Elliot D.H., 1985. Major and trace element geochemistry of the Kirkpatrick Basalt, Mesa Range, Antarctica. Earth and Planetary Science Letters, 72, 56-64.

Sisson T.W. & Grove T.L., 1993. Experimental investigations of the role of H_2O in calc-alkaline differentiation and subduction zone magmatism. Contributions to Mineralogy and Petrology, 113, 143-166.

Skinner D.N.B., Tessensohn F. & Vetter U., 1981. Lavas in the Ferrar Group of Litell Rocks, North Victoria Land, Antarctica. Geologisches Jahrbuch, B41, 251-259.

Smith J.V. & Brown W.L., 1988. Feldspar Minerals. Volume 1: Crystal structures, Physical, Chemical and Microtextural Properties. Springer Verlag, 758 pp.

Snow J.E. & Schmidt G., 1998. Constraints on Earth accretion deduced from noble metals in the oceanic mantle. Nature, 391, 166-169.

Storey B.C., 1995. The role of the mantle plumes in continental breakup: case histories from Gondwana. Nature, 377, 301-308.

Storey B.C., Alabaster T., Hole M.J., Pankhurst R.J. & Wever H.E., 1992a. Role of subduction-plate boundary forces during the initial stages of Gondwana break-up: evidence from the proto-Pacific margin of Antarctica. In: Storey B.C., Alabaster T. & Pankhurst R.J. (eds), Magmatism and the Causes of Continental Break-Up., Geological Society of London, Special Publication, 68, 149-163.

Storey B.C., Alabaster T. & Pankhurst R.J., 1992b. Magmatism and the Causes of Continental Break-Up. Geological Society of London, Special Publication, 68, 404 pp.

Storey B.C. & Kyle P.R., 1997. An active mantle mechanism for Gondwana break-up. South African Journal of Geology, 100, 283-290.

Storey B.C., Leat P.T. & Ferris J.K., 2001. The location of mantle plume centres during the initial stages of Gondwana breakup. In: Ernst R.E. & Buchan K.L. (eds.), Mantle Plumes: Their Identification Through Time. Geological Society of America Special Paper, 352, 71-80.

Storey B.C., Leat P.T., Weaver S.D., Pankhurst R.J., Bradshaw J.D. & Kelley S., 1999. Mantle plumes and Antarctica-New Zealand rifting: evidence from mid-Cretaceous mafic dykes. Journal of the Geological Society, London, 156, 659-671.

Storey B.C., Mahoney J.J. & Saunders A.D., 1997. Cretaceous Basalts in Madagascar and the Transition Between Plume and Continental Lithosphere Mantle Sources. In: Mahoney J.J. & Coffin M.F. (eds), Large Igneous Provinces: Continental, Oceanic, and Planetary Flood Volcanism, AGU Geophysical Monograph Series, 100, 95-122.

Stormer J.C., Jr., 1983. The effects of recalculation on estimates of temperature and fO_2 from analyses of multicomponent iron-titanium oxides. American Mineralogist, 68, 586-594.

Stone W.E., Crocket J.H. & Fleet M.E., 1990. Partitioning of palladium, iridium, platinum and gold between sulfide liquid and basalt melt at 1200°C. Geochimica et Cosmochimica Acta, 54, 2341-2344.

Sugawara T., 2001. Ferric iron partitioning between plagioclase and silicate liquid: thermodynamics and petrological applications. Contributions to Mineralogy and Petrology, 141, 659-686.

Sun S.-s. & McDonough W.F., 1989. Chemical and isotopic systematics of oceanic basalts: implications for mantle composition and processes. In: Saunders A.D. & Norry M.J. (eds), Magmatism in the Ocean Basins, Geological Society of London, Special Publication, 42, 313-345.

Tait S. & Jaupart C., 1996. The producing of chemically stratified and adcumulate plutonic igneous rocks. Mineralogical Magazine, 60, 99-114.

Takahashi E. & Kushiro I., 1983: Melting of a dry peridotite at high pressures and basalt magma genesis. American Mineralogist, 68, 859-879.

Taylor S.R. & McLennan S.M., 1985. The Continental Crust: its Composition and Evolution. Blackwell Scientific Publication, Oxford, 312 pp.

Thordarson T. & Self S., 1996. Sulfur, chlorine and fluorine degassing and atmospheric loading by the Roza eruption, Columbia River Basalt Group, Washington, USA. Journal of Volcanology and Geothermal Research, 74, 49-73.

Toplis M.J. & Carroll M.R., 1995. An Experimental Study of the Influence of Oxygen Fugacity on Fe-Ti Oxide Stability, Phase Relations, and Mineral-Melt Equilibria in Ferro-Basaltic Systems. Journal of Petrology, 36, 1137-1170.

Toplis M.J. & Carroll M.R., 1996. Differentiation of Ferro-Basaltic Magmas under Conditions Open and Closed to Oxygen: Implications for the Skaergaard Intrusion and Other Natural Systems. Journal of Petrology, 37, 837-858.

Turner S. & Hawkesworth C.J., 1995. The nature of the sub-continental mantle: constraints from the major-element composition of continental flood basalts. Chemical Geology, 120, 295-314.

Villiger S., Ulmer P., Müntener O. & Thompson A.B., 2004. The Liquid Line of Descent of Anhydrous, Mantle-Derived, Tholeiitic Liquids by Fractional and Equilibrium Crystallization – an Experimental Study at 1.0 GPa. Journal of Petrology, 45, 2369-2388.

Villiger S., Ulmer P. & Müntener O., 2007. Equilibrium and Fractional Crystallization Experiments at 0.7GPa; the Effect of Pressure on Phase Relations and Liquid Compositions of Tholeiitic Magmas. Journal of Petrology, 48, 159-184.

Vogel D.C. & Keays R.R., 1997. The petrogenesis and platinum-group element geochemistry of the Newer Volcanic Province, Victoria, Australia. Chemical Geology, 136, 181-204.

Wager L.R., 1960. The Major Element Variation of the Layered Series of the Skaergaard Intrusion and a Re-estimation of the Average Composition of the Hidden Layered Series and of the Successive Residual Magmas. Journal of Petrology, 1, 364-398.

Wager L.R. & Brown G.M., 1967. Layered Igneous Rocks. Oliver and Boyd, Edinburgh, 558 pp.

Walker R.J., Carlson R.W., Shirey S.B. & Boyd F.R., 1989. Os, Sr, Nd, and Pb isotope systematics of southern African peridotite xenoliths: Implications for the chemical evolution of subcontinental mantle. Geochimica et Cosmochimica Acta, 53, 1583-1595.

Walker R.J., Hanski E., Vuollo J. & Liipo J., 1996. The Os isotopic composition of Proterozoic upper mantle: evidence for chondritic upper mantle from Outokumpu ophiolite, Finland. Earth and Planetary Science Letters, 141, 161-173.

Wallace P. & Carmichael I.S.E., 1992. Sulfur in basaltic magmas. Geochimica et Cosmochimica Acta, 56, 1863-1874.

Watkinson D.H., Lavigne M.J. & Fox P.E., 2002. Magmatic-Hydrothermal Cu- and Pd-rich Deposits in Gabbroic Rocks from North America. In: Cabri L.J. (ed), The Geology, Geochemistry, Mineralogy and Mineral Beneficiation of Platinum-Group Elements. Geological Society of Canadian Institute of Mining, Metallurgy and Petroleum, Special Volume 54, 299-319.

Weaver S.D., Bradshaw J.D. & Laird M.G., 1984. Geochemistry of Cambrian volcanics of the Bowers Supergroup and implications for the Early Palaeozoic tectonic evolution of northern Victoria Land, Antarctica. Earth and Planetary Science Letters, 68, 128-140.

Wheelock M.M. & Marsh B.D., 1993. Bimodal differentiation: Silicic segregations in the Ferrar Dolerites. Antarctic Journal of the U.S., 28, 19-21.

White J.D.L. & McClintock M., 2001. Immense vent complex marks flood-basalt eruption in a wet, failed rift: Coombs Hills, Antarctica. Geology, 29, 935-938.

White R. & McKenzie D., 1989. Magmatism at Rift Zones: The Generation of Volcanic Continental Margins and Flood Basalts. Journal of Geophysical Research, 94, 7685-7729.

White R. & McKenzie D., 1995. Mantle Plumes and Flood Basalts. Journal of Geophysical Research, 100, 17,543-17,585.

Wignall P.B., 2001. Large igneous provinces and mass extinctions. Earth-Science Reviews, 53, 1-33.

Wilhelm S. & Wörner G., 1996. Crystal size distribution in Jurassic Ferrar flows and sills (Victoria Land, Antarctica): evidence for processes of cooling, nucleation, and crystallisation. Contributions to Mineralogy and Petrology, 125, 1-15.

Wilson M., 1989. Igneous Petrogenesis. Unwin Hyman, London, 466 pp.

Wilson T.J., 1993. Jurassic faulting and magmatism in the Transantarctic Mountains: implications for Gondwana breakup. In: Findlay R.H., Unrug R., Banks M.R. & Veevers J.J. (eds), Gondwana Eight: Assembly, Evolution and Dispersal. Balkema, Rotterdam, 563-572.

Wood S., 2002. The Aqueous Geochemistry of the Platinum-Group Elements with Applications to Ore Deposits. In: Cabri L.J. (ed), The Geology, Geochemistry, Mineralogy and Mineral Beneficiation of Platinum-Group Elements, Geological Society of Canadian Institute of Mining, Metallurgy and Petroleum, 54, 211-249.

Wood B.J. 1991, Oxygen Barometry of Spinel Peridotites. In: Lindsley D.H. (ed), Oxide Minerals: Petrologic and Magnetic Significance, Reviews in Mineralogy, 25, 417-431.

Wooden J.L., Czamanske G.K., Fedorenko V.A., Arndt N.T., Chauvel C., Bouse R.M., King B.-S.W., Knight R.J. & Siems D.F., 1993. Isotopic and trace-element constraints on mantle and crustal contributions to Siberian continental flood basalts, Noril'sk area, Siberia. Geochimica et Cosmochimica Acta, 57, 3677-3704.

Woodland A.B. & Koch M., 2003. Variation in oxygen fugacity with depth in the upper mantle beneath the Kaapvaal craton, Southern Africa. Earth and Planetary Science Letters, 214, 295-310.

Wright T.O., 1981. Sedimentology of the Robertson Bay Group, northern Victoria Land, Antarctica. Geologisches Jahrbuch, B41, 127-138.

Wright T.L. & Doherty P.C., 1970. A linear programming and least squares computer method for solving petrologic mixing problems. Bulletin of the Geological Society of America, 81, 1995-2008.

Yi V.Y. & Masuda A., 1996. Simultaneous determination of ruthenium, palladium, iridium, and platinum at ultratrace levels by isotope dilution inductively coupled plasma mass spectrometry in geological samples. Analytical Chemistry, 68, 1444-1450.

Yoder H.S. & Tilley C.E., 1962. Origin of basaltic magmas: an experimental study of natural and synthetic rock systems. Journal of Petrology, 3, 342-532.

Zuleger E. & Erzinger J., 1988. Determination of REE and Y in silicate materials with ICP-AES. Fresenius Zeitschrift fuer Analytische Chemie, 332, 140-143.

Appendix 1 List of sampled Ferrar occurrences from northern Victorialand (RH*) and George V Land (NWR*) including geographical information as well as short notes on the mode of magma emplacement if indicated by field relations. Sample description refers to the respective sample(s), which has (have) been analysed by any of the given methods. The analytical methods applied are given in the columns to the right.

Abbreviations of the applied analytical techniques:

OM   – Rock composition determined by optical microscopy including point counting

XRF   – Bulk-rock chemistry by X-ray fluorescence analysis at the Institut für Geowissenschaften Jena and at the GeoForschungsZentrum Potsdam.

EMP   – Mineral chemistry by electron microprobe analysis at the Mineralogisches Institut, Tübingen.

ICP-AES   – REE concentrations by atom emissions spectrometry with inductively coupled plasma at the GeoForschungsZentrum Potsdam.

ICP-MS   – PGE concentrations by mass spectrometry with inductively coupled plasma at the Institut für Mineralogie und Geochemie, Karlsruhe.

Sample number	Region	Location	GPS-coordinates (helicopter landing position)	Type of magma emplacement (extrusive / intrusive)	OM	XRF	EMP	ICP-AES	ICP-MS
RH1	Morozumi Range	above Unconformity Valley	71°40.402 / 161°53.948	sill above Beacon sediments, vertically thick platy jointing, coarse-crystalline, non-vesicular		X			
RH2/3	Litell Rocks	at 410 m high dolerite ridge, N of camp	71°24.6 / 162°03.2 (map coordinates)	(sill), thin columnar to vertically thick platy jointing, very fine-crystalline, non-vesicular, horizontal terracing	X RH3	X RH3			X RH3
RH4/5	Litell Rocks	Mandel Cliffs, foot of cliffs	71°26.75 / 162°04.0 (map coordinates)	lava flow sequence, very fine-crystalline, highly vesicular	X	X			
RH6	Litell Rocks	~ 2 km N of Mandel Cliffs, foot of cliffs	71°25.9 / 162°03.5 (map coordinates)	(sill), thin columnar to vertically thick platy jointing, fine-crystalline, non-vesicular, horizontal terracing	X	X	X	X	X
RH7-10	Litell Rocks	W of 410 m high dolerite ridge, N of camp	71°24.365 / 162°02.748	(sill), columnar to thick platy jointing, fine- (to medium-) crystalline, non-vesicular, horizontal terracing,	X RH7	X RH7, 9			X RH7, 9
RH11-15	Helliwell Hills	Mt. Alford	71°54.9 / 161°39.1	sill containing rafts of Beacon sediments, medium- to coarse crystalline, non-vesicular		X			X RH12
RH16	Helliwell Hills	nunatak W of Mt. Alford	71°57.360 / 161°28.055	(sill), regular thick columnar jointing, medium-crystalline, non-vesicular		X			
RH17	SSE of Helliwell Hills	Fitzsimmons Nunatak	71°08.666 / 161°42.875	(sill), thick columnar to platy jointing, medium-crystalline, non-vesicular		X			X
RH18	Neall Massif	on top of unnamed nunatak	72°03.785 / 164°24.934	dikes in Beacon sediments, very fine-crystalline, non-vesicular	X	X		X	X
RH19	Helliwell Hills	Boggs Valley	71°53.906 / 161°32.293	sill above Beacon sediments, thin columnar jointing, medium-crystalline, non-vesicular		X			
RH20	Morozumi Range	western margin	71°36.609 / 161°45.607	sill close to Beacon / basement unconformity, fine- to (medium-)crystalline, non-vesicular		X			
RH21	Neall Massif	W-flank of unnamed nunatak	72°03.504 / 164°27.105	sill in Beacon sediments, medium-crystalline, non-vesicular	X	X	X	X	X

Appendix 1 (continued)

Sample number	Region	Lokalität	GPS-Coordinates (Helicopter landing position)	Type of magma emplacement (extrusive / intrusive)	OM	XRF	EMP	ICP-AES	ICP-MS
RH22	Alamein Range	northern branch	71°53.251 / 163°05.180	sill above Beacon sediments, medium-crystalline, non-vesicular	X	X			
RH23	Alamein Range	northern branch	71°52.426 / 163°02.437	sill above Beacon sediments, (medium-) to coarse-crystalline, non-vesicular		X			
RH24	Alamein Range	northern branch	71°56.367 / 163°07.360	(sill), columnar jointing, coarse-crystalline, non-vesicular	X	X	X		X
RH25	Alamein Range	northern branch	71°57.711 / 163°00.248	(sill), columnar jointing, medium-crystalline, non-vesicular		X			
RH26-29	Monument Nunataks	Margret Nunatak	72°42.304 / 162°09.133	lava flow sequence, very fine- to fine-crystalline, highly vesicular	X	X			
RH30-33	Monument Nunataks	Mt. Burkett	72°42.046 / 162°14.750	lava flow sequence, very fine- to fine-crystalline, highly vesicular	X	X		X RH29	
RH34	Monument Nunataks	Mt. Lorius	72°29.740 / 162°20.523	lava flow, fine-crystalline, highly vesicular	X	X			
RH35	Monument Nunataks	northern branch	72°28.088 / 162°22.182	lava flow, fine- to medium-crystalline, highly vesicular	X	X			
RH36/37	S of Salamander Range	Mt. Apolotok	72°14.714 / 164°29.406	dike in granitoid basement, 36: very fine-crystalline, 37: fine-crystalline, non-vesicular	X	X	X		
RH38	S of Salamander Range	Mt. Apolotok	72°14.010 / 164°30.422	dike in granitoid basement, fine-crystalline, non-vesicular	X	X		X	X
RH39/40	S of Salamander Range	NW of Mello Nunatak	72°20.005 / 164°49.640	sill close to Beacon / basement unconformity, 39: very fine-crystalline / 40: coarse-crystalline, non-vesicular	X	X		X R40	X R40
RH41	Freyberg Mts.	Mt. Jackman	72°23.951 / 163°15.361	(sill), columnar jointing, medium-crystalline, non-vesicular		X			X
RH42	Freyberg Mts.	Mt. Jackman	72°23.909 / 163°11.009	(sill), thin columnar jointing, fine- to (medium-)crystalline, non-vesicular	X	X			
RH44	Crown Hills	NW of All Black Peak	71°47.119 / 163°51.203	(sill), vertically platy jointing, coarse-crystalline, non-vesicular	X	X	X	X	X
RH45	Crown Hills	All Black Peak	71°48.116 / 163°57.127	(sill), vertically platy jointing, coarse-crystalline, non-vesicular	X	X	X	X	X
RH46	E of Gallipoli Heights	unnamed nunatak	72°32.263 / 164°20.449	(sill), thick platy jointing, medium- to coarse-crystalline, non-vesicular	X	X		X	X
RH47	E of Gallipoli Heights	unnamed nunatak	72°23.232 / 164°14.904	(sill), thick platy jointing, medium- to coarse-crystalline, non-vesicular	X	X			
RH48	E of Morozumi Range	Sickle Nunatak	71°32.0 / 161°56.5 (map coordinates)	(sill), medium- to coarse-crystalline, non-vesicular	X	X		X	X

Sample number	Region	Location	GPS-Coordinates (Helicopter landing position)	Type of magma emplacement (extrusive / intrusive)	OM	XRF	EMP	ICP-AES	ICP-MS
RH49/50	Lanterman Range	saddle N of Mt. Lugering	71°40.861 / 162°53.429	sill close to Beacon / basement unconformity, medium-crystalline, non-vesicular		X			
RH51a-d	Lanterman Range	N below Mt. Lugering	71°40.034 / 162°54.432	dike in granitoid basement, a: micro-crystalline / d: coarse-crystalline, non-vesicular	X	X RH51a			
RH52	Lanterman Range	E of Linder Glacier	71°40.356 / 163°07.249	(sill), irregular columnar jointing, medium-crystalline, non-vesicular		X			X
RH53	Lanterman Range	Mt. Lugering	71°40.861 / 162°53.429	(sill), thick platy jointing, medium- to coarse-crystalline, non-vesicular	X	X	X		X
RH54a-f	Outback Nunataks	Mt. Bower	72°36.815 / 160°30.470	sill close to Beacon / basement unconformity, a: very fine-crystalline / f: coarse-crystalline, non-vesicular	X	X 54a, f	X 54a		X 54a
RH55	Freyberg Mts.	Smith's Bench	72°10.142 / 163°05.008	(sill), columnar jointing, medium-crystalline, non-vesicular	X	X			X
RH56	Freyberg Mts.	NW of Mt. Strandtmann	72°05.720 / 163°00.660	(sill), columnar jointing, medium- (to coarse-) crystalline, non-vesicular		X			X
RH57	Morozumi Range	Paine Ridge	71°36.609 / 161°45.607	sill above Beacon sediments, coarse-crystalline, non-vesicular		X			
RH58	SSE of Outback Nunataks	Johannessen Nunatak	72°50.5 / 161°09.0 (map coordinates)	sill above Beacon sediments, fine- to medium-crystalline, non-vesicular	X	X			
George V Land									
NWR25	Anxiety Nunataks		68°36′15′′/ 153°46′44′′	sill, columnar jointing, very coarse-crystalline, non-vesicular	X	X			
NWR26	Anxiety Nunataks		68°32′20′′/ 153°45′58′′	sill, columnar jointing, very coarse-crystalline, non-vesicular	X	X	X		
NWR27	SCAR Bluffs		68°48′12′′/ 153°31′65′′	sill, columnar jointing, very coarse-crystalline, non-vesicular	X	X			X
NWR28	SCAR Bluffs		68°48′12′′/ 153°31′65′′	sill, columnar jointing, very coarse-crystalline, non-vesicular	X	X			
NWR29	SCAR Bluffs		68°50′5′′ / 153°36′9′′	sill, columnar jointing, very coarse-crystalline, non-vesicular	X	X	X		X
NWR30	Anxiety Nunataks		68°32′2′′ / 153°45′5′′	sill, columnar jointing, very coarse-crystalline, non-vesicular	X	X			
NWR78	Horn Bluff		68°25′3′′ / 149°50′7′′	sill, columnar jointing, medium- to coarse-crystalline, non-vesicular	X	X			
NWR80	Horn Bluff		68°21′6′′ / 149°45′6′′	sill, columnar jointing, medium- to coarse-crystalline, non-vesicular	X	X			

Appendix 2 Petrographic data of selected Ferrar low-Ti samples and all Ferrar high-Ti samples (marked by an asterisk) with abundances of primary and secondary phases in vol% determined by thin section analyses (point counting). P – phenocryst (larger in size than average phases, which are in turn larger than matrix phases), Opx – orthopyroxene, Pig – pigeonite, Aug – augite, Plag – plagioclase, Chl – chlorite, Bt – biotite, Cc – calcite, Qz – quartz, acc. – accessory.

Part I: Intrusives from northern Victorialand

Sample number	RH3*	RH6*	RH7*	RH18	RH21	RH22	RH24*	RH36	RH37	RH38	RH39	RH40
Mesostasis	30	33	26	31	14	25	27	23	23	13	36	26
– secondarily altered	15	6	13	3	5	5	7	7	--	--	3	5
Total mesostasis	**45**	**39**	**39**	**34**	**19**	**30**	**34**	**30**	**23**	**13**	**39**	**31**
Orthopyroxene	--	--	--	3 P	5	--	--	<3 P	2	5	7 P	--
Plagioclase	25	28	32	29 + 4 P	38	34	32	35 + 3 P	36	39	18 + 3 P	34
Pigeonite + Augite	23 Pig < Aug	25 Pig < Aug	23 Pig < Aug	30	37 Pig >> Aug	35	29 Pig ~ Aug	27 + 1 P	37 Pig >> Aug	36 Pig >> Aug	34	31 Pig > Aug
Opaque phases	7	8	6	--	1	< 1	5	<2	2	2	--	2
Total primary minerals	**55**	**61**	**61**	**66**	**81**	**70**	**66**	**70**	**77**	**87**	**61**	**69**
Secondary in primary phases	2, altered Px, acc. titanite	1, altered Px, acc. titanite	5, altered Px, acc. titanite	--	3, brown secondary phase in Px	--	titanite	--	5, Bt + Chl in Pig; 15, colour-less in Px of high-order interference colours	5, Chl + Bt in Pig; 13, colour-less in Px of high-order interference colours	< 4, Bt +Chl in Opx	< 2, Bt + Chl in Pig
Secondary in mesostasis	15 Chl	6 Chl	13 Chl	3, Chl + Cc	5, brown radiating aggregates	5, Chl + Bt	7	7	--	--	3	5, Chl
Total secondary phases	**17**	**7**	**18**	**3**	**8**	**5**	**7**	**7**	**20**	**18**	**< 7**	**< 7**

Appendix 2 (continued) – Part I: Intrusives from northern Victorialand

Sample number	RH42	RH44	RH45	RH46	RH47	RH48	RH51a	RH53	RH54a	RH54f	RH55	RH58
Mesostasis	21	21	35	7	7	21	33	13	28	13	28	27
– secondarily altered	12	4	4	5	--	--	6	2	3	3	6	--
Total mesostasis	**33**	**25**	**39**	**12**	**7**	**21**	**39**	**15**	**31**	**16**	**34**	**27**
Orthopyroxene	3	--	--	1	11	13	2 P (mainly altered)	--	8 P	8	2 (incl. Bt)	> 1
Plagioclase	33	37	32	39	33 + 3 P	31	23 + < 1 P	33	29 + 3 P	44	40	33 + 5 P
Pigeonite + Augite	31	36 Pig >> Aug	24 Pig ~ Aug	48 Pig>>>Aug	45 Pig>>>Aug	35 Pig ~ Aug	35	51 Pig	29	30 Pig >> Aug	22 Pig ~ Aug	34
Opaque phases	< 1	2	< 5	--	< 1	--	--	< 1	--	< 2	< 2	< 1
Total primary minerals	**67**	**75**	**61**	**88**	**93**	**79**	**61**	**86**	**69**	**84**	**66**	**73**
Secondary in primary phases	--	--	1; acc. titanite	--	< 3, Bt	< 2, yellow secondary phase in Opx	< 2, green clay minerals in Opx	--	--	--	2, Bt in Opx	--
Secondary in mesostasis	12, Chl + Bt	4 Chl	4, brown / green clay minerals	5, Chl	--	--	6, Chl +Cc	< 2	3, brown radiating aggregates	3, brown radiating aggregates	--	--
Total secondary	**12**	**4**	**4**	**5**	**< 3**	**< 2**	**6**	**< 2**	**3**	**3**	**2**	**--**

Appendix 2   (continued) – Part II: Extrusives from northern Victorialand

Sample number	RH4	RH5	RH26	RH28	RH29	RH30	RH31	RH32	RH34	RH35
Mesostasis	71	39	26	5	29	16	28	71	73	--
– secondarily altered	--	9	--	11	5	14	--	--	--	17
Total mesostasis	**71**	**48**	**26**	**16**	**34**	**30**	**28**	**71**	**73**	**17**
Orthopyroxene	7, completely altered	--	--	< 1	< 1	3	2	< 1 P	--	--
Plagioclase	8 P very altered	16	22	29 + 5 P very altered	21	22 + 2 P very altered	16	5 P	--	30 + 12 P very altered
Pigeonite + Augite	7 P	11 Pig >> Aug	39	36 Pig >> Aug	28 Pig >>> Aug	33 Pig ~ Aug	20 Pig >>> Aug	5 P	--	24 Pig < Aug
Opaque phases	--	--	2	< 2	< 1	< 2	--	--	--	4
Total primary minerals	**22**	**27**	**63**	**73**	**50**	**62**	**38**	**10**	**--**	**70**
Secondary in primary phases	7, green clay minerals in Opx	--	--	5, in Plag	--	2, in Plag	--	--	--	12, in Plag
Secondary in mesostasis	--	9	--	11	--	14 Chl	--	--	--	17
Secondary, hydrothermal in vesicals	7, Chl + Cc + zeolites	25, Qtz + Chl + prehnite / pumpellyite + epidote	11, amorph SiO_2 + brown / green clay minerals	11, amorph SiO_2 + zeolites + green / brown clay minerals	14, brown radiating aggregates + zeolites	8, green / brown clay minerals + zeolites	34, zeolites + brown clay minerals + Chl	19, zeolites + brown / green clay minerals + amorph SiO_2	27, zeolites + amorph SiO_2 + green / brown clay minerals	13, zeolites + Chl
Total secondary	**14**	**34**	**11**	**27**	**14**	**24**	**34**	**19**	**27**	**42**

Appendix 3a Representative electron microprobe analyses of pyroxene; ph = phenocryst, mph = micro-phenocryst or matrix, location within individual pyroxene: c = core, r = rim, where to distinguish: cc = innermost core, rr = outermost rim; end-members: En = enstatite, Fs = ferrosilite, Wo = wollastonite; - = not determined

Sample	RH6	RH6	RH6	RH6	RH6	RH6	RH6	RH6	RH6	RH6	RH6	RH6	RH6	RH6	RH6	RH6	RH6	RH6	RH21	RH21	RH21	RH21	RH21	RH21	RH21	RH21	RH21
Magma Series	HTS	HTS	HTS	HTS	HTS	HTS	HTS	HTS	HTS	HTS	HTS	HTS	HTS	HTS	HTS	HTS	HTS	HTS	LTS	LTS	LTS	LTS	LTS	LTS	LTS	LTS	LTS
No.	mph1	mph2	mph3	mh3	mph4	mph5	mph6	mph6	mph7	mph7	mph8	mph8	mph8	mph9	mph10	mph	mph	mph	ph1	ph1	ph1	ph1	ph1	ph2	ph2	ph2	ph2
Location			c	r			c	r	c	r	c	r							ccc	cc	c	r	rr	cc	c	r	rr
wt%																											
SiO$_2$	49.81	50.45	49.85	48.47	48.64	49.91	51.09	50.87	50.68	48.76	49.70	48.16	48.03	47.56	48.67	47.37	47.19	46.55	56.23	55.98	54.91	53.78	52.11	56.44	55.57	52.99	51.01
TiO$_2$	0.60	0.72	0.80	0.78	0.51	0.64	0.61	0.65	0.68	0.59	0.62	0.74	0.75	0.73	0.55	0.68	0.58	0.65	0.16	0.13	0.27	0.15	0.45	0.08	0.05	0.19	0.62
Al$_2$O$_3$	1.09	1.41	1.30	1.07	0.88	1.15	1.42	1.32	1.43	0.98	1.21	1.06	1.05	1.05	0.97	0.82	0.89	0.77	1.14	1.18	0.89	0.87	0.60	0.74	0.98	1.60	1.38
Cr$_2$O$_3$	0.03	0.01	0.02	0.00	0.01	0.02	0.00	0.02	0.00	0.03	0.02	0.00	0.00	0.00	0.00	0.03	0.00	0.01	0.15	0.11	0.08	0.07	0.00	0.10	0.11	0.18	0.00
FeO	22.33	19.12	23.06	28.60	32.22	26.66	19.71	19.68	19.33	30.42	24.78	29.82	29.96	31.53	32.16	39.47	37.68	40.55	10.74	10.50	14.61	15.81	23.25	10.36	10.46	7.08	15.39
MnO	0.48	0.40	0.46	0.60	0.65	0.48	0.41	0.44	0.37	0.57	0.50	0.54	0.52	0.64	0.71	0.72	0.72	0.78	0.26	0.25	0.35	0.35	0.45	0.25	0.25	0.19	0.31
MgO	10.22	11.65	9.94	5.72	7.62	10.88	12.79	11.96	11.38	6.43	10.44	4.79	5.09	5.37	6.67	4.17	2.27	1.64	29.68	29.97	26.96	23.34	18.53	29.75	29.62	17.87	13.26
CaO	15.08	16.14	14.82	15.10	9.93	11.02	14.77	15.79	16.67	13.10	12.80	15.29	14.76	12.46	10.88	7.15	10.90	9.07	2.40	2.57	2.31	5.38	4.13	2.29	2.41	18.94	16.80
Na$_2$O	0.15	0.17	0.16	0.10	0.06	0.07	0.14	0.15	0.15	0.12	0.14	0.14	0.15	0.10	0.11	0.03	0.09	0.07	0.01	0.02	0.04	0.03	0.06	0.03	0.01	0.18	0.15
K$_2$O	0.00	0.00	0.01	0.01	0.01	0.00	0.01	0.00	0.02	0.01	0.01	0.02	0.01	0.02	0.01	0.04	0.04	0.03	0.00	0.01	0.00	0.00	0.02	0.01	0.00	0.00	0.01
Total	99.79	100.07	100.42	100.44	100.55	100.83	100.94	100.87	100.70	101.01	100.21	100.55	100.32	99.46	100.73	100.48	100.35	100.08	100.78	100.74	100.41	99.78	99.59	100.05	99.46	99.23	98.93
Formulae based on 4 cations and 6 oxygens																											
Si	1.947	1.941	1.942	1.946	1.951	1.945	1.942	1.942	1.940	1.947	1.943	1.943	1.940	1.945	1.956	1.963	1.965	1.962	1.974	1.963	1.970	1.972	1.980	1.990	1.975	1.953	1.956
Al	0.050	0.064	0.059	0.051	0.042	0.053	0.064	0.059	0.064	0.046	0.056	0.050	0.050	0.051	0.046	0.040	0.044	0.039	0.047	0.049	0.038	0.038	0.027	0.031	0.041	0.070	0.062
Ti	0.018	0.021	0.023	0.023	0.015	0.019	0.017	0.019	0.019	0.018	0.018	0.022	0.023	0.022	0.017	0.021	0.018	0.020	0.004	0.004	0.007	0.004	0.013	0.002	0.001	0.005	0.018
Cr	0.001	0.000	0.000	0.000	0.000	0.001	0.000	0.001	0.000	0.001	0.001	0.000	0.000	0.000	0.000	0.001	0.000	0.000	0.004	0.003	0.002	0.002	0.000	0.003	0.003	0.005	0.000
Fe^{3+}	0.031	0.025	0.023	0.019	0.030	0.024	0.028	0.030	0.028	0.034	0.031	0.032	0.037	0.024	0.019	0.000	0.000	0.005	0.000	0.016	0.007	0.011	0.000	0.000	0.005	0.022	0.001
Mg	0.595	0.668	0.577	0.342	0.456	0.632	0.725	0.681	0.649	0.383	0.608	0.288	0.306	0.327	0.399	0.258	0.141	0.117	1.553	1.567	1.442	1.276	1.050	1.564	1.569	0.982	0.758
Fe^{2+}	0.699	0.590	0.729	0.941	1.051	0.845	0.599	0.598	0.591	0.982	0.779	0.974	0.975	1.054	1.062	1.368	1.312	1.406	0.315	0.292	0.431	0.473	0.739	0.306	0.306	0.196	0.492
Mn	0.016	0.013	0.015	0.020	0.022	0.016	0.013	0.014	0.012	0.019	0.017	0.018	0.018	0.022	0.024	0.025	0.025	0.028	0.008	0.008	0.010	0.011	0.015	0.007	0.008	0.006	0.010
Ca	0.632	0.665	0.619	0.649	0.427	0.460	0.602	0.646	0.684	0.560	0.536	0.661	0.639	0.546	0.468	0.317	0.486	0.415	0.090	0.097	0.089	0.211	0.168	0.087	0.092	0.748	0.690
Na	0.011	0.013	0.012	0.008	0.005	0.006	0.010	0.011	0.011	0.010	0.010	0.011	0.012	0.008	0.009	0.002	0.007	0.006	0.001	0.002	0.002	0.002	0.004	0.002	0.001	0.013	0.011
K	0.000	0.000	0.001	0.000	0.001	0.000	0.000	0.000	0.001	0.001	0.000	0.001	0.001	0.001	0.001	0.002	0.002	0.002	0.000	0.000	0.000	0.000	0.001	0.000	0.000	0.000	0.000
Sum	4.000	4.000	4.000	4.000	4.000	4.000	4.000	4.000	4.000	4.000	4.000	4.000	4.000	4.000	4.000	3.998	4.000	3.999	3.997	4.000	4.000	4.000	3.996	3.992	4.000	4.000	4.000
mol%																											
En	30.2	34.1	29.4	17.3	23.0	32.0	36.9	34.6	33.1	19.3	30.9	14.6	15.5	16.6	20.2	13.1	7.2	5.9	79.0	79.2	72.8	64.3	53.3	79.7	79.3	50.2	38.8
Fe	37.8	32.0	39.1	49.7	55.6	44.7	32.5	32.6	32.1	52.3	41.9	51.9	52.1	55.8	56.0	70.8	68.1	73.0	16.4	15.9	22.7	25.0	38.2	15.9	16.1	11.5	25.8
Wo	32.0	33.9	31.5	32.9	21.5	23.3	30.6	32.8	34.8	28.3	27.2	33.5	32.3	27.7	23.7	16.1	24.8	21.1	4.6	4.9	4.5	10.7	8.5	4.4	4.6	38.3	35.4
Mg#	44.9	52.1	43.5	26.3	29.7	42.1	53.6	52.0	51.2	27.4	42.9	22.3	23.2	23.3	27.0	15.8	9.7	54.6	83.1	83.6	76.7	72.5	58.7	83.7	83.5	81.8	60.6

Appendix 3a   (continued)

Sample	RH21	RH21	RH21	RH21	RH21	RH21	RH21	RH21	RH21	RH21	RH21	RH24	RH24	RH24	RH24	RH24	RH24	RH24	RH24	RH24	RH24	RH24	RH24	RH24	RH36	RH36	RH36
Magma Series	LTS	LTS	LTS	LTS	LTS	LTS	LTS	LTS	LTS	LTS	LTS	HTS	HTS	HTS	HTS	HTS	HTS	HTS	HTS	HTS	HTS	HTS	HTS	HTS	LTS	LTS	LTS
No.	mph1	mph2	mph3	mph2	ph3	ph3	ph3	ph4	ph4	ph4	ph4	ph1	ph1	ph2	ph2	ph3	ph3	ph3	ph3	ph4	ph4	ph4	ph4	ph5	mph	ph1	ph1
Location	c	r	c	r	c	r	rr	cc	c	r	rr	c	r	c	r	c	r	rr	rrr	c	r	rr			cc	c	r
wt%																											
SiO_2	53.83	52.14	50.92	50.85	53.65	52.67	50.21	55.88	56.17	54.14	51.86	50.01	48.80	49.34	48.08	50.17	49.81	49.40	49.18	50.77	49.61	48.62	50.84	49.65	56.20	56.14	51.55
TiO_2	0.16	0.41	0.78	0.81	0.19	0.41	0.93	0.12	0.07	0.16	0.26	0.67	0.46	0.45	0.41	0.70	0.59	0.41	0.43	0.37	0.47	0.33	0.58	0.41	0.12	0.05	0.17
Al_2O_3	1.49	1.38	1.39	1.40	1.44	1.31	1.32	1.16	0.96	1.00	0.59	1.39	0.75	0.75	0.57	1.45	1.20	0.80	0.74	0.68	0.73	0.56	1.40	0.71	1.01	0.82	1.28
Cr_2O_3	0.08	0.05	0.02	0.03	0.10	0.02	0.04	0.10	0.10	0.11	0.02	0.00	0.00	0.05	0.00	0.00	0.00	0.05	0.01	0.00	0.00	0.00	0.00	0.02	0.06	0.06	0.05
FeO	6.99	13.29	15.61	15.99	7.41	11.94	18.98	11.07	11.85	16.47	25.51	19.97	33.35	31.34	37.25	19.48	23.56	26.38	35.85	29.04	31.54	36.53	18.80	34.92	11.28	11.44	26.10
MnO	0.20	0.32	0.32	0.35	0.23	0.29	0.39	0.26	0.28	0.33	0.56	0.43	0.69	0.61	0.78	0.40	0.48	0.47	0.70	0.58	0.65	0.69	0.44	0.70	0.27	0.27	0.48
MgO	18.69	15.09	13.01	12.86	17.83	15.51	11.25	28.94	28.79	25.25	17.58	10.66	8.48	11.61	8.29	11.28	9.08	5.63	7.68	15.01	11.59	7.79	10.60	10.11	29.27	29.37	17.79
CaO	18.35	17.36	17.39	16.78	18.54	17.36	16.44	2.40	2.35	2.26	4.01	16.00	7.20	5.21	3.84	16.28	15.39	17.18	6.56	3.73	5.01	5.38	17.01	5.19	2.40	2.37	2.32
Na_2O	0.15	0.15	0.18	0.21	0.12	0.13	0.17	0.02	0.02	0.00	0.05	0.17	0.08	0.07	0.00	0.12	0.17	0.22	0.04	0.04	0.04	0.08	0.18	0.04	0.02	0.05	0.00
K_2O	0.01	0.00	0.01	0.00	0.00	0.00	0.01	0.00	0.01	0.00	0.00	0.00	0.00	0.02	0.01	0.02	0.01	0.04	0.01	0.01	0.01	0.00	0.00	0.01	0.02	0.00	0.02
Total	99.95	100.19	99.63	99.27	99.50	99.64	99.75	99.95	100.59	99.71	100.45	99.29	99.80	99.44	99.22	99.89	100.28	100.57	101.20	100.23	99.65	99.99	99.85	101.75	100.65	100.58	99.76
Formulae based on 4 cations and 6 oxygens																											
Si	1.964	1.951	1.942	1.949	1.973	1.971	1.942	1.980	1.984	1.974	1.972	1.950	1.971	1.966	1.975	1.938	1.951	1.968	1.975	1.970	1.973	1.980	1.964	1.960	1.980	1.980	1.971
Al	0.064	0.061	0.062	0.063	0.062	0.058	0.060	0.048	0.040	0.043	0.026	0.064	0.036	0.035	0.027	0.066	0.055	0.038	0.035	0.031	0.034	0.027	0.064	0.033	0.042	0.034	0.058
Ti	0.004	0.011	0.022	0.023	0.005	0.011	0.027	0.003	0.002	0.004	0.007	0.020	0.014	0.014	0.013	0.020	0.017	0.012	0.013	0.011	0.014	0.010	0.017	0.012	0.003	0.001	0.005
Cr	0.002	0.002	0.001	0.001	0.003	0.001	0.001	0.003	0.003	0.003	0.001	0.000	0.000	0.001	0.000	0.000	0.000	0.001	0.000	0.000	0.000	0.000	0.001	0.002	0.002	0.001
Fe^{3+}	0.007	0.023	0.022	0.006	0.000	0.000	0.014	0.000	0.000	0.000	0.017	0.009	0.000	0.009	0.000	0.027	0.022	0.020	0.000	0.012	0.000	0.000	0.000	0.026	0.000	0.004	0.000
Mg	1.017	0.842	0.740	0.735	0.977	0.865	0.649	1.529	1.516	1.373	0.997	0.620	0.511	0.690	0.508	0.650	0.530	0.334	0.460	0.868	0.687	0.473	0.610	0.595	1.537	1.544	1.014
Fe^{2+}	0.206	0.393	0.476	0.507	0.228	0.374	0.600	0.328	0.350	0.502	0.794	0.642	1.127	1.035	1.280	0.602	0.750	0.859	1.204	0.931	1.049	1.244	0.607	1.127	0.332	0.333	0.835
Mn	0.006	0.010	0.010	0.011	0.007	0.009	0.013	0.008	0.008	0.010	0.018	0.014	0.024	0.021	0.027	0.013	0.016	0.016	0.024	0.019	0.022	0.024	0.014	0.023	0.008	0.008	0.015
Ca	0.717	0.696	0.711	0.689	0.730	0.696	0.681	0.091	0.089	0.088	0.163	0.669	0.312	0.222	0.169	0.674	0.646	0.733	0.282	0.155	0.214	0.235	0.704	0.220	0.091	0.090	0.095
Na	0.011	0.011	0.013	0.015	0.008	0.009	0.013	0.001	0.001	0.000	0.004	0.013	0.006	0.005	0.000	0.009	0.013	0.017	0.003	0.003	0.003	0.006	0.014	0.003	0.001	0.003	0.000
K	0.000	0.000	0.001	0.000	0.000	0.000	0.000	0.000	0.000	0.000	0.000	0.000	0.000	0.001	0.000	0.001	0.000	0.002	0.000	0.001	0.001	0.000	0.000	0.001	0.001	0.000	0.001
Sum	4.000	4.000	4.000	4.000	3.994	3.993	4.000	3.992	3.994	3.998	4.000	4.000	4.000	4.000	3.999	4.000	4.000	4.000	3.996	4.000	3.997	3.999	3.994	4.000	3.997	4.000	3.995
mol%																											
En	52.0	42.9	37.8	37.7	50.3	44.5	33.2	78.2	77.2	69.6	50.1	31.7	25.9	34.9	25.6	33.0	27.0	17.0	23.3	43.7	34.9	23.9	31.5	29.9	78.1	78.0	51.8
Fe	11.2	21.7	25.9	26.9	12.1	19.7	32.0	17.2	18.3	26.0	41.7	34.1	58.3	53.9	65.9	32.7	40.1	45.6	62.3	48.4	54.3	64.2	32.1	59.1	17.3	17.5	43.4
Wo	36.7	35.4	36.3	35.4	37.6	35.8	34.8	4.7	4.5	4.5	8.2	34.2	15.8	11.3	8.5	34.3	32.9	37.4	14.3	7.8	10.8	11.9	36.4	11.0	4.6	4.5	4.9
Mg#	82.7	66.9	59.8	58.9	81.1	69.8	51.4	82.3	81.2	73.2	55.1	48.8	31.2	39.8	28.4	50.8	40.7	27.6	27.6	48.0	39.6	27.5	50.1	34.0	82.2	82.1	54.9

Appendix 3a   (continued)

Sample	RH36	RH36	RH36	RH36	RH36	RH36	RH36	RH36	RH36	RH36	RH44	RH44	RH44	RH44	RH44	RH44	RH44	RH44	RH44	RH44	RH45	RH45	RH45	RH45	RH45	RH45	RH45
Magma Series	LTS	LTS	LTS	LTS	LTS	LTS	LTS	LTS	LTS	LTS	LTS	LTS	LTS	LTS	LTS	LTS	LTS	LTS	LTS	LTS	LTS	LTS	LTS	LTS	LTS	LTS	LTS
No.	mph1	mph2	ph2	ph2	ph2	mph3	ph3	ph3	mph4	ph4	ph1	ph1	ph1	ph2	ph2	ph3	ph4	ph4	ph5	ph5	ph1	ph1	ph1	ph2	ph2	ph3	mph1
Location	c	r	cc	c	rr		cc	c			c	r	rr	c	r	c	c	r	c	r	rr	c	r	c		c	c
wt%																											
SiO$_2$	53.18	52.01	55.93	56.58	53.34	52.22	56.38	56.28	54.05	55.77	53.83	51.76	48.36	52.75	53.15	52.45	51.07	49.59	54.17	49.78	49.54	48.79	48.61	50.16	49.08	50.78	49.12
TiO$_2$	0.31	0.30	0.06	0.12	0.22	0.42	0.08	0.05	0.26	0.08	0.17	0.27	0.72	0.24	0.38	0.36	0.49	0.60	0.20	0.59	0.39	0.44	0.59	0.43	0.31	0.49	0.39
Al$_2$O$_3$	2.47	1.86	1.20	0.85	2.01	2.15	0.95	1.11	2.30	0.74	0.75	0.84	0.90	1.32	1.37	1.26	1.25	1.03	0.77	1.07	0.62	0.82	1.16	0.57	0.60	1.52	0.59
Cr$_2$O$_3$	0.06	0.00	0.17	0.11	0.03	0.01	0.15	0.12	0.22	0.04	0.07	0.01	0.00	0.01	0.06	0.03	0.04	0.00	0.05	0.02	0.00	0.00	0.00	0.00	0.02	0.04	0.01
FeO	8.94	12.33	9.90	11.13	10.06	12.04	9.96	10.45	8.36	11.67	18.36	25.07	30.41	11.06	11.00	12.07	16.14	26.50	18.82	26.75	33.20	31.63	22.92	31.49	32.98	15.89	34.60
MnO	0.24	0.29	0.21	0.24	0.26	0.27	0.22	0.24	0.24	0.27	0.45	0.49	0.63	0.32	0.28	0.27	0.40	0.54	0.45	0.59	0.67	0.64	0.58	0.71	0.69	0.37	0.72
MgO	18.61	13.50	29.82	29.57	18.65	16.28	30.03	29.92	21.22	29.21	21.73	16.17	7.00	16.10	15.90	15.76	12.88	8.47	21.96	9.66	11.41	9.29	6.67	12.90	11.13	12.86	10.02
CaO	16.41	19.08	2.37	2.41	15.26	16.61	2.38	2.42	13.24	2.39	4.82	5.71	11.92	17.95	17.72	17.20	16.58	13.64	4.39	11.33	4.06	7.33	17.63	3.75	4.10	17.36	4.13
Na$_2$O	0.14	0.19	0.01	0.00	0.12	0.13	0.03	0.03	0.12	0.01	0.05	0.05	0.07	0.12	0.13	0.14	0.13	0.10	0.04	0.11	0.05	0.08	0.26	0.03	0.08	0.15	0.06
K$_2$O	0.01	0.01	0.00	0.01	0.00	0.01	0.01	0.00	0.00	0.00	0.00	0.00	0.00	0.00	0.00	0.00	0.00	0.02	0.00	0.02	0.01	0.00	0.01	0.01	0.00	0.02	0.00
Total	100.36	99.56	99.67	101.01	99.94	100.13	100.19	100.62	100.01	100.18	100.23	100.38	100.02	99.87	99.99	99.52	98.97	100.49	100.84	99.92	99.95	99.02	98.42	100.04	98.99	99.47	99.63
Formulae based on 4 cations and 6 oxygens																											
Si	1.940	1.962	1.977	1.984	1.958	1.940	1.983	1.976	1.954	1.977	1.986	1.977	1.948	1.963	1.973	1.966	1.963	1.958	1.986	1.966	1.974	1.972	1.956	1.978	1.976	1.941	1.980
Al	0.106	0.083	0.050	0.035	0.087	0.094	0.039	0.046	0.098	0.031	0.033	0.038	0.043	0.058	0.060	0.055	0.057	0.048	0.033	0.050	0.029	0.039	0.055	0.026	0.029	0.069	0.028
Ti	0.008	0.008	0.002	0.003	0.006	0.012	0.002	0.001	0.007	0.002	0.005	0.008	0.022	0.007	0.011	0.010	0.014	0.018	0.006	0.018	0.012	0.013	0.018	0.013	0.009	0.014	0.012
Cr	0.002	0.000	0.005	0.003	0.001	0.000	0.004	0.003	0.006	0.001	0.002	0.000	0.000	0.000	0.002	0.001	0.001	0.000	0.001	0.001	0.000	0.000	0.000	0.000	0.000	0.001	0.000
Fe^{3+}	0.006	0.000	0.000	0.000	0.000	0.012	0.000	0.000	0.000	0.011	0.000	0.000	0.023	0.011	0.000	0.002	0.000	0.010	0.000	0.000	0.003	0.000	0.018	0.000	0.006	0.032	0.000
Mg	1.012	0.759	1.572	1.545	1.020	0.901	1.574	1.566	1.144	1.544	1.195	0.921	0.420	0.893	0.880	0.881	0.738	0.498	1.200	0.569	0.678	0.560	0.400	0.758	0.668	0.733	0.602
Fe^{2+}	0.267	0.389	0.293	0.326	0.309	0.362	0.293	0.307	0.253	0.334	0.566	0.801	1.002	0.333	0.342	0.377	0.519	0.865	0.577	0.884	1.103	1.069	0.753	1.038	1.105	0.476	1.166
Mn	0.007	0.009	0.006	0.007	0.008	0.008	0.006	0.007	0.007	0.008	0.014	0.016	0.022	0.010	0.009	0.008	0.013	0.018	0.014	0.020	0.023	0.022	0.020	0.024	0.023	0.012	0.025
Ca	0.641	0.771	0.090	0.091	0.600	0.661	0.090	0.091	0.513	0.091	0.190	0.234	0.515	0.716	0.705	0.691	0.683	0.577	0.172	0.480	0.173	0.317	0.760	0.158	0.177	0.711	0.178
Na	0.010	0.014	0.001	0.000	0.008	0.009	0.002	0.002	0.008	0.001	0.004	0.004	0.006	0.009	0.009	0.010	0.010	0.008	0.003	0.008	0.004	0.006	0.020	0.002	0.006	0.011	0.005
K	0.000	0.001	0.000	0.001	0.000	0.000	0.000	0.000	0.000	0.000	0.000	0.000	0.000	0.000	0.000	0.000	0.000	0.001	0.000	0.001	0.001	0.000	0.000	0.000	0.000	0.001	0.000
Sum	4.000	3.996	3.994	3.995	3.997	4.000	3.994	3.999	3.991	4.000	3.994	3.998	4.000	4.000	3.990	4.000	3.998	4.000	3.992	3.995	4.000	3.998	4.000	3.998	4.000	4.000	3.996
mol%																											
En	52.3	39.4	80.2	78.5	52.7	46.3	80.2	79.4	59.7	77.6	60.8	46.7	21.2	45.5	45.5	45.0	37.8	25.3	61.1	29.1	34.2	28.4	20.5	38.3	33.8	37.3	30.5
Fe	14.5	20.6	15.3	16.9	16.4	19.7	15.2	15.9	13.6	17.8	29.5	41.4	52.8	18.0	18.1	19.8	27.2	45.4	30.1	46.3	57.0	55.4	40.5	53.7	57.3	26.5	60.4
Wo	33.2	40.0	4.6	4.6	31.0	34.0	4.6	4.6	26.8	4.6	9.7	11.9	26.0	36.5	36.4	35.3	35.0	29.3	8.8	24.6	8.8	16.1	39.0	8.0	8.9	36.2	9.0
Mg#	78.8	66.1	84.3	82.6	76.8	70.7	84.3	83.6	81.9	81.7	67.8	53.5	29.1	72.2	72.0	69.9	58.7	36.3	67.5	39.2	38.0	34.4	34.2	42.2	37.6	59.1	34.0

Appendix 3a   (continued)

Sample	RH45	RH45	RH45	RH45	RH45	RH45	RH45	RH45	RH53	RH53	RH53	RH53	RH53	RH53	RH53	RH53	RH53	RH53	RH54a	RH54a	RH54a	RH54a	RH54a	RH54a	RH54a	RH54a	RH54a
Magma Series	LTS	LTS	LTS	LTS	LTS	LTS	LTS	LTS	LTS	LTS	LTS	LTS	LTS	LTS	LTS	LTS	LTS	LTS	LTS	LTS	LTS	LTS	LTS	LTS	LTS	LTS	LTS
No.	mph1	mph2	mph2	ph4	ph4	mph3	mph4	mph4	ph1	ph1	ph2	ph2	ph2	ph3	ph3	ph5	ph5	ph4	ph1	ph1	ph2	ph2	ph3	ph3	ph4	ph4	ph5
Location	r	c	r	c	r		c	r	c	r	c	cc	rr	c	r	cc	c	rr	cc	c	cc	c	c	r	c	r	cc
wt%																											
SiO_2	49.05	50.19	49.15	52.53	49.49	48.60	50.54	49.69	54.15	51.79	53.95	54.21	50.91	53.92	51.26	53.68	53.91	49.88	56.04	55.94	55.44	55.66	55.80	53.63	55.50	53.02	55.57
TiO_2	0.72	0.37	0.30	0.20	0.34	0.51	0.34	0.75	0.08	0.16	0.13	0.16	0.30	0.17	0.38	0.10	0.10	0.58	0.02	0.04	0.12	0.07	0.09	0.14	0.16	0.30	0.15
Al_2O_3	1.37	0.64	0.63	0.77	0.54	0.59	0.70	1.68	0.76	0.48	0.82	0.69	0.62	0.62	0.64	0.75	0.78	0.75	0.89	1.34	1.29	1.05	0.92	0.57	1.63	1.92	1.34
Cr_2O_3	0.00	0.02	0.04	0.04	0.01	-	-	-	0.08	0.04	0.12	0.07	0.04	0.07	0.03	0.07	0.05	0.00	0.17	0.23	0.24	0.18	0.19	0.00	0.34	0.11	0.29
FeO	24.43	30.20	33.58	19.97	31.79	38.65	32.00	23.47	14.58	26.83	13.61	14.44	24.86	15.49	26.83	14.30	15.24	25.37	9.81	9.92	9.88	10.24	9.84	17.65	9.57	8.82	9.67
MnO	0.54	0.63	0.67	0.43	0.68	0.59	0.51	0.34	0.34	0.54	0.33	0.39	0.51	0.38	0.57	0.37	0.38	0.57	0.26	0.22	0.26	0.23	0.23	0.41	0.25	0.26	0.22
MgO	9.64	14.22	11.51	20.78	12.72	7.59	13.44	8.95	24.51	18.69	25.59	26.24	17.44	25.79	16.19	26.05	25.24	15.13	30.58	30.42	30.30	30.09	30.51	22.37	30.68	20.82	30.79
CaO	13.56	3.53	3.89	4.93	3.82	4.87	3.81	16.30	5.17	1.27	4.33	3.03	4.05	2.71	4.10	3.34	3.77	5.77	2.18	2.16	2.19	2.21	2.19	5.30	2.09	13.62	2.07
Na_2O	0.11	0.01	0.03	0.03	0.03	-	-	-	0.06	0.03	0.04	0.03	0.06	0.05	0.04	0.03	0.05	0.09	0.02	0.03	0.01	0.04	0.04	0.00	0.05	0.10	0.06
K_2O	0.01	0.00	0.01	0.01	0.02	-	-	-	0.00	0.01	0.00	0.00	0.00	0.00	0.00	0.01	0.01	0.02	0.00	0.00	0.01	0.01	0.00	0.00	0.01	0.00	0.00
Total	99.43	99.81	99.81	99.69	99.43	101.40	101.35	101.18	99.72	99.84	98.93	99.26	98.79	99.19	100.04	98.70	99.53	98.16	99.97	100.29	99.73	99.80	99.79	100.08	100.28	98.97	100.15
Formulae based on 4 cations and 6 oxygens																											
Si	1.938	1.968	1.962	1.964	1.966	1.963	1.964	1.931	1.972	1.979	1.968	1.971	1.966	1.969	1.974	1.962	1.964	1.959	1.973	1.964	1.958	1.967	1.968	1.976	1.945	1.945	1.950
Al	0.064	0.030	0.030	0.034	0.025	0.028	0.032	0.077	0.033	0.022	0.035	0.030	0.028	0.027	0.029	0.032	0.033	0.035	0.037	0.056	0.054	0.044	0.038	0.025	0.067	0.083	0.055
Ti	0.021	0.011	0.009	0.005	0.010	0.015	0.010	0.022	0.002	0.005	0.004	0.004	0.009	0.005	0.011	0.003	0.003	0.017	0.001	0.001	0.003	0.002	0.002	0.004	0.004	0.008	0.004
Cr	0.000	0.001	0.001	0.001	0.000	-	0.000	0.000	0.002	0.001	0.004	0.002	0.001	0.002	0.001	0.002	0.002	0.000	0.005	0.006	0.007	0.005	0.005	0.000	0.010	0.003	0.008
Fe^{3+}	0.026	0.013	0.029	0.029	0.024	0.015	0.020	0.018	0.021	0.013	0.021	0.021	0.026	0.027	0.002	0.039	0.035	0.021	0.013	0.011	0.018	0.017	0.019	0.015	0.027	0.013	0.033
Mg	0.568	0.831	0.685	1.158	0.753	0.457	0.779	0.518	1.331	1.065	1.392	1.422	1.004	1.404	0.930	1.419	1.371	0.886	1.605	1.592	1.595	1.585	1.604	1.229	1.603	1.139	1.611
Fe^{2+}	0.781	0.977	1.092	0.595	1.032	1.291	1.020	0.744	0.423	0.844	0.394	0.418	0.777	0.446	0.862	0.398	0.429	0.812	0.276	0.280	0.273	0.286	0.271	0.529	0.253	0.257	0.251
Mn	0.018	0.021	0.023	0.014	0.023	0.020	0.017	0.011	0.011	0.018	0.010	0.012	0.017	0.012	0.019	0.011	0.012	0.019	0.008	0.006	0.008	0.007	0.007	0.013	0.007	0.008	0.007
Ca	0.574	0.148	0.166	0.197	0.163	0.211	0.159	0.679	0.202	0.052	0.169	0.118	0.168	0.106	0.169	0.131	0.147	0.243	0.082	0.081	0.083	0.084	0.083	0.209	0.078	0.535	0.078
Na	0.009	0.001	0.002	0.002	0.002	-	0.000	0.000	0.004	0.002	0.003	0.002	0.005	0.003	0.003	0.002	0.003	0.007	0.001	0.002	0.001	0.003	0.003	0.000	0.003	0.007	0.004
K	0.001	0.000	0.000	0.000	0.001	-	0.000	0.000	0.000	0.000	0.000	0.000	0.000	0.000	0.000	0.000	0.000	0.001	0.000	0.000	0.000	0.001	0.000	0.000	0.000	0.000	0.000
Sum	4.000	4.000	4.000	4.000	4.000	4.000	4.000	4.000	4.000	4.000	4.000	4.000	4.000	4.000	4.000	4.000	4.000	4.000	4.000	4.000	4.000	4.000	4.000	4.000	4.000	4.000	4.000
mol%																											
En	28.9	41.8	34.3	58.1	37.8	22.9	39.0	26.3	67.0	53.5	70.1	71.4	50.4	70.4	46.9	71.0	68.7	44.7	80.9	80.8	80.7	80.1	80.9	61.6	81.4	58.3	81.4
Fe	42.0	50.8	57.3	32.0	54.1	66.5	53.0	39.3	22.9	43.9	21.4	22.6	41.2	24.3	44.6	22.4	23.9	43.0	15.0	15.1	15.1	15.6	15.0	27.9	14.6	14.3	14.7
Wo	29.2	7.4	8.3	9.9	8.2	10.6	8.0	34.4	10.2	2.6	8.5	5.9	8.4	5.3	8.5	6.5	7.4	12.3	4.1	4.1	4.2	4.2	4.2	10.5	4.0	27.4	3.9
Mg#	41.3	45.6	37.9	65.0	41.6	25.9	42.8	40.5	75.0	55.4	77.0	76.4	55.6	74.8	51.8	76.5	74.7	51.5	84.7	84.5	84.5	84.0	84.7	69.3	85.1	80.8	85.0

Appendix 3a   (continued)

Sample	RH54a	RH54a	RH54a	RH54a	RH54a	NWR26	NWR26	NWR26	NWR26	NWR26	NWR26	NWR26	NWR26	NWR26	NWR26	NWR26	NWR26	NWR26	NWR26	NWR29	NWR29	NWR29
Magma Series	LTS	LTS	LTS	LTS	LTS	LTS	LTS	LTS	LTS	LTS	LTS	LTS	LTS	LTS	LTS	LTS	LTS	LTS	LTS	LTS	LTS	LTS
No.	ph5	ph5	mph1	mph2	mph2	ph1	ph1	mph1	mph1	mph1	ph2	ph2	ph2	mph2	ph3	ph3	ph3	ph3	ph3	ph1	ph1	ph1
Location	c	r		c	r	c	r	c	r	rr	c	r	rr		cc	c	cr	r	rr	c	r	rr
wt%																						
SiO_2	55.51	51.56	52.08	53.06	49.56	53.98	48.96	49.98	48.95	48.21	53.57	52.52	49.53	48.42	52.50	52.20	51.33	50.66	49.39	52.69	52.68	52.49
TiO_2	0.11	0.25	0.42	0.21	0.58	0.15	0.37	0.74	0.60	0.53	0.13	0.18	0.60	0.65	0.29	0.31	0.38	0.46	0.65	0.24	0.28	0.32
Al_2O_3	1.33	0.86	2.38	2.20	2.26	0.69	0.63	1.36	1.05	0.82	0.70	0.70	1.07	1.04	1.35	1.15	1.17	1.19	0.98	1.32	1.28	1.27
Cr_2O_3	0.22	0.01	0.00	0.24	0.03	0.03	0.01	0.00	0.01	0.00	0.02	0.00	0.02	0.00	0.01	0.01	0.00	0.03	0.00	0.03	0.03	0.00
FeO	10.07	23.01	11.26	8.94	19.53	17.91	33.13	21.02	25.76	30.17	17.10	22.77	24.15	29.92	10.50	16.23	17.74	20.02	27.62	11.54	11.93	12.92
MnO	0.20	0.51	0.28	0.24	0.39	0.44	0.78	0.41	0.49	0.64	0.44	0.49	0.54	0.64	0.32	0.42	0.00	0.00	0.01	0.30	0.31	0.32
MgO	30.17	18.50	15.87	21.79	11.96	23.74	10.38	10.68	8.46	6.15	24.32	19.92	9.67	8.77	16.60	15.44	14.24	12.82	8.76	15.67	15.26	15.70
CaO	2.21	4.68	17.12	12.41	14.54	3.06	4.92	15.63	13.83	12.37	3.02	3.52	13.95	9.42	17.58	14.11	13.91	13.70	12.20	17.98	18.37	17.14
Na_2O	0.02	0.00	0.13	0.09	0.10	0.00	0.02	0.17	0.12	0.13	0.00	0.02	0.12	0.07	0.11	0.11	0.14	0.13	0.09	0.14	0.13	0.11
K_2O	0.00	0.03	0.01	0.03	0.01	0.00	0.01	0.00	0.01	0.00	0.00	0.01	0.00	0.00	0.01	0.01	0.01	0.01	0.00	0.01	0.00	0.00
Total	99.84	99.40	99.55	99.20	98.96	100.00	99.21	99.98	99.29	99.02	99.30	100.13	99.65	98.94	99.26	99.99	98.92	99.01	99.69	99.92	100.26	100.27
Formulae based on 4 cations and 6 oxygens																						
Si	1.960	1.963	1.943	1.935	1.925	1.981	1.975	1.940	1.952	1.967	1.972	1.973	1.952	1.956	1.960	1.968	1.969	1.963	1.965	1.965	1.963	1.957
Al	0.055	0.039	0.105	0.095	0.103	0.030	0.030	0.062	0.050	0.039	0.030	0.031	0.050	0.050	0.059	0.051	0.053	0.054	0.046	0.058	0.056	0.056
Ti	0.003	0.007	0.012	0.006	0.017	0.004	0.011	0.022	0.018	0.016	0.004	0.005	0.018	0.020	0.008	0.009	0.011	0.013	0.020	0.007	0.008	0.009
Cr	0.006	0.000	0.000	0.007	0.001	0.001	0.000	0.000	0.000	0.000	0.001	0.000	0.001	0.000	0.000	0.000	0.000	0.001	0.000	0.001	0.001	0.000
Fe^{3+}	0.015	0.022	0.000	0.024	0.019	0.000	0.000	0.028	0.018	0.003	0.018	0.014	0.019	0.003	0.013	0.003	0.000	0.002	0.000	0.009	0.011	0.019
Mg	1.588	1.050	0.883	1.185	0.693	1.299	0.624	0.618	0.503	0.374	1.335	1.116	0.568	0.528	0.924	0.868	0.814	0.741	0.520	0.871	0.848	0.873
Fe^{2+}	0.283	0.711	0.351	0.248	0.615	0.550	1.118	0.654	0.841	1.027	0.508	0.701	0.777	1.008	0.314	0.508	0.569	0.647	0.919	0.351	0.361	0.384
Mn	0.006	0.016	0.009	0.007	0.013	0.014	0.027	0.013	0.017	0.022	0.014	0.016	0.018	0.022	0.010	0.013	0.000	0.000	0.000	0.009	0.010	0.010
Ca	0.084	0.191	0.685	0.485	0.605	0.120	0.213	0.650	0.591	0.541	0.119	0.142	0.589	0.408	0.703	0.570	0.572	0.569	0.520	0.718	0.734	0.685
Na	0.001	0.000	0.010	0.006	0.008	0.000	0.002	0.013	0.009	0.010	0.000	0.002	0.009	0.005	0.008	0.008	0.010	0.009	0.007	0.010	0.009	0.008
K	0.000	0.001	0.000	0.001	0.000	0.000	0.001	0.000	0.001	0.000	0.000	0.000	0.000	0.000	0.000	0.001	0.001	0.000	0.000	0.000	0.000	0.000
Sum	4.000	4.000	3.998	4.000	4.000	3.999	4.000	4.000	4.000	4.000	4.000	4.000	4.000	4.000	4.000	4.000	3.999	4.000	3.996	4.000	4.000	4.000
mol%																						
En	80.4	52.8	45.8	60.8	35.6	65.5	31.5	31.5	25.5	19.0	66.9	56.1	28.8	26.8	47.0	44.2	41.7	37.8	26.5	44.5	43.2	44.3
Fe	15.4	37.6	18.7	14.4	33.3	28.4	57.8	35.4	44.5	53.5	27.1	36.8	41.3	52.5	17.2	26.8	29.1	33.1	46.9	18.8	19.4	21.0
Wo	4.2	9.6	35.5	24.9	31.1	6.1	10.7	33.1	30.0	27.5	6.0	7.1	29.9	20.7	35.8	29.0	29.2	29.0	26.5	36.7	37.4	34.8
Mg#	84.2	58.9	71.5	81.3	52.2	70.3	35.8	47.5	36.9	26.7	71.7	60.9	41.6	34.3	73.8	62.9	58.9	53.3	36.1	70.8	69.5	68.4

Appendix 3b Representative electron microprobe analyses of plagioclase; ph = phenocryst, mph = micro-phenocryst or matrix, location within individual plagioclase: c = core, r = rim, where possible to distinguish: cc = innermost core, rr = outermost rim; end-members: An = anorthite, Ab = albite, Or = orthoclase; - = not determined

Sample	RH6	RH6	RH6	RH6	RH6	RH6	RH6	RH6	RH6	RH6	RH6	RH6	RH21	RH21	RH21	RH21	RH21	RH21	RH21	RH21	RH21	RH21	RH21	RH21	RH21	RH21
Magma Series	HTS	HTS	HTS	HTS	HTS	HTS	HTS	HTS	HTS	HTS	HTS	HTS	LTS	LTS	LTS	LTS	LTS	LTS	LTS	LTS	LTS	LTS	LTS	LTS	LTS	LTS
No.	mph1	mph1	mph2	mph2	mph3	mph3	mph4	mph5	mph6	mph6	mph8	mph9	ph1	ph1	mph1	mph1	ph2	ph3	ph4	ph4	ph5	ph5	ph6	ph6	ph6	ph7
Location	c	r	c	r	c	r	c	c	c	r	c	c	cc	c	cc	c	c	c	c	r	c	r	c	r	rr	cc
wt%																										
SiO_2	54.15	56.75	55.14	57.82	54.39	57.96	54.18	54.22	54.60	56.27	55.83	55.26	47.94	48.49	52.84	52.91	47.90	47.28	48.06	50.95	48.30	54.67	47.66	49.93	50.29	48.29
TiO_2	0.06	0.04	0.05	0.06	0.07	0.06	0.05	0.05	0.06	0.06	0.06	0.06	-	-	-	-	-	-	-	-	-	-	-	-	-	-
Al_2O_3	28.18	26.53	27.58	26.15	28.08	26.16	27.40	27.87	27.04	26.01	27.37	26.84	32.46	32.32	29.24	28.86	32.42	32.65	32.52	30.32	32.29	28.14	32.53	30.74	30.49	32.18
FeO	0.95	0.90	0.88	0.88	0.97	0.77	0.75	0.85	1.75	2.61	0.85	2.16	0.64	0.64	0.69	0.62	0.57	0.60	0.51	0.73	0.65	0.76	0.58	0.64	0.73	0.54
MnO	0.00	0.00	0.01	0.00	0.00	0.00	0.00	0.01	0.02	0.02	0.00	0.00	-	-	-	-	-	-	-	-	-	-	-	-	-	-
BaO	0.00	0.01	0.00	0.07	0.00	0.01	0.00	0.04	0.00	0.03	0.00	0.01	0.03	0.07	0.06	0.01	0.00	0.00	0.00	0.00	0.00	0.00	0.03	0.02	0.00	0.05
SrO	0.00	0.02	0.00	0.00	0.00	0.00	0.00	0.00	0.00	0.00	0.00	0.00	0.16	0.15	0.18	0.13	0.15	0.13	0.15	0.17	0.17	0.16	0.16	0.12	0.11	0.12
CaO	12.30	10.16	11.79	9.53	12.68	9.54	11.68	12.12	11.01	9.55	11.15	10.77	16.70	16.54	12.99	12.99	16.78	17.16	16.80	14.46	16.59	11.73	17.05	15.48	14.88	16.57
Na_2O	4.40	5.51	4.68	5.87	4.49	5.92	4.66	4.47	4.76	5.32	5.17	4.88	1.94	2.17	4.12	4.17	1.94	1.76	1.98	3.21	2.12	4.86	1.88	2.74	3.08	2.16
K_2O	0.30	0.46	0.32	0.52	0.34	0.52	0.35	0.32	0.31	0.38	0.46	0.30	0.08	0.08	0.20	0.24	0.09	0.05	0.08	0.18	0.09	0.31	0.07	0.14	0.14	0.10
Total	100.34	100.38	100.46	100.90	101.02	100.94	99.06	99.95	99.55	100.25	100.88	100.28	99.95	100.45	100.32	99.93	99.84	99.63	100.09	100.01	100.20	100.63	99.96	99.81	99.72	100.00
Formulae based on 5 cations and 8 oxygens																										
Si	2.452	2.554	2.489	2.585	2.452	2.588	2.480	2.464	2.493	2.551	2.508	2.507	2.208	2.221	2.400	2.411	2.208	2.187	2.208	2.330	2.218	2.467	2.197	2.294	2.310	2.221
Ti	0.002	0.001	0.002	0.002	0.002	0.002	0.002	0.002	0.002	0.002	0.002	0.002	-	-	-	-	-	-	-	-	-	-	-	-	-	-
Al	1.504	1.407	1.467	1.378	1.492	1.376	1.478	1.493	1.455	1.390	1.449	1.435	1.762	1.745	1.565	1.550	1.761	1.780	1.761	1.634	1.748	1.497	1.767	1.664	1.650	1.745
Fe^{2+}	0.036	0.034	0.033	0.033	0.036	0.029	0.029	0.032	0.067	0.099	0.032	0.082	0.024	0.024	0.026	0.024	0.022	0.023	0.020	0.028	0.025	0.029	0.023	0.024	0.028	0.021
Mn	0.000	0.000	0.000	0.000	0.000	0.000	0.000	0.000	0.001	0.001	0.000	0.000	-	-	-	-	-	-	-	-	-	-	-	-	-	-
Ba	0.000	0.000	0.000	0.001	0.000	0.000	0.000	0.000	0.000	0.000	0.000	0.000	0.001	0.001	0.001	0.000	0.000	0.000	0.000	0.000	0.000	0.000	0.001	0.000	0.000	0.001
Sr	0.000	0.001	0.000	0.000	0.000	0.000	0.000	0.000	0.000	0.000	0.000	0.000	0.004	0.004	0.005	0.004	0.004	0.003	0.004	0.005	0.004	0.004	0.004	0.003	0.003	0.003
Ca	0.597	0.490	0.570	0.456	0.612	0.456	0.573	0.590	0.539	0.464	0.537	0.524	0.824	0.812	0.632	0.634	0.829	0.850	0.827	0.709	0.816	0.567	0.842	0.762	0.732	0.817
Na	0.386	0.481	0.410	0.509	0.392	0.512	0.414	0.394	0.421	0.468	0.450	0.429	0.173	0.193	0.363	0.368	0.173	0.158	0.176	0.285	0.189	0.425	0.168	0.244	0.274	0.193
K	0.018	0.026	0.019	0.029	0.020	0.030	0.021	0.018	0.018	0.022	0.026	0.017	0.005	0.005	0.012	0.014	0.005	0.003	0.005	0.010	0.005	0.018	0.004	0.008	0.008	0.006
Sum	4.995	4.995	4.990	4.993	5.006	4.993	4.996	4.994	4.996	4.997	5.004	4.997	5.001	5.005	5.004	5.005	5.001	5.004	5.001	5.000	5.005	5.006	5.005	5.000	5.006	5.006
mol%																										
An	59.6	49.1	57.1	45.9	59.8	45.7	56.9	58.9	55.1	48.7	53.0	54.0	82.2	80.4	62.8	62.4	82.3	84.1	82.0	70.6	80.8	56.2	83.1	75.1	72.1	80.4
Ab	38.6	48.2	41.0	51.2	38.3	51.3	41.1	39.3	43.1	49.0	44.4	44.2	17.3	19.1	36.0	36.2	17.2	15.6	17.5	28.4	18.7	42.1	16.6	24.1	27.0	19.0
Or	1.8	2.6	1.9	3.0	1.9	3.0	2.0	1.8	1.8	2.3	2.6	1.8	0.5	0.5	1.2	1.4	0.5	0.3	0.5	1.0	0.5	1.7	0.4	0.8	0.8	0.6

Appendix 3b (continued)

Sample	RH21	RH21	RH21	RH21	RH24	RH24	RH24	RH24	RH24	RH24	RH24	RH36	RH36	RH36	RH36	RH36	RH36	RH36	RH36	RH36	RH36	RH36	RH36	RH36	RH36	RH44
Magma Series	LTS	LTS	LTS	LTS	HTS	HTS	HTS	HTS	HTS	HTS	HTS	LTS	LTS	LTS	LTS	LTS	LTS	LTS	LTS	LTS	LTS	LTS	LTS	LTS	LTS	LTS
No.	ph7	ph8	ph8	ph8	ph1	ph1	ph2	ph2	ph3	ph3	ph3	ph1	ph1	ph1	ph2	ph2	ph3	ph3	ph4	ph4	ph4	mph1	mph2	mph3	mph4	ph1
Location	c	c	r	rr	c	r	c	r	c	r	rr	cc	c	r	cc	c	cc	c	cc	c	r					c
wt%																										
SiO_2	48.92	48.07	49.95	54.35	54.62	54.92	53.80	56.38	53.69	53.77	53.76	47.05	47.56	48.54	46.98	47.41	47.21	48.57	47.43	47.43	49.19	52.47	54.85	49.37	51.94	49.07
TiO_2	-	-	-	-	-	-	-	-	-	-	-	-	-	-	-	-	-	-	-	-	-	-	-	-	-	-
Al_2O_3	31.64	32.56	30.74	27.82	27.54	27.26	28.14	26.51	28.35	28.00	28.27	33.10	33.08	31.62	33.22	32.49	33.13	31.66	32.26	32.45	31.56	29.04	27.48	31.26	29.22	31.69
FeO	0.74	0.63	0.55	0.67	0.68	0.65	0.66	0.54	0.75	0.79	0.82	0.37	0.32	0.62	0.32	0.37	0.41	0.39	0.41	0.37	0.33	0.74	0.90	0.59	0.55	0.55
MnO	-	-	-	-	-	-	-	-	-	-	-	-	-	-	-	-	-	-	-	-	-	-	-	-	-	-
BaO	0.04	0.00	0.00	0.12	0.09	0.00	0.00	0.00	0.05	0.07	0.00	0.07	0.03	0.00	0.08	0.09	0.01	0.00	0.00	0.01	0.00	0.05	0.00	0.09	0.00	0.00
SrO	0.14	0.12	0.12	0.21	0.17	0.16	0.17	0.18	0.17	0.18	0.17	0.11	0.14	0.15	0.11	0.11	0.14	0.12	0.17	0.13	0.14	0.17	0.14	0.14	0.11	0.19
CaO	16.13	16.93	15.19	11.88	11.48	11.29	11.97	9.83	12.44	12.21	11.88	17.56	17.65	16.17	17.60	17.17	17.64	16.53	17.08	16.98	16.12	12.95	11.41	15.41	13.72	15.95
Na_2O	2.39	1.90	2.89	4.76	4.94	5.08	4.61	5.75	4.41	4.55	4.56	1.54	1.55	2.29	1.44	1.78	1.48	2.22	1.87	1.87	2.32	3.86	4.87	2.62	3.79	2.43
K_2O	0.10	0.08	0.16	0.30	0.31	0.34	0.27	0.40	0.25	0.27	0.31	0.07	0.08	0.12	0.07	0.10	0.06	0.11	0.09	0.10	0.12	0.43	0.44	0.21	0.29	0.14
Total	100.09	100.28	99.60	100.11	99.83	99.70	99.62	99.60	100.12	99.84	99.78	99.87	100.40	99.52	99.82	99.52	100.07	99.59	99.30	99.33	99.78	99.71	100.09	99.68	99.62	100.02
Formulae based on 5 cations and 8 oxygens																										
Si	2.247	2.206	2.297	2.468	2.484	2.498	2.453	2.555	2.440	2.451	2.449	2.171	2.181	2.242	2.168	2.194	2.173	2.240	2.200	2.197	2.260	2.400	2.488	2.273	2.380	2.253
Ti	-	-	-	-	-	-	-	-	-	-	-	-	-	-	-	-	-	-	-	-	-	-	-	-	-	-
Al	1.713	1.761	1.666	1.489	1.476	1.461	1.512	1.416	1.519	1.504	1.518	1.800	1.788	1.721	1.807	1.772	1.797	1.721	1.763	1.772	1.709	1.565	1.469	1.696	1.578	1.715
Fe	0.028	0.024	0.021	0.026	0.026	0.025	0.025	0.020	0.029	0.030	0.031	0.014	0.012	0.024	0.013	0.014	0.016	0.015	0.016	0.014	0.013	0.028	0.034	0.023	0.021	0.021
Mn	-	-	-	-	-	-	-	-	-	-	-	-	-	-	-	-	-	-	-	-	-	-	-	-	-	-
Ba	0.001	0.000	0.000	0.002	0.002	0.000	0.000	0.000	0.001	0.001	0.000	0.001	0.000	0.000	0.002	0.002	0.000	0.000	0.000	0.000	0.000	0.001	0.000	0.002	0.000	0.000
Sr	0.004	0.003	0.003	0.005	0.004	0.004	0.005	0.005	0.004	0.005	0.005	0.003	0.004	0.004	0.003	0.003	0.004	0.003	0.004	0.003	0.004	0.004	0.004	0.004	0.003	0.005
Ca	0.794	0.832	0.748	0.578	0.559	0.550	0.585	0.477	0.606	0.596	0.580	0.868	0.867	0.800	0.870	0.851	0.870	0.817	0.849	0.843	0.794	0.635	0.555	0.760	0.674	0.785
Na	0.213	0.169	0.258	0.419	0.436	0.448	0.408	0.505	0.389	0.402	0.403	0.138	0.138	0.205	0.129	0.160	0.132	0.199	0.168	0.168	0.207	0.342	0.428	0.234	0.337	0.216
K	0.006	0.005	0.009	0.018	0.018	0.020	0.016	0.023	0.015	0.016	0.018	0.004	0.005	0.007	0.004	0.006	0.003	0.007	0.005	0.006	0.007	0.025	0.026	0.012	0.017	0.008
Sum	5.006	5.000	5.003	5.005	5.005	5.005	5.003	5.002	5.002	5.006	5.003	5.000	4.996	5.004	4.995	5.003	4.996	5.002	5.005	5.004	4.992	5.001	5.004	5.002	5.008	5.002
mol%																										
An	78.4	82.7	73.7	57.0	55.2	54.1	58.0	47.5	60.0	58.8	57.9	86.0	85.9	79.0	86.8	83.7	86.5	79.9	83.0	82.9	78.8	63.3	55.0	75.5	65.6	77.8
Ab	21.0	16.8	25.4	41.3	43.0	44.0	40.4	50.2	38.5	39.6	40.3	13.6	13.7	20.3	12.8	15.7	13.1	19.4	16.4	16.5	20.5	34.2	42.5	23.2	32.8	21.4
Or	0.6	0.4	0.9	1.7	1.8	1.9	1.6	2.3	1.5	1.6	1.8	0.4	0.5	0.7	0.4	0.6	0.3	0.6	0.5	0.6	0.7	2.5	2.5	1.2	1.6	0.8

Appendix 3b   (continued)

Sample	RH44	RH44	RH44	RH44	RH44	RH44	RH44	RH44	RH44	RH44	RH44	RH44	RH44	RH44	RH44	RH45	RH45	RH45	RH45	RH45	RH45	RH45	RH45	RH45	RH45	RH45
Magma Series	LTS	LTS	LTS	LTS	LTS	LTS	LTS	LTS	LTS	LTS	LTS	LTS	LTS	LTS	LTS	LTS	LTS	LTS	LTS	LTS	LTS	LTS	LTS	LTS	LTS	LTS
No.	ph1	ph2	ph2	ph3	ph4	ph4	ph4	ph5	ph5	mph1	mph2	mph3	mph3	mph4	mph5	mph1	mph2	ph1	ph2	ph3	ph3	ph4	ph5	ph5	ph6	ph6
Location	r	c	r	c	cc	c	r	c	r			c	r			c	r	c	c	c	r	c	c	r	c	r
wt%																										
SiO$_2$	55.41	50.70	54.02	49.26	49.58	49.80	54.45	47.74	55.04	54.35	52.81	51.43	53.08	53.28	51.48	54.73	57.20	54.81	54.84	55.41	58.70	53.48	53.94	60.13	53.63	55.85
TiO$_2$	-	-	-	-	-	-	-	-	-	-	-	-	-	-	-	0.07	0.05	0.06	0.07	0.03	0.04	0.06	0.03	0.00	0.00	0.00
Al$_2$O$_3$	27.13	30.08	28.20	31.42	31.11	30.60	27.71	32.17	27.23	27.72	28.97	29.89	28.99	28.81	29.94	27.68	26.51	28.09	27.80	27.39	25.38	28.78	28.51	24.62	29.03	27.72
FeO	0.64	0.62	0.77	0.67	0.62	0.57	0.76	0.51	0.68	0.77	0.61	0.54	0.65	0.76	0.64	0.85	0.71	0.72	0.68	0.57	0.45	0.82	0.82	0.69	0.79	0.88
MnO	-	-	-	-	-	-	-	-	-	-	-	-	-	-	-	0.00	0.02	0.02	0.00	0.00	0.02	0.01	0.02	0.00	0.00	0.00
BaO	0.02	0.10	0.09	0.03	0.10	0.00	0.01	0.05	0.00	0.07	0.01	0.00	0.00	0.06	0.00	0.03	0.07	0.02	0.04	0.01	0.04	0.04	0.03	0.00	0.00	0.00
SrO	0.13	0.15	0.14	0.19	0.19	0.14	0.15	0.15	0.19	0.16	0.16	0.13	0.17	0.17	0.15	0.00	0.00	0.00	0.01	0.00	0.00	0.00	0.00	0.00	0.00	0.00
CaO	11.00	14.79	12.05	15.98	15.75	15.48	11.65	16.56	11.29	11.94	13.25	14.36	13.17	12.90	14.35	11.46	9.60	11.62	11.45	11.08	8.26	12.65	12.10	6.75	12.28	10.36
Na$_2$O	5.11	3.18	4.60	2.47	2.53	2.77	4.86	2.02	5.11	4.74	4.04	3.32	3.99	4.05	3.37	4.73	5.81	4.71	4.78	5.10	6.53	4.20	4.36	7.40	4.28	5.19
K$_2$O	0.37	0.17	0.29	0.13	0.15	0.14	0.31	0.10	0.32	0.30	0.24	0.19	0.23	0.23	0.18	0.38	0.38	0.37	0.36	0.28	0.50	0.28	0.33	0.68	0.37	0.57
Total	99.81	99.79	100.16	100.15	100.03	99.51	99.90	99.30	99.85	100.04	100.08	99.86	100.27	100.26	100.11	99.93	100.35	100.43	100.02	99.86	99.92	100.32	100.13	100.26	100.37	100.56
Formulae based on 5 cations and 8 oxygens																										
Si	2.513	2.328	2.453	2.260	2.276	2.295	2.475	2.212	2.500	2.470	2.405	2.352	2.410	2.420	2.350	2.483	2.569	2.474	2.484	2.508	2.635	2.425	2.446	2.684	2.427	2.511
Ti	-	-	-	-	-	-	-	-	-	-	-	-	-	-	-	0.002	0.002	0.002	0.002	0.001	0.001	0.002	0.001	0.000	0.000	0.000
Al	1.450	1.628	1.509	1.699	1.683	1.662	1.484	1.757	1.458	1.485	1.555	1.611	1.552	1.542	1.611	1.480	1.403	1.494	1.484	1.461	1.343	1.538	1.524	1.295	1.548	1.469
Fe^{2+}	0.024	0.024	0.029	0.026	0.024	0.022	0.029	0.020	0.026	0.029	0.023	0.021	0.025	0.029	0.025	0.032	0.027	0.027	0.026	0.021	0.017	0.031	0.031	0.026	0.030	0.033
Mn	-	-	-	-	-	-	-	-	-	-	-	-	-	-	-	0.000	0.001	0.001	0.000	0.000	0.001	0.001	0.001	0.000	0.000	0.000
Ba	0.000	0.002	0.002	0.001	0.002	0.000	0.000	0.001	0.000	0.001	0.000	0.000	0.000	0.001	0.000	0.001	0.001	0.000	0.001	0.000	0.001	0.001	0.001	0.000	0.000	0.000
Sr	0.003	0.004	0.004	0.005	0.005	0.004	0.004	0.004	0.005	0.004	0.004	0.003	0.004	0.005	0.004	0.000	0.000	0.000	0.000	0.000	0.000	0.000	0.000	0.000	0.000	0.000
Ca	0.535	0.728	0.586	0.786	0.775	0.764	0.567	0.822	0.549	0.581	0.646	0.704	0.641	0.628	0.702	0.557	0.462	0.562	0.556	0.537	0.397	0.615	0.588	0.323	0.595	0.499
Na	0.449	0.283	0.405	0.220	0.225	0.247	0.428	0.181	0.450	0.418	0.357	0.294	0.351	0.357	0.298	0.416	0.506	0.412	0.420	0.448	0.568	0.369	0.383	0.641	0.375	0.453
K	0.022	0.010	0.017	0.008	0.009	0.008	0.018	0.006	0.019	0.017	0.014	0.011	0.013	0.014	0.011	0.022	0.022	0.021	0.021	0.016	0.028	0.016	0.019	0.038	0.021	0.033
Sum	4.997	5.005	5.004	5.004	4.999	5.002	5.006	5.003	5.006	5.005	5.003	4.996	4.996	4.994	4.999	4.994	4.992	4.994	4.992	4.992	4.991	4.997	4.992	5.007	4.997	4.997
mol%																										
An	53.2	71.3	58.2	77.6	76.8	74.9	56.0	81.5	54.0	57.2	63.6	69.7	63.8	62.9	69.4	56.0	46.7	56.4	55.8	53.7	40.0	61.5	59.4	32.2	60.0	50.7
Ab	44.7	27.7	40.2	21.7	22.3	24.3	42.3	18.0	44.2	41.1	35.1	29.2	35.0	35.7	29.5	41.8	51.1	41.4	42.1	44.7	57.2	36.9	38.7	63.9	37.8	46.0
Or	2.1	1.0	1.7	0.8	0.9	0.8	1.8	0.6	1.8	1.7	1.4	1.1	1.3	1.4	1.0	2.2	2.2	2.2	2.1	1.6	2.9	1.6	1.9	3.8	2.1	3.3

Appendix 3b   (continued)

Sample	RH53	RH53	RH53	RH53	RH54	RH53	RH53	RH53	RH53	RH53	RH53	RH53	RH53	RH53	RH53	RH54a	RH54a	RH54a	RH54a	RH54a	RH54a	RH54a	RH54a	RH54a	RH54a
Magma Series	LTS	LTS	LTS	LTS	LTS	LTS	LTS	LTS	LTS	LTS	LTS	LTS	LTS	LTS	LTS	LTS	LTS	LTS	LTS	LTS	LTS	LTS	LTS	LTS	LTS
No.	mph1	mph1	ph1	ph1	ph2	ph2	ph3	ph3	ph3	ph4	ph5	mph2	mph2	mph3	mph3	ph1	ph1	mph1	ph2	ph2	mph2	ph3	ph3	ph4	ph4
Location	c	r	c	r	cc	c	cc	c	r	c	c	c	r	c	r	c	r		c	r		cc	c	cc	c
wt%																									
SiO_2	52.40	55.59	48.12	54.64	48.57	47.88	47.65	48.44	48.04	49.58	48.93	50.23	54.26	52.80	54.38	47.53	49.78	52.71	47.19	49.02	52.62	46.68	47.09	46.86	46.33
TiO_2	0.11	0.10	0.06	0.08	0.02	0.03	0.01	0.04	0.02	0.02	0.02	0.02	0.08	0.06	0.10	-	-	-	-	-	-	-	-	-	-
Al_2O_3	28.42	27.03	31.09	27.11	32.20	31.62	32.32	31.92	30.95	30.66	31.69	30.65	28.05	29.15	27.39	32.11	30.59	28.14	32.35	31.16	28.32	32.93	33.15	33.09	32.89
FeO	0.74	0.87	0.83	0.84	0.51	0.51	0.51	0.58	0.91	0.57	0.73	0.67	0.73	0.64	0.80	0.26	0.46	0.84	0.37	0.42	0.85	0.31	0.36	0.38	0.40
MnO	0.02	0.00	0.00	0.05	0.01	0.02	0.00	0.00	0.00	0.02	0.01	0.00	0.02	0.00	0.03	-	-	-	-	-	-	-	-	-	-
BaO	0.00	0.06	0.04	0.06	0.00	0.01	0.02	0.00	0.00	0.00	0.00	0.00	0.04	0.02	0.09	0.00	0.00	0.02	0.00	0.00	0.04	0.00	0.02	0.06	0.00
SrO	0.00	0.00	0.00	0.00	0.00	0.00	0.04	0.01	0.00	0.00	0.00	0.00	0.00	0.00	0.00	0.12	0.14	0.15	0.17	0.12	0.16	0.12	0.15	0.12	0.13
CaO	12.69	10.59	16.13	11.11	16.28	16.19	16.88	16.58	15.78	15.36	16.24	14.77	11.69	13.06	11.44	17.26	15.31	12.78	17.24	15.85	13.17	17.60	17.49	17.79	17.70
Na_2O	4.19	5.20	2.12	4.89	2.10	2.09	1.81	2.05	2.16	2.67	2.21	2.98	4.66	3.89	4.79	1.74	2.72	4.08	1.60	2.40	3.82	1.48	1.51	1.34	1.38
K_2O	0.24	0.40	0.11	0.41	0.11	0.10	0.09	0.11	0.11	0.15	0.11	0.15	0.29	0.23	0.35	0.06	0.15	0.30	0.07	0.13	0.28	0.07	0.06	0.08	0.08
Total	98.82	99.84	98.49	99.19	99.80	98.44	99.33	99.73	97.97	99.03	99.93	99.47	99.82	99.84	99.38	99.08	99.14	99.02	98.99	99.10	99.26	99.19	99.83	99.71	98.90
Formulae based on 5 cations and 8 oxygens																									
Si	2.414	2.519	2.246	2.498	2.232	2.232	2.206	2.231	2.252	2.292	2.248	2.309	2.465	2.405	2.483	2.206	2.299	2.426	2.194	2.268	2.418	2.168	2.172	2.166	2.160
Ti	0.004	0.004	0.002	0.003	0.001	0.001	0.000	0.001	0.001	0.001	0.001	0.001	0.003	0.002	0.004	-	-	-	-	-	-	-	-	-	-
Al	1.543	1.444	1.710	1.461	1.744	1.738	1.763	1.733	1.710	1.671	1.716	1.660	1.502	1.565	1.474	1.757	1.665	1.527	1.773	1.699	1.534	1.803	1.802	1.803	1.808
Fe^{2+}	0.029	0.033	0.032	0.032	0.020	0.020	0.020	0.022	0.036	0.022	0.028	0.026	0.028	0.024	0.031	0.010	0.018	0.032	0.014	0.016	0.033	0.012	0.014	0.015	0.016
Mn	0.001	0.000	0.000	0.002	0.001	0.001	0.000	0.000	0.000	0.001	0.000	0.000	0.001	0.000	0.001	-	-	-	-	-	-	-	-	-	-
Ba	0.000	0.001	0.001	0.001	0.000	0.000	0.000	0.000	0.000	0.000	0.000	0.000	0.001	0.000	0.002	0.000	0.000	0.000	0.000	0.000	0.001	0.000	0.000	0.001	0.000
Sr	0.000	0.000	0.000	0.000	0.000	0.000	0.001	0.000	0.000	0.000	0.000	0.000	0.000	0.000	0.000	0.003	0.004	0.004	0.005	0.003	0.004	0.003	0.004	0.003	0.003
Ca	0.626	0.514	0.807	0.544	0.802	0.809	0.837	0.818	0.793	0.761	0.799	0.727	0.569	0.637	0.560	0.859	0.758	0.630	0.859	0.786	0.648	0.876	0.864	0.881	0.884
Na	0.374	0.457	0.192	0.433	0.187	0.189	0.162	0.183	0.196	0.239	0.197	0.266	0.410	0.343	0.424	0.157	0.244	0.364	0.144	0.215	0.340	0.133	0.135	0.120	0.125
K	0.014	0.023	0.007	0.024	0.006	0.006	0.005	0.006	0.007	0.009	0.006	0.009	0.017	0.013	0.020	0.004	0.009	0.017	0.004	0.008	0.016	0.004	0.004	0.004	0.005
Sum	5.005	4.995	4.996	4.998	4.992	4.995	4.996	4.996	4.994	4.996	4.995	4.997	4.995	4.990	4.998	4.995	4.995	5.001	4.994	4.994	4.994	4.999	4.996	4.994	5.001
mol%																									
An	61.7	51.7	80.3	54.3	80.6	80.6	83.3	81.2	79.6	75.4	79.7	72.6	57.1	64.1	55.7	84.3	75.0	62.3	85.3	77.9	64.5	86.4	86.2	87.6	87.2
Ab	36.9	45.9	19.1	43.3	18.8	18.8	16.2	18.2	19.7	23.7	19.6	26.5	41.2	34.6	42.2	15.4	24.1	36.0	14.3	21.3	33.9	13.2	13.5	12.0	12.3
Or	1.4	2.3	0.7	2.4	0.6	0.6	0.5	0.6	0.7	0.9	0.6	0.9	1.7	1.3	2.0	0.4	0.9	1.7	0.4	0.7	1.6	0.4	0.4	0.4	0.4

Appendix 3b   (continued)

Sample	RH54a	RH54a	RH54a	RH54a	NWR26	NWR26	NWR26	NWR26	NWR26	NWR26	NWR26	NWR26	NWR26	NWR26	NWR26	NWR26	NWR29	NWR29	NWR29	NWR29	NWR29	NWR29
Magma Series	LTS	LTS	LTS	LTS	LTS	LTS	LTS	LTS	LTS	LTS	LTS	LTS	LTS	LTS	LTS	LTS	LTS	LTS	LTS	LTS	LTS	LTS
No.	ph4	ph5	ph5	mph3	mph1	mph2	mph3	mph4	ph1	ph1	ph2	ph2	mph5	mph6	ph3	ph3	ph1	ph1	ph2	ph2	ph3	mph
Location	r	cc	c						c	r	cc	c			c	r	c	r	c	r	c	
wt%																						
SiO_2	52.87	46.71	46.95	53.73	54.12	54.08	55.57	54.14	48.37	53.75	48.66	49.87	54.46	53.91	47.69	54.30	49.97	54.31	48.36	53.71	49.24	51.28
TiO_2	-	-	-	-	0.02	0.05	0.04	0.03	0.00	0.02	0.00	0.04	0.07	0.03	0.03	0.05	-	-	-	-	-	-
Al_2O_3	27.51	32.97	32.96	28.10	27.72	28.23	27.38	28.36	32.16	28.85	31.27	30.97	28.13	28.50	31.31	28.59	30.94	28.20	31.67	28.43	31.41	29.86
FeO	0.90	0.37	0.31	0.74	0.79	0.68	0.89	0.82	0.67	0.77	0.54	0.71	0.87	0.71	0.73	0.70	0.68	0.78	0.56	0.76	0.56	0.71
MnO	-	-	-	-	0.00	0.00	0.01	0.00	0.00	0.00	0.02	0.02	0.00	0.01	0.00	0.00	-	-	-	-	-	-
BaO	0.00	0.02	0.00	0.00	0.00	0.00	0.06	0.00	0.04	0.06	0.01	0.01	0.00	0.05	0.05	0.00	0.08	0.00	0.00	0.00	0.00	0.00
SrO	0.17	0.17	0.16	0.18	0.00	0.00	0.00	0.00	0.02	0.01	0.00	0.00	0.00	0.00	0.00	0.00	0.12	0.18	0.15	0.16	0.14	0.16
CaO	12.33	17.53	17.63	11.99	11.55	12.11	11.06	12.31	16.52	12.55	15.95	15.36	11.79	12.24	16.29	11.95	15.11	12.18	16.53	12.39	15.79	14.23
Na_2O	4.26	1.43	1.53	4.53	4.67	4.53	5.11	4.33	2.02	4.16	2.42	2.70	4.60	4.42	2.13	4.46	2.94	4.62	2.18	4.45	2.59	3.42
K_2O	0.31	0.05	0.06	0.33	0.32	0.30	0.30	0.27	0.10	0.27	0.13	0.14	0.30	0.26	0.10	0.29	0.15	0.32	0.09	0.31	0.11	0.20
Total	98.35	99.26	99.60	99.59	99.19	99.99	100.42	100.26	99.90	100.45	99.01	99.82	100.21	100.12	98.33	100.34	99.99	100.60	99.55	100.21	99.84	99.85
Formulae based on 5 cations and 8 oxygens																						
Si	2.448	2.168	2.172	2.452	2.473	2.454	2.506	2.451	2.225	2.431	2.255	2.289	2.465	2.445	2.231	2.453	2.292	2.455	2.234	2.439	2.263	2.348
Ti	-	-	-	-	0.001	0.002	0.001	0.001	0.000	0.001	0.000	0.001	0.002	0.001	0.001	0.002	-	-	-	-	-	-
Al	1.501	1.804	1.797	1.511	1.493	1.510	1.455	1.513	1.744	1.538	1.708	1.675	1.501	1.523	1.727	1.522	1.672	1.502	1.725	1.521	1.701	1.611
Fe^{2+}	0.035	0.014	0.012	0.028	0.030	0.026	0.034	0.031	0.026	0.029	0.021	0.027	0.033	0.027	0.028	0.026	0.026	0.030	0.022	0.029	0.021	0.027
Mn	-	-	-	-	0.000	0.000	0.000	0.000	0.000	0.000	0.001	0.001	0.000	0.000	0.000	0.000	-	-	-	-	-	-
Ba	0.000	0.000	0.000	0.000	0.000	0.000	0.001	0.000	0.001	0.001	0.000	0.000	0.000	0.001	0.001	0.000	0.001	0.000	0.000	0.000	0.000	0.000
Sr	0.005	0.005	0.004	0.005	0.000	0.000	0.000	0.000	0.001	0.000	0.000	0.000	0.000	0.000	0.000	0.000	0.003	0.005	0.004	0.004	0.004	0.004
Ca	0.612	0.872	0.874	0.586	0.566	0.589	0.534	0.597	0.814	0.608	0.792	0.755	0.572	0.595	0.817	0.578	0.742	0.590	0.818	0.603	0.778	0.698
Na	0.382	0.129	0.137	0.401	0.414	0.399	0.447	0.380	0.180	0.365	0.217	0.240	0.404	0.389	0.193	0.391	0.261	0.405	0.195	0.392	0.231	0.304
K	0.018	0.003	0.004	0.019	0.019	0.018	0.017	0.016	0.006	0.015	0.008	0.008	0.017	0.015	0.006	0.017	0.009	0.018	0.006	0.018	0.007	0.011
Sum	5.002	4.996	5.000	5.002	4.996	4.997	4.997	4.989	4.996	4.989	5.003	4.997	4.993	4.995	5.004	4.989	5.007	5.005	5.004	5.006	5.005	5.004
mol%																						
An	60.4	86.9	86.1	58.3	56.7	58.6	53.5	60.1	81.4	61.5	77.9	75.3	57.6	59.6	80.4	58.7	73.3	58.2	80.3	59.5	76.6	68.9
Ab	37.8	12.8	13.5	39.8	41.5	39.7	44.7	38.3	18.0	36.9	21.4	23.9	40.7	38.9	19.0	39.6	25.8	40.0	19.2	38.7	22.7	30.0
Or	1.8	0.3	0.4	1.9	1.9	1.8	1.7	1.6	0.6	1.6	0.8	0.8	1.8	1.5	0.6	1.7	0.9	1.8	0.5	1.8	0.6	1.1

Appendix 3c Representative electron microprobe analyses of titano-magnetite (Ti-mgt) and ilmenite (ilm). Recalculation of Fe^{3+} and Fe^{2+} after CARMICHAEL (1967); end-member calculation after STORMER (1983): Usp = ulvöspinel, Ilm = ilmenite, Mgt = magnetite, Hem = hematite; - = not determined.

Sample	RH6	RH6	RH6	RH6	RH6	RH6	RH21	RH21	RH21	RH21	RH21	RH21	RH21	RH21	RH24	RH24	RH24	RH24	RH24	RH24	RH24	RH24	RH24
Magma Series	HTS	HTS	HTS	HTS	HTS	HTS	LTS	LTS	LTS	LTS	LTS	LTS	LTS	LTS	HTS	HTS	HTS	HTS	HTS	HTS	HTS	HTS	HTS
Phase	Ti-mgt	Ti-mgt	Ti-mgt	ilm	Ti-mgt	Ti-mgt	ilm	ilm	ilm	ilm	ilm	ilm	ilm	ilm	Ti-mgt	ilm	ilm	ilm	ilm	ilm	ilm	ilm	Ti-mgt
No.	6_2	6_3	6_5	6_8	6_10	6_11	21_1	21_2	21_3	21_6	21_8	21_9	21_10	21_11	24_1	24_2	24_3	24_8	24_9	24_10	24_11	24_12	24_13
wt%																							
SiO$_2$	0.09	0.11	0.57	0.64	0.16	0.12	0.07	0.00	0.00	0.00	0.00	0.03	0.00	0.00	0.11	0.05	0.01	0.00	0.00	0.04	0.03	0.01	0.29
TiO$_2$	26.01	25.46	18.79	34.66	22.11	24.18	49.93	50.27	49.80	50.24	49.37	49.80	50.76	49.73	21.89	51.26	50.31	50.70	50.05	50.37	50.60	51.13	22.69
Al$_2$O$_3$	1.67	1.70	0.68	0.10	1.41	1.67	0.03	0.08	0.03	0.06	0.07	0.05	0.09	0.03	1.50	0.02	0.06	0.04	0.06	0.08	0.06	0.04	1.58
Cr$_2$O$_3$	0.05	0.07	0.01	0.00	0.02	0.09	0.02	0.05	0.03	0.05	0.01	0.09	0.03	0.04	0.14	0.02	0.03	0.00	0.06	0.04	0.03	0.09	0.15
ZnO	0.06	0.04	0.09	0.04	0.12	0.06	0.00	0.05	0.03	0.09	0.02	0.04	0.05	0.08	0.23	0.08	0.00	0.03	0.03	0.05	0.00	0.03	0.14
FeO$_{(T)}$	65.21	65.97	72.44	56.83	69.65	66.87	46.68	47.08	46.26	47.21	47.20	47.44	46.53	47.71	69.47	46.11	47.37	46.71	46.74	46.77	46.45	46.76	66.72
MnO	1.44	1.37	1.13	1.99	1.22	1.25	1.47	0.44	1.43	0.44	0.68	0.46	0.47	0.55	1.20	0.51	0.53	0.68	0.79	0.97	0.81	0.45	0.38
MgO	0.01	0.01	0.04	0.02	0.00	0.04	0.21	0.96	0.44	1.05	0.51	0.69	1.21	0.55	0.06	0.38	0.40	0.27	0.32	0.25	0.35	0.36	0.02
CaO	-	-	-	-	-	-	-	-	-	-	-	-	-	-	0.15	0.04	0.17	0.17	0.05	0.08	0.04	0.02	0.40
Total	94.55	94.74	93.75	94.28	94.68	94.26	98.42	98.94	98.02	99.13	97.86	98.60	99.14	98.69	94.76	98.47	98.88	98.59	98.09	98.64	98.36	98.90	92.37
Formulae based on 3 (2) cations and 4 (3) oxygens for magnetite (ilmenite)																							
Si	0.00	0.00	0.02	0.02	0.01	0.00	0.00	0.00	0.00	0.00	0.00	0.00	0.00	0.00	0.00	0.00	0.00	0.00	0.00	0.00	0.00	0.00	0.01
Al	0.08	0.08	0.03	0.00	0.06	0.08	0.00	0.00	0.00	0.00	0.00	0.00	0.00	0.00	0.07	0.00	0.00	0.00	0.00	0.00	0.00	0.00	0.07
Ti	0.76	0.74	0.55	0.69	0.64	0.70	0.96	0.96	0.96	0.95	0.95	0.95	0.96	0.95	0.63	0.98	0.96	0.97	0.96	0.97	0.97	0.98	0.67
Cr	0.00	0.00	0.00	0.00	0.00	0.00	0.00	0.00	0.00	0.00	0.00	0.00	0.00	0.00	0.00	0.00	0.00	0.00	0.00	0.00	0.00	0.00	0.00
Fe^{+3}	0.40	0.43	0.83	0.59	0.64	0.50	0.08	0.09	0.08	0.09	0.09	0.09	0.07	0.10	0.65	0.03	0.08	0.05	0.07	0.06	0.05	0.04	0.55
Mg	0.00	0.00	0.00	0.00	0.00	0.00	0.01	0.04	0.02	0.04	0.02	0.03	0.05	0.02	0.00	0.01	0.02	0.01	0.01	0.01	0.01	0.01	0.00
Fe^{+2}	1.71	1.70	1.53	0.66	1.60	1.67	0.92	0.91	0.91	0.90	0.92	0.92	0.90	0.92	1.58	0.96	0.93	0.94	0.93	0.93	0.94	0.95	1.65
Mn	0.05	0.04	0.04	0.04	0.04	0.04	0.03	0.01	0.03	0.01	0.01	0.01	0.01	0.01	0.04	0.01	0.01	0.01	0.02	0.02	0.02	0.01	0.01
Zn	0.00	0.00	0.00	0.00	0.00	0.00	0.00	0.00	0.00	0.00	0.00	0.00	0.00	0.00	0.01	0.00	0.00	0.00	0.00	0.00	0.00	0.00	0.00
Ca	-	-	-	-	-	-	-	-	-	-	-	-	-	-	0.01	0.00	0.00	0.00	0.00	0.00	0.00	0.00	0.02
Sum	3.00	3.00	3.00	2.00	3.00	3.00	2.00	2.00	2.00	2.00	2.00	2.00	2.00	2.00	3.00	2.00	2.00	2.00	2.00	2.00	2.00	2.00	3.00
mol%																							
Usp / Ilm	81.5	79.7	57.4	69.3	68.2	76.0	96.1	95.6	95.9	95.2	95.2	95.3	96.1	95.0	67.6	98.6	96.2	97.3	96.5	96.8	97.4	97.9	73.2
Mgt / Hem	18.5	20.3	42.6	30.7	31.8	24.0	3.9	4.4	4.1	4.8	4.8	4.7	3.9	5.0	32.4	1.4	3.8	2.7	3.5	3.2	2.6	2.1	26.8

Appendix 3c   (continued)

Sample	RH44	RH44	RH44	RH44	RH44	RH44	RH44	RH44	RH44	RH44	RH44	RH44	RH44	RH45	RH45	RH45	RH45	RH45	RH45	RH45	RH45	RH45	RH45
Magma Series	LTS	LTS	LTS	LTS	LTS	LTS	LTS	LTS	LTS	LTS	LTS	LTS	LTS	LTS	LTS	LTS	LTS	LTS	LTS	LTS	LTS	LTS	LTS
Phase	Ti-mgt	Ti-mgt	ilm	Ti-mgt	Ti-mgt	Ti-mgt	Ti-mgt	Ti-mgt	Ti-mgt	ilm	Ti-mgt	Ti-mgt	ilm	Ti-mgt	Ti-mgt	ilm	ilm	Ti-mgt	ilm	ilm	ilm	Ti-mgt	Ti-mgt
No.	44_1	44_2	44_4	44_5	44_7	44_8	44_12	44_13	44_14	44_15	44_18	44_19	44_22	45_1	45_2	45_8	45_9	45_12	45_13	45_14	45_17	45_19	45_20
wt%																							
SiO_2	0.11	0.10	0.06	0.08	0.05	0.06	0.03	0.05	0.07	0.02	0.09	0.08	0.09	0.04	0.06	0.00	0.00	0.02	0.00	0.00	0.00	0.00	0.05
TiO_2	21.20	19.59	37.84	12.96	16.26	25.14	14.30	17.84	20.71	50.26	15.43	23.20	34.32	17.43	17.68	50.47	50.89	12.44	50.42	50.76	50.80	13.16	14.44
Al_2O_3	1.25	1.29	0.57	2.40	2.05	1.35	2.03	1.77	1.88	0.00	1.32	1.23	0.69	0.73	1.00	0.03	0.05	0.96	0.02	0.03	0.00	1.61	0.82
Cr_2O_3	0.02	0.06	0.04	0.03	0.06	0.04	0.06	0.00	0.02	0.01	0.04	0.05	0.04	0.00	0.03	0.04	0.00	0.01	0.05	0.09	0.02	0.07	0.02
ZnO	0.20	0.22	0.13	0.27	0.34	0.11	0.28	0.36	0.13	0.00	0.18	0.18	0.02	0.26	0.16	0.02	0.08	0.17	0.10	0.07	0.06	0.23	0.17
$FeO(T)$	71.01	72.90	55.55	77.52	74.10	68.42	77.21	72.95	69.72	46.47	74.90	69.38	57.11	77.87	76.59	47.85	46.96	78.30	47.23	47.40	47.24	77.99	77.91
MnO	0.90	0.76	1.59	0.28	0.31	0.64	0.16	0.37	0.86	1.76	0.76	0.71	1.16	0.52	0.41	0.57	0.52	0.28	0.50	0.53	0.60	0.57	0.29
MgO	0.06	0.03	0.02	0.04	0.02	0.07	0.06	0.07	0.03	0.01	0.03	0.06	0.08	0.17	0.13	0.51	0.54	0.07	0.51	0.53	0.48	0.07	0.10
CaO	-	-	-	-	-	-	-	-	-	-	-	-	-	-	-	-	-	-	-	-	-	-	-
Total	94.76	94.94	95.80	93.58	93.20	95.82	94.12	93.40	93.42	98.53	92.76	94.91	93.50	97.01	96.07	99.48	99.05	92.24	98.84	99.42	99.21	93.70	93.81

Formulae based on 3 (2) cations and 4 (3) oxygens for magnetite (ilmenite)

Si	0.00	0.00	0.00	0.00	0.00	0.00	0.00	0.00	0.00	0.00	0.00	0.00	0.00	0.00	0.00	0.00	0.00	0.00	0.00	0.00	0.00	0.00	0.00
Al	0.06	0.06	0.02	0.11	0.09	0.06	0.09	0.08	0.09	0.00	0.06	0.06	0.02	0.03	0.04	0.00	0.00	0.04	0.00	0.00	0.00	0.07	0.04
Ti	0.61	0.57	0.74	0.37	0.47	0.72	0.41	0.52	0.61	0.97	0.45	0.67	0.68	0.49	0.50	0.96	0.97	0.37	0.96	0.96	0.97	0.38	0.42
Cr	0.00	0.00	0.00	0.00	0.00	0.00	0.00	0.00	0.00	0.00	0.00	0.00	0.00	0.00	0.00	0.00	0.00	0.00	0.00	0.00	0.00	0.00	0.00
Fe^{+3}	0.71	0.80	0.50	1.13	0.95	0.49	1.08	0.87	0.69	0.06	1.02	0.59	0.61	0.98	0.94	0.08	0.06	1.22	0.07	0.07	0.06	1.16	1.12
Mg	0.00	0.00	0.00	0.00	0.00	0.00	0.00	0.00	0.00	0.00	0.00	0.00	0.01	0.01	0.02	0.02	0.00	0.02	0.02	0.02	0.00	0.01	
Fe^{+2}	1.58	1.54	0.70	1.36	1.46	1.70	1.40	1.50	1.58	0.93	1.42	1.64	0.66	1.46	1.48	0.93	0.94	1.35	0.93	0.93	0.94	1.35	1.40
Mn	0.03	0.02	0.03	0.01	0.01	0.02	0.01	0.01	0.03	0.04	0.03	0.02	0.03	0.02	0.01	0.01	0.01	0.01	0.01	0.01	0.01	0.02	0.01
Zn	0.01	0.01	0.00	0.01	0.01	0.00	0.01	0.01	0.00	0.00	0.01	0.01	0.00	0.01	0.00	0.00	0.00	0.00	0.00	0.00	0.00	0.01	0.00
Ca	-	-	-	-	-	-	-	-	-	-	-	-	-	-	-	-	-	-	-	-	-	-	-
Sum	3.00	3.00	2.00	3.00	3.00	3.00	3.00	3.00	3.00	2.00	3.00	3.00	2.00	3.00	3.00	2.00	2.00	3.00	2.00	2.00	2.00	3.00	3.00
mol%																							
Usp / Ilm	64.7	59.7	74.1	41.7	52.0	76.6	45.1	56.2	65.8	96.7	47.9	71.0	68.8	50.3	52.4	95.8	97.0	38.1	96.3	96.5	96.7	40.7	43.4
Mgt / Hem	35.3	40.3	25.9	58.3	48.0	23.4	54.9	43.8	34.2	3.3	52.1	29.0	31.2	49.7	47.6	4.2	3.0	61.9	3.7	3.5	3.3	59.3	56.6

Appendix 3c   (continued)

Sample	RH45	RH45	RH45	RH45	RH53	RH53	RH53	RH53	RH53	RH53	RH53	RH53	NWR29	NWR29	NWR29	NWR29	NWR29	NWR29	NWR29	NWR29	NWR29	NWR29
Magma Series	LTS	LTS	LTS	LTS	LTS	LTS	LTS	LTS	LTS	LTS	LTS	LTS	LTS	LTS	LTS	LTS	LTS	LTS	LTS	LTS	LTS	LTS
Phase	ilm	Ti-mgt	Ti-mgt	Ti-mgt	ilm	ilm	ilm	ilm	ilm	ilm	ilm	ilm	ilm	Ti-mgt	Ti-mgt	ilm	ilm	Ti-mgt	Ti-mgt	ilm	Ti-mgt	Ilm
No.	45_22	45_27	45_30	45_33	53_2	53_3	53_4	53_5	53_6	53_8	53_9	53_10	29_1	29_2	29_3	29_6	29_7	29_10	29_11	29_12	29_13	29_14
wt%																						
SiO_2	0.00	0.06	0.06	0.05	0.04	0.02	0.04	0.07	0.00	0.01	0.00	0.04	0.00	0.07	0.05	0.00	0.00	0.05	0.06	0.00	0.09	0.00
TiO_2	49.41	22.91	12.09	24.65	49.16	48.22	48.88	47.87	49.52	48.04	49.20	48.43	50.40	15.31	13.97	50.50	50.75	16.10	13.35	50.90	14.73	50.32
Al_2O_3	0.05	0.96	1.25	1.12	0.01	0.05	0.03	0.05	0.00	0.03	0.04	0.04	0.01	1.35	1.22	0.00	0.03	1.56	1.98	0.04	1.92	0.03
Cr_2O_3	0.00	0.11	0.06	0.09	0.00	0.00	0.01	0.02	0.03	0.08	0.03	0.05	0.02	0.18	0.31	0.00	0.06	0.18	0.14	0.07	0.18	0.00
ZnO	0.08	0.49	0.57	0.26	0.04	0.00	0.00	0.03	0.01	0.03	0.00	0.02	0.06	0.18	0.26	0.01	0.06	0.19	0.19	0.02	0.18	0.00
$FeO_{(T)}$	47.83	68.77	77.40	66.96	47.09	46.02	46.29	45.18	45.51	46.05	45.95	45.69	48.54	78.38	78.42	48.36	48.09	76.75	79.91	47.80	78.48	48.13
MnO	0.52	0.69	0.78	0.95	1.68	3.44	2.70	3.73	3.10	3.47	3.47	3.55	0.44	0.28	0.27	0.55	0.46	0.30	0.30	0.44	0.25	0.48
MgO	0.43	0.04	0.04	0.18	0.68	0.05	0.28	0.07	0.39	0.03	0.07	0.03	0.27	0.11	0.09	0.16	0.21	0.19	0.08	0.11	0.10	0.13
CaO	-	-	-	-	-	-	-	-	-	-	-	-	0.02	0.02	0.03	0.02	0.00	0.02	0.03	0.02	0.02	0.02
Total	98.32	94.03	92.25	94.25	98.70	97.81	98.23	97.02	98.56	97.75	98.76	97.84	99.75	95.88	94.62	99.60	99.65	95.32	96.03	99.39	95.94	99.11

Formulae based on 3 (2) cations and 4 (3) oxygens for magnetite (ilmenite)

Si	0.00	0.00	0.00	0.00	0.00	0.00	0.00	0.00	0.00	0.00	0.00	0.00	0.00	0.00	0.00	0.00	0.00	0.00	0.00	0.00	0.00	0.00
Al	0.00	0.04	0.06	0.05	0.00	0.00	0.00	0.00	0.00	0.00	0.00	0.00	0.00	0.06	0.06	0.00	0.00	0.07	0.09	0.00	0.09	0.00
Ti	0.95	0.67	0.36	0.72	0.94	0.93	0.94	0.93	0.95	0.93	0.94	0.94	0.96	0.44	0.40	0.96	0.96	0.46	0.38	0.97	0.42	0.96
Cr	0.00	0.00	0.00	0.00	0.00	0.00	0.00	0.00	0.00	0.00	0.00	0.00	0.00	0.01	0.01	0.00	0.00	0.01	0.00	0.00	0.01	0.00
Fe^{+3}	0.10	0.61	1.22	0.50	0.12	0.13	0.12	0.13	0.10	0.14	0.11	0.12	0.09	1.06	1.13	0.08	0.07	1.00	1.15	0.06	1.07	0.08
Mg	0.02	0.00	0.00	0.01	0.03	0.00	0.01	0.00	0.01	0.00	0.00	0.00	0.01	0.01	0.01	0.01	0.01	0.01	0.00	0.00	0.01	0.00
Fe^{+2}	0.92	1.63	1.31	1.67	0.88	0.86	0.87	0.85	0.87	0.85	0.87	0.86	0.93	1.42	1.38	0.94	0.95	1.44	1.36	0.96	1.40	0.95
Mn	0.01	0.02	0.03	0.03	0.04	0.07	0.06	0.08	0.07	0.08	0.07	0.08	0.01	0.01	0.01	0.01	0.01	0.01	0.01	0.01	0.01	0.01
Zn	0.00	0.01	0.02	0.01	0.00	0.00	0.00	0.00	0.00	0.00	0.00	0.00	0.00	0.01	0.01	0.00	0.00	0.01	0.01	0.00	0.01	0.00
Ca	-	-	-	-	-	-	-	-	-	-	-	-	0.00	0.00	0.00	0.00	0.00	0.00	0.00	0.00	0.00	0.00
Sum	2.00	3.00	3.00	3.00	2.00	2.00	2.00	2.00	2.00	2.00	2.00	2.00	2.00	3.00	3.00	2.00	2.00	3.00	3.00	2.00	3.00	2.00
mol%																						
Usp / Ilm	94.9	70.0	37.2	75.5	93.7	93.1	93.9	93.2	94.7	92.8	94.1	93.6	95.5	46.2	42.6	95.9	96.5	49.2	41.1	97.1	45.5	96.1
Mgt / Hem	5.1	30.0	62.8	24.5	6.3	6.9	6.1	6.8	5.3	7.2	5.9	6.4	4.5	53.8	57.4	4.1	3.5	50.8	58.9	2.9	54.5	3.9

Appendix 4 XRF whole-rock analyses of major and trace element concentrations of Ferrar low-Ti samples and high-Ti samples (marked by an asterisk) from northern Victorialand and from George V Land analysed at the Institut für Geowissenschaften, Universität Jena and at the GeoForschungsZentrum Potsdam.

Sample	RH1	RH3*	RH4	RH5	RH6*	RH7*	RH9*	RH11	RH12	RH14	RH15	RH16	RH17	RH18	RH19	RH20
Major elements [wt%] normalised to 100 wt% without LOI / volatiles																
SiO_2	57.10	56.62	54.52	57.88	56.45	56.72	56.98	56.63	56.55	55.07	54.13	54.13	56.61	54.19	55.80	55.69
TiO_2	0.91	2.01	0.80	0.78	2.02	1.95	1.95	0.80	0.88	0.61	0.57	0.61	0.83	0.63	0.69	0.67
Al_2O_3	14.20	11.97	14.74	13.94	11.95	12.02	12.00	15.16	15.27	15.03	16.03	16.35	14.54	15.59	14.89	14.71
$FeO_{(T)}$	9.88	15.16	10.55	9.07	15.57	15.31	15.19	9.70	9.76	8.97	8.64	8.27	9.59	9.19	9.23	8.97
MnO	0.17	0.21	0.19	0.16	0.23	0.21	0.20	0.18	0.16	0.17	0.16	0.16	0.17	0.23	0.17	0.16
MgO	4.83	2.30	6.01	4.76	2.31	2.35	2.39	4.47	4.42	6.92	6.93	6.48	5.64	7.15	6.19	7.05
CaO	9.12	7.34	9.81	10.85	7.21	6.93	7.10	9.65	9.25	10.15	11.16	11.38	9.17	10.90	9.50	9.57
Na_2O	2.32	1.82	2.36	1.57	2.18	2.30	2.14	2.10	2.32	2.02	1.65	1.73	2.04	1.66	2.16	2.07
K_2O	1.33	2.30	0.90	0.90	1.84	1.94	1.76	1.18	1.26	0.97	0.64	0.79	1.28	0.35	1.26	1.00
P_2O_5	0.14	0.28	0.11	0.10	0.26	0.27	0.27	0.12	0.13	0.10	0.08	0.09	0.13	0.10	0.11	0.11
LOI [1]		0.38	1.77	3.04	0.01	0.06	0.39	0.68		0.39	0.51			0.80	0.67	
H_2O [2]	1.48								1.47			0.80	1.25			1.28
CO_2 [2]	0.04								0.09			0.08	0.21			0.08
Mg# [3]	50.6	24.1	54.4	52.4	23.7	24.4	24.8	49.2	48.7	61.8	62.7	62.2	55.2	62.0	58.5	62.2
Trace elements [ppm]																
Ba	324	491	320	113	394	461	358	299	308	191	154	161	309	446	372	214
Co	36	33	42	38	38	43	39	36	33	40	36	35	37	37	37	41
Cr	47	bld	85	52	bld	bld	<5	31	20	187	237	159	75	211	153	194
Cu	106	213	95	89	209	208	223	118	128	78	90	82	97	89	97	95
Ga	16	20	16	14	22	21	22	18	19	16	16	14	18	14	15	16
Nb	8	10	6	5	11	12	12	7	6	6	3	5	8	5	7	7
Ni	54	21	65	50	22	23	24	55	47	116	75	66	60	125	95	115
Pb	9	11	9	10	12	9	9	9	9	6	6	5	7	4	7	5
Rb	51	67	38	32	66	79	66	45	48	40	27	33	50	7	49	41
Sc	39	44	41	38	43	43	43	39	36	32	36	34	34	36	33	33
Sr	156	131	229	21	125	131	124	143	148	169	121	121	136	231	183	137
V	232	489	259	241	466	488	494	216	218	187	177	182	204	197	194	189
Y	30	52	25	22	54	53	52	30	29	22	21	21	28	21	23	23
Zn	94	146	90	80	146	148	149	86	91	77	72	72	85	77	83	80
Zr	149	244	125	115	244	242	236	137	143	92	77	82	140	100	110	105

[1] LOI – loss on ignition measured for samples analysed in Jena

[2] H_2O + CO_2 – volatiles measured for samples analysed in Potsdam

[3] Mg# – Mg-number calculated as 100 x Mg / [Mg+Fe^{2+}] from molecular portions setting Fe_2O_3/FeO = 0.15

Appendix 4   (continued)

Sample	RH21	RH22	RH23	RH24*	RH25	RH26	RH27	HR28	RH29	RH30	RH31	RH32	RH33	RH34	RH35	RH36

Major elements [wt%] normalised to 100 wt% without LOI / volatiles

	RH21	RH22	RH23	RH24*	RH25	RH26	RH27	HR28	RH29	RH30	RH31	RH32	RH33	RH34	RH35	RH36
SiO_2	54.04	54.16	54.88	56.51	56.30	53.33	55.03	54.95	55.00	53.55	55.83	54.90	53.91	55.04	54.20	54.18
TiO_2	0.56	0.57	0.55	1.72	0.81	0.67	0.67	0.63	0.64	0.65	0.63	0.66	0.63	0.62	0.61	0.63
Al_2O_3	14.26	15.73	14.98	12.80	15.07	15.57	14.78	14.72	14.92	15.77	14.53	14.90	16.34	14.64	16.56	15.02
$FeO_{(T)}$	8.89	8.34	8.60	13.96	9.41	9.50	9.48	9.32	9.33	9.31	8.90	9.56	9.31	9.11	8.91	9.12
MnO	0.18	0.29	0.16	0.20	0.16	0.17	0.18	0.18	0.14	0.16	0.17	0.18	0.15	0.19	0.15	0.18
MgO	8.98	7.53	8.06	3.01	4.94	6.97	6.66	6.72	7.17	6.77	6.67	6.65	6.53	7.17	5.67	7.17
CaO	10.86	10.98	10.06	7.72	9.87	10.75	11.06	11.16	10.05	10.76	9.22	11.19	10.45	10.90	11.43	11.12
Na_2O	1.46	1.67	1.82	2.43	2.10	1.86	1.57	1.42	1.68	1.99	1.63	1.62	1.68	1.74	1.64	1.73
K_2O	0.68	0.67	0.79	1.50	1.20	1.09	0.48	0.81	0.98	0.96	2.34	0.24	0.90	0.51	0.75	0.76
P_2O_5	0.08	0.07	0.09	0.15	0.12	0.10	0.09	0.08	0.09	0.09	0.09	0.09	0.09	0.08	0.08	0.09
LOI	0.25	0.59	0.38	0.58		2.49	5.15	3.74	2.14	2.56	6.86	6.35	1.33	5.1	3.99	0.53
H_2O					1.39											
CO_2					0.04											
Mg# *	67.9	65.4	66.3	31.2	52.4	60.6	59.6	60.2	61.7	60.4	61.1	59.3	59.5	62.3	57.2	62.2

Trace elements [ppm]

	RH21	RH22	RH23	RH24*	RH25	RH26	RH27	HR28	RH29	RH30	RH31	RH32	RH33	RH34	RH35	RH36
Ba	182	225	204	372	280	253	198	183	195	175	277	215	196	243	185	182
Co	41	44	35	49	35	42	36	35	39	36	37	36	32	37	36	39
Cr	274	69	283	<5	49	133	94	87	113	155	126	129	105	131	135	166
Cu	72	84	84	180	104	85	75	77	81	75	75	78	88	72	89	79
Ga	15	16	14	17	17	16	14	15	14	16	13	13	16	11	17	16
Nb	6	7	4	9	6	6	4	5	3	5	5	3	3	4	5	5
Ni	112	85	134	25	63	77	64	64	73	74	69	68	55	74	66	88
Pb	9	8	6	10	8	9	6	7	7	9	7	8	7	6	6	9
Rb	26	37	33	58	48	37	19	34	32	38	99	18	35	23	36	28
Sc	35	43	33	52	34	37	31	34	39	36	33	34	31	35	37	39
Sr	112	123	142	141	139	82	171	113	112	87	151	179	132	321	109	114
V	181	235	169	449	199	203	182	187	196	189	181	176	161	177	187	193
Y	19	24	19	35	27	23	19	23	19	19	22	21	20	18	24	23
Zn	71	83	72	126	83	77	66	67	74	73	70	68	67	69	72	78
Zr	86	112	83	172	124	104	98	97	101	94	95	96	82	95	91	98

Sample	RH37	RH38	RH39	RH40	RH41	RH42	RH44	RH45	RH46	RH47	RH48	RH49	RH50	RH51	RH52	RH53
Major elements [wt%] normalised to 100 wt% without LOI / volatiles																
SiO_2	54.26	54.17	55.22	55.41	59.04	55.38	55.23	59.22	53.70	53.83	53.63	56.17	55.18	55.74	53.89	54.21
TiO_2	0.65	0.60	0.66	0.80	1.11	0.73	0.72	1.21	0.39	0.43	0.46	0.74	0.63	0.68	0.45	0.46
Al_2O_3	15.24	14.53	15.09	14.53	13.49	13.59	14.35	13.27	13.37	13.21	12.99	14.63	14.89	14.94	13.07	11.19
$FeO_{(T)}$	9.15	9.23	9.28	10.06	11.13	10.00	9.88	11.60	8.65	8.35	8.54	9.57	8.86	9.16	8.21	9.36
MnO	0.18	0.17	0.16	0.18	0.18	0.20	0.18	0.17	0.19	0.18	0.18	0.18	0.16	0.16	0.17	0.19
MgO	6.83	8.13	6.54	5.66	3.20	6.90	6.13	2.72	10.35	10.98	10.90	5.57	7.32	6.23	11.08	11.96
CaO	11.29	10.89	10.34	9.96	7.35	10.40	10.55	7.03	11.56	11.17	11.36	9.99	10.29	9.82	11.36	10.88
Na_2O	1.74	1.55	1.86	2.02	2.54	1.79	1.86	2.64	1.25	1.29	1.25	1.96	1.75	2.18	1.22	1.14
K_2O	0.56	0.65	0.75	1.20	1.77	0.92	0.98	1.94	0.49	0.50	0.63	1.05	0.79	0.99	0.51	0.54
P_2O_5	0.10	0.08	0.10	0.18	0.20	0.09	0.11	0.19	0.05	0.06	0.06	0.12	0.11	0.11	0.06	0.07
LOI	0.74	0.45	0.51	0.71	0.92	0.40	0.99	0.72	0.57	0.28	0.62	0.48		0.41		
H_2O													1.13		0.55	1.01
CO_2													0.06		0.05	0.06
Mg# *	61.0	64.9	59.7	54.1	37.6	59.1	56.5	33.0	71.5	73.4	72.8	55.0	63.4	58.8	73.9	72.8
Trace elements [ppm]																
Ba	175	178	211	301	434	302	242	436	130	132	145	261	201	194	135	130
Co	38	40	39	35	32	38	39	36	48	45	43	40	40	35	43	51
Cr	139	212	178	58	8	143	59	bld	303	422	401	96	232	165	426	437
Cu	84	75	93	100	136	90	82	142	55	51	61	105	93	81	65	63
Ga	15	15	18	16	18	16	18	17	14	14	13	16	15	17	13	13
Nb	4	6	7	7	10	7	6	12	2	3	5	6	6	4	3	5
Ni	78	99	110	69	33	97	77	26	170	136	140	78	127	82	137	196
Pb	7	7	9	11	10	9	7	12	5	7	7	8	6	8	3	5
Rb	22	27	24	45	67	40	36	74	20	22	25	41	31	47	22	23
Sc	35	36	34	35	37	30	39	39	40	38	38	36	34	34	41	45
Sr	118	109	125	135	175	154	133	142	107	97	94	143	132	129	95	95
V	191	191	193	219	249	196	221	253	200	182	179	208	188	189	187	221
Y	22	20	23	28	38	24	26	42	16	15	16	25	22	23	16	15
Zn	78	76	80	85	103	78	81	107	67	66	67	84	78	76	67	75
Zr	98	91	108	126	202	111	119	218	58	63	68	114	95	97	57	60

Sample	RH54a	RH54f	RH55	RH56	RH57	RH58	NWR25	NWR26	NWR27	NWR28	NWR29	NWR30	NWR78	NWR80

Major elements [wt%] normalised to 100 wt% without LOI / volatiles

SiO_2	54.61	54.06	56.08	57.50	53.87	54.14	54.49	55.20	53.34	53.50	54.59	55.22	54.18	54.39
TiO_2	0.62	0.53	0.67	0.94	0.56	0.58	0.66	0.72	0.50	0.47	0.70	0.71	0.67	0.61
Al_2O_3	14.98	14.79	14.83	14.32	16.60	15.99	17.18	14.58	16.66	15.51	16.41	16.80	16.37	15.43
$FeO_{(T)}$	8.96	8.74	9.14	10.48	8.37	8.57	8.67	10.04	8.28	8.50	9.43	9.05	8.93	9.04
MnO	0.17	0.18	0.16	0.17	0.16	0.16	0.15	0.19	0.17	0.16	0.17	0.16	0.18	0.16
MgO	7.09	8.82	6.13	3.90	6.57	6.85	4.69	5.96	6.87	7.72	4.72	4.31	5.33	6.94
CaO	10.60	10.62	9.99	8.65	11.31	11.31	10.91	10.32	11.78	11.94	10.93	10.43	11.45	10.82
Na_2O	1.93	1.56	1.95	2.46	1.79	1.62	2.23	1.96	1.70	1.54	2.03	2.18	1.92	1.76
K_2O	0.94	0.62	0.95	1.43	0.70	0.70	0.92	0.95	0.62	0.58	0.92	1.03	0.88	0.76
P_2O_5	0.09	0.08	0.11	0.15	0.08	0.08	0.10	0.09	0.07	0.07	0.09	0.10	0.09	0.09
LOI	0.21	0.72	1.00		0.74	0.68	0.75	0.67	0.37	0.37	0.73	0.78	0.44	0.18
H_2O				1.45										
CO_2				0.07										
Mg#	62.4	67.9	58.4	43.8	62.2	62.6	53.2	55.4	63.5	65.6	51.2	50.0	55.6	61.7

Trace elements [ppm]

Ba	155	147	249	354	273	161	232	235	167	134	210	248	207	205
Co	35	41	33	36	35	37	33	42	37	45	36	30	37	41
Cr	286	373	145	10	186	214	50	64	138	155	33	34	73	208
Cu	79	74	93	149	93	85	92	107	73	67	111	112	101	86
Ga	16	14	17	18	16	15	15	13	15	13	16	14	13	13
Nb	4	4	5	8	3	5	6	7	4	4	7	6	4	6
Ni	86	99	96	40	73	76	44	62	76	91	43	44	64	76
Pb	7	7	8	9	8	7	6	7	3	4	8	6	3	6
Rb	27	27	34	55	30	27	36	36	26	22	33	38	33	32
Sc	35	34	32	35	34	35	29	40	38	41	34	33	38	40
Sr	118	110	148	148	119	127	162	116	121	109	131	164	123	114
V	184	173	193	223	162	183	168	220	178	194	193	193	204	205
Y	19	17	24	33	21	20	21	22	16	16	23	25	22	20
Zn	74	66	83	97	69	72	54	66	52	53	61	61	62	59
Zr	83	77	116	160	78	88	97	103	72	72	98	112	96	93

Appendix 5   Rare earth element as well as Y and Sc concentrations of selected Ferrar low-Ti (LTS) and high-Ti (HTS) samples measured by ICP-AES at the GeoForschungsZentrum Potsdam.

Sample	RH46	RH48	RH21	RH38	RH29	RH18	RH44	RH40	RH45	RH6
Magma Series	LTS	LTS	LTS	LTS	LTS	LTS	LTS	LTS	LTS	HTS

REE concentration in [ppm]

	RH46	RH48	RH21	RH38	RH29	RH18	RH44	RH40	RH45	RH6
La	6.7	7.5	10	10	11	12	13	16	24	26
Ce	13	16	21	22	23	24	28	35	52	54
Pr	1.9	2.1	2.7	2.7	3	3.1	3.5	4.3	6.5	7.2
Nd	7.7	8.2	11	11	12	12	14	18	25	30
Sm	1.9	2.1	2.6	2.7	2.9	2.9	3.4	4.1	6	7.3
Eu	0.58	0.58	0.72	0.74	0.76	0.83	0.97	1.1	1.4	1.8
Gd	2.1	2.3	2.9	2.9	3.1	3.2	3.7	4.5	6	8.2
Tb	0.35	0.37	0.51	0.49	0.54	0.54	0.64	0.69	1.1	1.5
Dy	2.4	2.5	3.2	3.3	3.4	3.6	4	4.6	6.7	9
Ho	0.5	0.54	0.66	0.72	0.7	0.74	0.89	0.97	1.4	1.8
Er	1.6	1.7	2.1	2	2.1	2.3	2.6	2.8	4.2	5.8
Tm	0.27	0.28	0.33	0.33	0.36	0.37	0.4	0.45	0.65	0.87
Yb	1.6	1.7	2.1	2.1	2.3	2.4	2.6	2.9	4.1	5.7
Lu	0.25	0.26	0.32	0.33	0.36	0.36	0.42	0.45	0.68	0.87
Y	14	15	19	19	18	20	23	26	39	51
Sc	44	44	41	41	43	40	45	43	39	44
La/Sm$_{(N)}$ [1]	2.22	2.25	2.42	2.33	2.39	2.61	2.41	2.46	2.52	2.24
Gd/Lu$_{(N)}$ [1]	1.04	1.10	1.13	1.09	1.07	1.10	1.09	1.24	1.10	1.17
Eu/Eu* [2]	0.89	0.81	0.80	0.81	0.77	0.83	0.84	0.78	0.71	0.71

[1] element ratios of normalised element concentrations using C1-chondrite normalisation values from EVENSON (1978)

[2] Eu anomaly calculated with Eu* as $\sqrt{Sm \times Gd}$

Appendix 6 Platinum-group element concentrations and Pd/Ir ratios of selected Ferrar low-Ti (LTS) and high-Ti (HTS) samples measured by ICP-MS at the Institut für Mineralogie und Geochemie Karlsruhe.

Sample	Magma Series	Ir	Ru	Rh	Pt	Pd	Pd/Ir
Platinum-group elements in [ppb]							
RH3	HTS	0.10	<0.20	0.74	22.70	16.73	167.3
RH6	HTS	0.13	0.26	0.56	14.50	12.14	90.7
RH7	HTS	<0.10	<0.20	0.56	12.94	10.37	-
RH9	HTS	0.12	<0.20	0.62	20.52	15.72	129.2
RH12	LTS	0.20	<0.50	0.21	10.89	7.57	37.4
RH17	LTS	0.18	<0.50	0.11	*3.04*	3.62	20.2
RH18	LTS	0.19	0.54	0.25	*2.80*	7.29	38.2
RH21	LTS	0.16	<0.20	0.22	5.77	7.16	43.7
RH24	HTS	0.11	<0.20	0.12	1.79	1.58	14.3
RH38	LTS	0.18	0.73	0.31	6.75	7.49	41.6
RH40	LTS	0.11	0.69	0.42	5.61	7.31	65.1
RH41	LTS	<0.10	<0.20	<0.10	2.40	1.22	-
RH44	LTS	0.13	0.44	0.34	4.90	2.18	17.0
RH45	LTS	0.10	0.77	0.23	12.57	8.78	87.3
RH46	LTS	0.20	0.72	0.19	4.43	3.68	18.4
RH48	LTS	0.20	0.54	0.22	5.41	5.43	26.6
RH52	LTS	0.31	0.63	0.28	4.80	3.32	10.6
RH53	LTS	0.23	0.76	0.26	4.54	3.00	12.9
RH54a	LTS	0.15	0.62	0.29	5.61	8.40	55.4
RH55	LTS	0.12	0.54	0.32	5.95	7.03	57.8
RH56	LTS	0.12	<0.20	<0.10	3.75	2.01	16.7
NWR27	LTS	0.11	0.99	<0.10	9.35	7.14	66.3
NWR29	LTS	0.11	0.73	<0.10	9.49	8.54	76.1

Appendix 7 Electron microprobe analyses of the experimental phases from experimental runs J1 to J8 in wt% recalculated to 100 wt%.

Run	phase	n^a	SiO$_2$	TiO$_2$	Al$_2$O$_3$	FeO$_{(T)}$	MnO	MgO	CaO	Na$_2$O	K$_2$O	Cr$_2$O$_3$	X^b
J4	mlt	12	56.88 (32)	0.80 (6)	14.87 (47)	9.82 (26)	0.17 (1)	5.00 (21)	9.52 (29)	1.99 (8)	0.94 (5)		47.6
	opx	6	54.04 (15)	0.18 (1)	2.48 (14)	13.29 (30)	0.33 (3)	27.18 (19)	2.48 (20)	0.02 (2)	0.01 (1)		78.5
	aug	7	52.13 (27)	0.28 (3)	3.01 (55)	9.00 (34)	0.24 (4)	17.22 (54)	17.88 (41)	0.20 (6)	0.05 (5)	0.13 (0)	77.3
	plag	7	51.24 (60)	0.12 (4)	27.96 (112)	2.15 (41)	0.05 (3)	1.22 (83)	14.77 (42)	2.29 (14)	0.20 (4)		77.1
J1	mlt	7	58.03 (22)	0.96 (2)	14.32 (16)	10.02 (25)	0.19 (6)	4.45 (9)	8.69 (17)	2.15 (9)	1.18 (7)		44.2
	aug	13	51.95 (35)	0.34 (4)	3.27 (48)	10.52 (58)	0.25 (3)	17.06 (53)	16.29 (80)	0.24 (6)	0.08 (4)	0.12 (2)	74.3
	pig	9	53.58 (47)	0.20 (3)	2.43 (61)	14.73 (42)	0.36 (3)	23.69 (59)	4.73 (55)	0.19 (10)	0.08 (4)	0.05 (1)	74.1
	plag	6	51.82 (61)	0.14 (2)	27.88 (69)	2.09 (21)	0.03 (2)	0.99 (26)	14.18 (35)	2.60 (14)	0.27 (2)		73.8
J2	mlt	8	57.91 (47)	0.98 (8)	14.76 (44)	9.68 (30)	0.15 (6)	4.23 (18)	9.05 (22)	2.11 (11)	1.14 (4)		43.8
	aug	6	51.82 (45)	0.35 (2)	3.41 (62)	10.81 (64)	0.28 (2)	17.06 (33)	15.97 (87)	0.24 (5)	0.07 (3)	0.11 (1)	73.8
	pig	4	53.33 (71)	0.20 (6)	3.04 (122)	14.81 (43)	0.38 (2)	23.09 (123)	4.82 (89)	0.26 (13)	0.08 (5)	0.07 (1)	73.5
	plag	7	52.56 (53)	0.14 (3)	27.23 (74)	2.12 (25)	0.03 (4)	0.98 (22)	14.03 (32)	2.62 (11)	0.31 (4)		73.3
J3	mlt	7	59.02 (38)	1.15 (7)	14.12 (26)	9.94 (29)	0.12 (10)	3.75 (17)	8.57 (30)	1.95 (13)	1.37 (9)		40.2
	aug	4	52.02 (20)	0.39 (1)	3.13 (2)	12.00 (26)	0.32 (3)	16.85 (29)	15.06 (47)	0.16 (3)	0.08 (1)		71.5
	pig	4	53.16 (34)	0.25 (3)	2.91 (45)	15.59 (56)	0.41 (3)	21.41 (63)	5.90 (72)	0.27 (5)	0.11 (4)	0.04 (0)	71.0
	plag	6	52.55 (42)	0.16 (3)	27.55 (61)	2.10 (35)	0.04 (4)	0.84 (12)	13.75 (25)	2.70 (8)	0.33 (4)		72.3
J5	mlt	15	56.60 (24)	0.68 (5)	15.80 (20)	8.35 (7)	0.17 (3)	5.79 (10)	9.85 (14)	1.96 (8)	0.80 (5)		55.3
	aug	5	53.07 (25)	0.25 (3)	2.49 (47)	8.66 (47)	0.25 (3)	17.85 (12)	17.23 (50)	0.16 (6)	0.04 (3)		78.6
	plag	1	52.44	0.19	26.53	2.03	0.16	1.76	14.10	2.43	0.35		74.6
J6	mlt	10	57.54 (15)	0.81 (4)	15.41 (18)	8.38 (7)	0.18 (2)	5.31 (16)	9.37 (12)	2.06 (7)	0.94 (3)		53.0
	aug	5	52.73 (27)	0.24 (3)	2.18 (21)	10.57 (28)	0.30 (6)	18.63 (47)	15.19 (38)	0.13 (4)	0.03 (3)	0.09 (1)	75.9
	pig	1	54.04	0.19	2.78	13.71	0.43	23.34	5.17	0.26	0.08		75.2
	plag	3	52.65 (24)	0.22 (3)	27.22 (10)	1.66 (21)	0.00	1.34 (15)	13.93 (7)	2.65 (12)	0.32 (1)		72.9
J7	mlt	12	57.69 (28)	0.84 (3)	15.35 (31)	8.63 (14)	0.16 (3)	5.01 (10)	9.28 (19)	2.05 (5)	0.99 (5)		50.8
	aug	12	52.28 (59)	0.33 (5)	3.47 (77)	10.88 (56)	0.28 (4)	17.68 (59)	14.82 (99)	0.20 (9)	0.06 (3)	0.11 (3)	74.3
	pig	5	54.24 (41)	0.20 (3)	2.87 (52)	13.84 (23)	0.32 (2)	22.76 (60)	5.37 (18)	0.28 (8)	0.13 (5)	0.04 (2)	74.6
	plag	5	52.53 (49)	0.21 (8)	27.54 (128)	1.69 (52)	0.07 (2)	1.23 (43)	13.68 (17)	2.72 (16)	0.34 (7)		72.3
J8	mlt	10	57.32 (31)	0.88 (5)	15.00 (34)	9.64 (35)	0.19 (3)	4.66 (12)	9.22 (22)	2.03 (8)	1.05 (4)		46.3
	aug	7	51.80 (43)	0.37 (5)	3.77 (63)	11.98 (41)	0.32 (2)	17.46 (56)	14.07 (71)	0.17 (3)	0.04 (2)	0.09 (0)	72.2
	pig	3	54.30 (13)	0.27 (3)	3.26 (13)	14.94 (25)	0.31 (4)	21.27 (31)	5.20 (25)	0.27 (4)	0.17 (2)		71.7
	plag	5	53.34 (17)	0.27 (2)	26.47 (39)	1.98 (7)	0.07 (5)	1.31 (7)	13.40 (24)	2.75 (13)	0.43 (2)		70.9

opx – orthopyroxene, *aug* – augite, *plag* – plagioclase, *pig* – pigeonite, *mlt* – glass

[a] number of analyses, numbers in parentheses are standard deviations *100

[b] compositional parameters: glass and pyroxenes – Mg# = 100*Mg/(Mg+Fe) (molar), all Fe as Fe^{2+}, plagioclase – anorthite content in mol%

ACKNOWLEDGEMENT

SELBSTÄNDIGKEITSERKLÄRUNG

Ich erkläre, dass ich die vorliegende Arbeit selbständig und unter Verwendung der angegebenen Hilfsmittel, persönlichen Mitteilungen und Quellen angefertigt habe.

....

Jena, 6. Juli 2007   Ricarda Hanemann